Medicinal Chemistry Division, Cardiff School of Pharmacy and Pharmaceutical Science, Cardiff University

Design and Synthesis of Novel CYP24A1

Inhibitors

A thesis submitted in accordance with the condition governing candidates for the degree of Philosophiae Doctor in Cardiff University

by

Ismail Taban

Supervisor

Dr. Claire Simons

20/07/2017

Dedicated to

my Father

my Mother

my Brothers

my Wife

my Son

my Daughter

ACKNOWLEDGEMENT

Lis of papers conference poster and workshop

1. **Taban, I**.; Zhu, J.; DeLuca, F. H.; Simons, C. Synthesis, molecular modelling and CYP24A1 inhibitory activity of novel of (*E*)-*N*-(2-(1*H*-Imidazol-1-yl)-2-(Phenylethyl)-3/4 Styrylbenzamides. Bioorganic & Medicinal Chemistry. 2017, 25(15), 4076-4087.

2. **Taban, I**.; Zhu, J.; DeLuca, F, H.; Simons, C. Analysis of the binding sites of vitamin D 1α-hydroxylase (CYP27B1) and vitamin D 24-hydroxylase (CYP24A1) for the design of selective CYP24A1 inhibitors: homology modelling, molecular dynamics simulations and identification of key binding requirements. Bioorganic & Medicinal Chemistry. Accepted on 20/08/2017. https://doi.org/10.1016/j.bmc.2017.08.036.

3. **Taban, I**.; Touran, B, W.; Zucchini, B.; Williamson, C.; Altuwairigi, D.; Adeline, S, T.; Girvan, H, N.; McLean, J, K.; Sood, S.; Marino, L, B.; Munro, W, A.; Carvalho, D, L.; and Simons, C. Novel aryl substituted pyrazoles as small molecule inhibitors of cytochrome P450 CYP121: synthesis and antimycobacterial evaluation. Journal of Medicinal Chemistry in preparation.

4. Moe molecular modeling workshops 23-24/02/27 (Cambridge)

5. DL- Poly molecular modeling workshop 03-06/12/ 2016 (Daresbury)

6. Enzymatic assay for CYP24A1 and CYP27B1 enzymes training 25/07/2015 to 31/08/2015 (University Wisconsin/ USA)

7. Ismail Taban, Claire Simons, design and synthesis of novel CYP24A1 inhibitors. BMCS 8TH Postgraduate Symposium, Cambridge University, UK, 2014

Abbreviations

$1\alpha,25\text{-(OH)}_2\text{-D}_3$	$1\alpha,25$-dihydroxyvitamin D_3 (calcitriol)
25-(OH)-D_3	25-hydroxyvitamin D_3
3 D	three-dimensional
2D	two-dimensional
Å	angstrom
Bcl-2	B-cell lymphoma 2
Bcl-xL	B-cell lymphoma-extra-large
BPH	benign prostate hyperplasia
cAMP	cyclic adenosine monophosphate
CDI	1,1 -carbonyldiimidazole
CDK	cyclin-dependent kinase
CYP24A1	$1\alpha,25$-dihydroxyvitamin D-24-hydroxylase
CYP27A1	vitamin D_3-25-hydroxylase
CYP27B1	25-hydroxyvitamin D_3-1α-hydroxylase
CYP2C5	cytochrome P450 2C5
DBP	vitamin D binding protein
DHT	dihydrotachysterol
DMF	dimethylformamide
DMSO	dimethylsulfoxide
ExPASY	expert protein analysis system
FAD	flavin adenine dinucleotide
GH	growth hormone
FGF-23	fibroblast growth factor 23
FMN	flavin mononucleotide
Gln	glutamine
Gly	glycine
GFR	glomerular filtration rate
h	hour
HIF-1α	hypoxia-inducible factor 1-alpha
HRMS	high Resolution Mass Spectroscopy
Hz	hertz
IGF-I	insulin-like growth factor-1
Ile	isoleucine
IL-8	interleukin-8
IL-17A	interleukin-17A
IL-17F	interleukin-17F
KTZ	ketoconazole
Leu	leucine

MD	molecular Dynamics
Met	methionine
MOE	molecular operating environment
mRNA	messenger ribonucleic acid
NF-κB	nuclear factor κ-light-chain-enhancer of activated B- cells
NADPH	nicotinamide-adenine dinucleotide phosphate (reduced form)
NMR	nuclear magnetic resonance
ns	nanoseconds
PDB	protein data bank
PGE2	prostaglandin E2
Phe	phenylalanine
PTH	parathyroid hormone
r.t.	room temperature
Rf	retention factor
RMSD	root-mean-square deviation
SAR	structure-activity relationship
Ser	serine
T1D	type 1 diabetes
T2D	Type 2 diabetes
Thr	threonine
TLC	thin layer chromatography
Trp	tryptophan
tyr	tyrosine
UVβ	ultraviolet β
VDR	vitamin D receptor

Table of Contents

List of tables

List of figures

Abstract

CYP24A1 (25-hydroxyvitamin D-24-hydroxylase) is a useful enzyme target for a range of medical conditions including cancer, cardiovascular and autoimmune disease, which show elevated CYP24A1 levels and corresponding reduction of calcitriol (the biologically active form of vitamin D). Calcitriol has antiproliferative and pro-differentiating properties, however use of calcitriol as a therapeutic drug is limited by hypercalcaemia. An alternative approach is the use of CYP24A1 inhibitors to prevent the metabolism of calcitriol. The aim of this research is to design and synthesise novel inhibitors of CYP24A1 to enhance the endogenous levels of circulating calcitriol. Furthermore, it is important to develop compounds that are selective for CYP24A1 over CYP27B1 so that the generation of calcitriol itself is not blocked. In order to understand the requirements of inhibitor binding to the enzyme-active site, it would be useful to have a 3D structure of both human CYP24A1 and CYP27B1. However, to date, no human crystal structures are available for either of these enzymes. Therefore, a homology model for CYP24A1 has been developed and published. A CYP27B1 homology model was developed, using a combination of homology modelling, molecular dynamics simulations, and molecular docking to understand the satisfactory explanation of the binding selectivity of the CYP27B1 model with the natural substrate and with selective inhibitor complexes. Docking results for CYP27B1 showed amino acids Arg107, Asn387 and Asp320 have an important role in binding interactions to form hydrogen bonds with inhibitors. The development of potent and selective inhibitors from three azole series was investigated. Development of series one using pyridine, imidazole and triazole as the haem binding group was synthesised successfully. The compounds exhibited weak potency and IC_{50} ranging between 10.2 to 28.4 μM against CYP24A1. Owing to the low CYP24A1 inhibitory activity the compounds were not evaluated against CYP27B1. The series two bis(3-methyl-1-phenyl-1H-pyrazol-5ol) was synthesised successfully. Two compounds were the moderate CYP24A1 inhibitors and so were further evaluated against CYP27B1. However, these compounds showed enzymatic inhibition (IC_{50} = 0.57 μM and 0.41 μM) against CYP27B1, that is they were more selective for CYP27B1 which could be rationalised from docking experiments. A series of (*E*)-*N*-(2-(1*H*-imidazol-1-yl)-2-(phenylethyl)-3/4-styrylbenzamides have been synthesised using an efficient synthetic route and shown to be potent inhibitors of CYP24A1 (IC_{50} 0.11 - 0.35 μM) compared with the standard ketoconazole. Molecular modelling using our CYP24A1 homology model showed the inhibitors to fill the hydrophobic binding site, forming key transition metal interaction between the imidazole nitrogen and the haem Fe^{3+} and multiple interactions with the active site amino acid residues.
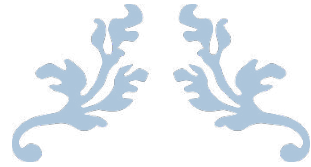
CHAPTER ONE

Introduction

1　Introduction

1.1　Introductory remarks

The sun is the primary source of energy in this biosphere, providing earth's heat and light, protecting people from disease, and governing photosynthesis in the plant kingdom. Notably, the sun works as a cofactor to enhance the production of vitamins, such as vitamin D, which is synthesised from the skin by exposure to ultraviolet β radiation to produce vitamin D_3 (cholecalciferol) through a non-enzymatic pathway[1]. Production of sufficient vitamin D from the skin depends on the strength of the ultraviolet β radiation, the length of time spent in the sun, the amount of pigment in the skin[2], and the exposure of arms and legs for around 30 minutes between 10 am and 3 pm twice a week[3]. Depending on the intensity of the ultraviolet β radiation from sunlight, which varies according to season and latitude, this can be adequate to prevent vitamin D deficiency[4].

1.2　History of Vitamin D

McCollum[3] discovered vitamin D in 1913, and termed it "D" as it was the fourth known vitamin[3,5]. Vitamins are classified into two classes depending on whether they attract (hydrophilic) or repel (hydrophobic) water[6]. The hydrophobic vitamins, comprising A, D, E and K, are stored mostly in adipose tissues and the liver whereas hydrophilic vitamins, such as C and the B complex (B_1, B_2, B_3, B_6 and B_{12})[7], cannot be stored in the tissues, and therefore, humans need to obtain these vitamins from their diet[2,8,9]. Vitamin D is a lipophilic compound known as a pro-hormone, and there are two major physiologically active forms, namely, vitamin D_2 (calciferol) and vitamin D_3 (cholecalciferol) [10]. Vitamin D has no hormonal activity, and therefore, it is converted to biologically active 1α,25-dihydroxyvitamin D_3 (1,25$(OH)_2D_3$), also known as calcitriol[11], by two successive hydroxylations, the first in the liver and the second in the kidneys[12,9,13].

1.3　Transport of Vitamin D

Vitamin D and its metabolites are hydrophobic in nature; therefore, their transportation in the circulatory system is facilitated by binding to serum proteins, such as vitamin D-

binding protein (DBP) and albumin[14,15.] DBP is the primary transport protein for calcitriol, contributing approximately 88% of the total bound calcitriol[16] ; the remainder is bound to albumin, leaving less than 1% of $25(OH)D_3$ in an unbound state[17]. DBP influences how cells can access vitamin D either by defining the amount of free vitamin D metabolites available for passive diffusion into the cell or by actively facilitating the acquisition of vitamin D metabolites[18].

In the glomerulus, DBP-bound $25(OH)D_3$ and other vitamin D metabolites are filtered out of the blood into the filtrate. Therefore, DBP-$25(OH)D_3$ is reabsorbed from the luminal filtrate in the renal proximal tubule by binding to megalin[19]. In addition, cubilin is another membrane receptor expressed on the apical side of the proximal tubule that plays a role in the renal uptake of DBP-$25(OH)D_3$ complexes[20].

1.4   Physiological role of vitamin D

1.4.1   Mineral homeostasis

Vitamin D, commonly regarded as the sunlight hormone or sunshine vitamin, plays an essential role in calcium and phosphorus homeostasis[21]. A deficiency of vitamin D results in osteomalacia and has been shown to affect approximately 50% of the population worldwide within all ethnic and age groups[22]. Hypovitaminosis D disease can be attributed mostly to reduced outdoor activities as well as air pollution factors that reduce exposure to sunlight, which is required for ultraviolet-β-induced vitamin D production in the skin[23]. Indeed, one of the best-described functions of calcitriol is the control of circulating calcium levels in the body[24]. When extracellular calcium levels are low, the calcium-sensing receptor of the parathyroid gland responds by stimulating the synthesis and secretion of parathyroid hormone (PTH)[25]. Consequently, PTH stimulates the synthesis of calcitriol by increasing CYP27Bl[26]. Simultaneously, PTH suppresses the renal expression of CYP24A1, which results in a rise in the circulating levels of calcitriol[20]. Furthermore, calcitriol stimulates the active absorption of dietary calcium from the small intestine by stimulating the key proteins involved, such as calbindin-D9k and calcium transporter-1[27]. In addition, calcitriol increases the reabsorption of calcium in the distal renal tubules by stimulating the gene transactivation of the receptor activator of nuclear factor KB (NF-KB)[28,29].

Vitamin D-regulated mineralisation of the skeleton and the maintenance of calcium levels are accomplished by the following two mechanisms[30] (Figure 1).

1. Proteins involved in the active intestinal absorption of calcium are induced by stimulating the active intestinal absorption of phosphate[31].

2. Blood calcium concentrations remain in the normal range even when there is no calcium from the diet. Therefore, if the calcium concentration is inadequate, renal 1α-hydroxylase is activated, and calcitriol, the active form of vitamin D_3, is synthesised[32].

Vitamin D-dependent rickets type I is related to defects in CYP27B1[33] and is quickly relieved by the administration of calcitriol[33]. Likewise, vitamin D-dependent rickets type II appears to result from a mutation in the vitamin D receptor gene and is also managed by the administration of calcitriol[34].
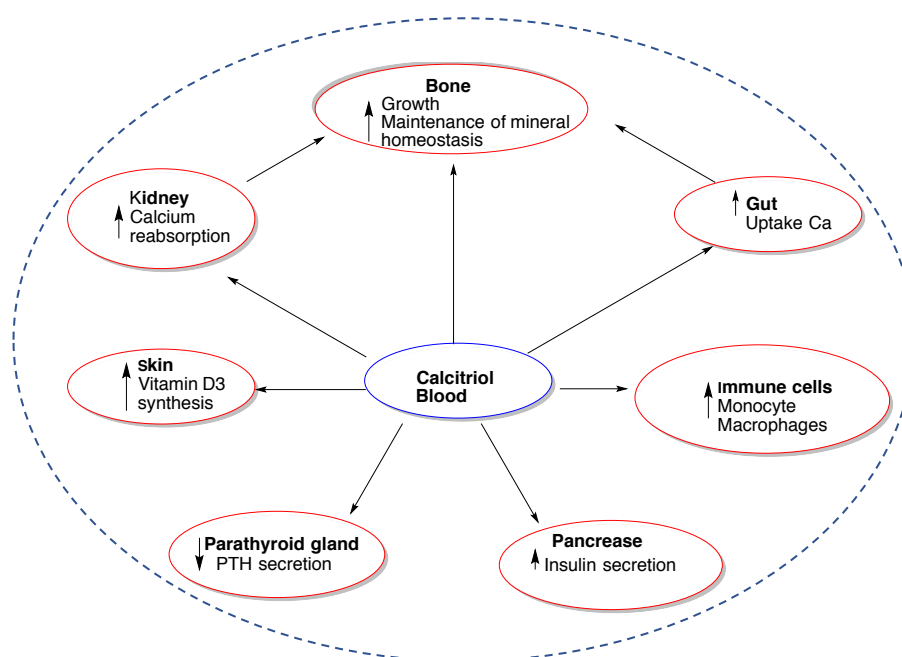
Figure 1: Effect of calcitriol on calcium

1.4.2 Kidney disease

Vitamin D is thought to play a pivotal job in several disease processes that are closely related to chronic kidney disease (CKD)[35], for example, mineral bone disorder, anaemia, and inflammation. Calcitriol governs multiple signalling routes that are related to renal damage, and in adults with CKD, treatment with vitamin D derivatives is beneficial in reducing proteinuria and inflammation[36].

Abnormalities in vitamin D metabolism have been linked to the pathogenesis of secondary hyperparathyroidism in CKD[37]. There are several mechanisms involved in the reduction in the levels of calcitriol that occur in kidney disease[38]. Therefore, a reduction in renal mass will limit the quantities of 1 α -hydroxylase that are available for the production of calcitriol. A reduction in the glomerular filtration rate could limit the delivery of substrate to the 1 α -hydroxylase, which may also limit the ability of the kidney to produce calcitriol. Chronic renal failure, such as that resulting from polycystic kidney disease or diabetic nephropathy, is related to severe metabolic bone disease[39,40]. Several studies have reported that treatment with vitamin D analogues, such as calcitriol, alfacalcidol, and paricalcitol, results in an increase in the life expectancy of patients with renal failure[41].

Recent observations have demonstrated that kidney disease seems to be associated with a high incidence of vitamin D deficiency[38]. Fortunately, vitamin D receptors are present in the parathyroid gland, and a major function of vitamin D is to suppress parathyroid cell proliferation. Several vitamin D analogues have been developed to treat the secondary hyperparathyroidism linked with chronic renal failure (Figure 2), such as 19-nor-1 α ,25-dihydroxyvitamin D_2 and 1 α -hydroxyvitamin D_2 and 22-oxa-1 α ,25-dihydroxyvitamin D_3.
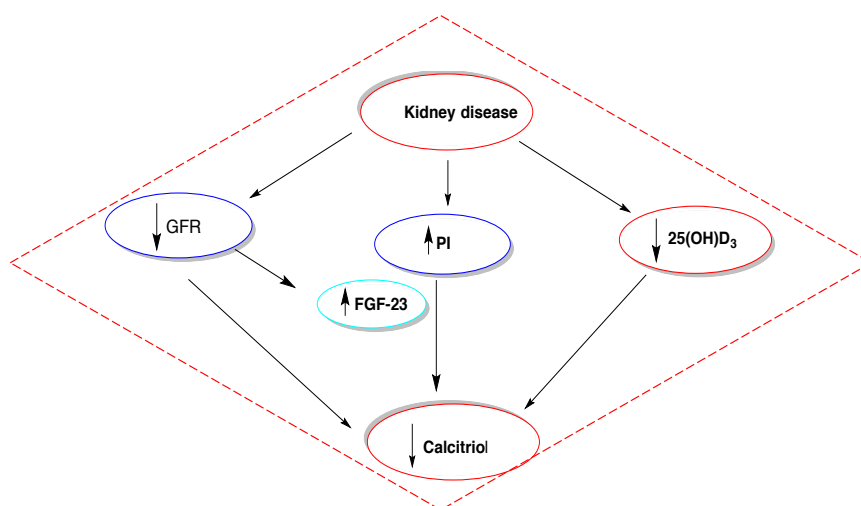
Figure 2: Effect of chronic kidney disease (CKD) on vitamin D, glomerular filtration rate (GFR), fibroblast growth factor-23 (FGF-23) and Pi phosphate (inorganic).

1.4.3 Cardiovascular system complications

Heart disease is currently considered as one of the leading causes of illness and death in the world. Vitamin D insufficiency has been distinguished as a possible risk factor

for numerous illnesses not traditionally associated with vitamin D[42], for example, tumour and cardiovascular disease, and there is evidence to confirm the relation between low 25-hydroxyvitamin D levels and cardiovascular disease[31]. In particular, vitamin D deficiency is reported to be linked to risk factors of heart disease, such as hypertension and diabetes mellitus; atherosclerosis events, for example, myocardial infarction and stroke; as well as congestive heart failure[43]. Vitamin D receptors are expressed in a variety of tissues, including cardiomyocytes, vascular smooth muscle cells, and endothelial cells, and vitamin D deficiency has been shown to affect inflammation, and cell proliferation and differentiation[44]. Furthermore, recent studies have disclosed a relationship between blood levels of calcitriol and the incidence of stroke[45]. Moreover, the association between vitamin D deficiency and hypertension, metabolic syndrome, and diabetes mellitus has also been studied[46,47] (Figure 3).
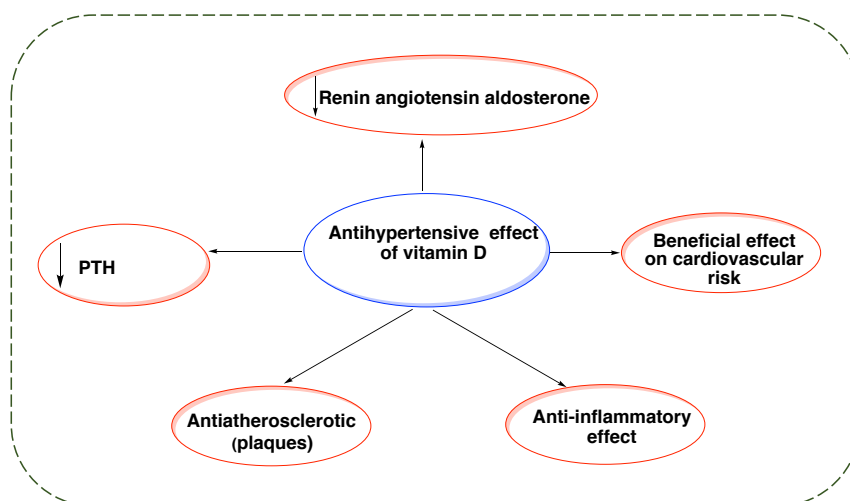
Figure 3: Relationship between vitamin D and cardiovascular risk

1.4.4 Skin complication

Vitamin D imparts therapeutic benefits to acne, which has traditionally been treated by retinoic acid[48]. The skin is a target of vitamin D action, and numerous literature reports have clearly established the presence of the vitamin D receptor in keratinocytes, sebocytes, and dermal papilla cells by the treatment of acne and psoriasis using calcitriol, calcipotriol and 22-oxa-1,25-$(OH)2D_3$[40].

Recently, it has been shown that analogues of the vitamin D hormone can be useful in the Rhino mouse model of acne[49], indicating the potential use of such compounds for the treatment of this disorder[49].

Furthermore, several studies have shown vitamin D analogues to be efficient treatment options for psoriasis[50]. Vitamin D_3 analogues are also used in combination with phototherapy to manage psoriasis through their immunomodulatory properties by suppressing T-cell proliferation[51]. In addition, vitamin D analogues influence the regulation of antimicrobial peptides, cathelicidin, and human β-defensin 2, which are involved in the pathogenesis of psoriasis[52].

1.4.5 Psoriasis

Psoriasis is a chronic inflammatory skin disease affecting approximately 5 % of the global population[48]; it is characterised by the hyperproliferation of keratinocytes leading to the redness, thickening, and scaling of the epidermis followed by itching and the appearance of lesions (Figure 4)[49]. Although, the pathogenesis of psoriasis is not entirely clear, there is evidence of dysregulation of the immune cells in the skin, acutely T cells, which play a critical function in psoriasis expansion[53]. Mostafa *et al.*[54] reviewed the possible role of vitamin D deficiency in psoriasis. However, calcitriol is known to suppress the T helper1 cell and T helper17 cell proliferation[55]. Likewise, topical treatment with calcipotriol has been revealed to pointedly decrease cutaneous levels of human β defensins 2, human β defensins 3[56], IL-17A, IL-17F, and IL-8, which play critical roles in psoriasis[56].

Figure 4: Clinical symptom of psoriasis[57]

1.4.6 Autoimmune diseases

The role of vitamin D cannot be ruled out in several autoimmune diseases[58], including inflammatory bowel disease, autoimmune thyroiditis, rheumatoid arthritis, diabetes mellitus type 1, mixed connective tissue disease, scleroderma, systemic lupus erythematosus, and allergic encephalomyelitis[59]. A few studies have suggested that the

risk of rheumatoid arthritis and type I diabetes mellitus is reduced in humans with a high vitamin D intake[60]. In addition, it influences a broad range of immune cells, such as T lymphocytes, B lymphocytes, and dendritic cells[61]. Furthermore, it has been observed that vitamin D receptors are located in immune cells, including antigen-presenting cells, macrophages, and activated T cells, which could be inhibited notably by calcitriol[62,63]. In line with this, an inverse relationship between exposure to ultraviolet light and the incidence of multiple sclerosis has been noted[64]. The impact of multiple sclerosis cases was observed to be low in countries near the equator whereas it increases progressively in countries closer to the poles[65].

1.4.7   Type 1 diabetes (T1D)

Type 1 diabetes (T1D) is an autoimmune disease in which β cells are destroyed and vitamin D elicits its preventive function. Treatment with calcitriol alleviates the symptoms of type I diabetes[66]. Moreover, recent studies have established a relationship between sunlight exposure and the incidence of type I diabetes[67] where calcitriol prevents the disease in animal models by modifying the T-cell differentiation, the modulation of dendritic cell action, the induction of cytokine secretion and the shifting of the balance to regulatory T cells[68].

In general, T1D is a consequence of the T-cell mediated destruction of insulin-producing pancreatic β-cells with a distinctive inception in childhood or adolescence[68]. Therefore, vitamin D administration during the juvenile period is considered a protective measure against the development of T1D[69]. Similarly, a 33% reduced risk of developing T1D was noted among children who received vitamin D supplementation during their infantile stage[70]. Additionally, in non-obese diabetic mice, the supplementation of calcitriol or vitamin D analogues prevented or at least postponed the onset of diabetes[71].

Moreover, vitamin D receptor (VDR) polymorphism is associated with type I diabetes mellitus[72]. Several studies have reported associations of T1D with polymorphisms in the CYP27B1 gene and have provided evidence of their association with T1D[73]. Therefore, VDR can be regarded as a master regulator of transcription, which is present in pancreatic β-cells, and vitamin D is essential for normal insulin secretion[71,74].

1.4.8   Type 2 diabetes (T2D)

Type 2 diabetes (T2D) is a disease that threatens the health and life quality of citizens. Presently, 285 million people worldwide are suffering from this disease[75], and this number is projected to reach 439 million after 2025[75]. Type 2 diabetes mellitus is a multifactorial disease characterised by chronic hyperglycaemia, based on two factors: altered insulin secretion and insulin resistance. In addition, it can also be expressed by diminished glucose tolerance, which results from islet β cell dysfunction, followed by insulin deficiency in skeletal muscle, liver, and adipose tissues[76]. The role of vitamin D in insulin secretion is justified by the presence of vitamin D receptors in β-cells and vitamin D-dependent calcium binding proteins in pancreatic tissue[77]. Similarly, vitamin D deficiency has been proven to alter insulin synthesis and secretion in humans[78]. Vitamin D deficiency may also affect glucose intolerance, altered insulin secretion, and type II diabetes mellitus[79]. Moreover, vitamin D deficiency results in decreased pancreatic insulin secretion, without altering glucagon secretion[80].

1.4.9   Cancer

Vitamin D deficiency leads to cancer. Genes coding the metabolic enzymes, CYP24A1 and CYP27B1, are discovered to remain down-regulated among numerous tumours, for example, breast and prostate tumours[81].

The antitumour mechanism of calcitriol is the promotion of cell apoptosis. Key mediators of apoptosis, such as the anti-apoptotic, pro-survival proteins Bcl-2 and Bcl-XL, are repressed through calcitriol, although it induces the expression of pro-apoptotic proteins, for example, BAX, BAK, and BAD[82]. Huang and Bao[83] reported that calcitriol also has a role in angiogenesis inhibition by inhibiting vascular endothelial growth factor and enhancing the potent anti-angiogenic factor thrombospondin 1[83].

E-cadherin, a transmembrane linker of the intercellular junctions, is a membrane protein that is categorised as a cancer suppressor gene[84]. E-cadherin binds to β-catenin, preventing its nuclear translocation. In the nucleus, β-catenin binds to T-cell transcription factor/lymphoid enhancer-binding factor 1 (TCF/LEF1), a transcription factor involved in cell proliferation control. Calcitriol treatment increases the level of E-cadherin, resulting in the sequestration of β-catenin in the cytoplasm and obstructing the TCF/LEF1 gene regulation[85]. Moreover, Chakraborti[86] has demonstrated that calcitriol displays antiproliferative and differentiation properties towards many cell

types by controlling many of the genes involved in proliferation, differentiation, apoptosis, and angiogenesis[86]. Colston *et al.*[87] reported that many malignant cell types have been shown to respond by intake of calcitriol, as they possess VDR. Calcitriol-mediated action on tumour cells revealed that the incubation of malignant melanoma in the presence of calcitriol-inhibited cell proliferation showed a noticeable increase in cell doubling time[87]. Several reports have documented the cancer activity of calcitriol in a varied range of normal and tumour cells. However, clinical trials of calcitriol for the treatment of prostate cancer and leukaemia have been unsuccessful due to its toxic hypercalcaemic side effect. The risk of toxicity can be thwarted by reducing the dosage[88]. Brawer[89] reported a randomised phase II clinical study for the treatment of prostate cancer, which demostrated that using a weekly treatment regimen consisting of high dose (45 μ g) calcitriol and docetaxel was associated with improved survival compared with placebo and docetaxel[89] alone. Therefore, it can be concluded that calcitriol has antiproliferative, anti-inflammatory, and immunomodulatory activities. Calcitriol suppresses the growth of numerous malignant cells by arresting cell cycle and motivating apoptosis[90]. So, calcitriol inhibits cell proliferation by

1. Expression and significant down-regulation cyclins and the cyclin-dependent kinase after calcitriol treatment were showed in pancreatic cancer[88,91]
2. inducing apoptosis through mitochondrial disruption and activating the intrinsic pathway [92]
3. thwarting cancer angiogenesis, stimulating healthy cells and promoting the inhibition of proliferation. Angiogenesis, the process of the formation of new blood vessels from the existing vasculature, is a crucial step in the continued growth, progression, and metastasis of tumours. Moreover, COX-2 promotes tumour development by stimulating angiogenesis. COX-2 inhibitors have been used to block angiogenesis and tumour proliferation. The pro-angiogenin effect of COX-2-produces PGE_2, which might increase HIF-1 α protein synthesis in cancer cells.

Thus, calcitriol plays a vital role in the development of specific types of cancers, such as oesophageal, stomach, colon, rectal, gall bladder, pancreatic, lung, breast, uterus, ovary, prostate, urinary bladder, kidney, skin, thyroid, and hematopoietic system (e.g., Hodgkin's lymphoma, non-Hodgkin's lymphoma, multiple myeloma)[93].

1.4.9.1 Breast cancer

There is a reverse relation between the intake of calcitriol and the risk of breast cancer. An improvement has been observed with patients given a high dosage of vitamin D [94]. Indeed, vitamin D insufficiency has been found in a majority of women suffering from breast cancer[95]. In addition, growth inhibition has been found in patients using a combination of vitamin D_3 and tamoxifen[96]. Calcitriol inhibits action by preventing the synthesis and blocking the biological action of oestrogens and reducing the gene coding aromatase[97]. Furthermore, calcitriol helps to regulate the oestrogen receptor and is effective against both oestrogen receptor positive and negative breast cancers. Moreover, Masuda and Jones have also reviewed that some vitamin D analogues inhibit angiogenesis and decrease metastatic potential[98].

1.4.9.2 Prostate cancer

Benign prostate hyperplasia (BPH) is the most prevalent prostate medical condition in the elderly and one of the most frequent chronic conditions in the male population, with a histological prevalence of 50% in men aged 50 to 60 years and 90% in men aged over 80 years[99]. Furthermore, prostate cancer is the most frequently diagnosed and the second leading cause of cancer mortality in males in the United States[100]. Clinical indication of BPH associated with benign prostatic enlargement leads to blockage of the urethra. BPH[101] is caused by complex cellular alterations including changes in proliferation, differentiation, apoptosis, and senescence[101]. Prostate cancer occurrence and mortality rates are found more in patients with vitamin D insufficiency[102]. The prostate is recognized as an extra renal site of vitamin D synthesis and action through the expression of CYP27B1 and the vitamin D receptor[103]. Maj *et al.*[104] have shown in their data reports that calcitriol has a significant anticancer effect and might increase the efficacy of chemotherapy[104]. Krishnan *et al.*[105] showed the antiproliferative effect of calcitriol in prostate cancer cells, including the promotion of cell cycle arrest, the induction of apoptosis, and the modulation of kinase pathways[105,106]. Calcitriol is used in the treatment of many diseases[106], for example, psoriasis, cardiovascular system complications and cancers. Nonetheless, there is a limitation in the broader clinical use of calcitriol as a single anticancer agent due to its toxicity at higher doses (hypercalcemia). In addition, calcitriol has limited bioavailability at the tumour site. Calcitriol anticancer activity is mainly dependent on its dose, and its serum

concentration ranges escalate from 0.5 to 41 ng/ml, resulting in significant changes[107]. Furthermore, Kaeding *el al.*[108] showed the efficiency of calcitriol to inhibit the proliferation of both prostate cancer types (androgen dependent and androgen independent)[108]. It also induces apoptosis and inhibits the cell growth in androgen-sensitive and androgen-independent prostate cancer cells[102].

1.4.9.3 Colorectal cancer

Colorectal cancer is a malignant tumour, which is caused by a group of tumorous cells developing in either the colon or the rectum. A colon tumour starts in the cells of the colon, while colorectal cancer starts in either the colon or the rectum[109]. Ma *et al.*[110] found a relation between low levels of calcitriol and colorectal tumours[110]. Individuals who have high levels of calcitriol in their human body are less likely to progress to colorectal cancer, and patients with higher calcitriol levels who previously have had colorectal cancer are more likely to have better outcomes. The mortality rates from colorectal cancer are higher in the northern and north eastern United States, compared with the Southwest, Hawaii and Florida and this correlate directly with an individual's vitamin D status[111]. Calcitriol helps to maintain a standard calcium gradient in the various colon epithelial cells[112]. With elevated levels of blood serum calcitriol associated with a noticeable decrease in proliferation of non-cancerous cells[111], calcitriol significantly increases the expression and activity of alkaline phosphatase and induces colonic differentiation inhibition of proliferation[113]. Endogenous synthesis of calcitriol from 25-hydroxyvitamin D_3 in gut mucosa plays a significant role in the control of cellular growth and differentiation in the colorectal mucosa[114].

Lin *et al.*[115] established that there is an inverse correlation between the serum levels of vitamin D and the incidence of polyps and adenomas with the inverse relationship between dietary vitamin D_3 intake or sunlight exposure and human colorectal cancer[115,116].

1.4.9.4 Blood cancer

Calcitriol in human myeloid leukaemic cells inhibits proliferation and enhances the differentiation of monocytes and macrophages[117]. Intake of calcitriol in acute myleloid leukaemia leads to growth inhibition, the stimulation of monocyte differentiation, and apoptosis[118]. Recent gene expression profiling experiments of lymphocytic leukaemia have recognised that the vitamin D receptors were prominent compared with normal B

and T lymphocytes. The growth of a malignant tumour is delayed by intake of calcitriol in patients suffering from blood cancer[119].

1.4.9.5   Skin cancer

Calcitriol has a critical function in the prevention of the induction and development of severe skin tumours, as it is involved in the regulation of several signalling pathways that have implications in carcinogenesis[119], including the inhibition of the hedgehog signalling pathway, the pathway underlying the development of basal cell carcinomas, and the upregulation of nucleotide excision repair enzymes[120]. Furthermore, skin cancer metastasis depends on the tumour microenvironment, where calcitriol plays a significant role in the inhibition of certain molecular events involved in cancer development[120]. Calcitriol regulates cellular growth and apoptosis in human keratinocytes, plays an antioxidative, cytoprotective and immunomodulatory role in the skin, and protects human keratinocytes. Calcitriol works to decrease the number of cyclobutane pyrimidine dimers, which are the more common DNA photoproducts caused by insufficient DNA repair after UV radiation[121,122]. Melanoma cells express the vitamin D receptor and can convert the $25(OH)D_3$ into calcitriol. Calcitriol slows down the proliferation of these cells, promotes apoptosis, and inhibits the proliferation of human melanoma cells *in vitro*[123].

1.5   Metabolism pathway of vitamin D

Vitamin D consists of 3 rings with 27 carbons. There are two forms of vitamin D: vitamin D_3 (cholecalciferol) and vitamin D_2 (ergocalciferol). Vitamin D_3 is produced by the conversion of 7-dehydrocholesterol (7-DHC) in the epidermis and dermis of humans, and ergocalciferol is formed in mushrooms and yeast and is synthesised by the ultraviolet β irradiation of ergosterol. The chemical difference between cholecalciferol and ergocalciferol is in the side chain (ergocalciferol has a double bond between C22 and C23 and a methyl group on C24)[7] (Figure 5).

Chemical Formula: $C_{27}H_{44}O$
Molecular Weight: 384.65
Cholecalciferol

Chemical Formula: $C_{28}H_{44}O$
Molecular Weight: 396.66
Ergocalciferol
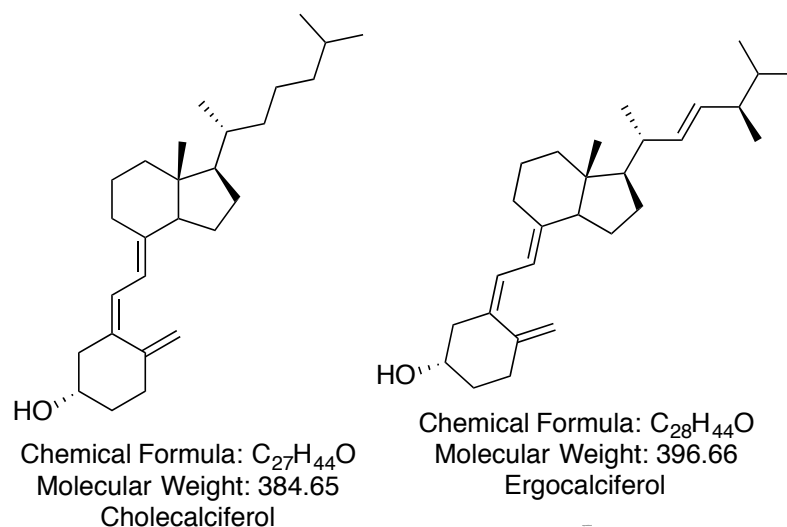
Figure 5: Chemical structure of cholecalciferol and ergocalciferol

Vitamin D is part of an endocrinal system, which plays a major role in the maintenance of calcium and phosphate homeostasis and is essential for the maintenance of a healthy skeleton[124]. Vitamin D is synthesised in the skin by the reaction of 7-dehydrocholestrol, which is found in the epidermal layers, with ultraviolet β radiation (when skin is exposed to the sun), or it is obtained from the diet. Provitamin D_3 is produced by opening of the steroid nucleus (B ring broken by UV light with spectrum 280 - 320 ultraviolet β radiation [125]). Provitamin D_3 is an unstable compound and isomerises into vitamin D_3[126].

The three most important steps in vitamin D metabolism, 25-hydroxylation, 1α-hydroxylation, and 24-hydroxylation, are all performed by cytochrome P450 enzymes[4]. The initial step of vitamin D metabolism is the hydroxylation of vitamin D_3 at position C25 of vitamin D_3 by CYP27A1 (endoplasmic reticulum) and CYP2R (mitochondrial) (25-droxylase), found in the liver to produce $25(OH)D_3$ (an inactive form of vitamin D)[125] (Scheme 1). Calcitriol, an active form of vitamin D, is produced by a second hydroxylation in the renal distal convoluted tubule at position 1 α by CYP27B1, a cytochrome P450 monooxygenase, which helps in many of the reactions involved in drug metabolism and the synthesis of cholesterol, steroids, and other lipids[127].
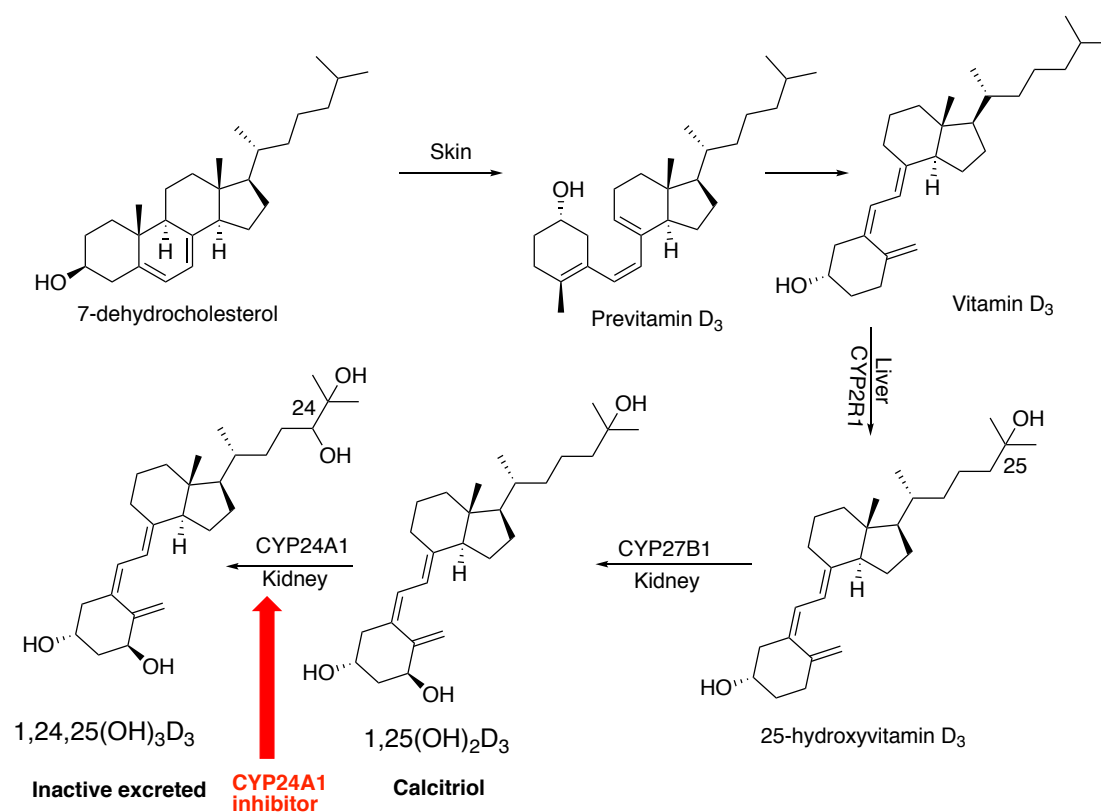
Scheme 1: Vitamin D metabolic pathway

CYP27B1 contains 508 amino acids and was classified as a class I cytochrome located in the mitochondria and is stimulated by PTH, hypophosphatemia, and hypocalcaemia and leads to the direct stimulation of the absorption of calcium in the duodenal intestine. However, the regulation of CYP27B1 in other tissues is independent of PTH, which does not induce the expression of CYP27B1 despite its strong stimulation of CYP27B1 gene expression in the kidney[128], and it is indirectly deactivated by fibroblast growth factor (23 FGF-23). Calcitriol deficiency in humans produces defects in bone formation and mineralisation, for example, rickets in children and osteomalacia in adults[129]. Recently, a CYP27B1 gene expression has been reported in non-renal tissues and is expressed widely in the human body, such as in keratinocytes, lungs, liver, placenta, thymus, stomach, brain, lung cancer, breast and skin in normal and cancer tissues,[130] cultured bone cells, macrophages [131], prostate cells, colon and islet cells of the pancreas. The function of CYP27B1 in renal and non-renal tissues is to produce calcitriol[132] (Scheme 2). Subsequently, the VDR binds with calcitriol to enhance the production of target genes[133]. Calcitriol was positively regulated with CYP27B1, and there is negative feedback regarding hydroxylation at position C24 of $25(OH)D_3$ due to the effect of CYP24A1 producing polar inactive compounds that are readily excreted from the body

(e.g. calcitroic acid)[134]. Also, 20,23-dihydroxyvitamin D_3 [20, 23$(OH)_2D_3$] is a biologically active metabolite produced by the action of CYP11A1 on calcitriol[134]. Several reports have illustrated the effect of P450 families on calcitriol to produce 20-hydroxyvitamin D_3 [20$(OH)D_3$], 20,23-dihydroxyvitamin D_3, and 17,20,23-trihydroxyvitamin D_3[135]. 20$(OH)D_3$ and 20,23$(OH)_2D_3$, possess many of the properties of calcitriol, such as the inhibition of proliferation, the promotion of differentiation, and the suppression of inflammation[136].
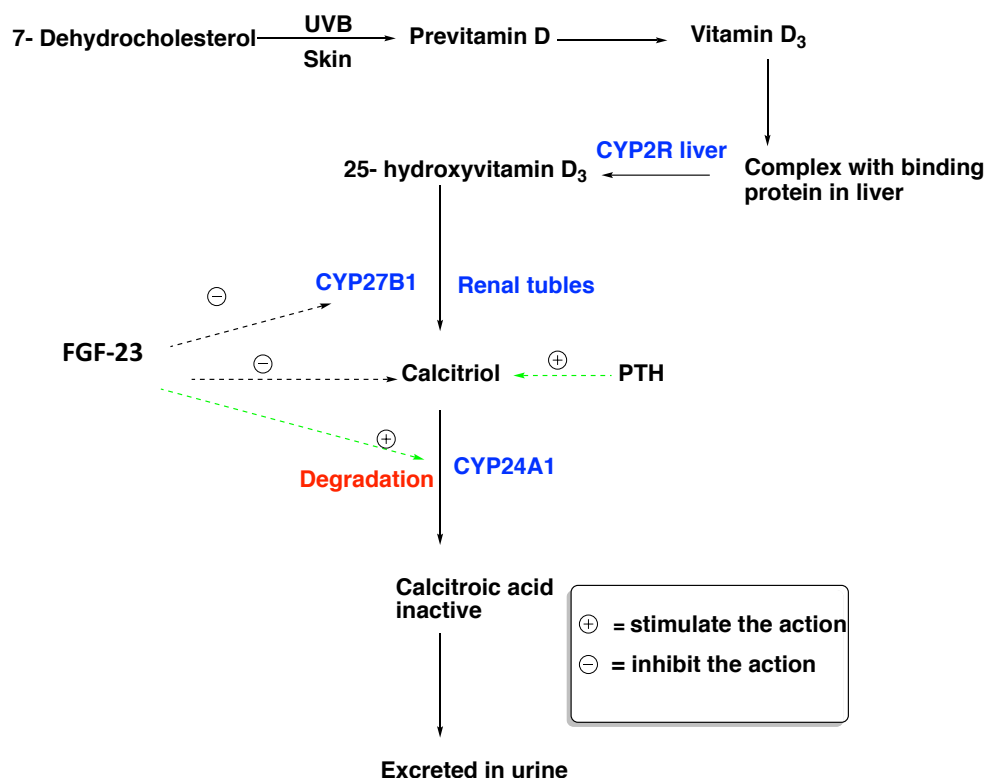
Scheme 2: Metabolic pathway for vitamin D with negative feedback loop

Importantly, defects in vitamin D metabolism include vitamin D deficiency, resistance, and vitamin D biosynthesis, which include mutations in CYP27B1 and CYP2R1[136] (Scheme 2). These disorders lead to rickets. There are two forms of vitamin D-dependent rickets, namely, type 1, also called pseudo-vitamin D deficiency rickets, and type 2 rickets, which is due to inactivating mutations in the vitamin D receptor. Failure in the positive and adverse regulation between CYP27B1 and CYP24A1 can result in tumours, and there are pathologic diseases, where CYP27B1 is elevated, such as in basal cell carcinoma or the decreased action of CYP27B1 on active metabolites resulting in colon tumour[137].

1.6 Vitamin D analogues

The active vitamin D metabolite, calcitriol, has shown cancer activities *in vitro* and *in vivo* in several cancer types. Hypercalcemia may be the dose-limiting factor for the application of calcitriol in the hospital; therefore, efforts have been made to develop analogues of calcitriol with antiproliferative and low calcaemic effects. Vitamin D analogues are chemically classified as secosteroids, which are steroids with one broken bond. In addition, both the synthetic analogues and the natural analogues of vitamin D are called vitamers:

1. Vitamin D_1 is a molecular complex of ergocalciferol (D_2) and lumisterol in a 1:1 ratio.

2. Ergocalciferol is a secosteroid and is the least expensive among the vitamin D analogues. As indicated in its name, 9,10 is the seco portion whereas ergosta shows the presence of 28 atoms in the carbon skeleton. The half-life is 19 hours, and the duration of action is up to 24 weeks[138].

3. Vitamin D_4 is an analogue known as 22-dihydroergocalciferol or 9,10-ergosta-5,7,22-trien-3-ol.

The primary role of calcitriol is to balance serum calcium and phosphorus concentrations. Therefore, designing calcitriol analogues with selective actions against certain diseases is a great challenge because newly designed compounds should be devoid of plasma calcium-increasing activity[139]. DeLuca[28] reported that C2 analogous of vitamin D produced a much more stable transcription complex compared with vitamin D analogues without C2 modifications[28]. In addition, analogues can be designed, for example, 2-methylene-19-nor-20*S*-1α,25-dihydroxyvitamin D_3 (2MD), which are very selective for their action on bone, with 2MD approximately 90 times more active than calcitriol in effecting bone calcium mobilisation[140]. Moreover, the main side effect when treating human osteoblasts with 2MD is the formation of bone nodules within two weeks[141, 142] (Figure 6). However, incubation of the same cells with high concentrations of calcitriol produced slight bone nodules or no change[28,143,144].
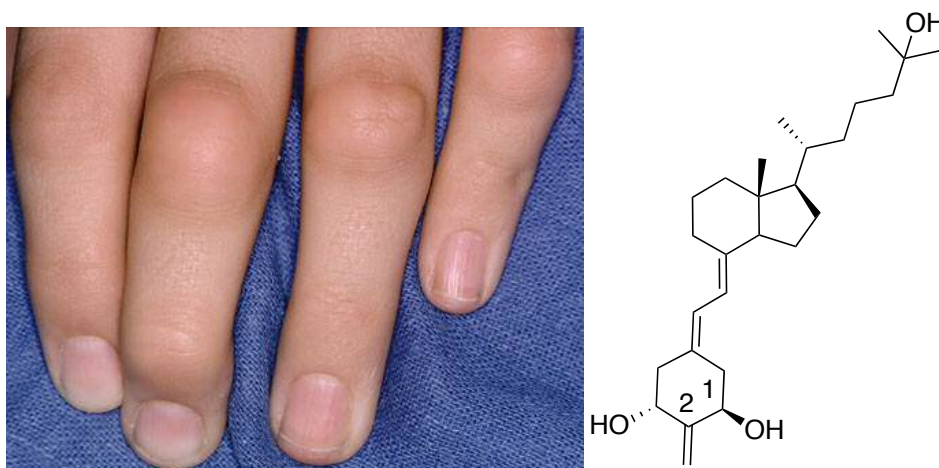
Figure 6: Bone nodules caused by 2MD[145]

Two other analogues modified at C2 (2MP and 2MbisP)[146] (Figure 7)) bind well to the VDR and are active in transcription, but, even when given orally to animals at high doses, are unable to increase serum calcium[28].

2MP   **2MbisP**
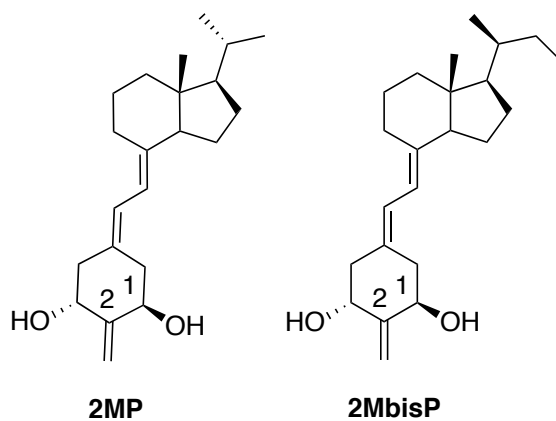
Figure 7 :Vitamin D analogues modified at C2

1.6.1   19-nor-1 α ,25(OH)$_2$D$_2$ (19-norD$_2$) (paricalcitol)
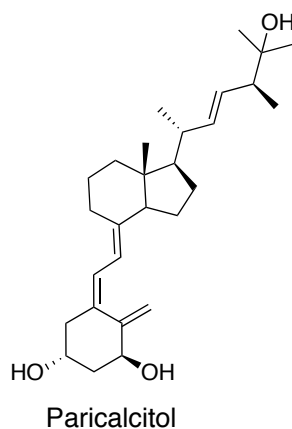
Paricalcitol

Figure 8: Chemical structure of paricalcitol

Paricalcitol differs from calcitriol in that it lacks the exocyclic carbon 19 and has a vitamin D_2 side chain instead of a vitamin D_3 side chain[147] (Figure 8). In normal and uremic rats, paricalcitol was approximately ten times less calcaemic and phosphatemic, but only three times less active in suppressing PTH. Intravenous paricalcitol was for use in dialysis patients in 1998 and for oral use in 2005 and is marketed by Abbott Laboratories under the brand name Zemplar[®]. Hyperparathyroidism is a very common complication of chronic renal failure[148]. For patients on haemodialysis intravenous calcitriol achieves active the suppression of elevated PTH levels[149]. Nevertheless, hypercalcaemia is a frequent complication that limits the calcitriol therapy. The newly approved synthetic vitamin D analogue paricalcitol appears to represent an efficient agent to control the secondary hyperparathyroidism associated with end-stage renal disease[150]. Calcitriol and paricalcitol have the same vitamin D binding protein affinity and circulating half-life. Also, paricalcitol is capable of reducing parathyroid gland weight while calcitriol is not able to reduce the parathyroid gland[151].

1.6.2 1 α (OH)D_2 (doxercalciferol)

Doxercalciferol is a prodrug and, like vitamin D_3, it must be activated *in vivo*. 1 α (OH)D_2 is reported to be less toxic than calcitriol[13]. Doxercalciferol has been tested directly in patients on dialysis; studies in experimental animal models of renal failure have been reported only recently[152]; oral doxercalciferol was approved for use in patients in the US in 1999 under the brand name Hectorol[®].

1.6.3 Calcipotriol

Calcipotriol has been recognised as a successful treatment strategy for psoriasis in numerous countries because it can be applied topically to the skin where it undergoes biotransformation, thus avoiding systemic circulation[153].
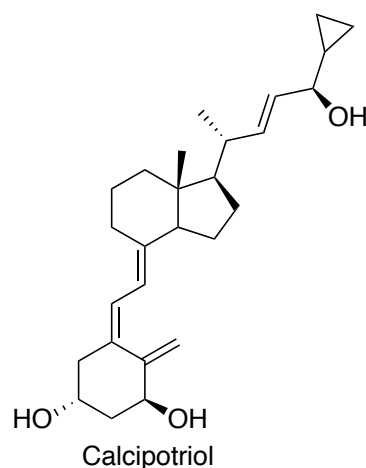
Figure 9: Chemical structure of calcipotriol

Calcipotriol is composed of a C22-C23 double bond, a C24 hydroxyl group (Figure 9), and a cyclopropane ring and has been employed in tumour trials[126]. This compound has been reported to have anti-proliferative and pro-differentiative properties towards human keratinocytes and prostate cancer cells[154].

1.6.4   OCT (maxacalcitol) [155]

OCT has an oxygen atom instead of carbon at the 22 position[126] (Figure 10); it is approved for the treatment of psoriasis and secondary hyperparathyroidism in Japan[156] and is now available in Japan under the brand name Ox (Chugai Pharmaceuticals) for patients who have CKD with secondary hyperparathyroidism (HPT)[157]. OCT was found to be substantially less hypercalcaemic than calcitriol[158,154].
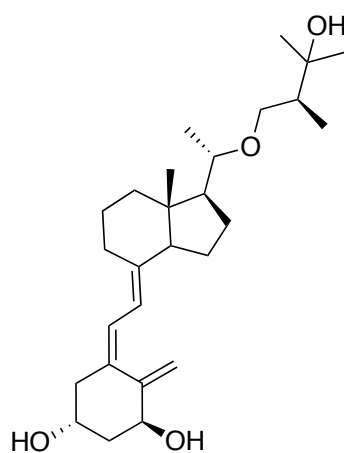
Figure 10: Chemical structure of OCT

1.6.5 ED-71 (eldecalcitol)

Eldecalcitol has been found to restore bone mass with minimal effect on serum calcium levels[126] (Figure 11). ED-71 has a higher affinity for vitamin D binding protein with a longer half-life in blood, which may contribute to its particular effect on bone[159,160].
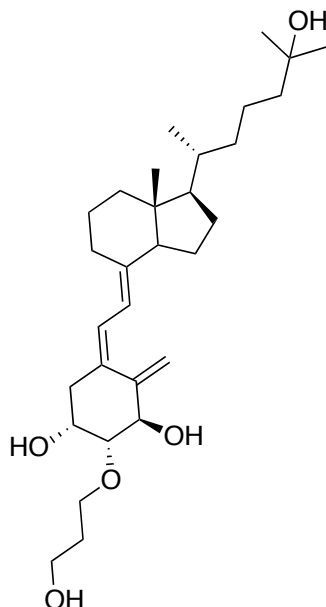
Figure 11: Chemical structure of eldecalcitol

1.6.6 Inecalcitol

Since calcitriol causes hypercalcaemia, the dose that can be given to patients is less than the amount ideally required for antitumour activity. Therefore, new analogues of vitamin D_3 that are potent but less calcaemic have been synthesised and tested. 19-nor-14-epi-23-yne-1α,25(OH)$_2$D$_3$ (inecalcitol) is a synthetic analogue of vitamin D_3 that has a 14-epi modification[107] (Figure 12).
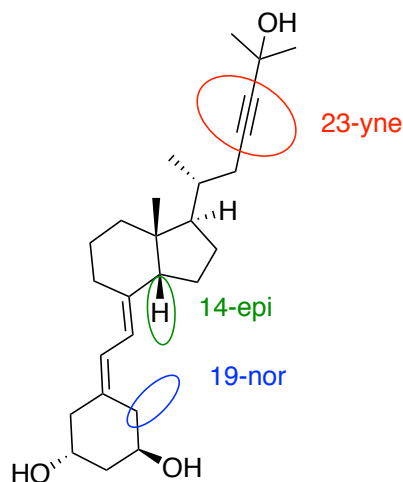
Figure 12: Chemical structure of inecalcitol

This reduction of hypercalcaemic effects might be due to the proprietary chemical structure of inecalcitol, a unique conformation of the carbon atom in position 14. Consequently, inecalcitol binds to the VDR but in a different conformation than calcitriol.

1.7   Cytochromes P450s

The cytochrome P450 monooxygenases are catalytic enzymes, and they have been found in all animals, plants, and microorganisms. Around 12 different types of reaction are related to cytochromes. They are present either in the endoplasmic reticulum or the mitochondria. Most of the cytochrome P450 enzymes have unknown functions, especially in microorganisms. Most human cytochromes belong to the CYP1, CYP2, and CYP3 families, and most of them are in the endoplasmic reticulum of the liver[137]. The cytochrome P450 enzymes are proteins that contain a haem (iron-protoporphyrin IX) prosthetic group that is the active centre for catalysis. Furthermore, the haem also interacts with the thiolate of the conserved cysteine residue that functions as the fifth ligand. Cytochrome P450 enzymes can be divided into four classes depending on how the electrons from Nicotinamide adenine dinucleotide phosphate (NADPH) are delivered to the catalytic site. Class I proteins require both an flavin adenine dinucleotide (FAD)-containing reductase and an iron-sulfur redox. Class II proteins need only a FAD/ flavin adenine mononucleotide (FMN) containing cytochrome P450 reductase to transfer electrons. Class III enzymes are self-sufficient and require no electron donor; however, cytochrome P450 enzymes from class IV receive electrons straight from NADPH. The structural conservation is established in the core of the protein around the haem and reveals a common mechanism of electron and proton transfer and oxygen activation. The conserved centre is formed by a four-helix (D, E, I and L) bundle, helices J and K, two sets of β sheets, and a coil called the 'meande[161]. Also conserved are the haem-binding loop, containing the most specific cytochrome P450 consensus sequence (Phe-X-X-Gly-X-Arg-X-Cys-X-Gly), placed on the proximal face of the haem just before the L helix and the conserved Glu-X-X-Arg motif in helix K. Moreover, the proximal side of haem is needed to stabilise the core structure[162]. Furthermore, the central part of the I helix, containing another consensus sequence considered as a cytochrome P450 signature (Ala/Gly-Gly-X-Asp/Glu-Thr-Thr/Ser), corresponds to the proton transfer channel on the distal side of the haem[163].

The haem group in cytochrome P450 enzymes includes four pyrrole rings linked by four methyl bridges, which form a tetrapyrrole ring. Pyrrole rings that have numbers IV and I relate to a methyl group, and pyrrole rings II and III each contain a vinyl and methyl group.

Cytochrome P450 enzymes are classified as per the rules set by a nomenclature committee. These rules depend on amino acid identity and phylogenetic criteria [163]. The cytochrome P450 enzymes are divided into families; for each family, the prefix CYP is linked with a capital letter and a number, for example, (CYP1A1, CYP4A2, CYP7B1, etc.) (Table 1).

Family	No of subfamily	genes	Function
CYP1	2	3	metabolism of foreign chemicals, arachidonic acid, eicosanoids
CYP2	13	16	metabolism of foreign chemicals, arachidonic acid, eicosanoids
CYP3	1	4	metabolism of foreign chemicals, arachidonic acid, eicosanoids
CYP4	5	12	metabolism of fatty acids, arachidonic acid, eicosanoids
CYP5	1	1	metabolism of thromboxane A_2 synthase
CYP7	2	2	cholesterol, bile acid synthesis
CYP8	2	2	prostacyclin synthase, bile-acid synthesis
CYP11	2	3	steroidogenesis
CYP17	1	1	steroid 17α-hydroxylase, 17/20-lyase
CYP19	1	1	aromatase to form oestrogen
CYP20	1	1	unknown
CYP21	1	1	steroid 21-hydroxylase
CYP24	1	1	vitamin D_3 24-hydroxylase
CYP26	3	3	retinoic acid hydroxylase
CYP27	3	3	bile acid biosynthesis, vitamin D_3 hydroxylations
CYP39	1	1	24-hydroxycholesterol-7 α -hydroxylase
CYP46	1	1	cholesterol 24-hydroxylase
CYP51	1	1	lanosterol 14 α -desmethylase

Table 1: Cytochrome P450 mammalian families[164]

1.7.1   Catalytic cycle of cytochrome P450 enzymes

Cytochrome P450 enzymes catalyse different types of reactions, such as dehalogenations, oxygenations, deaminations, dealkylations, dehydrogenations and isomerisations, and of these, the most vital reaction is oxygenation. The cytochrome

P450 enzymes are usually named as mixed-function oxidases or monooxygenases, as they insert one atom of O_2 into the substrate and one atom of O_2 into H_2O. When the system is uncoupled, the reducing equivalents and oxygen consumed deviate from the normal pathway of substrate hydroxylation, resulting in the formation of one or more of the side products of oxygen reduction (H_2O, H_2O_2 and O_2^-)[165]. The H_2O_2 and O_2^- can be converted into the highly toxic OH radicals in the presence of reduced transition metals, such as iron in cytochrome P450 enzymes[165,166]

The hydroxylation of the saturated R-H bond, the epoxidation of double bonds, the oxidation of heteroatoms, dealkylation reactions, and the oxidations of aromatics[167] occur when O_2 inserts one of its oxygen atoms into a substrate (S), and transforms the second oxygen atom into an H_2O molecule, utilising two electrons that are provided by NADPH via a reductase protein[168].

$$S + O_2 + 2e^- + 2H^+ \xrightarrow{\text{Cytochrome P450}} SO + H_2O$$
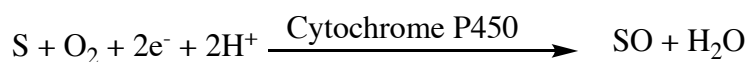
Cytochrome P450 enzymes have been categorised according to the electron-transfer proteins that deliver electrons from NADH or NADPH to the oxygenase protein[168]; this is classified as class I, which refers to mammalian mitochondrial enzymes involved in steroid synthesis and which transfer the electrons by Fe_2S_2[168].

Class II is placed in the endoplasmic reticulum of liver cells; the electrons are afforded by FAD and FMN, which contain reductases and which are involved in drug metabolism.

Estabrook *et al.*[169] observed a cyclic reaction for cytochrome P450 enzymes by oxygenation reactions. The reaction starts when the substrate binds to the active site of the cytochrome P450 enzyme to form a substrate ferric haem complex,[170]. NADPH-cytochrome P450 reductase, which holds two flavin prosthetic groups, can receive two electrons from NADPH and concurrently transfer one electron each to two different cytochrome P450 enzymes[171]. The first electron works on Fe in the cytochrome P450 enzyme, which is reduced to Fe^{II}, and O_2 binds to the cytochrome P450 complex. A second electron is provided to the cytochrome P450 enzymes from NADPH-cytochrome P450 reductase (the proportion of NADPH-cytochrome P450 reductase to cytochrome P450 enzymes in liver microsomal is around 19:1)[171] and leads to the generation of H_2O or H_2O_2 (Figure 13).

$$R + O_2 + NADPH + H^+ + 2e^- \longrightarrow RO + H_2O + NADP^+$$

Where:
R   = substrate
RO = product
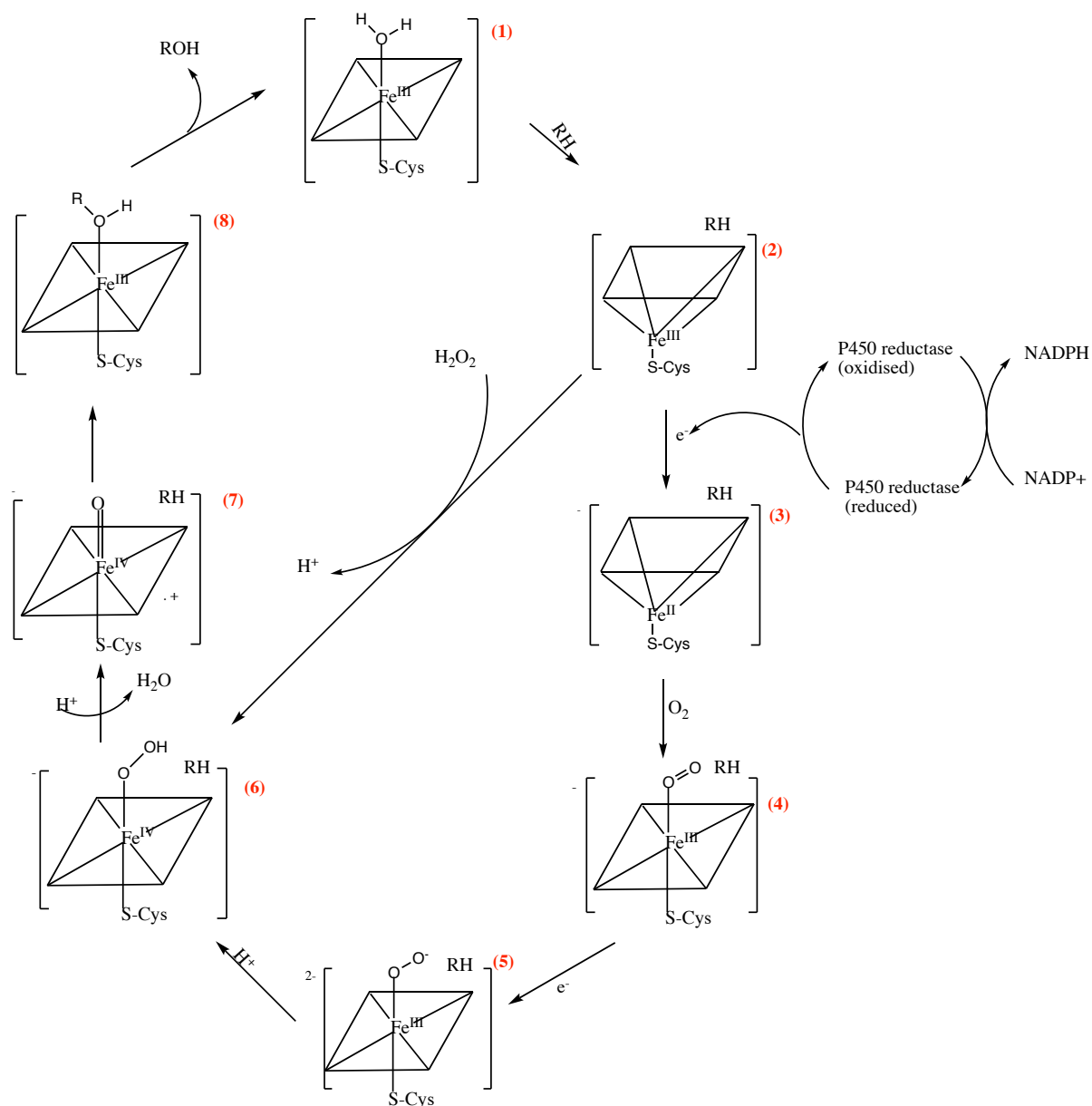
Figure 13: Catalytic cycle of cytochrome P450 enzymes. RH is substrate, and ROH is product.

Hrcay and O'Brien[172] illustrated the reductive activity of cytochrome P450 enzymes, whereby the haem protein decreases and detoxifies biological peroxides such as H_2O_2, lipid hydroperoxides, steroid hydroperoxides, and organic peroxides. The cytochrome P450 enzymes use H_2O_2 and other peroxy molecules as oxygen providers to catalyse the oxygenation of substrates. The cycle begins with cytochrome P450 haem $Fe^{III}(A)$,

and regenerates according to the following steps. In the first step, the substrate binds to low spin ferric cytochrome P450 enzymes and forms a high spin ferric cytochrome P450-substrate complex, which is reduced to Fe^{II} state (B), with the first electron provided by NADPH through redox protein partners. The reduction of ferric cytochrome P450 enzymes depends on the existence of the substrate and can be linked with substrate-induced changes in the spin state and the oxidation reduction potential. In the second step, ferrous haem iron binds O_2 to generate a stable nucleophilic ferrisuperoxo anion complex

$$(Fe^{III} \longrightarrow O^-_2)$$
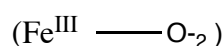
Next, in the third step, the move of a second electron produces a super nucleophilic dinegatively charged ferriperoxo intermediate(D) containing one (-) on the oxygen and a second (-) delocalised above the whole cysteine.
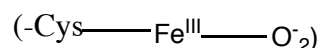
$$(^-Cys \longrightarrow Fe^{III} \longrightarrow O^-_2)$$

The above intermediate has sometimes been inaccurately described as an oxygen dianion complex
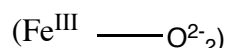
$$(Fe^{III} \longrightarrow O^{2-}_2)$$

In the fourth step, a proton is added to O_2 to generate a ferrihydroperoxo intermediate ($^-Cys–Fe^{III}–OOH$) (E) holding one (-) cysteine. In the fifth step, a second distal protonation produces a transient iron oxo–H_2O adduct ($Fe^{III}–OOH_2$), which directly dissociates by a heterolytic O–O bond and generates H_2O with a π radical Fe^{IV} oxo intermediate as ($Por^+ Fe^{IV}=O$) (F). In the sixth step, the $Por^+ Fe^{IV}=O$ oxotransfer entity moves O_2 to the substrate, creating a product (AO) and a renewed ferric cytochrome P450. In the fifth step, the formal oxidation state of the cytochrome P450 iron centre increases from Fe^{III} to Fe^V. The steps 2A and 3A are shown to be H_2O_2 producing pathways. Furthermore, ferric cytochrome P450 Fe^{III} is able to react with oxotransfer (RO) and XOOH to produce the $Por^. + Fe^{IV}=O$ (F) through the shunt pathway (step 7). The H_2O_2 produced in step 3A of the cytochrome P450 cycle can be changed to hydroxy with the availability of ferrous iron through the Fenton reaction (Figure 14).
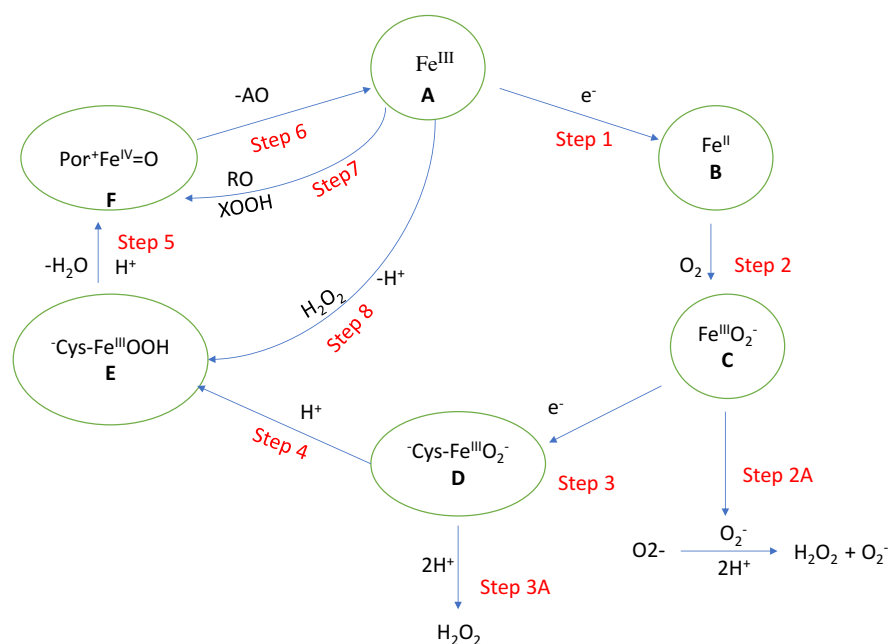
Figure 14: General cytochrome P450 catalytic cycle

1.7.2   General Function of cytochrome P450 enzymes

Cytochrome P450 enzymes help to metabolise large numbers of drugs by phase I metabolism, such as oxidation, reduction, hydroxylation, and demethylation, and so convert medicines into generally more water-soluble compounds that are easily eliminated. This metabolism is also called functionalisation metabolism. Cytochrome P450 enzymes are also responsible for thromboxane A_2, cholesterol, and steroid synthesis. Cytochrome P450 enzymes are distinguished from other proteins, such as collagen, insulin, and albumin, by their capacity to catalyse naturally important chemical reactions[173]. Cytochrome P450 enzymes are most commonly found in the liver, kidneys, small intestine, and lungs[174]. Cytochrome P450 enzymes work as cofactors and support the hydroxylation of carbon atoms of methyl groups, methylene carbons, and aromatic rings to hydrophilic metabolites. The human cytochrome P450 superfamily includes 57 genes. These genes code for enzymes that can have a function in the metabolism of medicines and biochemical compounds. Currently, there are more than 270 different cytochrome gene families, in which 18 are noted in mammals[161]. In addition, cytochrome P450 molecules have a role in antibiotic synthesis from fungi, that is, herbicide resistance in plants, as well as in multiple biosynthetic and metabolic pathways in bacterial species[175]. For example, the biotechnological purposes of the cytochrome P450 enzymes include the bioremediation of herbicide-contaminated soils, such as the catalysis of various chemical reactions, which are costly when achieved by

laboratory procedures. Furthermore, the synthesis of prostaglandins and polyethylene can be generated only by the cytochrome P450 molecule. The cytochrome P450 molecule also has many medical applications, such as the production of the anticancer drug, synthetic progesterone; hydrocortisone; vitamin D precursors; and antibiotics. In addition, human cytochrome P450 enzyme deficiency leads to monogenic disorders related to steroid hormones, cholesterol, eicosanoids, and vitamin D_3. As a result, the main function of cytochrome P450 molecules can be summarised as follows:

1. Detoxification - many substrates are lipid-soluble and affect the metabolism of foreign chemicals.
2. Metabolism of arachidonic acid, and eicosanoids.
3. Metabolism of fatty acids and eicosanoids, which are essential in eukaryotic sterol biosynthesis.
4. Production of steroid hormones, vitamins A and vitamin D.

1.7.2.1 Metabolism of foreign chemicals

Foreign chemicals include medicines, secondary metabolites from plants or fungi consumed with food, and pollutants, for example, polycyclic aromatic hydrocarbons, arylamines, the ingredients of industrial mixtures, pesticides, and cigarettes. Human cytochromes like P450 enzymes, which metabolise xenobiotics, are found especially in CYP1, CYP2, CYP3, and CYP4 [164]. Class I and class II cytochrome P450 enzymes from all organisms contribute to the detoxification or, occasionally, the activation of xenobiotics. Besides, class II cytochrome P450 enzymes are the most common in eukaryotes. Type II cytochrome P450 enzymes from plants are involved in the biosynthesis or catabolism of a range of hormones[176]. Furthermore, cytochrome P450 enzymes are the major site of drug metabolism, mainly hydroxylation reactions in the presence of particular electron transport systems and molecular oxygen[177]. Therefore, the cytochrome P450 enzymes play an important role in maintaining the therapeutic level of a drug in the body[174]. However, most side effects of medicines are related to the cytochrome P450 enzymes. The side effects can result in more than one effect, such as drug-drug interactions. Furthermore, the drug-induced toxicity can also result from reactive oxygen species generated during drug metabolism, due to the uncoupling of oxygen utilisation and drug hydroxylation, which is a problem with many drugs[165].

1.7.2.2   Metabolism of arachidonic acid, and eicosanoids

Cytochrome P450 enzymes undoubtedly have twin purposes; these can be seen in the cytochrome P450 enzymes, which metabolise arachidonic acid, which is changed into more than 100 eicosanoid metabolites[178]. The metabolism of arachidonic acid appears in different tissues, such as the liver, the kidneys, and the heart[179]. The cytochrome P450 enzymes work on arachidonic acid metabolism in two definite ways: first, by the ω-hydroxylase, and second, by epoxygenase pathways[180]. Prostaglandins and leukotrienes, which are products of arachidonic acid metabolism, are potent mediators of inflammation. In addition, the prostaglandins D2, F2, and E2 have several functions including vasoconstriction, bronchial dilation/constriction, smooth muscle contraction, allergic response, inhibition of platelet aggregation, and pain response. Furthermore, CYP5A1 (the thromboxane A2 synthase) and CYP8A1 (prostacyclin synthase) have opposite functions in blood clotting. Thromboxane A2, the product of the CYP5A1 enzyme, reduces cyclic AMP levels in platelets and so stimulates their aggregation[181]. However, CYP8A1 raises intracellular cyclic AMP concentrations and inhibits platelet aggregation. Mutations in the CYP5A1 or CYP8A1 genes are thus predicted to lead to clotting and inflammatory disorders, including coronary artery disease and pulmonary hypertension[182].

1.7.2.3   Cholesterol metabolism, bile acid biosynthesis and steroid metabolism

Cytochrome P450 enzymes have a function for changing acetate into sterols and bile acids[181]. CYP51A1 is essential for synthesising cholesterol[183]. In addition, the synthesis of bile acids from cholesterol was found in the main catabolic pathway for the clearance of cholesterol in mammals[184]. Furthermore, sexual differentiation of the genital ridge in early embryogenesis is mainly regulated by P450 enzymes involved in steroid hormone synthesis, i.e. CYP11A1, CYP11B1, and CYP11B2 [182]. Cortisol, testosterone, and oestrogen are synthesised by CYP17A1; however, CYP19A1 changes androgen into oestrogens. The hydroxylation of steroid precursors at C21 is an important point in the production of glucocorticoids and mineralocorticoids, which are catalysed by CYP21A2. Any mutations that occur, which interrupt 21-hydroxylation, cause more than 90% of congenital adrenal hyperplasia, which can be caused by mutations in CYP11A1, CYP11B1, CYP11B2, CYP17A1 or CYP19A1 (Figure 15).
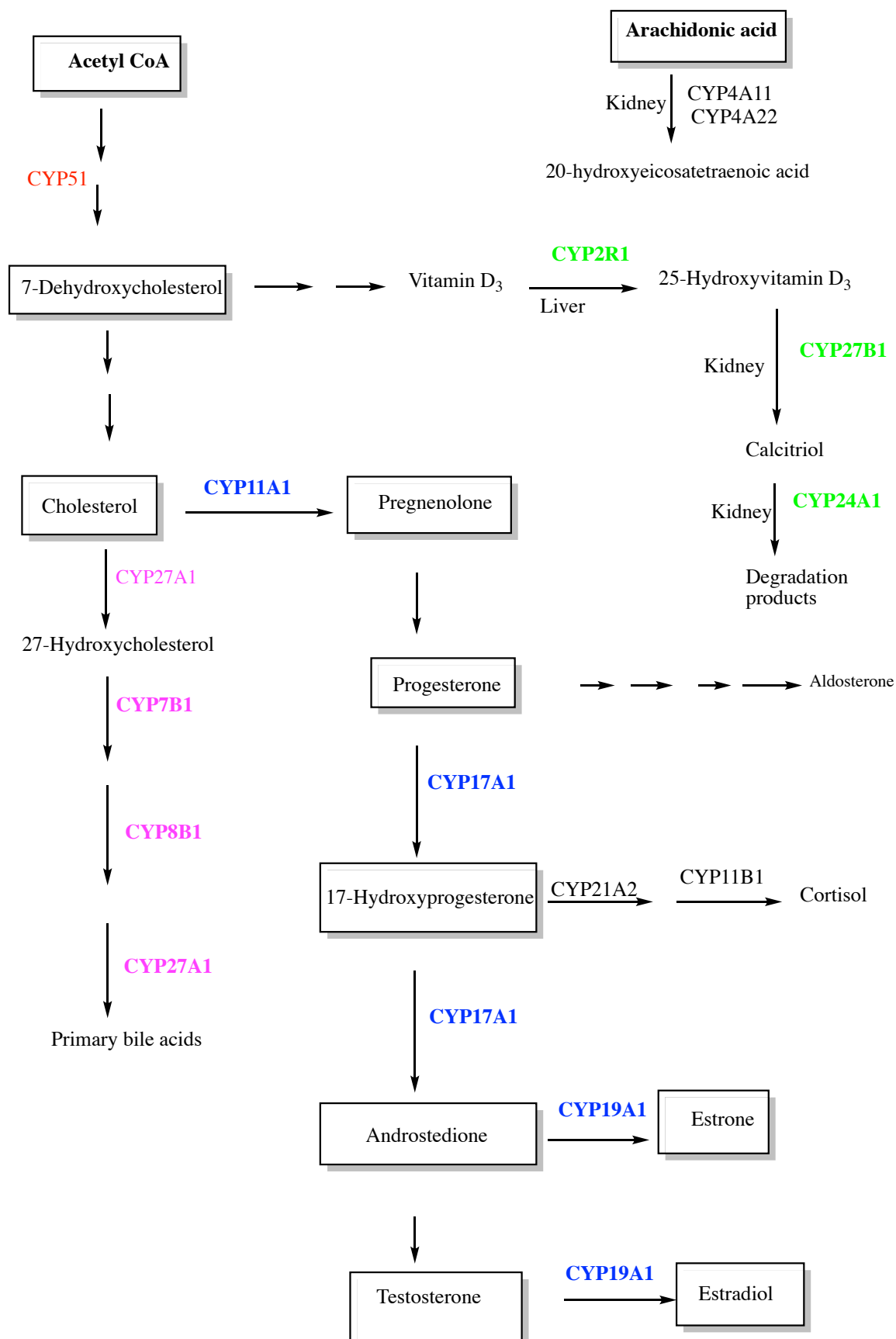
Figure 15: Pathways and cytochrome P450 enzymes involved in the biosynthesis and metabolism of different sterols

1.7.2.4 Retinoic acid hydroxylation

Retinoic acid (RA), the active form of vitamin A, is vital during vertebrate development; it operates through many retinoic acid receptors and retinoid X receptors and plays an important role in development, differentiation, and homeostasis inside the human body. Retnoic acid is metabolised primarily by CYP26A1, however CYP26B1 and CYP26C1 also have roles in the metabolic pathways of all-*trans*-RA and 9- and 13-cis-RA.

1.7.2.5 Vitamin biosynthesis

Vitamin D is previously described in detail in this Chapter.

1.7.3 25-hydroxyvitamin D_3-24-hydroxylase (CYP24A1)

CYP24A1 was recognised as the main enzyme responsible for calcitriol catabolism; CYP24A1 works in balance with CYP27B1, which is responsible for changing 25-hydroxyvitamin D_3 to calcitriol in the kidney[185] (Scheme 2). CYP24A1 was first described in the early 1970s[186], and the enzyme activity is the result of a combination of three constituents: ferredoxin, ferredoxin reductase, and CYP24A1[187]. CYP24A1 catalyses the conversion of calcitriol into 24-hydroxylated products, which are metabolised further to produce calcitroic acid, identified as a biliary catabolite[188]. Most species of CYP24A1 have Ala326, resulting in 24-hydroxylation to calcitroic acid while embryonic organisms have Gly326, resulting in mainly 23-hydroxylation to give a 23,26-lactone product[189,190]. Annalora *et al.*[190] elucidated the crystal structure of rat CYP24A1, which revealed a canonical cytochrome P450 structure of helices and β-sheets surrounding a prosthetic haem group and a substrate binding cavity (Figure 16).
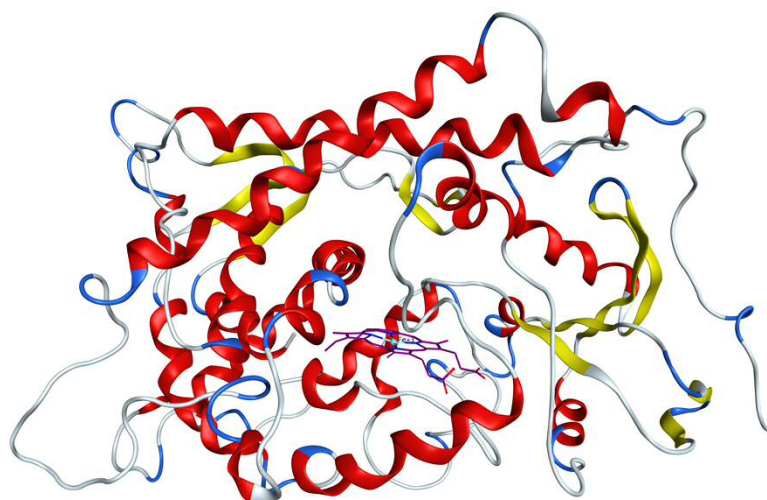
Figure 16: CYP24A1 model[191]

The CYP24A1 gene is found at position 13 on chromosome 20 long arms (q). The interaction of calcitriol with the VDR, followed by the binding of the calcitriol-VDR complex to retinoid-X-receptor regulates the CYP24A1 enzyme[91]. The selective inhibition of the CYP24A1 enzyme decreases the catabolism rate and prolongs the serum calcitriol half-life. This increases the endogenous levels of calcitriol and enhances the cells exposure to calcitriol. More efficacy and inhibition potency could be achieved with ligands designed to target the CYP24A1 binding pocket[191]. Thus, the development of CYP24A1 enzyme inhibitors based upon the calcitriol structure is a feasible option[191].

Calcitriol is transformed first into 1α,23*S*,25-$(OH)_3$D and then into 1α,23*S*,25,26-$(OH)_4$D by successive hydroxylations at carbon 23 and carbon 26[192]. Then, it is transformed into 1,25-$(OH)_2$D-26,23-lactol, which is subsequently metabolised to the final product 1α,25-$(OH)_2$D-26,23-lactone, which is then eliminated by the kidney[193,194]. The same steps apply to 25-(OH)D, which is first transformed into 23,25-$(OH)_2$D, then 23,25,26-$(OH)_3$, and is then converted into 25-(OH)D-26,23-lactol and finally, 25-(OH)D-26,23-lactone[193]. The pharmacological effect of the C23- pathway metabolites remains slightly doubtful, but it is assumed that the lactone product could work as a VDR antagonist[126]. The second hydroxylation pathway for calcitriol by CYP24A1 at C24, includes five individual enzymatic steps and finally produces the metabolite calcitroic acid. Calcitriol is first hydroxylated at carbon 24 to produce 1,24,25-$(OH)_3$D; that is then converted to 24-oxo-1α,25-$(OH)_2$D. The next step is the hydroxylation of carbon 23 providing 24-oxo-1α,23,25-$(OH)_3$D. The oxidative cleavage of the bond between C23 and C24 leads to the generation of 24,25,26,27-tetranor-1α,23-$(OH)_2$D; this is converted to calcitroic acid, which is eliminated in the bile[126,194] (Scheme 3).
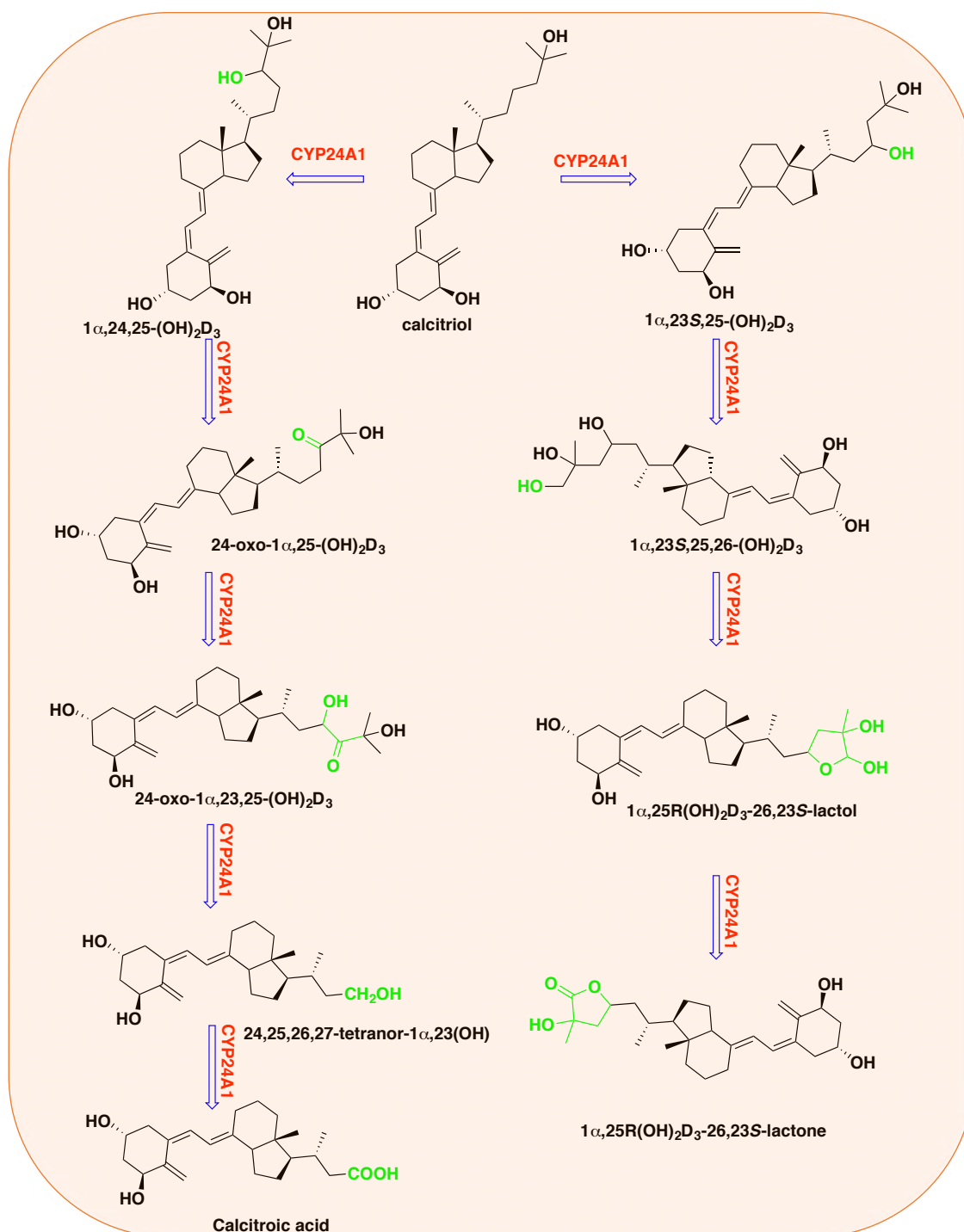
Scheme 3: Catabolism pathway of calcitriol

1.7.4 CYP27B1

CYP27B1 is a gene located on chromosome 12 that encodes 25-hydroxyvitamin D_3 1 α -hydroxylase, a vitamin D-activating enzyme that plays an essential role in vitamin D metabolism in humans. CYP27B1 has 508 amino acids with a molecular mass of around 55 kDa[195].

Entry of 25-(OH)D into the proximal renal tubular cells requires receptor-mediated uptake by a vitamin D binding protein (DBP), degradation of DBP by legumain, and endocytic internalisation and translocation of 25-(OH)D to mitochondria [196]. Megalin, a member of the low density lipoprotein receptor family, is essential for the reabsorption of filtered DBP-bound 25 vitamin D[197]. Several considerations are related to the tight regulation of CYP27B1 enzyme expression and activity in the kidney. These include calcium, PTH, calcitonin, growth hormone (GH), insulin-like growth factor-1 (IGF-I), and fibroblast[198]. CYP27B1 activity is regulated by PTH and calcitriol, and the expression of CYP27B1 mRNA is regulated by intracellular Cyclic adenosine monophosphate (cAMP)[199]. A homology model of human CYP27B1 based on the crystal structure of rabbit CYP2C5 as a template[200] has been reported, and the sequence identity between CYP2C5 and CYP27B1 is 23.5 %[200].

1.7.5   CYP24A1 inhibitors

Selective inhibitors of CYP24A1 might be useful to enhance the anticancer activities of calcitriol, and they have the potential to be used clinically for cancer treatment. In addition, there is also a link between increased CYP24A1 levels in diseased states such as cancer, which suggests that CYP24A1 may be a useful therapeutic target[152]. However, while the inactivation of CYP24A1 leads to hypercalcaemia, many cancer cell lines display elevated levels of CYP24A1 expression as they progress to more tumourigenic phenotypes, suggesting that these tumours have an increased ability to catabolise calcitriol. Subsequently, several CYP24A1 inhibitors have been designed for the treatment of diseases associated with elevated vitamin D catabolism. However, the challenge in the design of CYP24A1 inhibitors is designing CYP24A1 inhibitors selective over CYP27B1. CYP24A1 inhibitors could be classified into two main categories: azole and non-azole inhibitors

1.7.5.1   Vitamin D derivatives as CYP24A1 inhibitor

Chiellini *et al.*[201] designed two 19-nor-1-OH-vitamin D type analogues containing the azole VIMI or CPA1 (cyclopropylamine) in the side chain[201] (Figure 17). Both VIMI and CPA1 are potent competitive inhibitors of CYP24A1. However, VIMI showed a 4.3-fold moderate selectivity for the inhibition of CYP24A1 over CYP27B1 whereas CPA1 showed 80 times more selectivity in inhibiting CYP24A1 over CYP27B1[201].
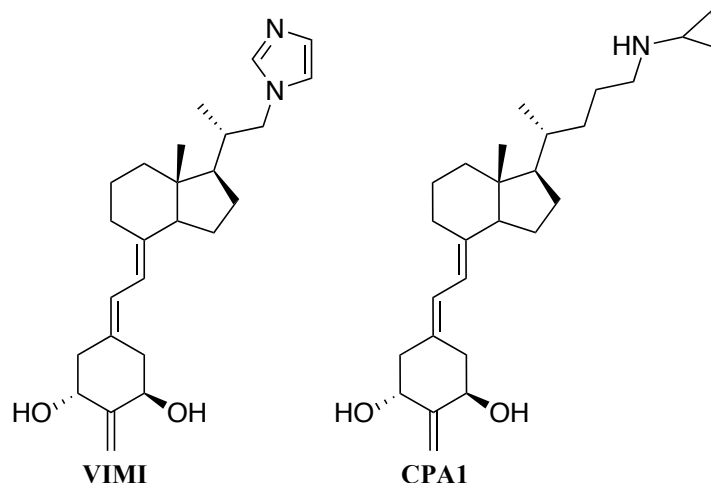
VIMI   **CPA1**
Figure 17: Vitamin D derivatives as CYP24A1 inhibitor

Posner *et al.*[202,203] reported sulfone and sulfoxime derivatives of calcitriol, CTA018 and CTA091, respectively (Figure 18). CTA091 is classified as a pure CYP24A1 inhibitor with low calcaemic activity and an IC_{50} of 6.5 $\pm$ 0.2 nM, which is 40-fold more potent than ketoconazole[202]. Studies with lung cancer cells have shown that CTA091 increases the stability of calcitriol by slowing its catabolism and enhancing the half-life of calcitriol. The antiproliferative effects of calcitriol were improved about 45-fold when it was co-administered with CTA091 *in vitro*, indicating that they can work synergistically[106]. Unlike CTA091, the sulfone analogue, CTA018, is a mixed CYP24A1 inhibitor/VDR agonist, as it binds to the VDR, although with a 15-fold lower affinity than that of calcitriol.[204] CTA018 is also a low calcaemic inhibitor of CYP24A1 and is ten times more potent than ketoconazole. When administered to rats with induced CKD, both CTA091 and CTA018 suppressed parathyroid hormone levels and increased serum calcitriol[202]. Thus, CTA018 is a selective drug candidate to treat CKD and hyperphosphatemia[205] .
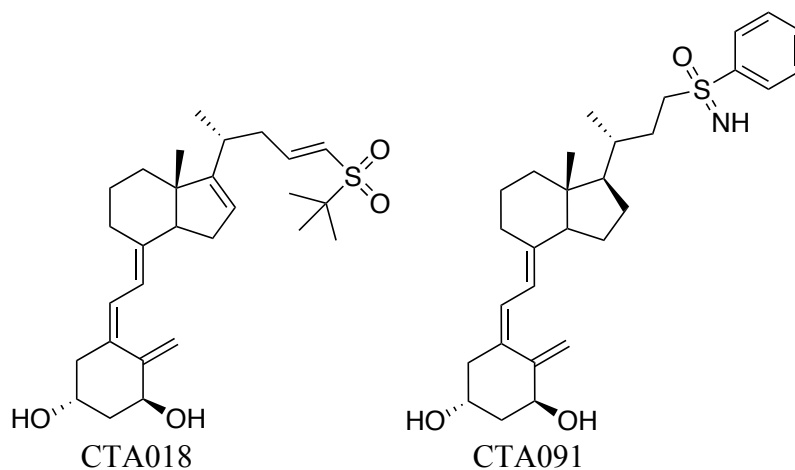
CTA018   **CTA091**
Figure 18: Sulfone and sulfoxime derivatives

1.7.5.2 Cyclopropylamine derivativas

Hanzlik *et al.*[206] reported cyclopropylamine derivatives can be used as CYP24A1 inhibitors. *N*-benzyl-*N*-cyclopropylamine (Figure 19) is a suicide substrate for cytochrome P450 enzymes; in addition, a 1′ -methyl-substituted analogue of 1,*N*-(1′ - methylcyclopropyl)amine lacking the hydrogen atom at the position of cyclopropyl group was also capable of inactivating CYP24A1[207].
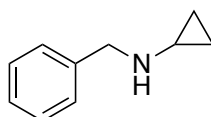
Figure 19: *N*-benzyl-*N*-cyclopropylamine

1.7.5.3 Azole derivatives as CYP24A1 inhibitor

Azole-based compounds can inactivate a broad range of cytochrome P450 enzymes by binding to the haem moiety present in the enzyme active site. Azole compounds have a nitrogen heterocyclic ring, frequently an imidazole or triazole, and it is through a nitrogen of the heterocyclic ring that binding occurs with the haem iron. Ketoconazole and liarozole were shown to extend the half-life of calcitriol in prostate cancer cells *in vitro* and *in vivo*[208,202]. Nevertheless, azole compounds have the possibility to cause significant systemic side effects due to the poor selectivity among cytochrome P450 enzymes. Thus, the development of novel CYP24A1 inhibitors with good selectivity and low toxicity are necessary[209]. Ketoconazole is an azole compound with CYP24A1 inhibitory activity and is a nonselective inhibitor for CYP24A1 and CYP27B1[210,211]. Schuster *et al.*[212] described the azole compounds (Table 2); which inhibit CYP24A1 and CYP27B1. Chiellini *et al.*[201] reviewed the non selective cytochrome inhibitor ketoconazole, which has been shown to inhibit CYP24A1 and act synergistically with vitamin D analogues in cell cultures. In addition, Peehl *et al.*[213] reported that the combination of 0.1 μg/mL ketoconazole potentiated antitumor activity of calcitriol 50-fold and EB 1089 (vitamin D analogue) 10-fold. Ly *et al.*[214] showed that liarazole has also been shown to inhibit CYP24A1 and act synergistically with calcitriol in the treatment of prostate cancer. The development of azole type inhibitors of CYP24A1 was started in Novartis in the early 1990s[201]. Around 400 different azole inhibitors have been evaluated, using primary human keratinocytes as a model system. R-(-)VID400 displayed potent selective CYP24A1 inhibitor activity, and so it was chosen for development in the indication of psoriasis[215,216]. Aboraia *et al.*[210] illustrated how *N*-(2-

(1*H*-imidazol-1-yl)-2-phenylethyl)arylamides were evaluated for their inhibitory activity against human CYP24A1 and IC_{50} ranging from 0.3 to 0.72 μM compared with the standard ketoconazole 0.3 μM (Figure 20).
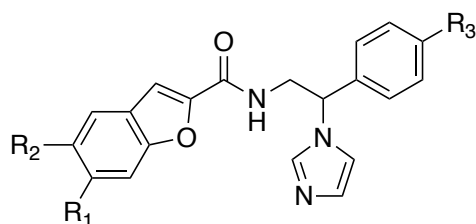
Where R:
R₁ = H, NO₂
R₂ = H, OCH₃
R₃ = H, F, Cl

Figure 20: *N*-(2-(1*H*-imidazol-1-yl)-2-phenylethyl)arylamides
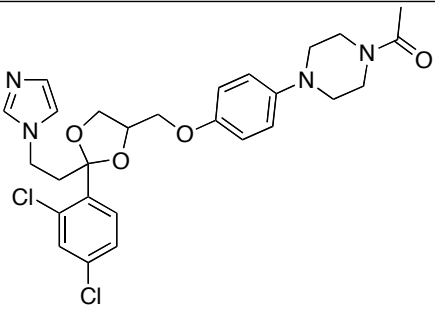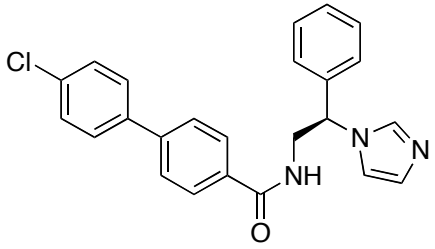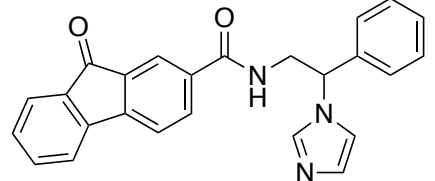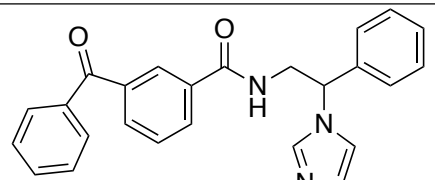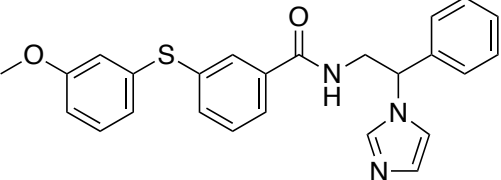
Compound	Chemical structure	IC$_{50}$ (nM)	
		CYP27B1	CYP24A1
Ketoconazole		28.3	126.0
R-(-)VID400		616.1	15.2
SDZ-286907 (R)		1696.9	34.9
SDZ-287871 (R)		1271.6	29.9
VAB636 (R)		266.1	5.08

Table 2: Example of azole non selective and selective inhibitors of CYP24A1[215]

1.7.5.3.1 Styryl azole derivatives as CYP24A1 inhibitor

Aboraia *et al.*[210] found that the styryl nucleus plays an important role in improving CYP24A1 inhibitor activity[191]. Ferla *et al.*[211] synthesised the styryl indole imidazole derivatives and styryl indole sulphonyl derivatives (Table 3). The imidazole styryl indole derivatives were found to be potent inhibitors of CYP24A1 with IC$_{50}$ ranging between 0.19 and 0.52 μM, which is more active than the standard ketoconazole (Figure 20). In addition, the sulfonate and sulfonamides displayed only weak CYP24A1

inhibitory activity, thus indicating the importance of the imidazole azole group in interacting with the active site haem moiety. In general, styryl indole imidazole derivatives and styryl indole sulphonyl derivatives displayed a small selectivity for CYP24A1 over CYP27B1, which was comparable with that of ketoconazole (Figure 21).

Chemical structure	Chemical structure
Where R: **1** = R = H **2** = R = OCH₃	Where R: **3** = R = H **4** = R = OCH₃
5	**6**
Where R: **7** = R = H **8** = R = OCH₃	Where R: **9** = R = H **10** = R = OCH₃
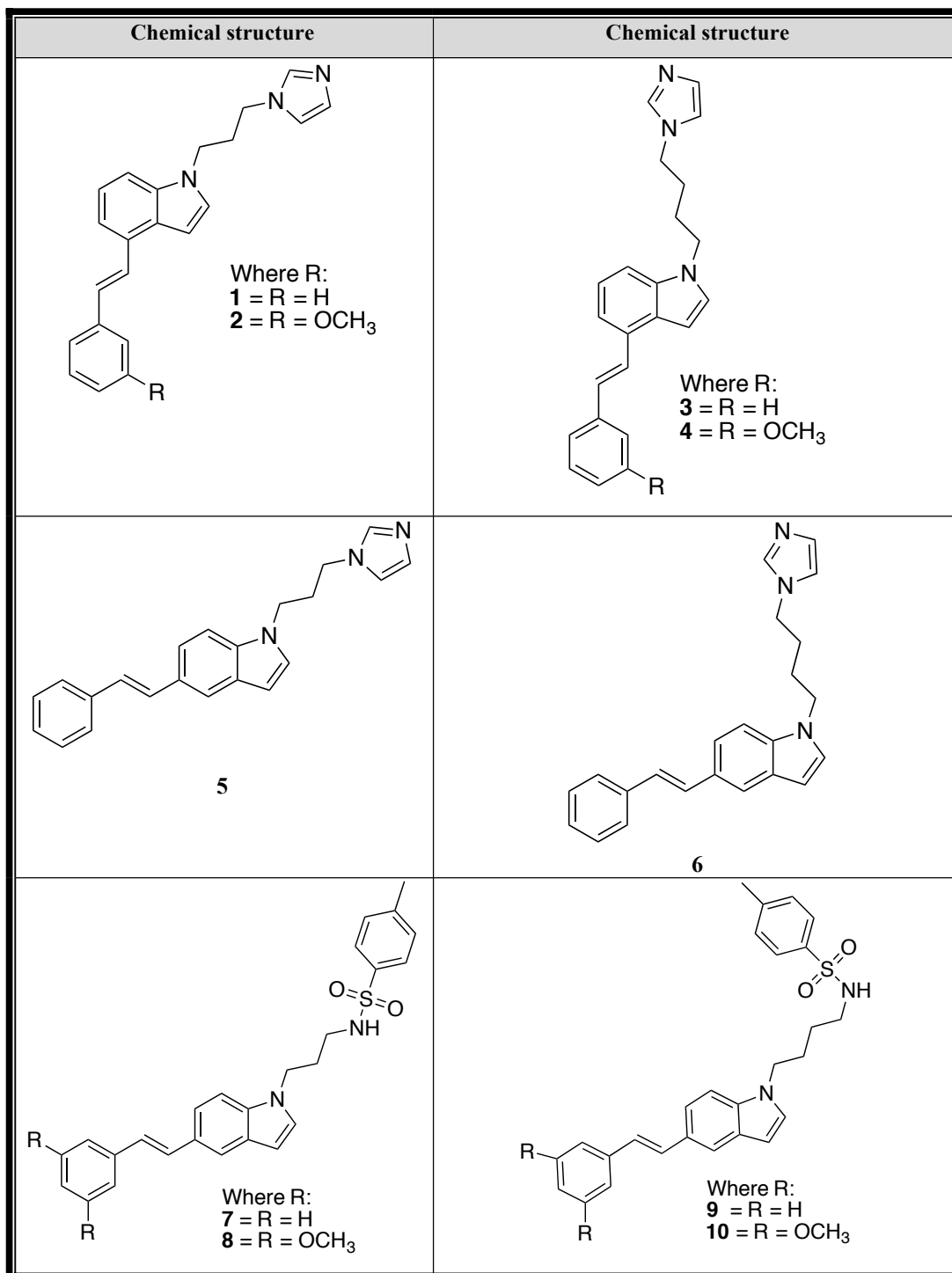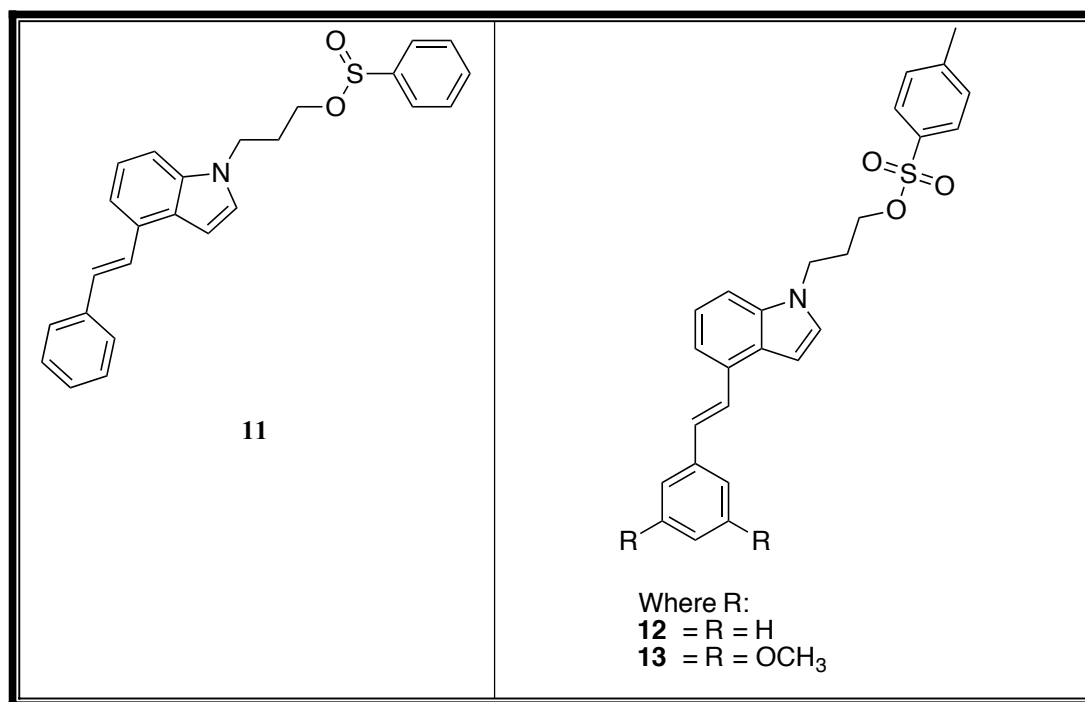
Table 3: styryl indole imidazole derivatives and styryl indole sulphonyl derivatives
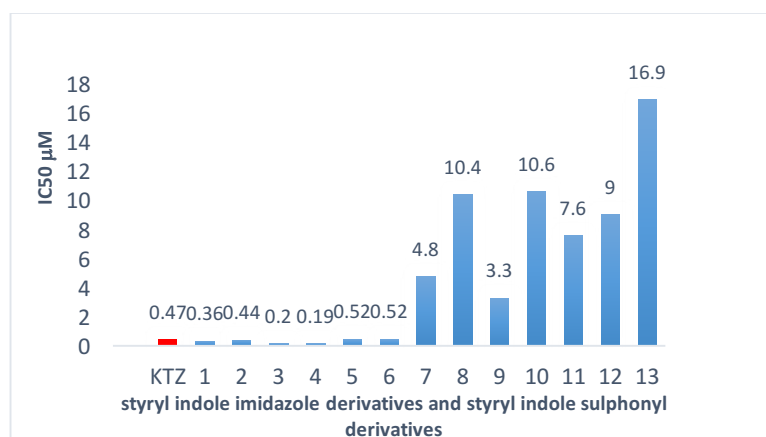
Figure 21: IC50 data for styryl indole imidazole derivatives and styryl indole sulphonyl derivative against CYP24A1

Ferla et al.[191] demonstrated that styryl derivatives had stronger inhibitory activity, (Figure 22) with an IC_{50} value of 0.11 µM, than ketoconazole (IC_{50} = 0.47 µM) against human CYP24A1 (Table 4). A structure-activity relationship study that investigated the reduction of the styrene double bond resulted in a reduced level of inhibitory (IC_{50} = 0.51 µM), and changing the double bond for a sulfonamide group resulted in a more remarkable decrease in activity (IC_{50} = 1.3 µM).
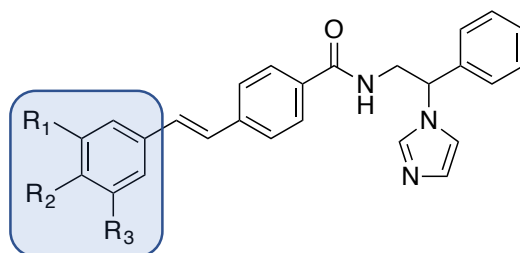
Where R:
a = R_1 = H, R_2 = H, R_3 = H
b = R_1 = H, R_2 = F, R_3 = H
c = R_1 = H, R_2 = OCH_3, R_3 = H
d = R_1 = OCH_3, R_2 = H, R_3 = OCH_3
e = R_1 = OCH_3, R_2 = OCH_3, R_3 = OCH_3

Figure 22: Styryl imidazole derivatives

Cpd	IC50 (μM)	
	CYP24A1	**CYP27B1**
a	0.40	0.50
b	0.26	0.60
c	0.34	0.24
d	0.11	0.16
e	0.14	0.33

Table 4: IC$_{50}$ data for CYP24A1 and CY27B1

1.7.5.4 Tetralone derivative as CYP24A1 inhibitor

Non-azole compounds without the nitrogen heterocycle bind within the active site including hydrogen bonding and hydrophobic interactions. Nevertheless, the strength of these interactions is mostly less than that observed with azole compounds resulting in less potent inhibitors. The tetralone derivatives enhance the antiproliferative action of calcitriol. The ability of tetralones to inhibit the CYP24A1 enzyme is less than that of their azole. However, tetralone derivatives have more selectivity through their binding to the active site; the enzyme inhibitory effect of tetralone derivatives is mediated through hydrogen bonds and hydrophobic interactions with the active site of the enzyme. Yee and Simons[217] reported that benzylidenetetralone derivatives were found to be very weak inhibitors (IC$_{50}$ 20 to >100 μM), whereas the 2-benzyltetralone derivatives showed promising inhibitory activity (IC$_{50}$ 0.9 μM for the most active derivative) compared with ketoconazole (IC$_{50}$ 20 μM). Also, Aboraia *et al.*[218] demonstrated that tetralone derivatives displayed potent inhibitory activity compared with ketoconazole (Figure 23).
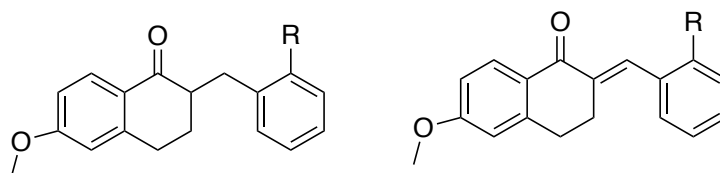
R = alkyl, aryl, bromide

Figure 23: Tetralone derivative

Yee *et al.*[219] illustrated that 2-(4-hydroxybenzyl)-6-methoxy- 3,4-dihydro-2*H*-naphthalen-1-one (Figure 24) was found to be a potent inhibitor (IC$_{50}$ 3.5 µM); indeed, it was shown to be a more potent inhibitor than standard ketoconazole.
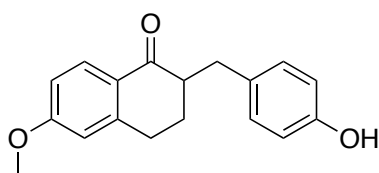
Figure 24: 2-(4-hydroxybenzyl)-6-methoxy- 3,4-dihydro-2*H*-naphthalen-1-one

1.8   Aims and Objectives

Therapy using calcitriol is limited owing to the short duration of action; $25OHD_3$ has a life of two weeks, and the half-life of calcitriol has been measured in hours[220], due to CYP24A1, which metabolises calcitriol to inactive products. The aim of this research is to design and synthesise novel inhibitors of CYP24A1 to enhance the endogenous levels of circulating calcitriol. In addition, it is important to develop compounds that are selective for CYP24A1 over CYP27B1 so that the generation of calcitriol itself is not blocked (Figure 25).
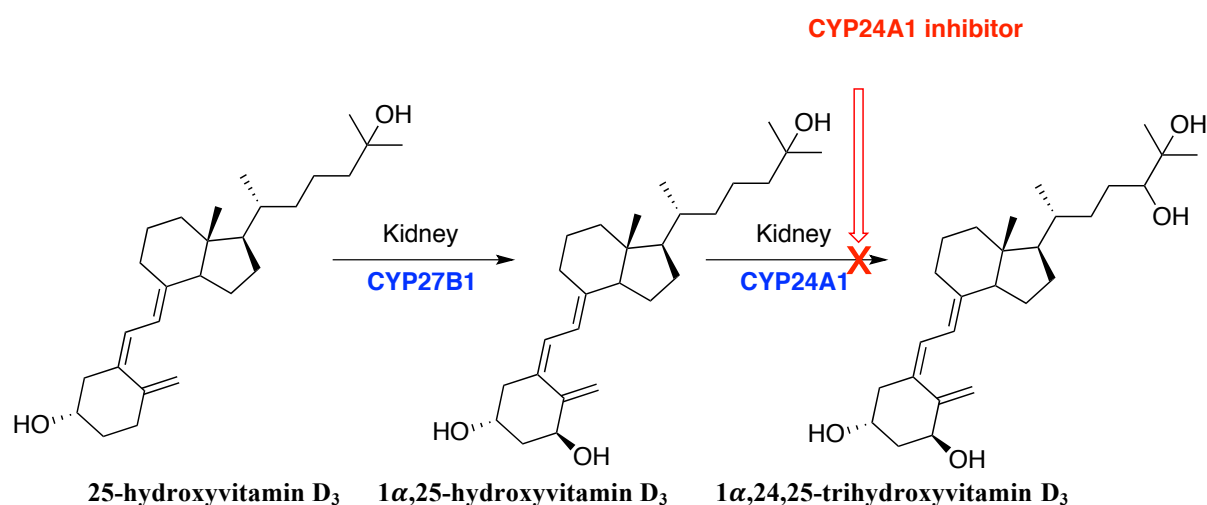
Figure 25: Site of CYP24A1 inhibitor action

Although potent CYP24A1 inhibitors have been described, selectivity versus CY27B1 has proved more challenging. In order to understand the requirements of inhibitor binding to the enzyme-active site, it would be useful to have a 3D structure of both human CYP24A1 and CYP27B1. However, to date, no human crystal structures are available for either of these enzymes. Therefore, a homology model for CYP24A1 has been developed and published[191]. In this project, a homology model of CYP27B1 will be developed, validated, optimised, and subsequently analysed for both CYP24A1 and CYP27B1 enzyme active sites. Identification of the differences in both substrate binding and active site architecture will be used to assist in the design of selective inhibitors.

Previously, screening of the SPECS database[221] has identified some promising CYP24A1 inhibitors with moderate inhibitory activity[222] (Figure 26). Two of these compounds (Lead 2 and 3) will be taken as lead compounds for further development. In addition, Ferla *et al.*[191] investigated how the imidazole styrylbenzamide derivatives

(lead 3) furnished optimal activity (Figure 23).

Lead 1 IC$_{50}$ = 4.2 µM   **Lead 2 IC$_{50}$ = 5.5 µM**   **Lead 3 IC$_{50}$ = 0.4 µM**
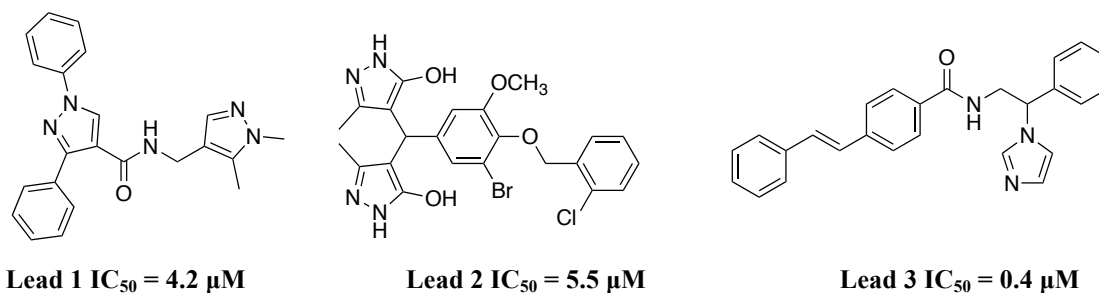
Figure 26: CYP24A1 inhibitors with moderate inhibitory activity

Owing to the lack of potential CYP24A1 inhibitors in the market, the development of potent and selective inhibitors after the modification of Lead 1, Lead 2 and Lead 3 was investigated.

Firstly, the study investigated the modification of lead 1[222], specifically through (i) replacement of the dimethyl pyrazole with a basic heterocycle to enhance binding interaction with the haem moiety, (ii) substitution of the benzene rings to explore structure-activity relationship, and (iii) variation in the length of the linker to determine optimum length to allow complete filling of the hydrophobic pocket of the CYP24A1 active site (Figure 27).
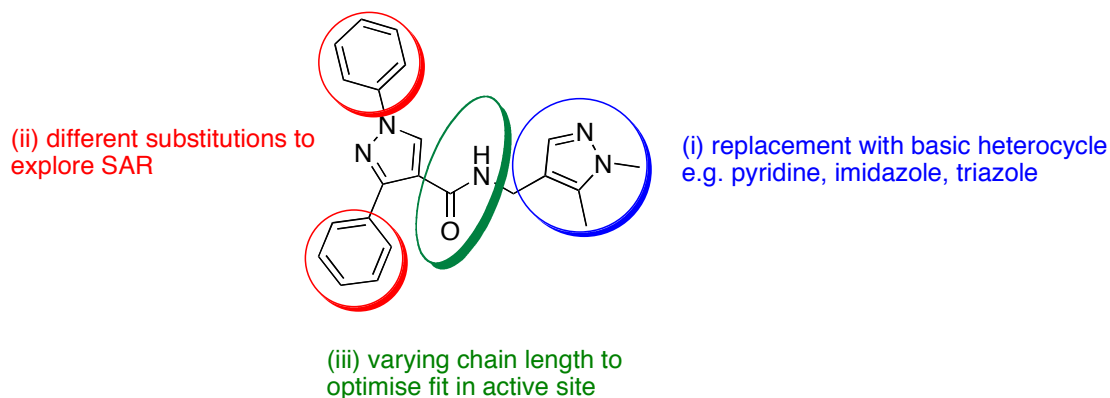
Figure 27: Modifications of lead 1 compound

Secondly, the study investigated the modification and development of Lead 2[222], specifically through (i) replacement of the phenyl with a basic heterocycle to enhance the binding interaction with the haem moiety, (ii) simplifying of the bromophenyl with an unsubstituted phenyl ring, (iii) the addition of phenyl substituents to dipyrazole rings or replacement of the dipyrazole rings with a basic heterocycle to allow complete filling in the active site of the CYP24A1 active site, and (iv) variation of the ether position to allow complete filling in the active site of CYP24A1 (Figure 28).
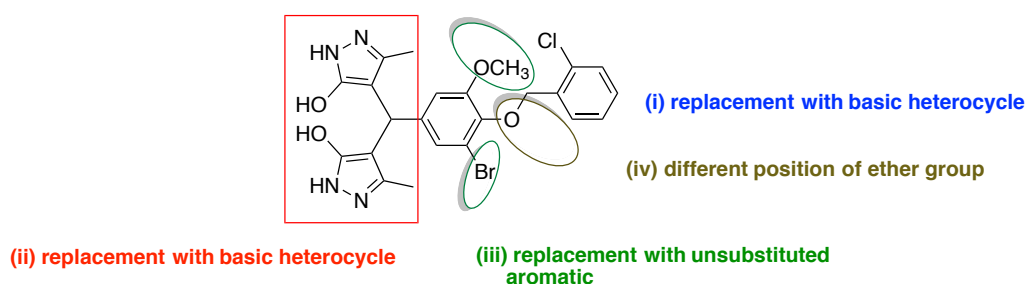
Figure 28: Modification of lead 2 compound

Finally, the study investigated the modification and development of Lead 3[191], specifically through (i) substitution of the phenyl ring of imidazole to explore the structure-activity relationship, (ii) substitution of the phenyl ring of styrene to explore the structure-activity relationship, and (iii) alteration of the alkene position to allow complete filling of the active site of the CYP24A1 (Figure 29).
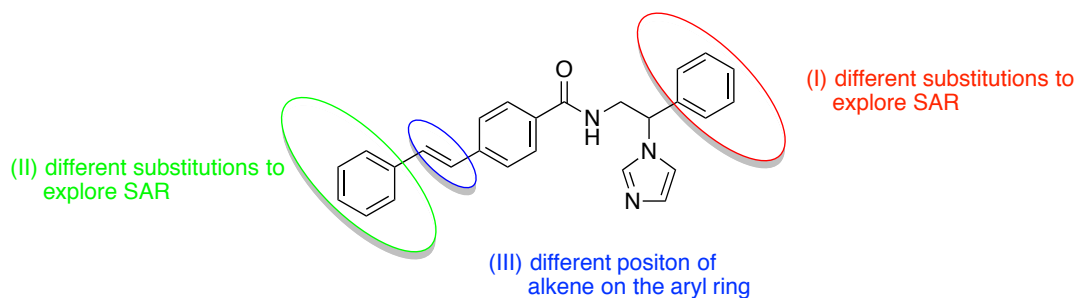
Figure 29: Modification of lead 3 compound

The main objective of the research can be summarised as follows:

1. Development of a theoretical CYP27B1 homology model based on homologous templates using Molecular Operating Environment (MOE) and validation of the model using Verify 3D, Errat, ProSA and Ramachandran plot

2. Optimisation of the model using molecular dynamics by using Maestro software

3. Further validation of the optimised CYP27B1 model by docking with the natural substrate (25-hydroxyvitamin D_3); analysis of the enzyme active sites of both CYP27B1 and CYP24A1 using described inhibitors (both selective and non-selective) to identify any differences in the two proteins

4. Chemical synthesis for modified Lead 1, 2 and 3 and evaluation *in vitro* of the development of lead 1, lead 2 and lead 3 regarding their inhibitory activities against CYP24A1 and CYP27B1 enzymes.
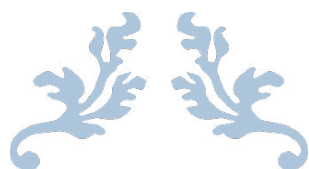
CHAPTER TWO

Molecular modelling

2   Molecular modelling

2.1   General consideration

The improvement of new medications is undoubtedly a very complex and demanding interdisciplinary process. Driven by the joint endeavour of the pharmaceutical companies, biotech companies, and academia, the approaches and methodologies used in drug design have changed after some time, exploiting and driving new technological advances to solve the various bottlenecks found along the way. Today, the field of medication improvement might appear to be riper than any time in recent memory, with limitless measures of data made accessible from molecular modelling. There is no single answer for a drug design difficulty. The suitable test strategies or computational techniques to be utilised will rely upon the qualities of the framework itself and the data available[223,224].

Molecular modelling can be considered as a range of computerised procedures based on hypothetical science techniques and experimental data that can be utilised to analyse molecules to predict molecular and physicochemical properties[225]. Molecular modelling serves as a bridge between theory and experiment. In addition, molecular modelling and drug design are economical and save time. During the past two decades, research centres have changed the method of research to generate novel bioactive molecules by using advances in molecular modelling techniques through identification of enzymes using X-ray crystallography, after which, drugs were designed which could bind with enzymes as ligands. Moreover, molecular modelling helps to compare experimental results with theoretical predictions for the model. Molecular modelling also helps to understand and to interpret experimental observations and provide data not available from genuine experiments. Therefore, molecular modelling can be characterised as the generation, manipulation, calculation, and expectation of reasonable molecular structures and associated physicochemical as well as biochemical properties using a computer. However, the traditional method of drug discovery is the experimental screening of huge quantities of chemicals to find out their biological action by enrolling hundreds of compounds. Unfortunately, it is an expensive and time-consuming method. Furthermore, molecular modelling is a computational technique used in pharmaceutical research to design and discover potentially useful proteins, which are visualised as three dimensional structures. There are two types of molecular

modelling studies in drug design: either the structure of the target is known or unknown[226].

Proteins are essential to life, as they play critical roles in most biological processes. X-ray crystallography is the main method for determining the structure of proteins, including the ability to elucidate how they work based on their three dimensional structures to study active sites and the interaction between the protein and the ligand. Unfortunately, the majority of proteins are currently difficult to crystallise or are too large for NMR studies. This can be a time-consuming process, and it will succeed only if it is possible to find suitable conditions for growing crystals. This can therefore easily become a bottleneck in drug design projects[227]. The protein data bank (PDB) is an available source of protein crystal structures, but only 12 % of all known proteins are available as three dimensional structures[228]. Homology modelling is used for the determination of a protein structure based on the crystal structure of a protein (template), which has a similar amino acid sequence.

Human CYP27B1 and CYP24A1 are part of the huge cytochrome P450 (CYP) superfamily; both enzymes are integrally placed in the inner mitochondrial membrane, and, as for almost all mammalian CYPs, structural data from X-ray crystallography or NMR analyses is even now inaccessibility. Currently, the aim of this chapter is to develop a human CYP27B1 homology model as a tool in the design of a selective inhibitor of vitamin D metabolism, specifically to aid in the design of chemical compounds with a selective inhibition of CYP24A1 and not the inhibition of CYP27B1, which inactivates the active form of vitamin D, calcitriol. A model of human CYP24A1 using the rat CYP24A1 crystal structure as a template[191] has previously been described by our group. To assist in the design of a selective CYP24A1 inhibitor, a CYP27B1 homology model was required.

2.2   Homology modelling

Three-dimensional protein structures are of extraordinary value for the rational design of a wide range of biological experiments, for example, site-coordinated mutagenesis or the structure-based discovery of particular inhibitors. Nevertheless, the number of structurally characterised proteins is small compared with the number of known protein sequences. Different computational strategies for modelling three-dimensional structures of proteins have been produced to conquer this restriction. Since the number

of possible folds in nature appears to be limited, homology modelling has proven to be the method of choice to generate a reliable 3D model of a protein from its amino acid sequence[229]. Homology modelling mixes sequence investigation and molecular modelling to predict three-dimension structures. Homology modelling depends on the identification of known protein structures with sequences similar to the structure of the query protein. Ideally, the similarity between a query sequence and the template sequence should be above 20 %[230]. The sequence alignment and template structure are used to produce a homology model; several stages are involved in the homology process. First, one or more appropriate structural templates are identified from the PDB[228]. The second stage aligns the query sequence with the template sequence. The third stage develops the general skeleton from the alignment. Finally, the homology model is subject to validation.

2.3   Identification of a template

The (Expert Protein Analysis System) (ExPASy) was used to obtain the amino acid sequence of the target gene human CYP27B1. ExPASy was obtained from the Swiss Institute of Bioinformatics (SIB), which contains a variety of information regarding proteins[223]. Using the UniProt KB/TrEMBL tool from the ExPASy server and a search target of the protein CYP27B1 showed 79 hits for many different organisms. The complete human protein sequence (CYP27B1 human) was selected.

The amino acid sequence for human CYP27B1 has entry number O15528, and it is also known as CYP 1 α－hydroxylase[223] (Table 5). CYP27B1 is composed of 508 amino acids (Figure 30).

Entry name	Accession number	Entry state	Entry history
CP27B1 Human	O15528	Reviewed (UniPortKB/Swiss-Port)	Integrated into UniPortKB/Swiss-Prot July 15, 1998. Last sequence update Jan. 1,1998 Last modified February 19, 2014

Table 5: CYP27B1 Human (O15528)

>sp|O15528|CP27B_HUMAN 25-hydroxyvitamin D-1 alpha hydroxylase, mitochondrial OS=Homo sapiens GN=CYP27B1 PE=1 SV=1
MTQTLKYASRVFHRVRWAPELGASLGYREYHSARRSLADIPGPSTPSFLAELFCKGGLSR
LHELQVQGAAHFGPVWLASFGTVRTVYVAAPALVEELLRQEGPRPERCSFSPWTEHRRCR
QRACGLLTAEGEEWQRLRSLLAPLLLRPQAAARYAGTLNNVVCDLVRRLRRQRGRGTGPP
ALVRDVAGEFYKFGLEGIAAVLLGSRLGCLEAQVPPDTETFIRAVGSVFVSTLLTMAMPH
WLRHLVPGPWGRLCRDWDQMFAFAQRHVERREAEAAMRNGGQPEKDLESGAHLTHFLFRE
ELPAQSILGNVTELLLAGVDTVSNTLSWALYELSRHPEVQTALHSEITAALSPGSSAYPS
ATVLSQLPLLKAVVKEVLRLYPVVPGNSRVPDKDIHVGDYIIPKNTLVTLCHYATSRDPA
QFPEPNSFRPARWLGEGPTPHPFASLPFGFGKRSCMGRRLAELELQMALAQILTHFEVQP
EPGAAPVRPKTRTVLVPERSINLQFLDR

Figure 30: The query sequence of the CYP7B1 protein in FASTA format

The critical initial step in homology modelling is the determining of the best template structure. The least complex strategy of template identification depends on serial pairwise sequence alignments supported by database search systems, for example, BLAST. The BLAST[231] tool from the ExPASy server was used to identify suitable crystal structures, which are similar to the query protein sequence by alignment of the query protein against crystal structures from the PDB. In addition, molecular computer techniques can be used to support the choice of the best homology model. The selections of templates depend on factors and parameters such as length alignment, E-value (a better protein sequence when E-value < 0.005), % sequence identity, and BLAST score (Table 6). Nine different cytochrome enzymes that have various % sequence identities and E-values were identified. CYP24A1 (3K9V-A) for rat[232], has the best E-value of $1e^{-54}$, and the % sequence identity was 30%. Human cytochrome enzymes might be more reliable and could take priority such as CYP11A1 (3N9Y-A), CYP11A1 (3NA0-A) and CYP11B2, which all have a sequence identity of 29%, and E-values of $6e^{-51}$, $6e^{-51}$ and $1e^{-42}$ respectively. This result agreed with the CYP27B1 model, which was built by Zalewski et al.[233]

PDB code	BLAST score	Sequence identity	% Positive	% Sequence identity	Chain length	E-value	Accession number
CYP24A1 (rat) 3K9V-A	210	144	44	30	482AA	$1e^{-54}$	Q09128
CYP11A1 (human) 3N9Y-A	198	142	44	29	487AA	$6e^{-51}$	P05108
CYP11A1 (human) 3NA0-A	198	142	44	29	471AA	$6e^{-51}$	P05108
CYP11A1 (bovine) 3MZS-A	197	141	43	29	486AA	$1e^{-50}$	P00189
CYP11B2 (human) 4DVQ-A	171	128	43	29	483AA	$1e^{-42}$	P19099
CYP3A4 (human) 1W0E-A	107	75	48	32	485AA	$1e^{-23}$	P08684
CYP3A4 (human) 3UA1-A	107	75	48	32	487AA	$1e^{-23}$	P00191
CYP21A (bovine) 3QZ1-A	90.1	65	47	33	496AA	$3e^{-18}$	P00191
CYP46A1 (human) 2Q9F-A	89.4	66	46	31	456AA	$5e^{-18}$	Q9Y6A2

Table 6: Different selected protein crystal structures from BLAST search

2.3.1   Multiple sequence alignments

Running the Clustal omega tool[234] from the European Bioinformatics Institute, part of the European Molecular Biology Laboratory (EMBL-EBI), alignment of the query amino acid sequence with other protein sequences of selected crystal structure (PDB) was performed. Amino acids that have the same physicochemical properties appear with the same colour (Figure 31).

                          H HELIX acid-alcohol I Helix   J Helix

```
CYP11A1    LGDSKMSFEDIKANVTEMLAGGVDTTSMTLQWHLYEMARNLKVQDMLRAEVLAARHQ--
A      323
CYP27B1    LFREELPAQSILGNVTELLLAGVDTVSNTLSWALYELSRHPEVQTALHSEITAALSPGSS 356
CYP24A1    YQQDHLSKKELYAAVTELQLAAVETTANSLMWILYNLSRNPQAQRRLLQEVQSVLPD--N
       331
           ..: ::.: ***: ..*.*.:.* * **:::.:.* * *:..
```

                       K HELIX   1-4 2-1   1-3

```
CYP11A1    QGDMATMLQLVPLLKASIKETLRLHPISVTLQRYLVNDLVLRDYMIPAKTLVQVAIYALG
       383
CYP27B1    AYPSATVLSQLPLLKAVVKEVLRLYPVVPGNSRVPDKDIHVGDYIIPKNTLVTLCHYATS
       416
CYP24A1    QTPRAEDLRNMPYLKACLKESMRLTPSVPFTTRTLDKPTVLGEYALPKGTVLTLNTQVLG
       391
            * * .*.*** .**.:*** * *   * :  : ..*.:.* *::: ..
```

                                     Haem pocket   L-HELIX

```
CYP11A1    REPTFFFDPENFDPTRWLSKDKNITYFRNLGFGWGVRQCLGRRIAELEMTIFLINMLENF
       443
CYP27B1    RDPAQFPEPNSFRPARWLGEGPTPHPFASLPFGFGKRSCMGRRLAELELQMALAQILTHF
       476
CYP24A1    SSEDNFEDSHKFRPERWLQKEKKINPFAHLPFGIGKRMCIGRRLAELQLHLALCWIIQKY
       451
      .  *:.:* * ***:.  * * ** * * *:.***.***::.* .:: ::
```

Figure 31: Illustration of multiple amino acid sequence alignment of the query protein. (*) means the residues are identical, (.) means the residues are similar, and (:) means the residues are highly conserved. The conserved cysteine in FXXGXXXCXG motif in each of these sequences is a crucial residue. The residues are coloured per their chemical properties: red small hydrophobic (AVFPMILWY), blue acidic (DE), magenta basic (RHK), green hydroxyl+ amine +basic (STYHCNGQ). 3K9V-A is CYP24A1 (rat), CYP11A1 human (3N9Y-A).

The phylogenetic tree result of twenty crystal structure proteins and the protein query (VIRT6852) placed the query protein in the same branch with 3N9Y-A, 3NA0-A, 3MZS-A and 4DVQ-A and rat crystal structure (3K9V-A)[235], (Figure 32).


```
pdb|3n9y|A 0.00013
pdb|3na0|A -0.00013
pdb|3mzs|A 0.12861
pdb|4dvq|A 0.30911
VIRT9734 0.32691
pdb|3k9v|A 0.3445
pdb|1tqn|A 0.00959
pdb|3ua1|A 0.0096
pdb|1w0e|A 0.01871
pdb|3qz1|A 0.33138
pdb|3ruk|A 0.33157
pdb|2pg5|A 0.00076
pdb|2pg7|A 0.0014
pdb|2pg6|A 0.00165
pdb|1z10|A 0.0017
pdb|3ebs|A 0.00454
pdb|3e4e|A 0.21069
pdb|1pq2|A 0.21355
pdb|3czh|A 0.00025
pdb|3c6g|A -0.00025
pdb|2q9f|A 0.39409
```
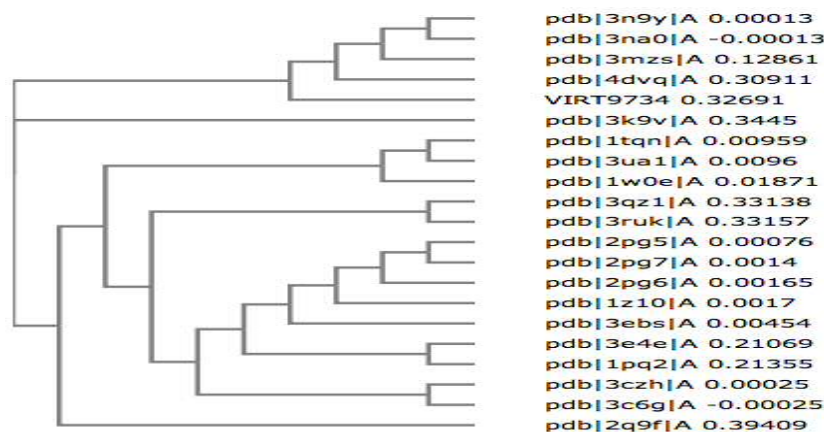
Figure 32: Phylogenetic tree for twenty-crystal structure proteins and query protein, CYP24A1 rat (3K9V-A), CYP11A1 human (3N9Y-A and 3NA0-A), CYP11A1 bovine (3MZS-A), CYP11B2 human (4DVQ-A), CYP3A4 human (1W0E-A, 1TQN-A and 3UA1-A), CYP21A bovine (3QZ1-A), CYP46A1 (2Q9F-A), VIRT6852 is query, CYP17A1 human (3RUK-A), CYP2A6 human (3EBS-A, 2PG6-A, 2PG5-A, 2PQ7-A and 1Z10-A), CYP2E1 human (3E4E-A), CYP2R1 human (3CZH-A), CYP2R1 human (3C6G-A) and CYP2C8 human (1PQ2-A)

The nine crystal structures were aligned with the query protein to find conserved regions by using PRATT[236]; 31 amino acids in each sequence were conserved which contained the FXXGXXXCXG) characteristic of the haem-binding motif (Table 7).

PDB code	Sequence	Conserved sequence	Accession No
CYP24A1rat 3K9V-A	455 - 485	FGiGkRmCIGrRLAelQLhLaLcwIIqkydI	Q09128
CYP11A1 human 3N9Y-A	455 - 485	FGwGvRqCLGrRIAelEMtIfLinMLenfrV	P05108
CYPA1 human 3NA0-A	455 - 485	FGwGvRqCLGrRIAelEMtIfLinMLenfrV	P05108
CYPA1 bovine 3MZS-A	454 - 484	FGwGvRqCVGrRIAelEMtLfLihILenfkI	P00189
CYP11B2 human 4DVQ-A	443 - 473	FGfGmRqCLGrRLAeaEMlLlLhhVLkhflV	P19099
CYP3A4 human 1W0E-A	435 - 465	FGsGpRnCIGmRFAlmNMkLaLirVLqnfsF	P08684
CYP3A4 human 3UA1-A	435 - 465	FGsGpRnCIGmRFAlmNMkLaLirVLqnfsF	P00191
CYP21A bovine 3QZ1-A	420 - 450	FGcGaRvCLGeSLArlELfVvLlrLLqaftL	P00191
CYP46A1 human 3Q9F-A	430 - 460	FSlGhRsCIGqQFAqmEVkVvMakLLqrleF	Q9Y6A2
Query	448 - 478	FGfGkRsCMGrRLAelELqMaLaqILthfeV	O15528

Table 7: PRATT result illustrating the 31 amino acid residues of the conserved Motif

In conclusion analysis confirmed rat CYP24A1 as the optimal template.

2.4   Homology building

Using the amino acid sequence of human CYP27B1 and CYP24A1 rat (3K9V-A) as templates, a homology model was built using Molecular Operating Environment (MOE) software[237]. Force-fields were used to construct the homology models including MMFF94. MOE generates ten intermediate models for each template, and the final model was taken as the Cartesian average of all the intermediate models.

2.5   Homology validation

Every homology model contains errors, with the number of errors depending on various factors: first, regarding the % sequence identity between template and target, if it is

greater than 90 %, the accuracy of the model can be compared with the crystal structure, except for a few individual side chains[238]. From 25 % to 90 % identity, the error will start. If the sequence identity is 25 % or less, the homology model will have very large errors. If errors in the template are located far from the active site, the error becomes less important. Once the homology modelling of the CYP27B1 model derived from CYP24A1 rat (3K9V-A) was finished, the templates and its model should be validated to evaluate the CYP27B1 model. Such validation considers the physicochemical quality to confirm that the stereochemistry and side chain environment of the model is correct[238,239].

2.5.1 Validation of active the site cysteine

The distance between the thiolate of the cysteine residue at the active site and the haem for template CYP24A1 rat (3K9V-A) and the CYP27B1 model was determined (Table 8). This shows the distance for the template was 2.36 $\mathring{A}$. In the human CYP27B1 model, the distance between the thiolate of the cysteine and the iron of the haem was found to be 2.41 $\mathring{A}$, which is close to the template. As a result, the distance in the human CYP27B1 model was very suitable for interaction between the thiolate and the haem.

Distance between thiolate of cysteine at the active site and haem iron		
PDB	**Template**	**Homology model**
3K9V-A CYP24A1 rat	**2.36 $\mathring{A}$**	**2.41 $\mathring{A}$**

Table 8: The distance between the thiolate of the cysteine residue at the active site and haem iron for template and model

2.5.2 Validation by Ramachandran plots

Ramachandran plots were generated by using the RAMPAGE server[240]. A Ramachandran plot interprets phi-psi torsion angles for all residues in the structure. Importantly, glycine residues appear unique and separated from other residues in the plot region. In addition, glycine and proline residues are represented in different plots due to a difference in the phi-psi angles.

PDB	No of residues in favoured region	No of residues in allowed region	No of residues in outlier region	Amino acid outlier
3K9V-A CYP24A1 rat	**448**	**14**	**0**	**NIL**
CYP27B1 model	**398**	**64**	**12**	**Phe48, Arg99, Gly176, Pro180, Ser205, Gly290, Pro359, Glu424, Thr439, His441, Leu446 and Ser454**

Table 9: Ramachandran plot evaluated the template and the corresponding model

A Ramachandaran plot program was used to check the quality of the template and the corresponding model (Table 9). The template had no residue in the outlier region. The result of the Ramachandran plot for the CYP27B1 model showed 12 amino acid residues in the outlier region. Visualisation of the outlier amino acid residues in the CYP27B1 model by MOE, showed them to be far from the active site (Figure 33). As a result, the CYP27B1 model passed the Ramachandaran examination.
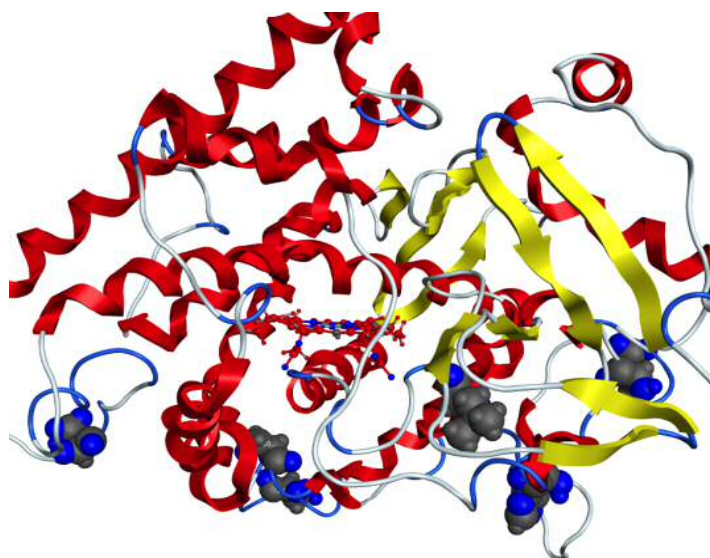
Figure 33: Outlier amino acids (space filled) identified by Ramachandran plot for CYP27B1 model

2.5.3 Validation by ERRAT

The ERRAT program works by analysing the statistics of non-bonded interactions between different atom types. The error is represented in the ERRAT diagram as a confidence limit that measures the structural error at each residue in the protein. Moreover, it calculates an overall score for the structure[241]. The ERRAT program is sensitive in detecting unusual atomic environments in protein molecules. In addition, this empirically derived atomic distribution was used as the basis for statistically

discriminating between correctly and incorrectly modelled regions of a query protein structure. The overall ERRAT score given for a structure signifies the percentage of residues falling below the 95 % confidence limit. Most quality structures are 80 - 100 % below the 95 % confidence limit.

In this work, ERRAT validation outputs for the template gave an overall score of 96.48 %. The CYP27B1 model, derived from rat CYP24A1 (3K9V-A) had the problematic areas appearing in residues around amino acids 200, 430, 440 and 460 (Figure 34). ERRAT showed them to be far from the active site. As a result, the CYP27B1 model passed the validation by ERRAT (Figure 35).
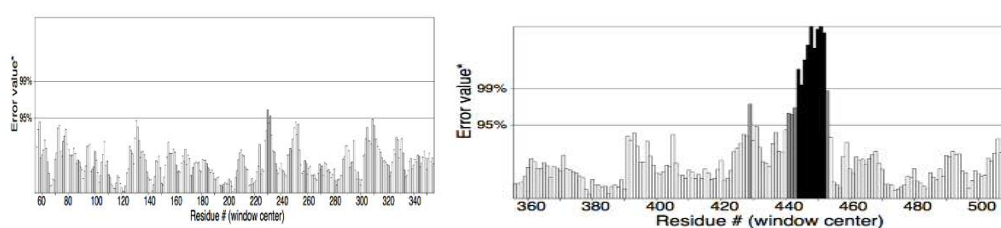
Figure 34: ERRAT validation for 3K9V-A CYP24A1 rat template
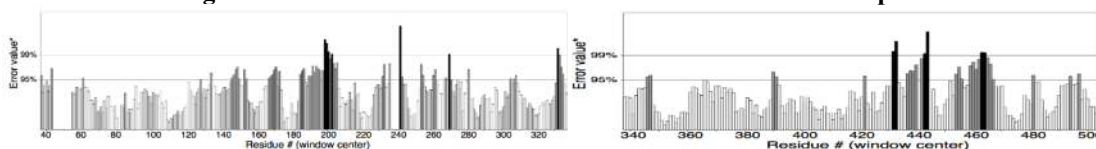
Figure 35: ERRAT validation for the CYP27B1 model

2.5.4   Validation by Verifiy 3D[242]

Verify 3D is a program that examines the compatibility of a three dimensional atomic model with its own amino acid 1D sequence[243]. Three dimensional verification is an effective tool for detecting errors in a protein structure, such as the wrong folding. The program examines how compatible the three-dimensional structure is with the primary structure[244]. Each of the twenty amino acids is given three parameters describing its preference for: secondary structure, degree of buried surface area and the fraction of side-chain area that is covered by polar atoms.

These three parameters are evaluated for each residue in the structure and a correlation is calculated between this set of observed parameters and the ideal parameters of the amino acid type to which it has been assigned. Verified 3D should stay above 0.2 and not fall under zero. The scores for the first 9 and the final 9 sequence positions have no meaning and are just for control. The rat CYP24A1 (3K9V-A) template and CYP27A1

model passed the validation without any residue below zero, and the residue percentage of amino acid is 94.5 % and 86 % above 0.20 respectively.

2.5.5 ProSA validation

ProSA (protein structure analysis) is a commonly used program to check faults in three-dimensional protein structure based on statistical analysis. A major issue in structural biology is the recognition of errors in experimental and theoretical models of protein structures. The ProSA program, which invests the benefits of interactive web-based applications for the show of scores and energy, plots potential issues seen in the protein structures[245].

In this work, the template and CYP27B1 homology model was evaluated by ProSA, and the outcomes are represented in two diagrams, the first diagram for Z- score by X-ray and NMR which measure the total Z-energy of the structures. The second diagram shows problematic residues in the template and CYP27B1 homology model. The ProSA-web service, which examines a PDB file and produces a score based on the quality of local structure surrounding each residue, based on the typical ranges of dihedral angles and side chain contacts observed in real protein. Also, ProSA calculates an overall for structural quality with Z score $\leqslant$ -10. So, (Table 10) the template and the CYP27B1 model showed two green lines to be present on the error axis to indicate the confidence with which the residues exceed error value. In addition, ProSa displayed quite a similar overall Z-score for the template (-10.35) and the CYP27B1 model (-7.82). Indicating a good quality for the CYP27B1 homology model (Table 10).

PDB	Z score	Local model quality	Overall model quality (X- ray, NMR)
3K9V-A CYP24A1 rat	**-10.53**		
CYP27B1 model	**-7.82**		

Table 10: 3D proSA validation for templates and their models.

2.5.6   Superimpose

To further increase the confidence of the acceptability of the CYP27B1 model, the root-mean-square deviation (RMSD) was run by MOE to estimate the RMSD between 3K9V-A CYP24A1 rat templates and the CYP27B1 homology model. The output for the RMSD homology model was superimposed with good RMSD below 2 $\mathring{A}$ (Table 11).

PDB	RMSD
3K9V-A CYP24A1 rat	0.956 $\mathring{A}$

Table 11: RMSD data

2.5.7   Prediction of secondary structure

The secondary structure of the CYP27B1 model was generated to identify α helices, β sheets, coils, and loops. The secondary structure prediction showed a high similarity in helices and beta sheets between the template and its model. The first 30 amino acids at the N-terminal segment, which is the membrane anchor peptide, have many hydrophobic residues. The polyproline motif follows the membrane anchor peptide[246]. As all of the selected sequences and query sequences of CYP27B1 were CYP subfamilies, the features common to all sequences revealed the presence of the haem-binding motif, an essential part of all cytochromes by using PRATT[236] and Psipred[247]. The patterns conserved over a set of sequences were identified, and it was found that 31 amino acids were similar in every protein. These 31 amino acids contained the conserved cysteine in all proteins, and this was the haem-binding motif. The cysteine ligand loop of the FXXGXXXCXG motif is a conserved region, which is found either before or toward the beginning of the L helix. The motif also contains a phenylalanine residue, which has an important role in modulating the thermodynamic properties of the haem iron[248] (Table 12). Another conserved region, the EXXR motif is believed to contribute to the catalytic activity of the cytochrome P450, and it helps to support 3D folding of the secondary structure.

Most cytochrome enzymes have the important acid - alcohol pair situated in the I-helix with the conserved sequence (A/G) GX (E/D) (T/S). The CYP27B1 model has the alcohol pair as AGVDT, that is, Ala317, Gly318, Val319, Asp320, and Thr321.

Using the nomenclature of Gotoh[249,250] six Substrate Recognition Site (SRS) regions were identified in all selected sequence alignments based on a CYP2 family analysis.

SRS-1 forms part of the B′ -helix region followed by the inter helical loop region, SRS-2 is within the F-helix, SRS-3 lies in a region of the G-helix, SRS-4 lies at the centre of the I-helix, while SRS-5 (β 1-4) and SRS-6 are just after the L-helix[251].

The haem is typically sandwiched between helix L on the side of the haem proximal to the surface of the protein and helix I in the inside of the protein.

The 3K9V-A CYP24A1 rat template and CYP27B1 model[232,251] were selected to run secondary structures by using the PSIPRED program[252]. The output result from PSIPRED is different from the MOE secondary structure result; this might result from a difference in calculations and logarithms between them.

The observed secondary structures of both proteins using PSIPRED demonstrated a high degree of similarity in terms of helices and β sheets. There is good overlap between the template and CYP27B1 model especially the L and I helices. Noticeably, helix α I for the CYP27B1 model has 14 amino acid residues, which is too short to cover the haem binding site, requiring the combination of the α I and α H helices to cover the haem binding site (Figure 36 and 37).

PDB	Helix template	Helix CYP27B1 model	Strand template	Strand CYP27B1 model
3K9V-A CYP24A1 (rat)	Ser67 -Trp75 = α A' Lys81-Lys92 = α A Pro112-Thr121 = α B Pro133 - His140 = α B' Gln153 - Phe162 = α C Lys164 - Lys165 = α C Pro169 - Asp195 = α D Leu203 - Tyr220 = α E Glu233 - Met253 = α F Val257 - His260 = α G' Val267 - Ser294 = α G Phe301 - Gln307 = α H Lys313 - Lue342 = α I Pro346 -Val359 = α J Ala368 - 371Leu = α K Tyr376 - Ser384 = α K Asn418 -Val420 = α K, α K' ' Cys462 - Lys482 = α L	Ser47 - Lys55 = α A' Arg60 - Phe72 = α A Pro91 - Gln100 = α B Trp113 - Cys119 = α B' Glu132 - Leu141 = α C Pro148 - Arg173 = α D Val186 - Leu202 = α E Pro216 - Arg243 = α F Trp250 - Arg278 = α G' Ser289 - Phe298 = α G Ala304 - Ala317 = α H Asp320 - Leu333 = α I Pro337 - Ala350 = α J Ala361 - Leu364 = α K Leu369 - Val377 = α K His412-Thr415 = α K ' , α K' ' Met456 -His475 = α L	Phe96 - Met99 = β 1-1 Asp106 - Leu109 = β 1-2 Thr402 - Leu404 = β 1-4 Tyr407 - Leu409 = β 2-1 Val414 - Leu417 = β 1-3 Leu422 - Met461 = Cys Loop Asp484 - Val486 = β 3-1 Leu496 - Ile500 = β 4-1 Ile509 - Arg512 = β 3-2	Trp76 - ala78 = β 1-1 Thr85 - Ala89 =B1-2 Ile395 - Val397 = β 1-4 Tyr400 - Ile402 = β 2-1 Leu407 - Cys411 = β 1-3 Ser416 - Cys455 = Loop Cys Glu477 - Gln479 = β 3-1 Thr491 - Val496 = β 4-1 Leu503 - Asp507 = β 3-2

Table 12: Secondary structure data for the template and CYP27B1 model
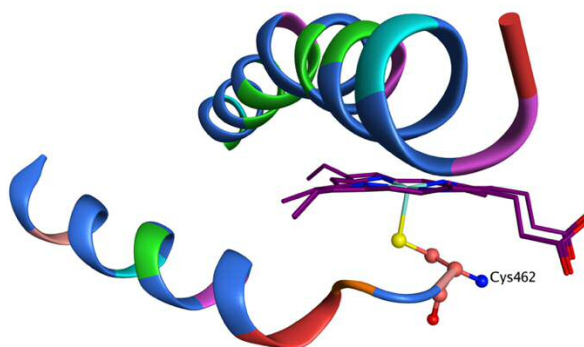
Figure 36: Haem binding site for template 3K9V-A
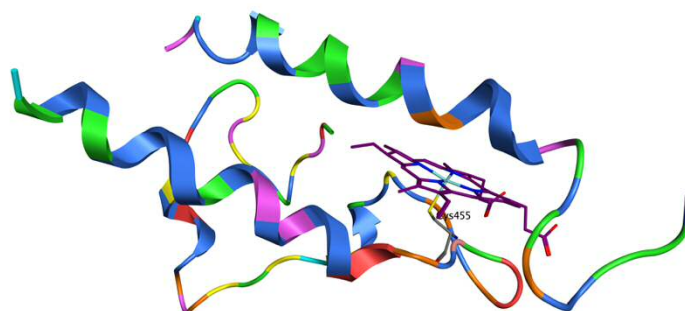
Figure 37: Haem binding site for CYP27B1 model 3K9V-A

2.6   Molecular dynamic studies

2.6.1   Molecular dynamic for the CYP27B1 model at 300 K

Molecular dynamics can be used to correct protein structure issues, for example, folding, conformational flexibility, and stability. The molecular dynamics simulations on CYP27B1. First used a 5 ns simulations carried out at two different temperatures, 300 K and 312 K. Molecular dynamics simulation at 300 K and 312 K represent normal body temperature and elevated body temperature.

The RMSD values of the backbone atoms were plotted as a time-dependent function of the molecular dynamics simulation. The outcomes support the CYP27B1 model structure, as they show time dependence of constant RMSD (Å) of the backbone atoms throughout the whole simulation process. This demonstrates that the model achieved equilibrium after some initial fluctuations. The chart plainly shows that there is an adjustment in the RMSD from 0.9 Å to 2.4 Å and that it reached the 2.02 Å at 1.39 ns and then declined to 1.83 Å at 1.83 ns, but after that, it reached a plateau from 2.25 ns (Figure 38).
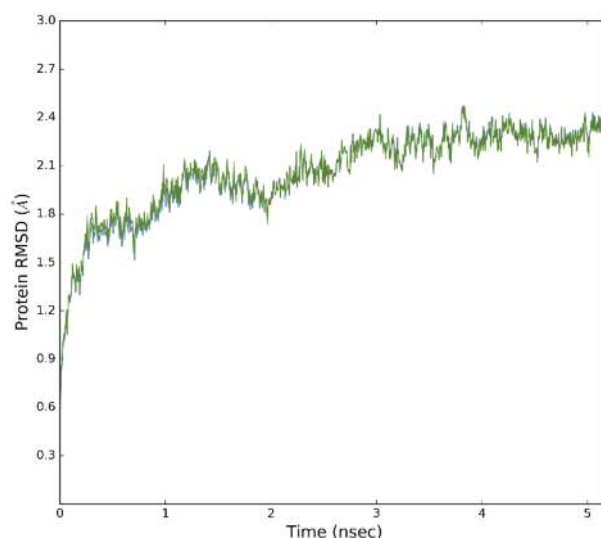
Figure 38: Time-dependent RMSD (Å) of backbone atoms of the CYP27B1 model at 300 K

Root mean square fluctuation (RMSF) showed the differences of structural behaviours and flexibilities in each residue for the CYP27B1 model; the amino acid residue (Pro440) was shown to be highly fluctuated (Figure 39).
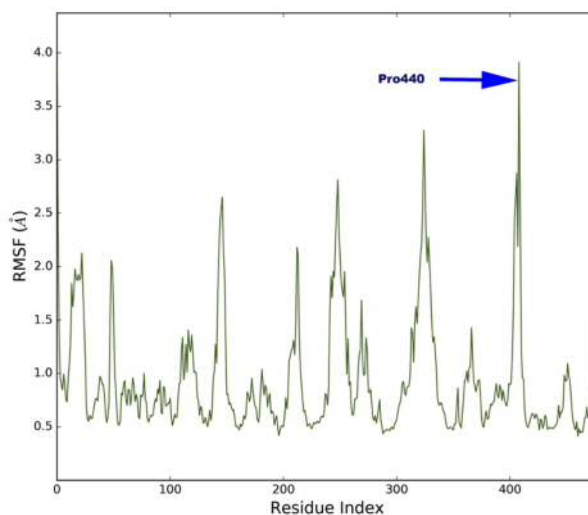
Figure 39: The RMSFs for the CYP27B1 model at 300 K. Root mean square fluctuation (RMSF) showed the differences of structural behaviours and flexibilities in each residue for the CYP27B1 model; the amino acid residue Pro440 was shown to be highly fluctuated

2.6.2   Molecular dynamic for the CYP27B1 model at 312 K

The RMSD of the backbone atom values for CYP27B1 at 312 K simulations were not much different from the simulations at 300 K (Figure 37). However, the graph clearly indicates that there is a change in the RMSD from 0.9 Å to 2.5 Å, and it reaches a plateau from 2.48 ns. The RMSF showed the amino acid residue Gly281 to be highly fluctuated (Figure 40 and 41).

The results of the molecular dynamics simulation for 5 ns at temperatures 300 K and 312 K showed that there are similar effects on the CYP27B1 model. Overall, it can be said that there is no significant difference in structure during molecular dynamics simulations at temperatures 300 K and 312 K. This means that at 312 K, the model still has activity, and no structural damage has happened.
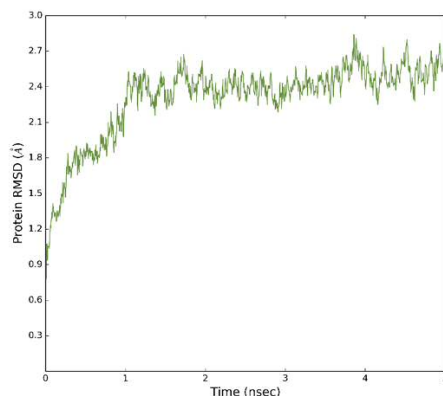
Figure 40: Time-dependent RMSD (Å) of backbone atoms of the CYP27B1 model at 312 K
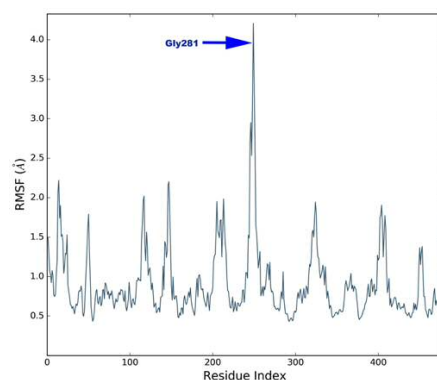
Figure 41: The RMSFs for the CYP27B1 model at 312 K. Root mean square fluctuation (RMSF) showed the differences of structural behaviours and flexibilities in each residue for the CYP27B1 model; the amino acid residue Gly281 was shown to be highly fluctuated.

2.6.3 Ramachandran plot validation for CYP27B1 model after molecular dynamics simulation

To validate the CYP27B1 model structure, Ramachandran plots were run before as well as after molecular dynamics simulation, and structures were analysed using RAMPAGE Ramachandran Plot Assessment (Table 13). After MD and it shows that the phi/psi angles of 90.9 % are in the most favoured regions, with 8.1 % in additional allowed regions, and 1.1 % amino acid residues were in disallowed regions. Therefore, the CYP27B1 model had improved after molecular dynamics simulation. However, the 1.1 % disallowed region might be attributed to the fact that the human CYP27B1 sequence has a low similarity to any of the crystal structures in the protein database

(PDB), and the modelling server utilised the only available template with reasonable resemblance.

PDB	No of residues in favoured region	No of residues in allowed region	No of residues in outlier region	% Amino acid outlier
Post-MD	428	38	5	1.1
Pre-MD	398	64	12	2.5

Table 13: Ramachandran plot evaluated the CYP27A1 model before and after molecular dynamics simulations

2.6.4   Molecular dynamic for the CYP27B1 model - SDZ-88357 at 300 K

SDZ-88357 is a selective inhibitor of the CYP27B1 enzyme and prevents the formation of calcitriol (Table 15). Molecular dynamics simulations were carried out on the CYP27B1 model-SDZ-88357 docking complex system to improve the understanding of the binding mode obtained from molecular docking. The dynamic stabilities of the complex system were predicted using RMSD changes during the molecular dynamics simulations.

Firstly, a molecular dynamics simulation for the CYP27B1 model-SDZ-88357 complex system was run for 5 ns (Figure 42). RMSDs increased progressively, fluctuations were observed until 5 ns, and the curve did not reach a plateau. Therefore, a molecular dynamics simulation for 5 ns was not enough to optimise the CYP27B1 model-SDZ-88357 complex system.
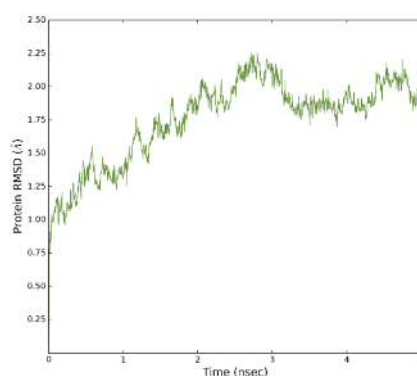
Figure 42: Time-dependent RMSD (Å) of backbone atoms of the CYP27B1 model - SDZ-88357 at 5 ns

Secondly, molecular dynamics simulations were carried out on the CYP27B1 model-SDZ-88357 complex system for 50 ns. The RMSD changed from 1.37 Å at zero time to 3.57 Å at 33.44 ns; then the protein was equilibrated with no evident RMSD fluctuations observed after 33.44 ns. The stability of the CYP27B1 model-SDZ-88357 complex structure during the molecular dynamics simulation was measured by its

deviation from the initial structure in terms of RMSD. This indicates that, after an initial increase in the magnitude of the fluctuation of the ligand atoms, the ligand reached a state of equilibrium characterised by the RMSD profile (Figure 43), showing that the complex has attained equilibration and is stable.
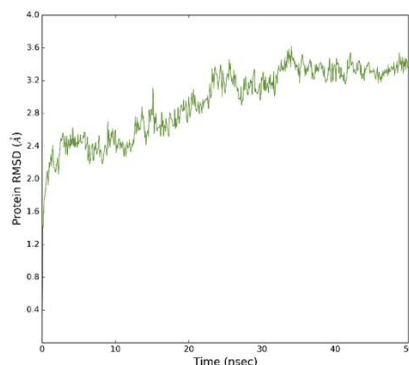
Figure 43: Time-dependent RMSD (Å) of backbone atoms of the CYP27B1 model - SDZ-88357 complex at 50 ns

Ligand RMSD (right Y- axis, Figure 44) demonstrates how stable the ligand is regarding the protein and its binding pocket. The red line indicates the RMSD of a ligand when the CYP27B1 model-SDZ-88357 complex is initially aligned on the protein backbone of the reference and then the RMSD of the ligand heavy atoms is measured. If the values observed are significantly larger than the RMSD of the protein, then it is likely that the ligand has diffused far from its initial binding site[253]. A pink line (Lig fit Lig) indicates the RMSD of a ligand that is aligned and measured just on its reference conformation. This RMSD value measures the internal fluctuations of the ligand atoms.
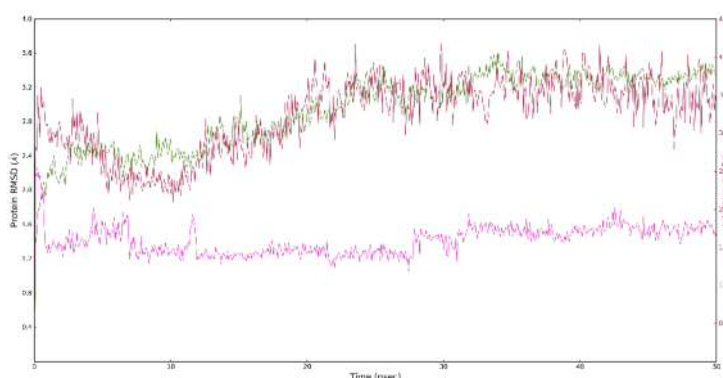
Figure 44: Protein and ligand root mean square fluctuation (RMSD). The above plot indicates the RMSD evolution of a protein (left Y-axis). All protein frames are first aligned on the reference frame backbone, and then the RMSD is calculated based on the atom selection. Ligand RMSD (right Y-axis) demonstrates how stable the ligand is with respect to the protein and its binding pocket, A pink line indicates the RMSD of a ligand when the protein ‒ ligand complex is first aligned on the protein backbone of the reference, and then the RMSD of the ligand heavy atoms is measured.

The RMSF of all the CYP27B1 model-SDZ-88357 complex structure generated during the MD simulation were calculated to characterise the mobility of the individual residues. The side chain residues from Met277 to Gly280 had high peaks during the MD simulations of the CYP27B1 model-SDZ-88357 complex and showed remarkable fluctuation events in the RMSF plot (Figure 45), indicating large fluctuations of those residues. The protein RMSF is useful for characterising local changes along the protein chain. On this plot, the peaks show the ranges of the protein that fluctuate the most during the simulation. Ordinarily, the tails (N- and C-terminal) fluctuate more than any other sequence of the protein. Secondary structure components, such as alpha helices and beta strands, are typically more inflexible than the unstructured part of the protein, and do not fluctuate as much as the loop regions. From the diagram, it is apparent that the vast majority of residue fluctuations were localised in the loop areas.
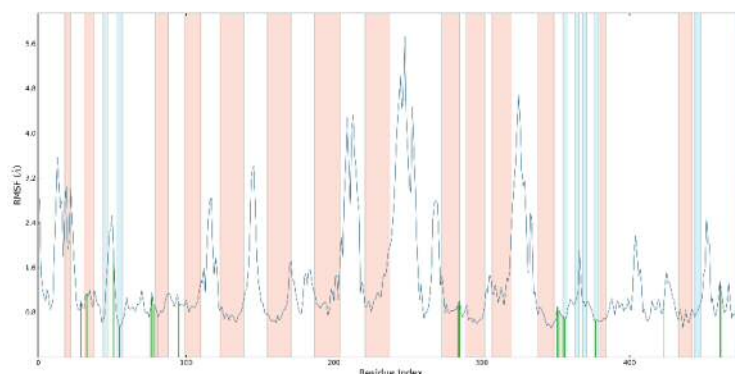
Figure 45: The RMSF for the CYP27B1 model-SDZ-88357 graph showed secondary structure elements, alpha-helical and beta-strand regions are highlighted in red and blue backgrounds, respectively. Ligand contacts and protein residues that interact with the ligand are marked with green coloured vertical bars.

Protein ligand interaction for the CYP27B1 model-SDZ-88357 complex is showed in (Figure 46). Protein interactions with the ligand were checked all through the simulation and interactions are ordered by their sort shown specifically hydrogen bonds, hydrophobic, ionic, and water bridges.
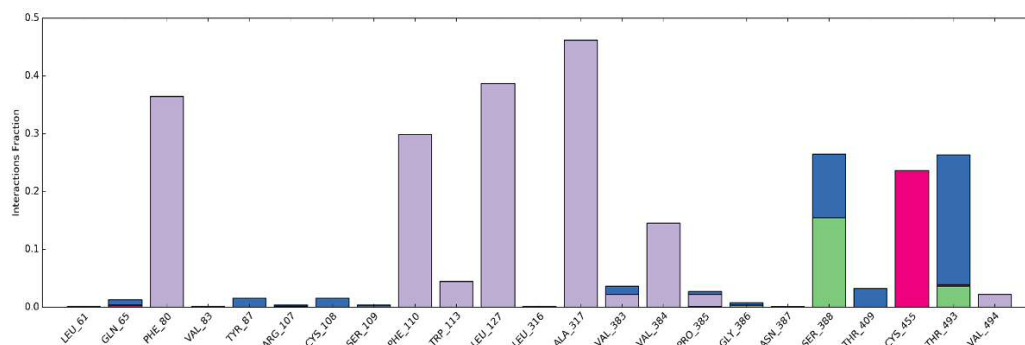
Figure 46: Illustration of protein interactions with the ligand. The red column means ionic bond, green column means a hydrogen bond, blue column means water bridges, and a purple column means a hydrophobic bond. The stacked bar charts are normalised over the course of the trajectory: for example, a value of 0.5 suggests that for 50% of the simulation time, the specific interaction is maintained.

The influence of SDZ-88357 on the dynamical properties of the CYP27B1 model active site has been clarified by analysing the trajectory data obtained from the molecular dynamics simulations. The CYP27B1 model-SDZ-88357 docking interactions were reproduced during the entire simulations period. The analysis revealed the crucial role of water molecules in the CYP27B1 model-SDZ-88357 docking interactions. In most of the trajectories, active site residues of the CYP27B1 model-SDZ-88357 complex were involved in H-bonding through water bridges. The hydrogen bonds observed for Ser388 and Thr493 in the CYP27B1 model-SDZ-88357 docking complex remained stable throughout the simulation period. Ser388 and Thr493 formed a H-bond with one water bridge

2.7 Docking the natural substrate in the optimised CYP27B1 model

Yamamoto *et al.*[254] reported the substrate binding pocket for the CYP27B1 model based on rabbit CYP2C5 to be Leu61, His62, Gln65, Phe80, Trp113, Leu127, Val225, Val228, Leu316, Ala317, Thr321, Pro385, Gly386, Asn387, Ser388, Thr409, Val496, and Pro497. In addition, Yamamoto *et al.*[255] showed that the side chain of 25-(OH)D$_3$ was situated to close Gln65 and Thr409, and the distances between the 25-hydroxyl group and Gln65 and the 25-hydroxyl group and Thr409 are 2.83 and 2.82 Å, respectively. This suggests that the 25-hydroxyl group forms pincer-type hydrogen bonds with Gln65 and Thr409. The 1α-hydrogen of 25-(OH)D$_3$, which will be subjected to hydroxylation, orients to the haem iron atom. Conformation of 25-(OH)D$_3$ accommodated in CYP27B1, 25-(OH)D$_3$ is docked with a stable conformation in which the A-ring adopts the chair form, and the side chain adopts the gauche(+) conformation (43°) at C16-17-20-22 and the following anti-conformation from C20 to the terminal

methyl group. The A-ring adopts the β-form. In this conformation, the distance between C1 and iron is 4.3 Å and between hydrogen at the 1α-position and iron is 3.3 Å.

In this chapter, the CYP27B1 model was optimised before undergoing docking studies. The docking was performed using LeadIT 2.1.2 for the CYP27B1 model derived from rat CYP24A1. The natural substrate (25-hydroxyvitamin D_3) (Figure 47) was docked in the CYP27B1 model to see how it interacted with the model and to identify the amino acids which interacted with the substrate. The docking result for the CYP27B1 model are given in Table 14. Docking was run for 10 conformations. The distance between the haem iron of the CYP27B1 model and carbon number 1 in the 25-hydroxyvitamin D_3 was 4.58 Å, which had interactions between 16 amino acid residues and the ligand. This result agreed with Yamamoto et al.[255]
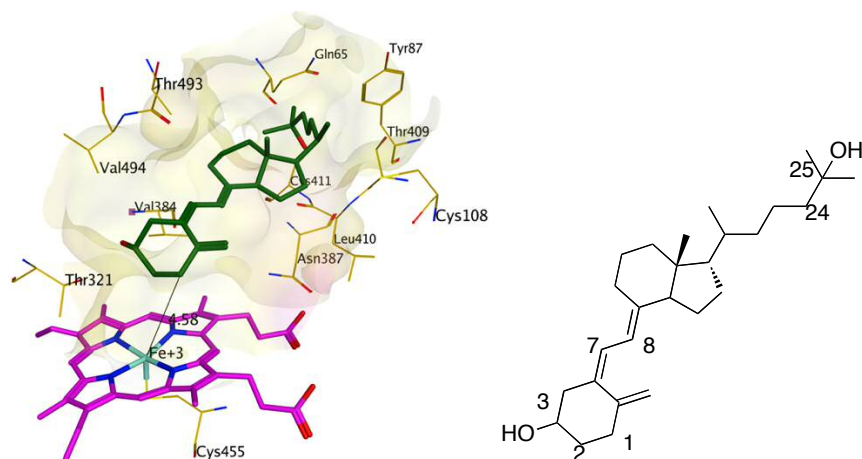
Figure 47: 3D and 2D for 25-hydroxyvitamin D_3

A	B	C
25-hydroxyvitamin D_3	**4.58 Å**	**Gln65, Tyr87, Cys108, Thr321, Val384, Asn387, Thr409, Leu410, Cys411, Thr493 and Val494.**

Table 14: (A) Docking output for the CYP27B1 model, (B) distance between carbon number 1 and the haem iron and (C) amino acids in the active site making interactions with the ligand.

2.7.1 Selective inhibitors of CYP27B1 model and the CYP24A1 model after molecular dynamics simulations

Powerful inhibitors of cytochrome P450 enzymes are found in azole compounds, which directly bind to the prosthetic haem iron through a pair of electron from heterocyclic nitrogen. Moreover, they interact with other amino acids in the binding site. Azole compounds block both oxygen binding and activation at the haem iron as well as substrate accommodation in the active site. The antifungals ketoconazole and clotrimazole are examples of azole drugs, which inhibit CYP24A1 and CYP27B1.

More selective inhibitors of vitamin D metabolism have been designed. For example, (*R*)-(-)VID400 has good selectivity for CYP24A1; however, SDZ-284971 and SDZ-88357 have more effect on CYP27B1 (Table 15).
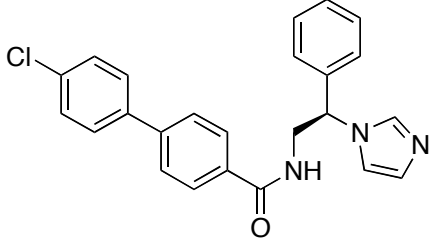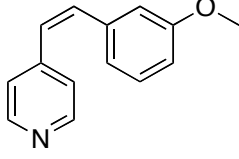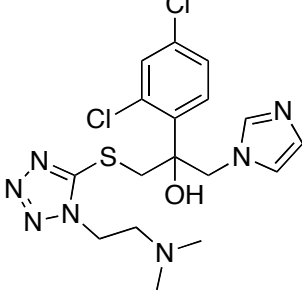
Compound	Chemical structure	IC$_{50}$ (nM)	
		CYP27B1	CYP24A1
R-(-)VID400		616.1	15.2
SDZ-284971		78.8	10000
SDZ-88357		60.2	>10000

Table 15: Example of selective inhibitors of CYP24A1 and CYP27B1[215]

2.7.1.1 Docking (R)-(-)VID400 inhibitor in the CYP27B1 model

(*R*)-(-)VID400 was a weak inhibitor of CYP27B1 based on the docking distance between the nitrogen of the imidazole ring and the haem iron, which was 4.16 $\mathring{A}$ (Table 16). This agrees with the literature IC$_{50}$ data (Table 15). In addition, there were some poses of compound (*R*)- (-)VID400 that form different interactions with the haem. e.g. the chloro substituent of the phenyl ring interacts with the iron.
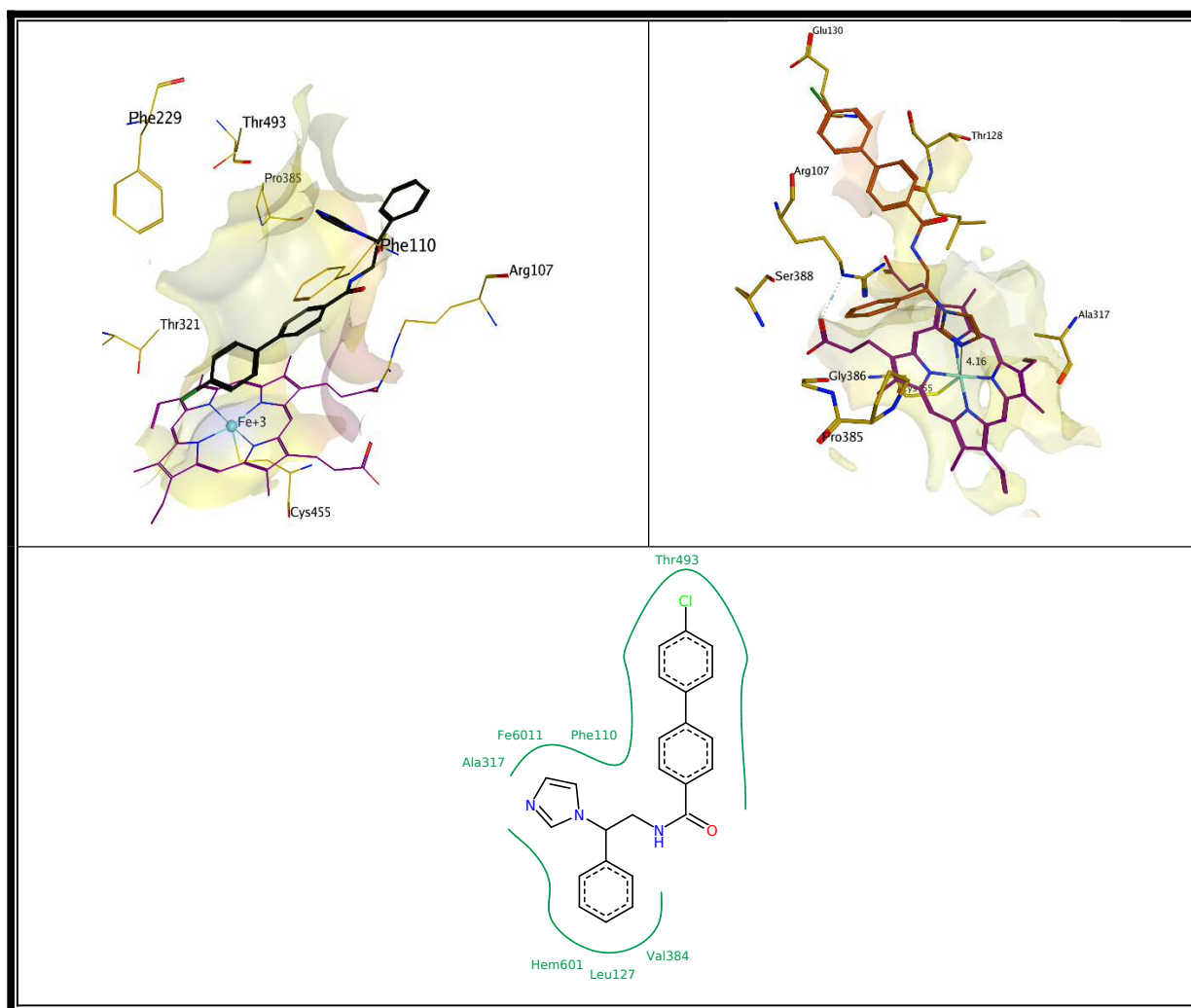
Table 16: 3D and 2D for (*R*)-(-)VID400 inhibitor in the CYP27B1 model

2.7.1.2 Docking (R)-(-)VID400 inhibitor in the CYP24A1 model

On the other hand, when (*R*)-(-)VID400 was docked inside the pocket of the CYP24A1 model[191], the distance between the nitrogen of imidazole and the haem iron was 2.31 $\mathring{A}$. (*R*)-(-) VID400 interacted with amino acid residues from the active site by hydrophobic interaction (Leu148, Met246, Phe249, Thr330, Ala326) (Figure 48).
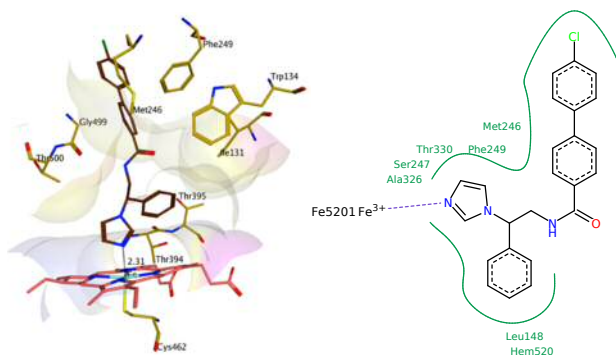
Figure 48: 3D and 2D for (R)-(-) VID400 inhibitor on the CYP24A1 model

Overall, the docking output showed that (*R*)-(-)VID400 was more selective for the CYP24A1 model than the CYP27B1 model.

2.7.1.3 Docking SDZ-88357 selective inhibitor in the CYP27B1 model

SDZ-88357 is a selective inhibitor of the CYP27B1 enzyme and prevents the formation of calcitriol. Docking results showed the interaction between the nitrogen lone pair of tetrazole ring and the haem iron at a distance of 2.25 *Å*. There were hydrophobic interactions between the inhibitor with amino acid residues in the active site (Phe110, Leu127, Pro385 and Gly386) (Figure 49). In addition, SDZ-88357 was observed making three additional hydrogen bonds with amino acids Arg107, Asn387 and Asp320 (Table 17).

	Distance	Hydrogen bond
1	2.07 Å	Between imidazole of SDZ-88357 and Arg107
2	2.80 Å	Between hydroxyl group of SDZ-88357 and Asn387
3	3.42 Å	Between tertiary amine of SDZ-88357 and Asp320

Table 17: Hydrogen bonds between SDZ-88357 and amino acid residues of CYP27B1 model
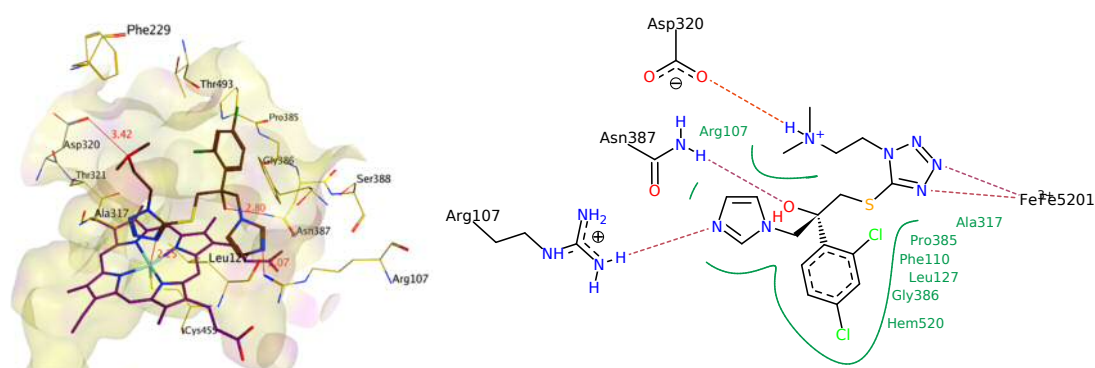
Figure 49: 3D and 2D for SDZ-88357 selective inhibitor on the CYP27B1 model

Noticeably, Asp320 was part of the α I helix for the CYP27B1 model, which covers the haem binding site and contains SRS-4, and plays a key role in orientating the ligand at the active site by electrostatic interactions[166]. Asp320 has the important acid - alcohol pair situated in the I-helix with the conserved sequence (A/G) GX (E/D) (T/S), which assumes an essential role in the binding of an oxygen molecule for catalysis.

2.7.1.4 Docking SDZ-88357 selective inhibitor in the CYP24A1 model

Schuster *et al.*[215] showed SDZ-88357 was a weak inhibitor of the CYP24A1 enzyme (> 1000 nM). Docking results showed the interaction between the nitrogen lone pair of

tetrazole and the haem iron at a distance of 5.56 $\mathring{A}$. There were hydrophobic interactions between the inhibitor with amino acid residues in the active site (Arg128, Leu129, Ile131, Trp134, Leu148, Met246, Phe249, Leu325, ala326, Val391, Pro392, Phe393, Thr395, His497, Gly499 and Thr500) (Figure 50). There was no hydrogen bond between SDZ-88357 and the CYP24A1 model. Overall the selectivity of DZ-88357 for CYP27B1 rather than CYP24A1 can be explains from docking experiments.
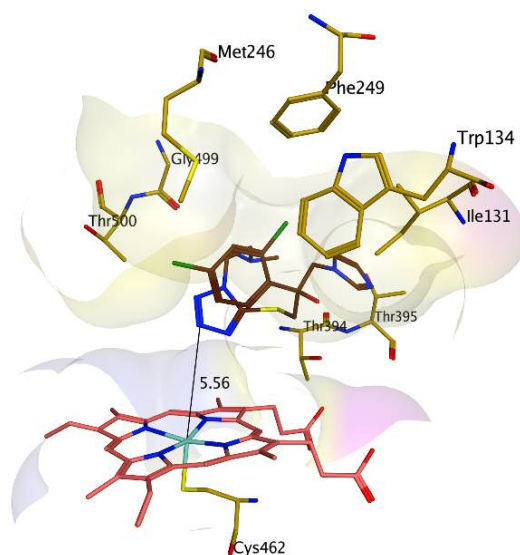
Figure 50: Docking output for SDZ-88357 inhibitor on the CYP24A1 model

2.7.1.5 Docking SDZ-88357 selective inhibitor in the mutant CYP24A1 model

The observation from the docking output for the SDZ-88357 inhibitor on the CYP27B1 model showed the hydrogen bonds between amino acid residues in CYP27B1 model Arg107, Asn387 and Asp320, which play an important role in fixing the SDZ-88357 inhibitor in the active site close to the haem iron of the CYP27B1 model.

Furthermore, to confirm the role of Arg107, Asn387 and Asp320 in CYP27B1, mutations were introduced in CYP24A1 by changing the amino acid residues Leu148, His497 and Gly499 in mutant for amino acid residues Asp148, Arg497 and Asn499.

The docking results showed the interaction between SDZ-88357 and the mutant CYP24A1 model was the same as the docking output result of SDZ-88357 complexed with the CYP27B1 model. In addition, the distance between the lone pair of electrons of terazole and the haem iron was 2.38 Å. There were hydrophobic interactions between the inhibitor with amino acid residues in the active site (Ile131, Ala326, Val391, Pro392 and Thr500) (Figure 51). In addition, SDZ-88357 making three additional hydrogen

bonds with amino acids Asp148, Arg497 and Asn499, the length of the hydrogen bonds in mutant CYP24A1 were the same as in the CYP27B1 model (Table 18)
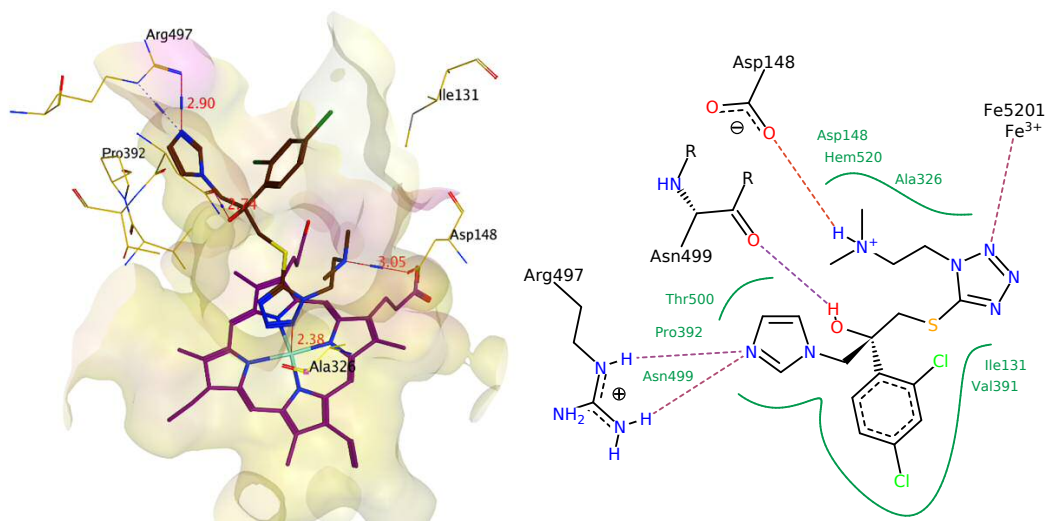
Figure 51: 3D and 2D for SDZ-88357 selective inhibitor on the mutant CYP24A1 model

	Distance	Hydrogen bond
1	2.90 Å	Between imidazole of SDZ-88357 and Arg497
2	2.74 Å	Between hydroxyl group of SDZ-88357 and Asn499
3	3.03 Å	Between tertiary amine of SDZ-88357 and Asp148

Table 18: Hydrogen bonds between SDZ-88357 and amino acids residues of CYP27B1 model

2.8   Conclusions

A homology model of CYP27B1 was built using MOE and was approved for stereochemical and amino acid environment quality using appropriate programmes, with further optimisation of the active site architecture achieved by molecular dynamics simulations. Understanding protein-ligand interactions is essential for designing more selective and potent CYP24A1 inhibitors. This chapter uses a combination of homology modelling, molecular dynamics simulations, and molecular docking to understand the satisfactory explanation of the binding selectivity of the CYP27B1 model with a natural substrate and with selective inhibitor complexes. Monitoring RMSD during simulations indicated that it is a structurally stable homology model. Docking results for CYP27B1 showed amino acids Arg107, Asn387 and Asp320 have an important role in binding interaction to form hydrogen bonds with inhibitors. Asp320 was part of the α I helix for the CYP27B1 model, which covers the haem binding site and contains SRS-4, and plays a key role in orientating the ligand at the active site by electrostatic interactions. Asp320 has the important acid - alcohol pair situated in the I-helix with the conserved sequence (A/G) GX (E/D) (T/S), which assumes an essential role in the binding of an oxygen molecule for catalysis.

The main strategy that can be used to build an inhibitor selective for CYP24A1 over CYP27B1, is to design compound unable to form hydrogen bonding interactions with CYP27B1 especially with Arg107, Asn387 and Asp320. Although additional H-bonds can improve binding and potentially inhibitory activity of hCYP24A1 this is at the expense of selectivity. Incorporating larger hydrophic pharmacophores capable of filling the active site cavity and formation of multiple hydrophic interactions with active site amino acids would result in CYP24A1 inhibitory activity and crucially selectivity with respect to CYP27B1.

2.9 Experimental

2.9.1 Docking method

The important amino acid residues of the active pocket Gln82, Ile131, Trp134, Met246, Ala326, Glu329, Thr330, Val391, Phe393, Thr394, Ser498, Gly499 and Tyr500[191,190] were selected, and then the selection was extended to 12.5 Å in order to include in the docking site the haem and the access tunnel to the catalytic site. Ligand database in mol 2 format, prepared using MOE[237], was used as input for the docking calculations. The iron atom of the catalytic site was set as an essential pharmacophoric feature. Ligand docking was performed using the default values, configured with flexible torsion, external formal charges, Corina for generation, volume overlap factor 2.9, and ligand clash factor 0.6, and no water molecules were considered. 100 output solutions were obtained from each compound, and visual inspection in MOE was used to identify the interaction between ligand and protein.

2.9.2 Method of Molecular dynamic

A molecular dynamics simulation was run on the CYP27B1 model alone and the CYP27B1 model in complex with SDZ-88357. Both PDB files were first optimised with protein preparation wizard in Maestro, version 11.0.015[256] by assigning bond orders, adding hydrogen, and correcting incorrect bond types. A default quick relaxation protocol was used to minimise the MD systems with the Desmond program[256]. In Desmond, the volume of space in which the simulation takes place (the global cell) is built up by regular 3D simulation boxes, which was utilised as part in this system for protein interactions. The orthorhombic water box (volume = 501882 $Å^3$) allowed for a 10 $Å$ buffer region between protein atoms and box sides. Overlapping water molecules were deleted, and the systems were neutralised with Na^+ ions and salt concentration 0.15 M.

Force-field parameters for the CYP27B1 model and the CYP27B1 model-SDZ-88357 complex were assigned using the OPLS_ 2005 force-field, that is, a 5 ns or 50 ns molecular dynamic run in the NPT ensemble ($T = 300$ K) at a constant pressure of 1 bar. Energy and trajectory atomic coordinate data were recorded at each 1.2 ns.

Molecular dynamics simulation for drug design is ideally conducted at a temperature range of 300 -314 K. In this study, molecular dynamics simulation was done at 300 K and 312 K.
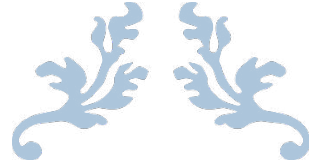
CHAPTER THREE

Lead 1

3   Lead compounds

Previous screening of the SPECS database[221] identified some promising CYP24A1 inhibitors with moderate inhibitory activity[222]. The most potent CYP24A1 inhibitors were selected as lead compounds (lead 1 and lead 2) for further development. In addition, lead 3 was synthesised in our laboratory[191] and showed potent CYP24A1 inhibitory activity (Figure 52).

LEAD1
$IC_{50} = 4.2$ µM [222]

LEAD 2
$IC_{50} = 5.5$ µM [222]

LEAD 3
$IC_{50} = 0.40$ µM [191]
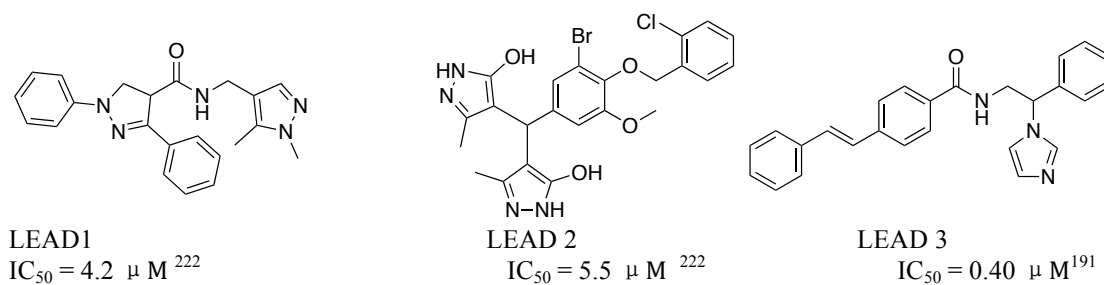
Figure 52: CYP24A1 inhibitors with moderate inhibitory activity

Firstly, docking of lead 1 into its binding site of the CYP24A1 model[191] was performed. Lead 1 was able to access the channel of the active site, and the nitrogen atom of heterocycle of lead 1 interacted perpendicularly with the haem iron with a distance of 2.35 Å. In addition, there were hydrophobic interactions between lead 1 and the amino acids of the active site of the human CYP24A1 model[191] (Arg128, Leu148, Ala326, Thr330, Val391, Phe393 and Thr394). Furthermore, docking studies showed there was no hydrogen bond between lead 1 and the active site of the CYP24A1 model (Figure 53).
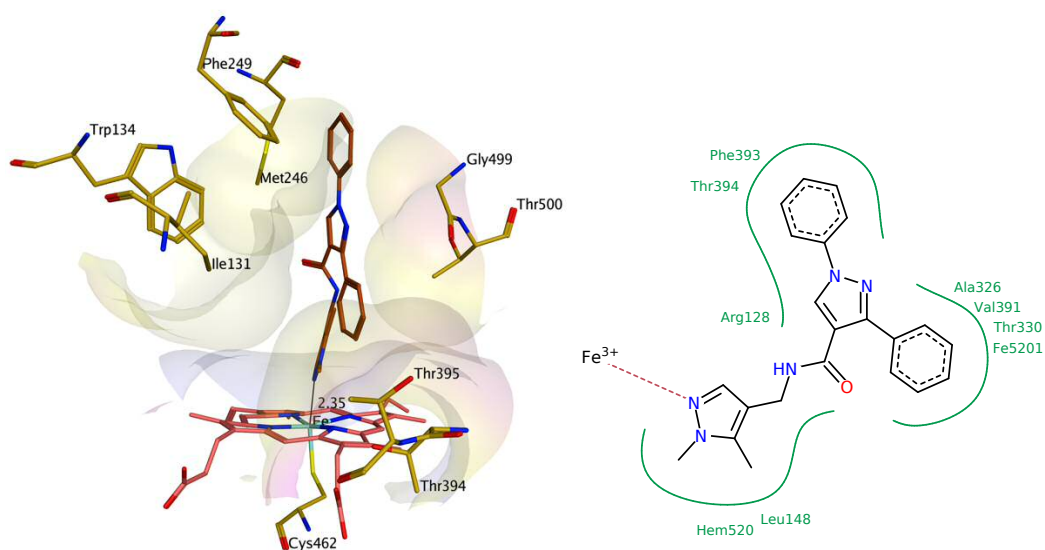
Figure 53: Docking data for lead 1

This chapter is concerned with the modification and development of lead 1, specifically through (i) replacement of the dimethyl pyrazole with basic heterocyclic rings to enhance binding interaction with the haem moiety (ii) substitution of the benzene rings to explore structure-activity relationship, and (iii) variation in the length of the linker to determine the optimum length to allow complete filling of the hydrophobic channel of the CYP24A1 active site (Figure 54).

(ii) different substitutions to explore SAR

(i) replacement with basic heterocycle e.g. pyridine, imidazole, triazole

(iii) varying chain length to optimise fit in active site
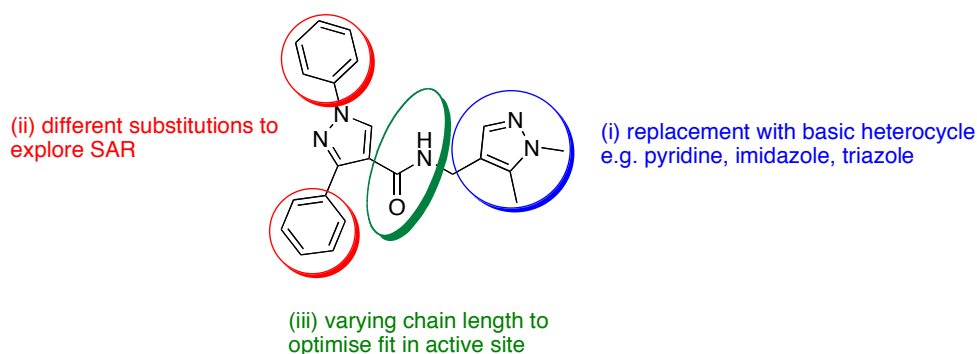
Figure 54: The modification of lead 1

This chapter is divided into 8 parts as follows:

1. Development of lead 1 by replacement with pyridine (pyridine pyrazole derivatives)
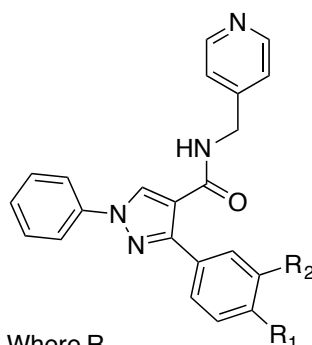
Where R
5a = R_1 = H, R_2 = H
5b = R_1 = F, R_2 = H
5c = R_1 = Cl, R_2 = H
5d = R_1 = H, R_2 = OCH$_3$
5e = R_1 = CH$_3$, R_2 = H

Figure 55: 3-(substituted/ unsubstituted phenyl)-1-phenyl-*N*-(pyridin-4-ylmethyl)-1*H*-pyrazole-4-carboxamide derivatives

2. Development of lead 1 by variation of the liker and replacement with imidazole
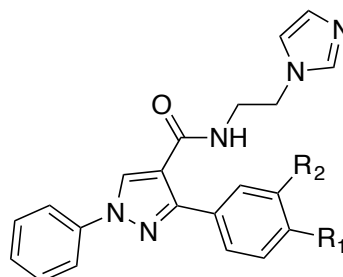
Where R
10a = R$_1$ = H,   R$_2$ = H
10b = R$_1$ = F,   R$_2$ = H
10c = R$_1$ = Cl,   R$_2$ = H
10d = R$_1$ = H,   R$_2$ = OCH$_3$
10e = R$_1$ =CH$_3$, R$_2$ = H

Figure 56: *N*-(2-(1*H*-imidazol-1-yl) ethyl)-3-(substituted/ unsubstituted phenyl)-1-phenyl-1*H*-pyrazole-4-carboxamide derivatives

3. Development of lead 1 by variation of the liker and replacement with triazole
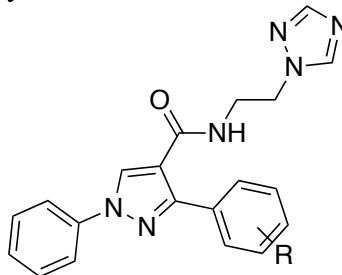
Where R
R = H, F, Cl,OCH$_3$ and CH$_3$

Figure 57: *N*-(2-(1*H*-1,2,4-triazol-1-yl)ethyl)-1-phenyl-3-(substituted/ unsubstituted phenyl)-1*H*-pyrazole-4-carboxamide derivatives

4. Development of lead 1 by changing the heterocycle
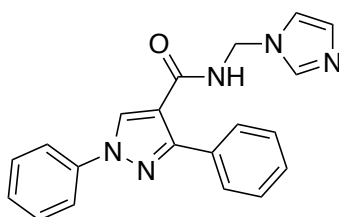
Figure 58: 1-(1,3-diphenyl-1*H*-pyrazol-4-yl)-2-(1*H*-imidazol-1-yl)ethan-1-one

5. Molecular modelling
6. Biological assay
7. Conclusions
8. Experimental
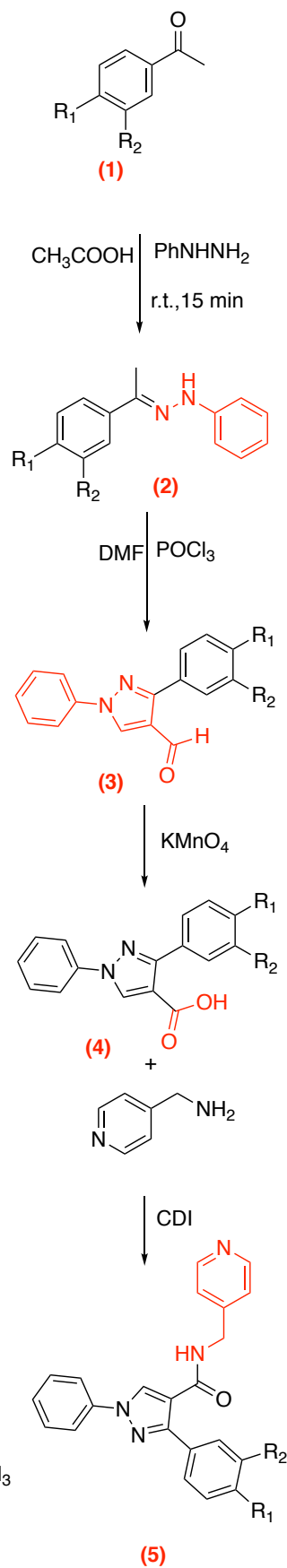
Where R
a = R_1 = H, R_2 = H
b = R_1 = F, R_2 = H
c = R_1 = Cl, R_2 = H
d = R_1 = H, R_2 = OCH_3
e = R_1 = CH_3, R_2 = H

Scheme 4: Synthetic pathway of pyridine pyrazole derivatives

3.1   Synthetic pathway of pyridine pyrazole derivatives

Literature methodology was searched using SciFinder® to determine the appropriate methods for the synthesis of the pyridine series. A four-step synthetic pathway was devised and is shown in (Scheme 4).

3.1.1   Synthesis of imines (2)

2a = R₁ = H,   R₂ = H
2b = R₁ = F,   R₂ = H
2c = R₁ = Cl,   R₂ = H
2d = R₁ = H,   R₂ = OCH₃
2e = R₁ =CH₃, R₂ = H
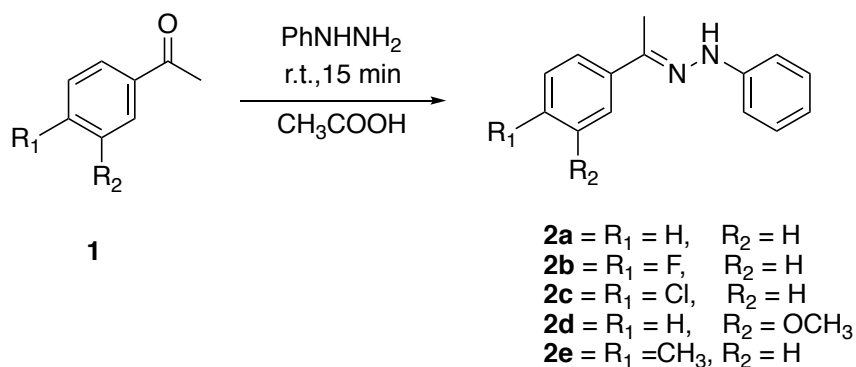
Scheme 5: Synthesis of imines

Acetophenone derivatives were reacted with phenyl hydrazine and acetic acid as the catalyst and solvent at room temperature, which provided the corresponding imines **2a - 2e**. The yield for *N*-[1-(4-fluorophenyl)ethylidene]-*N'* -phenyl-hydrazine (**2b**) was much lower than the theoretical yield and also lower than the literature yield[257] with loss during filtration (Scheme 5).

Compounds **2a - 2e** were synthesised with yields ranging from 20 - 100 %. Unfortunately, this method did not work particularly well with the 3-methoxyacetophenone **2d**, as the expected product **2d** did not precipitate out in acetic acid. This could be due to the polar nature of the methoxy group, as compound **2d** was very soluble in acetic acid preventing it from precipitating out.

Furthermore, this was also supported by a lower Log P (2.86) compared with **2a**, **2b**, **2c** and **2e** where Log P was between 2.98 and 3.54. As a result, the procedure for 3-methoxyacetophenone derivatives **2d** was attempted using ethanol as the solvent and acetic acid as the catalyst. Evaporation under vacuum was performed to remove the ethanol resulting in a precipitate. TLC was performed for all the imine reactions and the same R_f value was obtained for the products and their corresponding acetophenone, suggesting that both were the same compound. However, different colours were observed due to discolouration on light exposure. Therefore, storing the compounds

wrapped in foil was very important (Table 19). Owing to the light and air sensitivity of the compounds, they were not stable enough to perform NMR (rapid discolouration and decomposition), therefore they were used immediately in the next reaction step.

cpd	Yield %	m.p.		Colour and appearance
		Practical	Lit.	
2a	100	80 - 82°C	108 °C[258]	White solid
2b	20	88 – 90°C	134 - 136°C[257]	light yellow crystals
2c	89	109 - 111°C	102°C[259]	light yellow crystals
2d	78	61 - 62 °C	Unrecorded	light yellow solid
2e	100	80 - 82 °C	80°C[260]	light yellow solid

Table 19: Synthesis data for step (1)

3.1.2   Synthesis of pyrazole-4-carbaldehyde derivatives (3)

The Vilsmeier-Haack reaction is an important method for the synthesis of various aromatic aldehydes[261]; in 1927 Vilsmeier and Haack observed that *N*-dimethylformamide in the presence of $POCl_3$. Furthermore, the reaction of carbonyl compounds with the Vilsmeier reagent, *N,N*-dimethylformamide, and phosphorus oxychloride (DMF/$POCl_3$) is also used in a variety of cyclisation and cyclo aromatisation reactions[262]. The Vilsmeier reagent serves not only as a formylating agent, but also as an activating reagent for carboxylic acids to give esters, amides, and acid chlorides and for alcohols to give alkyl chlorides. Overall, the Vilsmeier reagent is used to generate a halomethyleneiminium salt used in the production of many heterocyclic compounds. Phosphorus oxychloride reacts with tertiary amides to give an adduct that exhibits salt-like properties, as shown in (Figure 59).

Initial electrophilic attack of Vilsmeier-Haack reagent on hydrazone yielded the intermediate I which subsequently looses a molecule of HCl to provide intermediate II. The nucleophilic attack by N-H group initiates the cyclisation and the resulting pyrazole intermediate losses $(CH_3)_2NH$ to give the more stable pyrazole derivative. The pyrazole formed reacts with another molecule of Vilsmeier-Haack reagent in an electrophilic substitution process giving an iminium salt (Intermediate III), which is hydrolysed to corresponding 4-formyl pyrazole[262]. The electrophilic attack of first Vilsmeier-Haack complex at the probable attacking site of hydrazones results into cyclisation. While

electrophilic attack of second Vilsmeier-Haack complex forms formyl product after hydrolysis.

The optimum reaction temperature was 60 °C; at lower temperatures, the reaction did not reach completion. Hydrolysis was done by pouring the reaction mixture on crushed ice (100 mL), and was made basic (pH 8.0) using 10% NaOH (Figure 59).
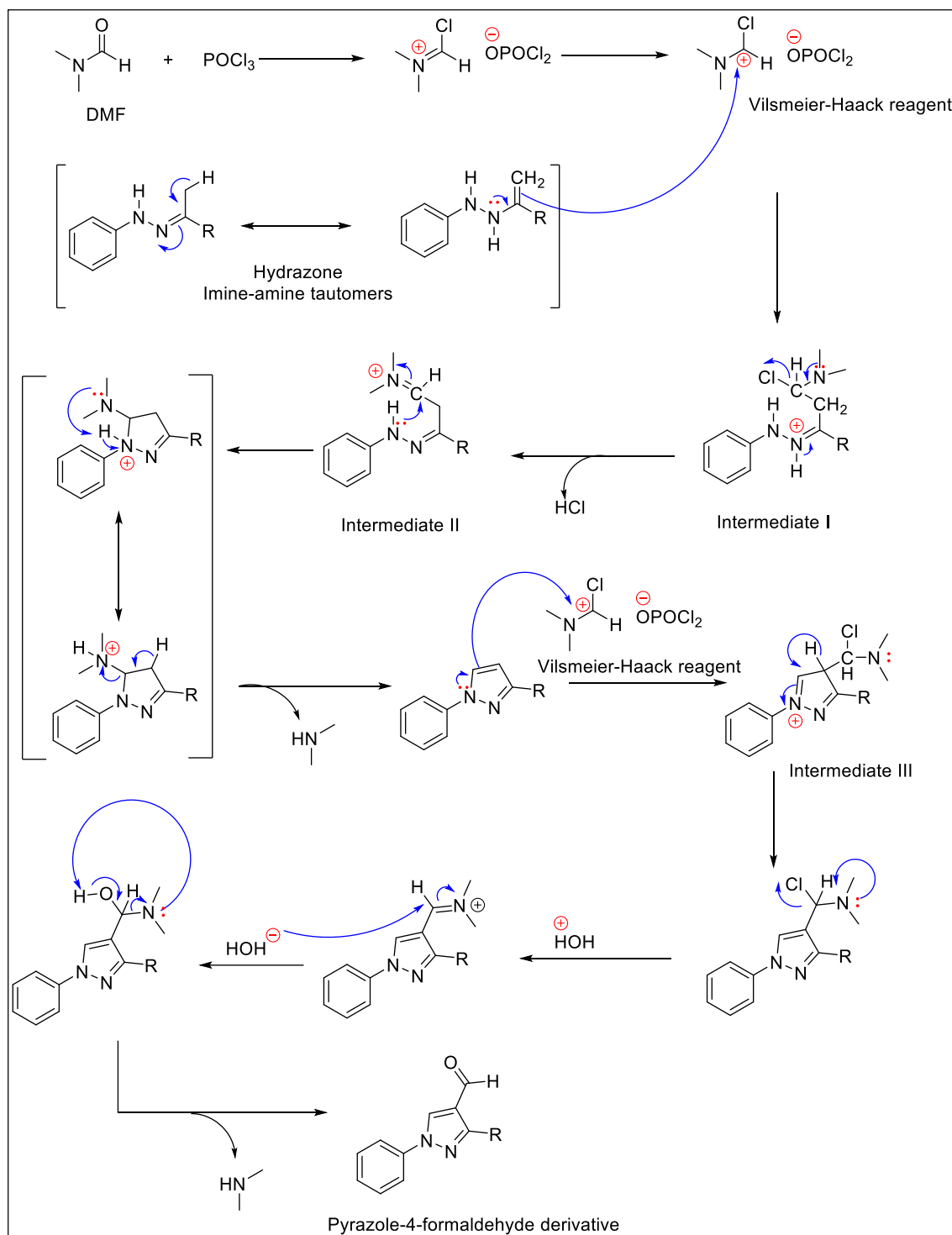
Figure 59: Vilsmeier-Haack reaction mechanism
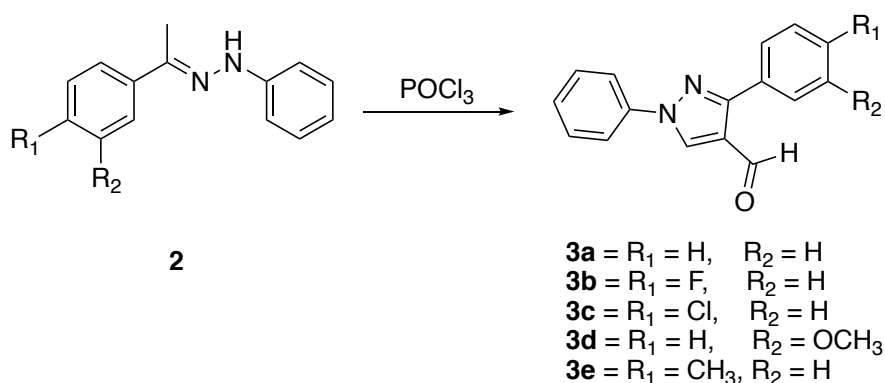
Scheme 6: Synthesis of pyrazole-4-carbaldehyde (3)

The method used by Yadlapalli *et al.*[263] was followed to prepare compounds **3a - 3e**. This method began with the imines **2a - 2e** being dissolved in dry DMF, then $POCl_3$ was added slowly dropwise at 0 ℃ as a catalyst, and the mixture was stirred for 2 h at 90 ℃. 10 % aqueous NaOH solution was added to neutralise the solution to form the corresponding pyrazole-4-carbaldehyde; **3a - 3e** were obtained in yields ranging from 39 to 60 % (Scheme 6).

This method was straightforward and successful although flash column chromatography was performed on **3d** to purify the product. Good yields were obtained for all the aldehydes (Table 20).

^{1}H NMR confirmed the presence of the CHO group with a peak at approximately $\delta \cong 10.07$ for **3a - 3e** as a singlet. In addition, the H group for pyrazole appeared as a singlet at $\delta \cong 8.5$ for all the compounds, thus confirming the presence of pyrazole.

cpd	Yield %	m.p.		Colour and appearance
		Practical	**Lit.**	
3a	66	128 - 130℃	144 -146℃[258]	light yellow solid
3b	44	150 - 154℃	173 -175℃[257]	light yellow crystals
3c	61	139 - 142℃	138 - 140℃[1]	light yellow crystals
3d	69	70 - 74℃	102℃[6,7]	light yellow crystals
3e	39	125 - 128℃	120℃[8]	light yellow solid

Table 20: Synthesis data for step (2)

3.1.3   Synthesis of 1*H*-pyrazole-4-carboxylic acid derivatives (4)

Aldehydes can be oxidised to carboxylic acids with both mild and strong oxidising agents. Typical oxidising agents for aldehydes include potassium permanganate and potassium dichromate in acid solution and Tollens reagent[264].

Potassium permanganate, which is an inexpensive oxidant that has been widely used in organic synthesis and is a highly efficient and effective nonselective oxidant when used in aqueous solutions[265]. Potassium permanganate is preferred when an organic compound contains only one site for oxidation. In addition, when the aqueous solution is made acidic by the addition of mineral acid, the rate of reaction increases. Under acidic conditions, permanganate is reduced to soluble manganese (II) or (III) salts; in addition, the rate of the reaction is also accelerated by the addition of sodium or potassium hydroxide as a basic medium[266].

The oxidation of aldehydes to carboxylic acids occurs in two steps. In the first step, one molecule of H_2O is added in the presence of an acid catalyst to generate a hydrate (Scheme 7).
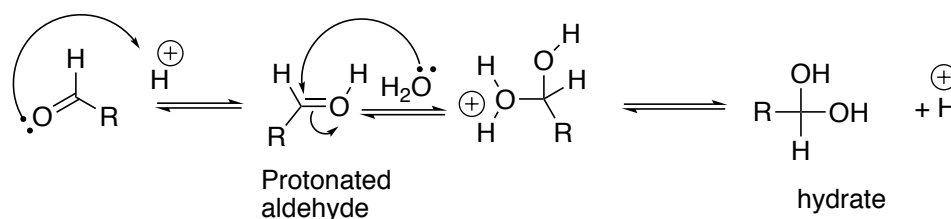
Scheme 7: Formation hydrate ion

In the second step, the hydrate is oxidised to the carboxylic acid, thus formally eliminating H_2O.

The method of Pandey *et al.*[258] was followed to synthesise compounds **4a - 4e**. This procedure involved compounds **3a - 3e,** which were dissolved in a mixture of *t*-butanol/H_2O, and then, a solution of $KMnO_4$ was added dropwise with stirring at 75 ℃. Aqueous KOH solution was then added until alkaline pH to dissolve the product in water (as salts). The mixture was filtered to produce a dark paste-like solid, and the

filtrate was acidified with conc. HCl to release the carboxylic acid group. Next, the product was recrystallised to give the corresponding compounds **4a - 4e.**

4a = R_1 = H, R_2 = H
4b = R_1 = F, R_2 = H
4c = R_1 = Cl, R_2 = H
4d = R_1 = H, R_2 = OCH_3
4e = R_1 = CH_3, R_2 = H
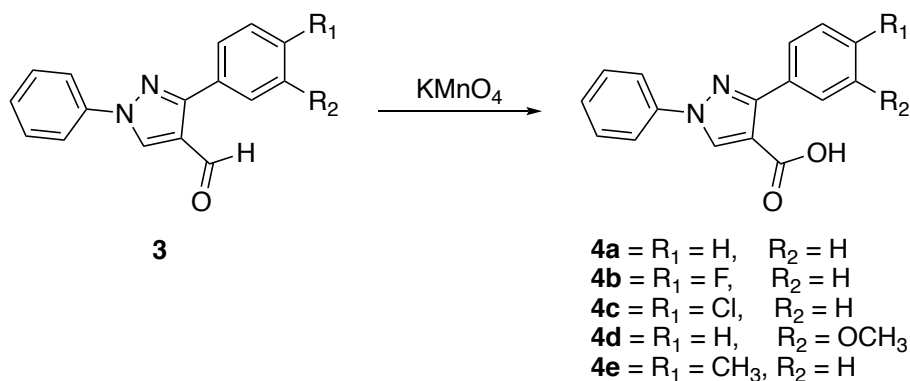
Scheme 8: Synthesis of 1*H*-pyrazole-4-carboxylic acid derivatives (4)

Pyrazole carboxylic acids were obtained in yields ranging from 54 to 80% for compounds **4a, 4c, 4d** and **4e**. These compounds precipitated as a white solid and appeared as one spot in TLC (CH_2Cl_2: CH_3OH, 9:1 v/v). Compound **4b** contained impurities and required two recrystallisations, the first using ethanol, and then the second with acetonitrile; subsequently, a lower yield of 37 % was obtained (Scheme 9). ^{1}H NMR confirmed the presence of the COOH group with a peak at $\delta \cong 12.59$ for **4a** - **4e** as a singlet. In addition, the H group for pyrazole appeared as a singlet at δ 9.03 to 9.08, thus confirming the presence of pyrazole. The compound 3-(3-methoxyphenyl)-1-phenyl-1*H*-pyrazole-4-carboxylic acid **4d** was a novel compound, so was further characterised by the ^{13}C NMR spectra, which confirmed the COOH group at δ 163.74. Finally, 3-(3-methoxyphenyl)-1-phenyl-1*H*-pyrazole-4-carboxylic acid **4d** was analysed with microanalysis, which confirmed $C_{17}H_{14}N_2O_3$ and M. Wt. 294.30 by calculation of the % of C, H and N (Table 21).

Cpd	Yield %	m.p.		Microanalysis	Colour and appearance
		Practical	Lit.		
4a	83	198 - 200 ℃	200 - 202℃ [258]	-	pale yellow solid
4b	37	222 - 223℃	229 - 230℃ [257]		white crystals
4c	80	238 - 240 ℃	240 - 242℃ [257]		white solid
4d	70	139 - 140℃	Novel	Anal. Calcd for $C_{17}H_{14}N_2O_3$ (294.30): C 69.38%, H 4.79%, N 9.51%. Found C 69.40%, H 4.66%, N 9.51%	white solid
4e	54	235 – 238℃	191 - 193℃ [258]	-	white solid

Table 21: Synthesis data for step (3)

3.1.4 Synthesis of 1*H*-pyrazole-4-carboxamide derivatives (5)

N,N′ -Carbonyldiimidazole (CDI) is one of several commonly used reagents for coupling carboxylic acids with aliphatic or aromatic amines to form an amide[267]. The mechanism involves a nucleophilic attack of the carboxylate to the carbonyl carbon of CDI, resulting in the formation of the active imidazolide and the liberation of carbon dioxide. The aliphatic amine then attacks the intermediate structure leading to coupling of the amine with the carboxylic acid to form an amide group.

4

5a = R_1 = H, R_2 = H
5b = R_1 = F, R_2 = H
5c = R_1 = Cl, R_2 = H
5d = R_1 = H, R_2 = OCH_3
5e = R_1 = CH_3, R_2 = H
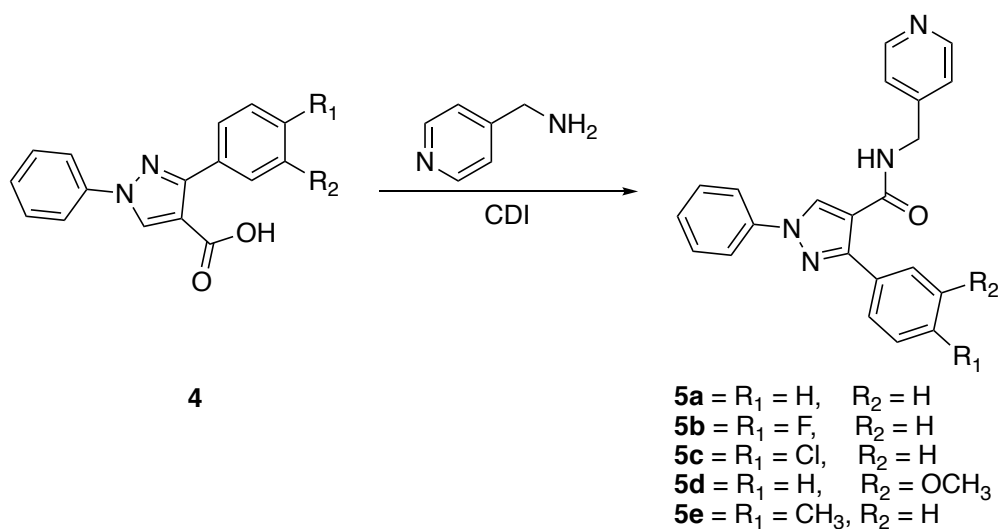
Scheme 9: Synthesis of 1*H*-pyrazole-4-carboxamide derivatives

The procedure of Aboraia *et al.*[210] was used to synthesise the final compounds **5a - 5e**. This was achieved by reaction of carboxylic acids **4a - 4e** with in *N,N'* -carbonyldiimidazole for 1 h at 0 ℃ to form the intermediate compound, followed by a solution of 4-aminomethylpyridine. After 20 h at room temperature, the product was obtained in a yield ranging from 4 to 58 %. Compound **5e** did not precipitate and required further purification (Scheme 9).

^{1}H NMR confirmed the presence of the amide group with a peak at $\delta \cong 8.80$ for **5a - 5e** as a triplet except for compound **5b,** which was found as a pseudo triplet.^{13}C NMR spectra confirmed the amide group (CONH), which was observed at $\delta \cong 162.7$ for **5a - 5e** (Table 22).

cpd	Yield %	m.p.	Microanalysis/ HRMS	Colour and appearance
5a	39	188 - 190℃	**Anal. Calcd for C$_{22}$H$_{18}$N$_4$O (354.40): C 74.56%, H 5.12%, N 15.80%. Found C 74.36%, H 5.04%, N 15.84%**	White solid
5b	58	199 - 200℃	**Calculated mass: 373.1459 [M + H]$^+$, measured mass: 374.1493 [M + H]$^+$**	White crystals
5c	37	222 - 223℃	**Anal. Calcd for C$_{22}$H$_{17}$ClN$_4$O (388.85): C 67.95%, H 4.41%, N 14.41%. Found C 67.87%, H 4.31%, N 14.58%**	White solid
5d	33	143 - 144℃	**Anal. Calcd for C$_{17}$H$_{14}$N$_2$O$_3$ (294.30): C 69.38%, H 4.79%, N 9.51%. Found C 69.40%, H 4.66%, N 9.51%**	White solid
5e	4	191 - 193℃	**Anal. Calcd for C$_{23}$H$_{20}$N$_4$O · 0.3 H$_2$O (373.85): C 73.89%, H 5.47%, N 14.98%. Found C 73.72%, H 5.40%, N 14.59%**	White solid

Table 22: 1*H*-pyrazole-4-carboxamide derivatives

3.2   Development of lead 1 by replacement with imidazole

This involved the coupling of the carboxylic acid with aminoethylimidazole dihydrochloride salt (**9**), which was synthesised as shown in Scheme 11.

a = R_1 = H, R_2 = H
b = R_1 = F, R_2 = H
c = R_1 = Cl, R_2 = H
d = R_1 = H, R_2 = OCH$_3$
e = R_1 = CH$_3$, R_2 = H
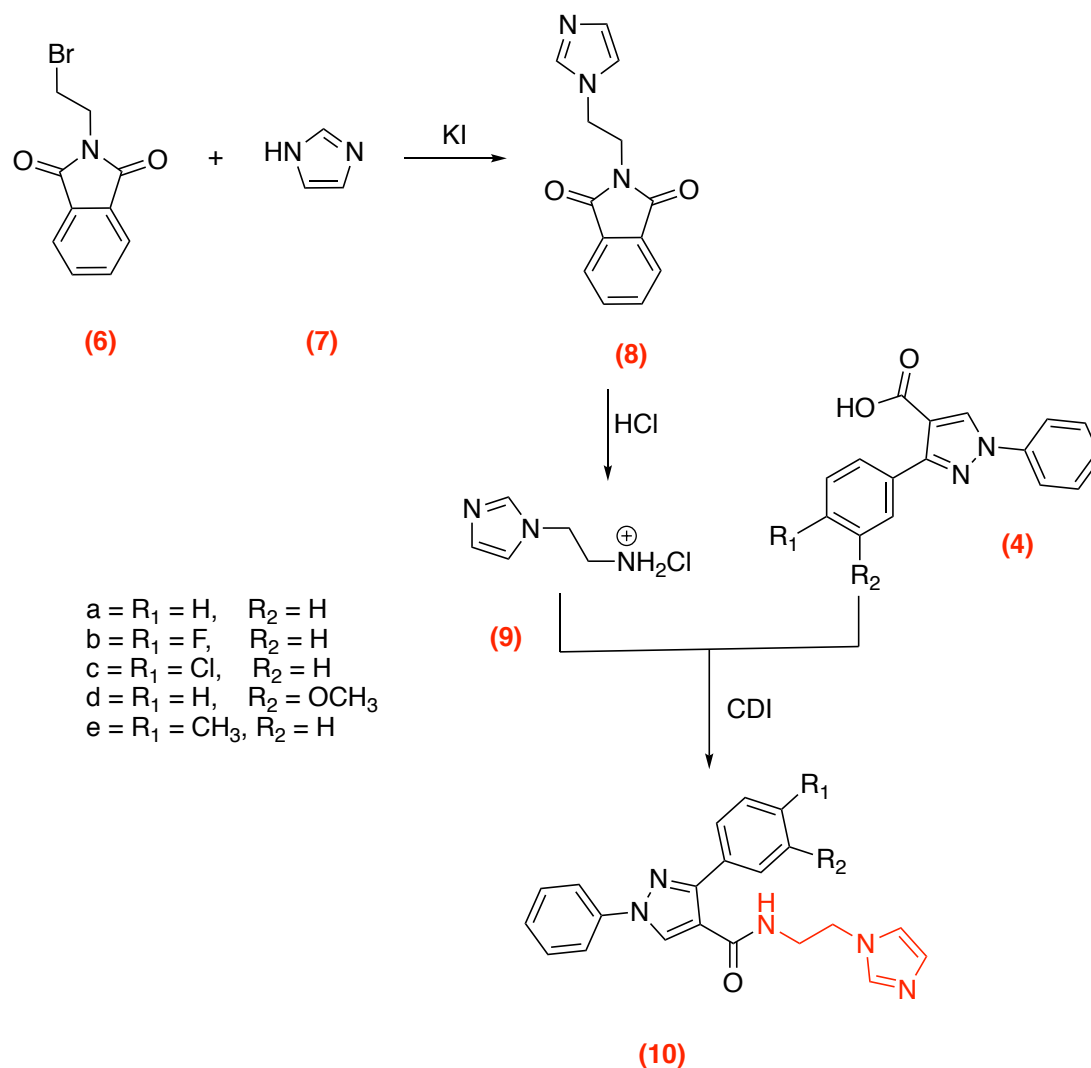
Scheme 10: Synthetic pathway of imidazole-pyrazole derivatives

3.2.1   Synthesis of *N*-(2-(1*H*-imidazol-1-yl)ethyl)-3-(substituted/ unsubstituted phenyl)-1-phenyl-1*H*-pyrazole-4-carboxamide (10)

3.2.1.1   Synthesis of 2-(2-(1*H*-imidazol-1-yl)ethyl) isoindoline-1,3-dione (8)
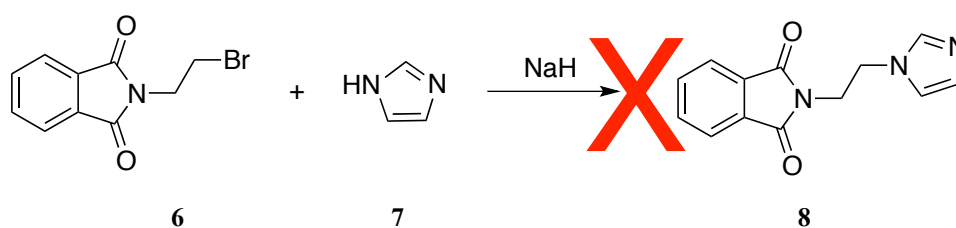
Scheme 11: 2-(2-(1*H*-imidazol-1-yl)ethyl) isoindoline-1,3-dione (8)

Many methods were attempted to prepare compound **8**. The first method followed the procedure of Buchhoiz *et al.*[268]; this method involved a reaction between 2-(2-bromoethyl)isoindoline-1,3-dione **6** and imidazole **7** in the presence of NaH (Scheme 12) as a base catalyst to form compound **8**, which gave a yellow viscous liquid that was recrystallised with isopropanol (Scheme 11). The resulting white precipitate was analysed by ^{1}H NMR. However, this confirmed that a carboxylic acid rather than the product was obtained. The reported carboxylic acid resulted from ring opening of imidazolylethylphthalamide, as reported by Ye *et al.*[269] where the presence of imidazole can enhance the rate of hydrolysis of the adjacent amide in a basic medium. As a result, the method of Buchhoiz *et al.*[268] was unsuccessful for producing compound **8** (Scheme 12)
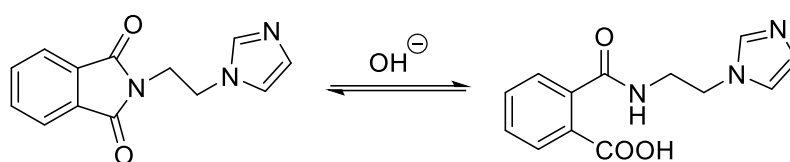
Scheme 12: Ring opening of imidazolylethylphthalamide

A second method followed the procedure of Hay *et al.*[270]; this used another base catalyst (potassium carbonate) rather than NaH in an attempt to synthesise 2-(2-(1*H*-imidazol-1-yl)ethyl)isoindoline-1,3-dione **8**.
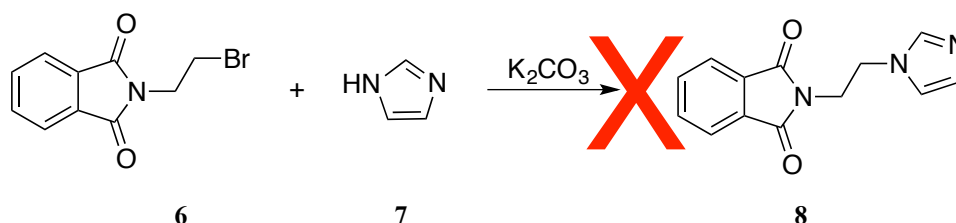
Scheme 13: Unsuccessful method to produce compound 8

This method was unsuccessful for producing compound **8** (Scheme 13), and the resulting product on analysis by ^{1}H NMR shows that carboxylic acid rather than the product was obtained[271] (Scheme 14).
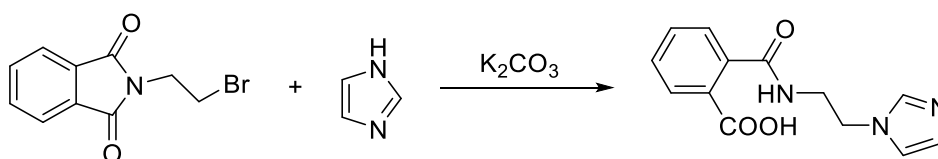
Scheme 14: Effect of K$_2$CO$_3$ on bromoethylphthalamide

Lastly, the method of Popkov and Skvortsova[272] was attempted, in which melted imidazole **7** was refluxed with bromoethylphthalamide **6**, and potassium iodide was added to convert bromide into iodide, as it is a better leaving group (Scheme 15).

6   **7**   **8**
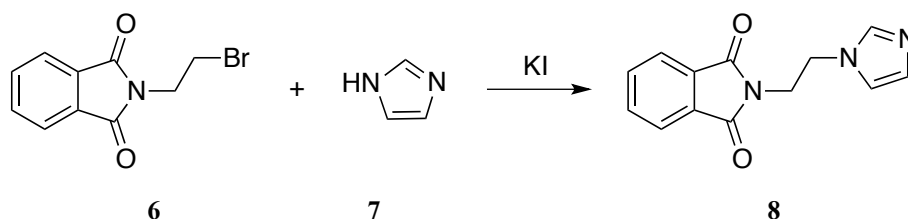
Scheme 15: Using the imidazole as both reactant and solvent

The reaction was refluxed for 3 h, after which toluene was added, and the reflux continued for a further 20 h. The product was obtained in a yield of 49 % after recrystallisation with isopropanol (Table 23).

Cpd	Yield %	m.p.		Colour and appearance
		Practical	**Lit.**	
8	83	126 - 130℃	155 – 157 ℃[272]	White solid

Table 23: Identification data for compound 8

3.2.1.2   Synthesis of 1-(2-ammonioethyl)-1*H*-imidazol-3-ium chloride (9)

The Gabriel synthesis[273], for converting halides to primary amines, involves two major steps: the first step is the synthesis of alkylphthalimide. The second step is a synthesis of primary amines from *N*-alkylphthalimide. The formation of a primary amine from the *N*-substituted phthalimide involves either hydrolysis, by using an acid or a base, or hydrazine, and is called the Ing-Manske procedure[274] (Scheme 16).

Treatment of **8** with 1 *N* aqueous HCl and hydrazine monohydrate gave the product **9** in a yield of 82%. ^{1}H NMR confirmed the amine as a singlet at 8.61 (Table 24).

8   **9**
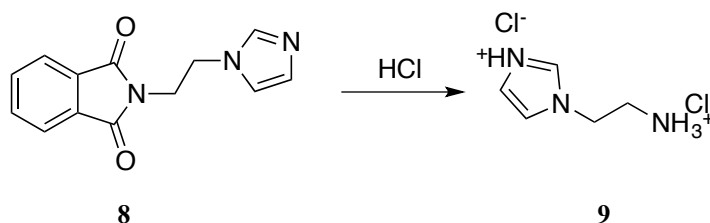
Scheme 16: 1-(2-Ammonioethyl)-1*H*-imidazol-3-ium chloride (9)

Cpd	Yield %	m.p.		Colour and appearance
		Practical	Lit.	
9	82	170 - 175℃	217 - 220℃[272]	Pale yellow solid

Table 24: Identification data for compound 9

3.2.1.3 Synthesis of: *N*-(2-(1*H*-imidazol-1-yl) ethyl)-3-(substituted/unsubstituted phenyl)-1-phenyl-1*H*-pyrazole-4-carboxamide (10)
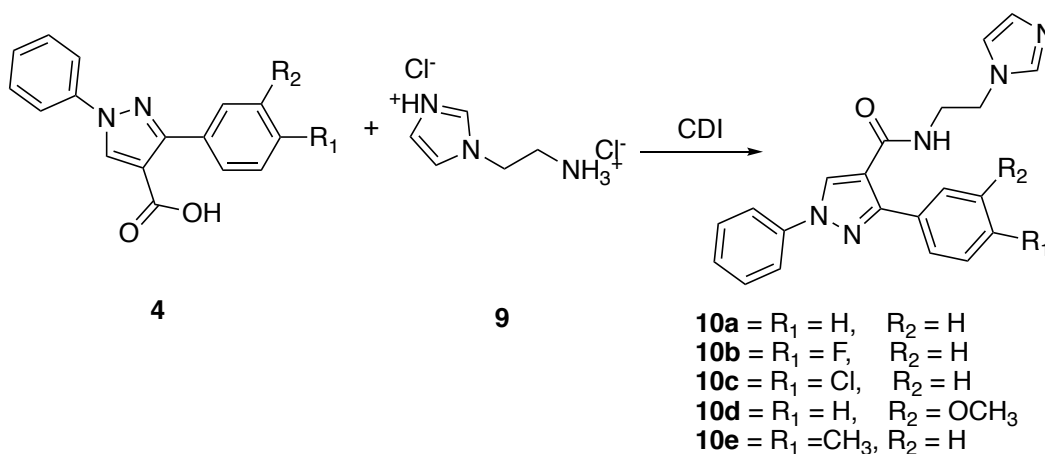
Scheme 17: *N*-(2-(1*H*-imidazol-1-yl) ethyl)-3-(substituted/unsubstituted phenyl)-1-phenyl-1*H*-pyrazole-4-carboxamide derivatives (10)

The procedure of Aboraia *et al.*[210] was used to synthesise the final sproducts of **10a - 10e**, achieved by reacting **4a - 4e,** with CDI as previously described (section 3.1.4). The carboxamide compounds **10a - 10e** were obtained in yields ranging from 6% to 40 % (Scheme 18). The methoxy derivative **10d** was an incomplete reaction after 20 h and an additional 2 eq of CDI was added and heated overnight at 60 ℃. The methyl derivative **10e** was obtained in a low yield because of impurities, as noted by TLC (EtOAc-CH$_3$OH 9:1 v/v) where three spots were observed (Table 25).

cpd	Yield %	m.p.	Microanalysis/ HRMS	Colour and appearance
10a	40	136 - 138℃	Anal. Calcd for $C_{21}H_{19}N_5O$ (357.42): C 70.57%, H 5.36%, N 19.59%. Found: C 70.28%, H 5.19%, N 19.29%	White solid
10b	29	158 - 160 ℃	Anal. Calcd for $C_{21}H_{18}FN_5O \cdot 0.3\ H_2O$ (380.81): C 66.60%, H 4.90%, N 18.31%. Found: C 66.57%, H 4.82%, N 17.99%	White crystals
10c	19	184 - 186 ℃	Anal. Calcd for $C_{21}H_{18}ClN_5O \cdot 0.1\ H_2O$ (393.66): C 64.07%, H, 4.65% N 17.79%. Found: C 63.92% H 4.33% N, 17.76%	White crystals
10d	32	108 - 112℃	Anal. Calcd for $C_{22}H_{21}N_5O_2 \cdot 0.2\ H_2O$ (391.04): C 67.57% H 5.51% N 17.91%. Found: C 67.21%, H 5.25% N 17.56%	Bright yellow crystals
10e	6	76 - 80℃	Anal. Calcd for $C_{22}H_{21}N_5O$ (371.44): C 71.14%. H 5.70%, N, 18.85%. Found: C 70.87%, H 5.74%, N 18.67%	White solid

Table 25: *N*-(2-(1*H*-imidazol-1-yl) ethyl)-3-(substituted/unsubstituted phenyl)-1-phenyl-1*H*-pyrazole-4-carboxamide derivatives (10)

3.3   Development of lead 1 by replacement with triazole

The method of synthesis for triazole derivatives was the same as described for imidazole derivatives (**10**) involving the reaction of the carboxylic acid (4) with corresponding aminoethyltriazole dihydrochloride salt (Scheme 18 and Figure 58).
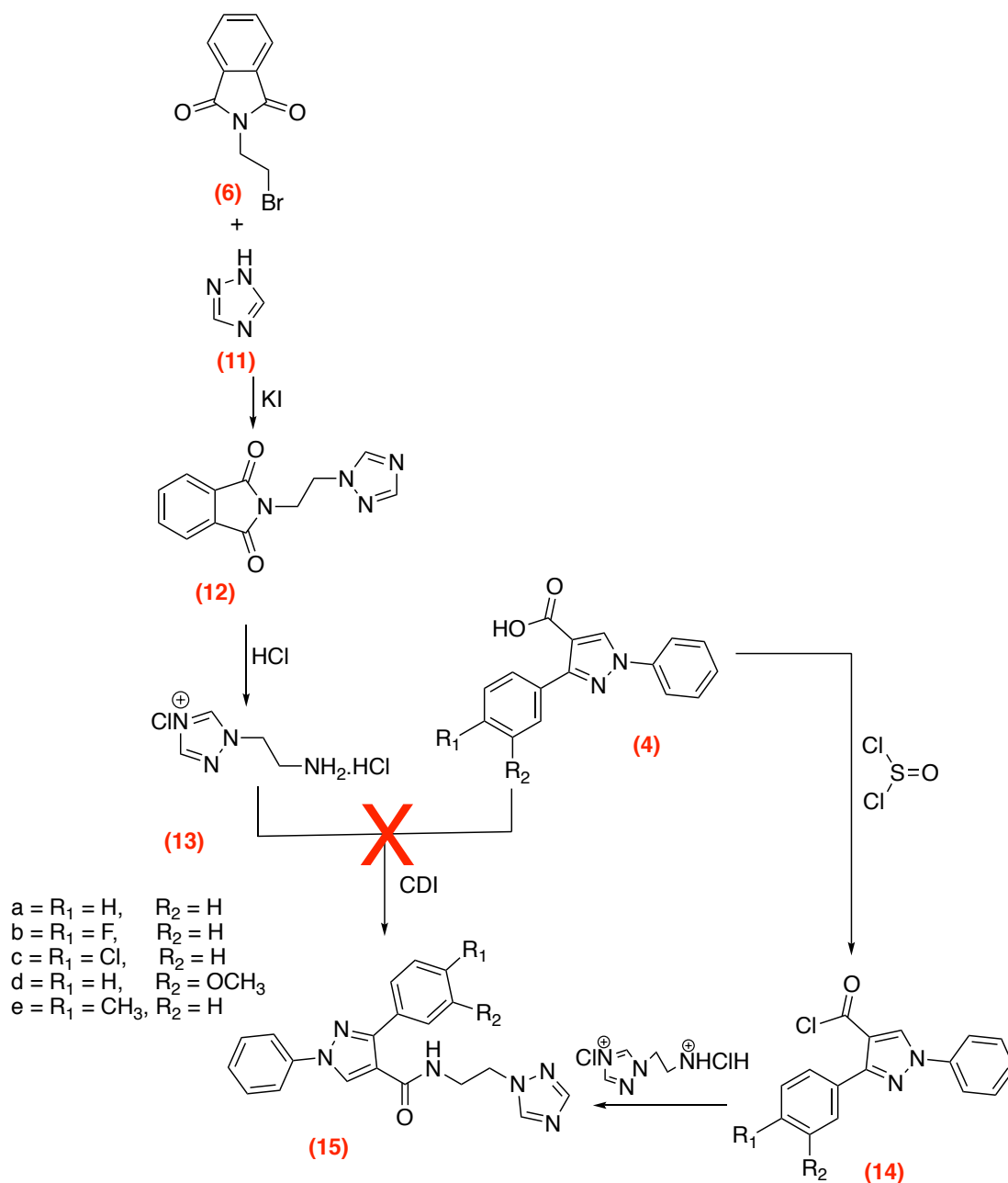
Scheme 18: Synthetic pathway of triazole-pyrazole derivatives

a = R$_1$ = H,   R$_2$ = H
b = R$_1$ = F,   R$_2$ = H
c = R$_1$ = Cl,   R$_2$ = H
d = R$_1$ = H,   R$_2$ = OCH$_3$
e = R$_1$ = CH$_3$, R$_2$ = H

3.3.1 Synthesis of *N*-(2-(1*H*-1,2,4-triazol-1-yl)ethyl)-1-phenyl-3-(substituted/ unsubstituted phenyl)-1*H*-pyrazole-4-carboxamide derivatives (15)

R$_1$ = H, F, Cl,OCH$_3$ and CH$_3$

Figure 60: *N*-(2-(1*H*-1,2,4-triazol-1-yl)ethyl)-1-phenyl-3-(substituted/unsubstituted phenyl)-1*H*-pyrazole-4-carboxamide derivatives

3.3.1.1 Synthesis of 2-(2-(1H-1,2,4-triazol-1-yl)ethyl)isoindoline-1,3-dione (12)

Preparation of compound **12** followed the same procedure as described for **8** (see 3.2.1.1) where triazole **11** instead of imidazole **7** was refluxed for 3 h, after which toluene was added and reflux continued for 20 h. The product was obtained in a yield of 46% after recrystallisation with isopropanol (Scheme 19).
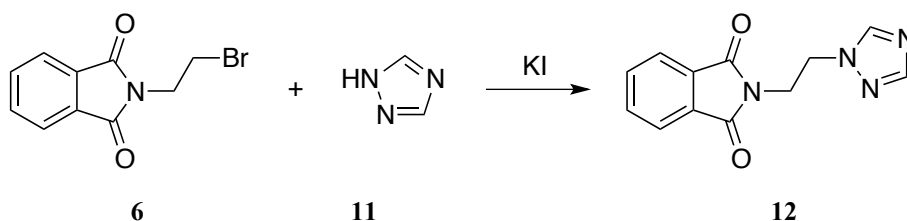
Scheme 19: 2-(2-(1*H*-1,2,4-triazol-1-yl)ethyl)isoindoline-1,3-dione (12)

^{1}H NMR confirmed the presence of triazole with peaks at δ 8.5 and 7.90. In addition, the ethyl linker appeared as triplets at δ 4.57 and δ 4.12 (Table 26).

Cpd	Yield %	m.p.		Colour and appearance
		Practical	Lit.	
12	46	152 - 156℃	166 - 169℃[272]	Yellow crystals

Table 26: Identification data for compound 12

3.3.1.2 Synthesis of 1-(2-ammonioethyl)-1*H*-1, 2,4-triazol-4-ium chloride (13)

Preparation of compound **13** followed the same procedure as described for **9** (see 3.1.4) where **12** was used instead of **8**. 1 N aqueous HCl and hydrazine monohydrate was added to help the breakdown of **12**. The product was obtained in a yield of 85 %. ^{1}H NMR confirmed the presence of the amine with peaks at δ 8.85. ^{13}C NMR spectra,

confirming the ethyl linker (CH$_2$), were observed at δ 46.7 and 37.7 (Table 27 and Scheme 20).

(12)   **(13)**
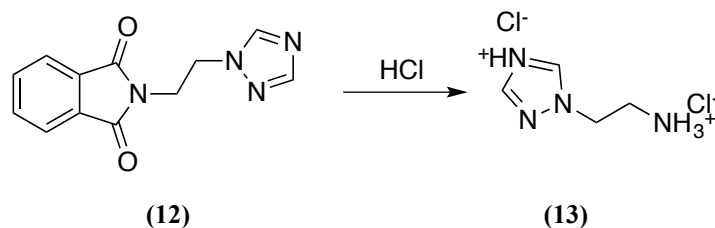
Scheme 20: 1-(2-Ammonioethyl)-1*H*-1, 2,4-triazol-4-ium chloride (13)

Cpd	Yield %	m.p.		Colour and appearance
		Practical	Lit.	
13	85	162 - 166℃	182 - 183℃[272]	Pale yellow crystals

Table 27: Identification data for compound 13

3.3.1.3   Synthesis of *N*-(2-(1*H*-1,2,4-triazol-1-yl)ethyl)-1-phenyl-3-(substituted/ unsubstituted phenyl)-1*H*-pyrazole-4-carboxamide derivatives (15)

The method followed was according to the procedure of Aboraia *et al.*[210], as previous described (see 3.1.4). The triazole-pyrazole series was difficult to synthesise by using coupling reagent CDI (Scheme 22). The carboxylic acids **4a - 4d** reacted with the coupling reagent rather than with 1-(2-ammonioethyl)-1*H*-1,2,4-triazol-4-ium chloride **13** and produced the imidazole-pyrazole compound. As a result, this method was unsuccessful for synthesising **15a - 15e** (Scheme 21).

Where R
R = H, F, Cl,OCH$_3$ and CH$_3$
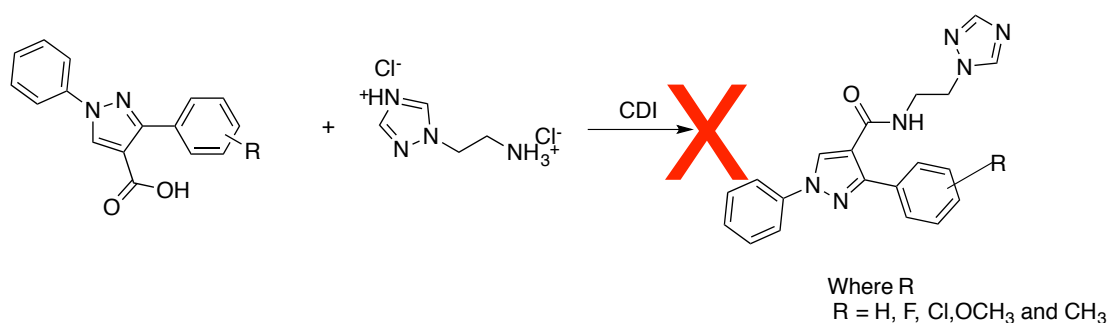
Scheme 21: The procedure of Aboraia *et al.*[210] which was used with the triazole-pyrazole series

a = R = H
b = R = F
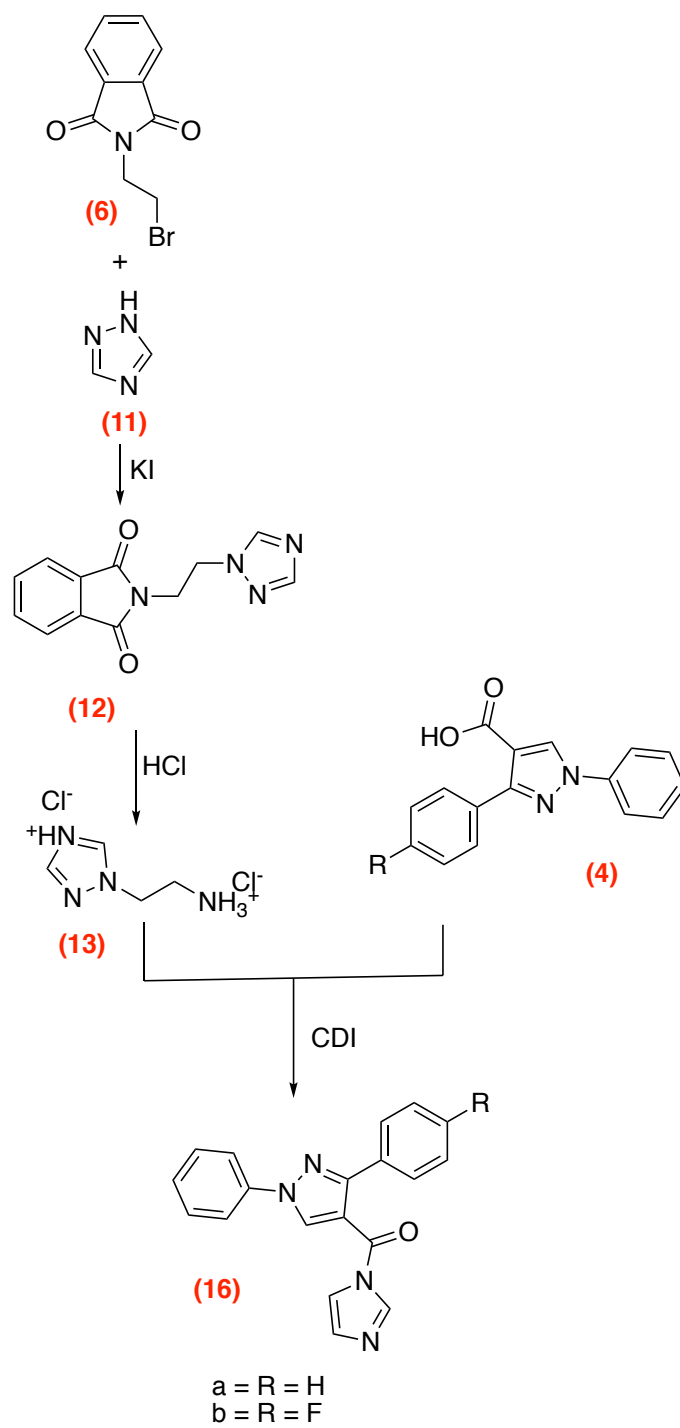
Scheme 22: Reacting the CDI with carboxylic acid instead of triazole

3.3.1.4 Synthesis of (3-(unsubstituted/substituted)-1-phenyl-1*H*-pyrazol-4-yl)(1*H*-imidazol-1-yl)methanone (16)

Where R
16a = R_1 = H
16b = R_1 = F
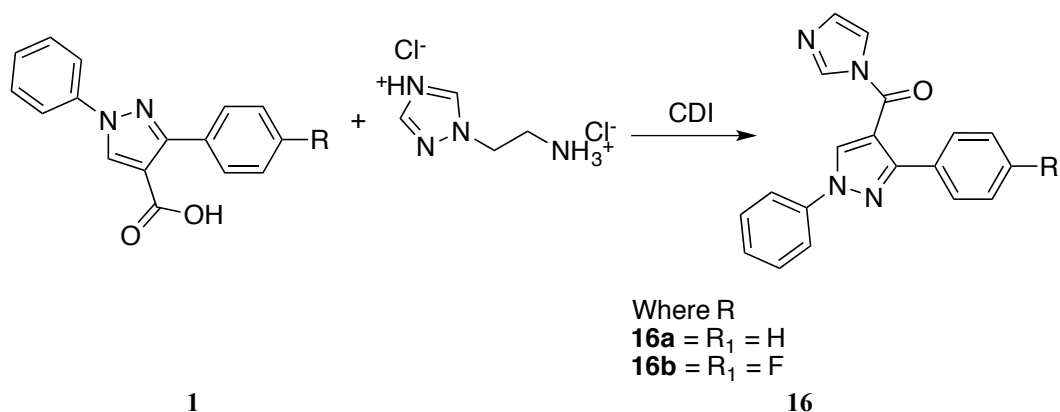
Scheme 23: Synthesis of (3-(unsubstituted/ substituted)-1-phenyl-1*H*-pyrazol-4-yl)(1*H*-imidazol-1-yl)methanone (16)

These compounds were produced by reacting the CDI with a carboxylic acid instead of with triazole (Scheme 23). The intermediate products had a yield of 42 and 39% respectively. ^{1}H NMR confirmed the presence of the imidazole, and there was no ethyl group in the aliphatic region (Table 28 and Scheme 22).

Cpd	Yield %	m.p.	HRMS	Colour and appearance
16a	42	118 - 120℃	Calculated mass: 314.1217 [M + H]$^+$, measured mass: 314.1209 [M + H]$^+$	White solid
16b	39	130 - 134℃	Calculated mass: 333.1152 [M + H]$^+$, measured mass: 333.1146 [M + H]$^+$	White solid

Table 28: Reacting of CDI with carboxylic acid

A second method followed the procedure of Khan e*t al.*[275] In this method, a two-step strategy for the preparation of **15a - 15e** was initiated using the acid chlorides **14b**, **14d** and **14e** rather than carboxylic acids **4** (Scheme 24).

14b = R_1 = F, R_2 = H
14d = R_1 = H, R_2 = OCH$_3$
14e = R_1 = CH$_3$, R_2 = H
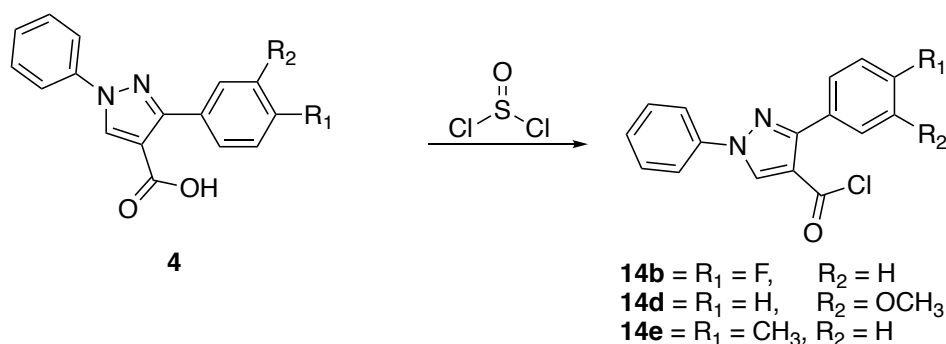
Scheme 24: Acid chloride derivatives

Carboxylic acid derivatives **4b, 4d** and **4e** were reacted with thionyl chloride. The reaction was refluxed for 6 h, which provided the corresponding acid chlorides, and the product was obtained in a yield ranging from 57 to 78 %. ^{1}H NMR confirmed the disappearance of the carboxylic acid (Table 29). The acid chlorides **14b**, **14d** and **14e** were coupled with **13** using CDI.

Cpd	Yield	m.p.		Colour and
	%	Practical	Lit.	appearance
14b	57	112 - 166℃	140 - 141℃[276]	White solid
14d	74	98 - 100℃	Unrecorded	White solid
14e	78	92 - 94℃	Unrecorded	White solid

Table 29: Identification data for compound 14

4e   **15e**
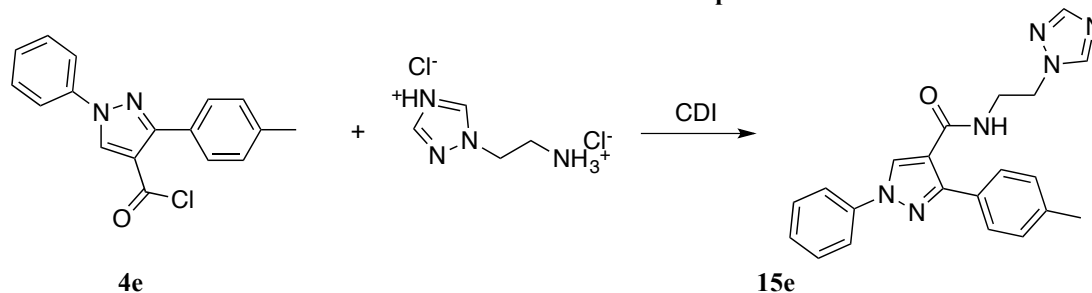
Scheme 25: *N*-((1*H*-1, 2, 4-triazol-1-yl) methyl)-3-phenyl-1-(*p*-tolyl)-1*H*-pyrazole-4-carboxamide **15e**

The reaction was successful for one derivative *N*-((1*H*-1, 2, 4-triazol-1-yl) methyl)-3-phenyl-1-(*p*-tolyl)-1*H*-pyrazole-4-carboxamide **15e** with a yield of 6 % (Scheme 26). The reaction resulted in a complex mixture (five spots on TLC), resulting in a very low yield after recrystallisation with methanol. However, it was unsuccessful for other derivatives (Table 30 and Scheme 25)

Cpd	Yield%	m.p.	HRMS	Colour and appearance
15e	6	142 - 148℃	Calculated mass: 373.1771 [M + H]$^+$, measured mass: 373.1772 [M + H]$^+$	White solid

Table 30: Identification data for compound 15e

3.4   Development of lead 1 by changing heterocycle

Variation in the length of the linker from two carbons to one carbon was investigated (Scheme 26)
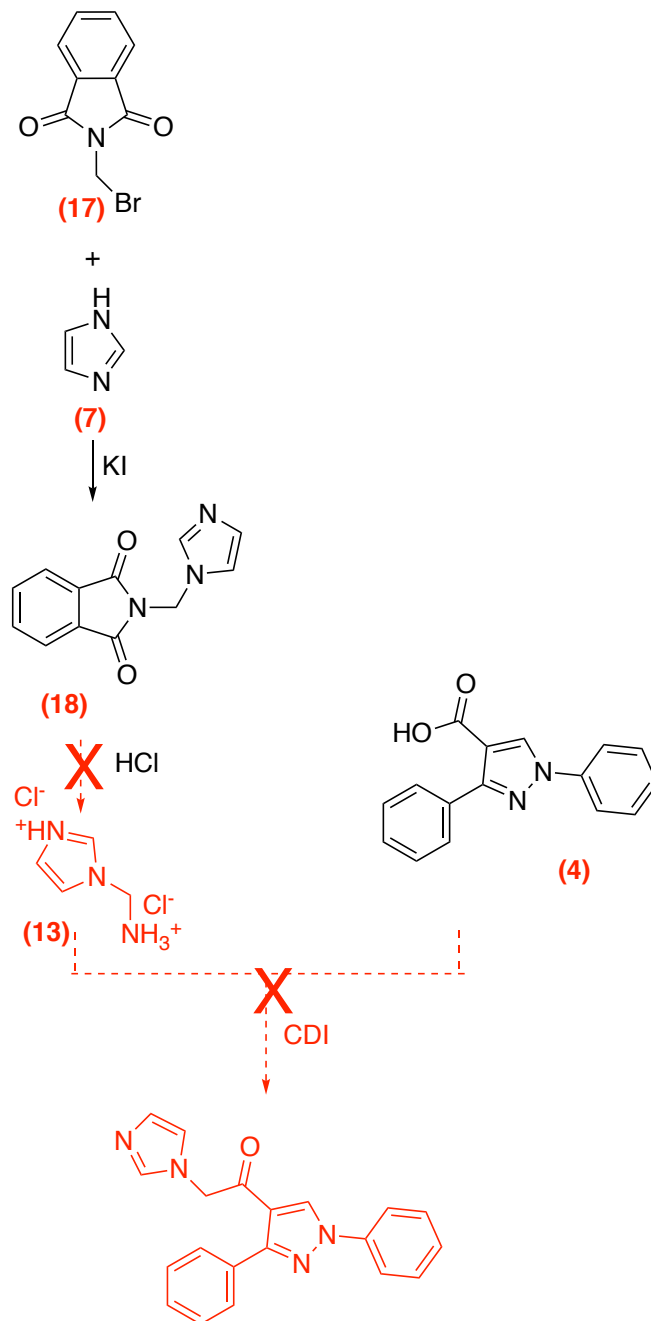
Scheme 26: Development of lead 1 by variation the linker

3.4.1 Synthesis of 2-((1*H*-imidazol-1-yl)methyl)isoindoline-1,3-dione (18)

The method of Popkov and Skvortsova[272] was followed, which used melted imidazole **7** refluxed with bromomethylphthalamide **17**, and potassium iodide was added. The reaction was refluxed for 3 h, after which time toluene was added and reflux continued for a further 20 h. The product was then recrystallised with methanol, and the product was obtained in a yield of 38% (Scheme 27).
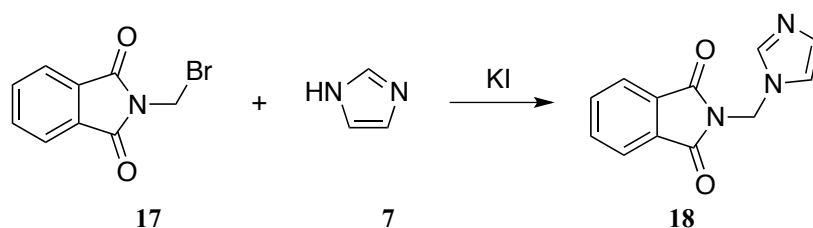
Scheme 27: 2-((1*H*-imidazol-1-yl)methyl)isoindoline-1,3-dione (18)

3.4.1.1 Synthesis of 2-((1*H*-1, 2, 4-triazol-1-yl) methyl)isoindoline-1,3-dione (19)

The method of Popkov and Skvortsova[272] was followed, which used melted triazole **11** refluxed with bromomethylphthalamide **17,** and potassium iodide was added (Scheme 28). The reaction was refluxed for 3 h, after which toluene was added and reflux continued for a further 20 h. The product was obtained in a yield of 57 % (Table 31).

cpd	Yield %	m.p.		Colour and appearance
		Practical	Lit.	
18	38	168 - 172℃	185 -187℃[277]	White crystals
19	57	164 - 168℃	169 - 170℃[272]	White crystals

Table 31: Identification data for 18 1and 19
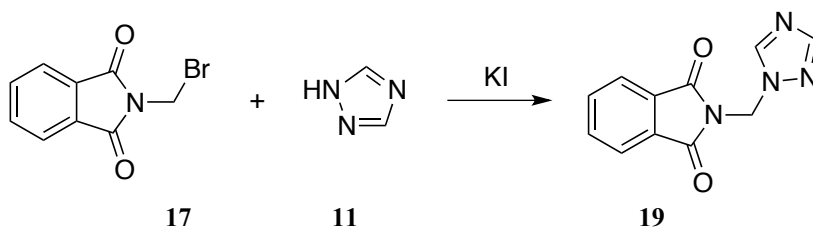
Scheme 28: 2-((1*H*-1, 2, 4-triazol-1-yl) methyl)isoindoline-1,3-dione (19)

Hydrolysis of compounds **18** and **19** was unsuccessful using hydrazine monohydrate and HCl, and instead produced an unknown compound was obtained (Scheme 29).
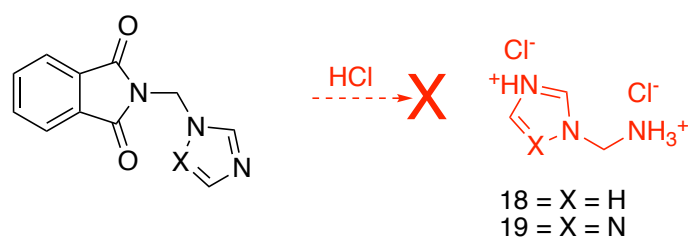
Scheme 29: Unsuccessful hydrolysis 18 and 19

This could be because compounds **18** and **19** have a self-destruct feature. The CH_2 linker was made stable by steric electronic effects, and imidazole has a catabolic effect leading to the hydrolysis of **18** and **19** to produce imidazolylmethylphthalamic acid. As a result, synthesis of **18** and **19** was unsuccessful, which led to the pathway of synthesis of the final compounds being blocked.

3.5   Molecular modelling

Our aim was to design inhibitors of CYP24A1 that are highly potent compared with ketoconazole and that would inhibit the catabolism of calcitriol while avoiding impairment of its synthesis. Furthermore, the designed compounds should be easily synthesised in our laboratory facilities. Crystal structures for human CYP24A1 and CYP27B1 are not available; therefore, the human CYP24A1 homology model was built in our laboratory[191] (the CYP27B1 model is detailed in Chapter 2). Ligands were designed and energy minimised using MOE[237], and then these were saved as a database file (mdb). Docking studies were performed using LeadIT 2.1.2 by BioSolve.IT[278]; this was used as it is one of the most suitable software programmes to perform docking studies.

3.5.1   Docking studies on the human CYP24A1 model with development of lead 1 by replacement with pyridine

To design new selective CYP24A1 inhibitors, the objective in this chapter was to create a new library of compounds and to dock them in the active site of the human CYP24A1 model[191]. The compounds were designed based on the structure of lead1[222], which has IC_{50} = 4.2 µM. Introducing the pyridine ring instead of the pyrazole ring in lead 1 gave compounds **5a** - **5e**, which accessed the CYP24A1 enzyme channel and reached the active site, and they were able to carry out hydrophobic interaction with amino acid residues in the active site (Table 32). **5a** - **5e** interacted perpendicularly with the haem iron of the CYP24A1 model with a distance ranging between 2.19 Å and 2.87 Å (Figure 61). Furthermore, **5a** and **5e** could make a hydrogen bond between the amide group and Glu329. However, there were poses for compound **5d**, where the methoxy group bonded perpendicularly with the haem iron with a distance of 2.35 Å. In addition, there were two extra hydrogen bonds – the first one between the amide group and Ala326 and the second bond between the pair of electron on the nitrogen atom of pyrazole and Glu329 (Figure 62).
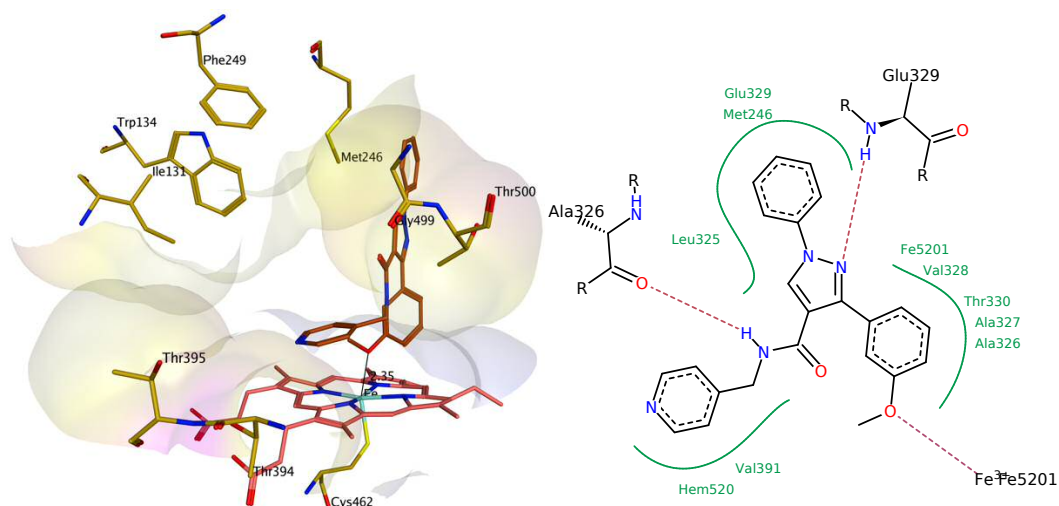
Figure 61: Example of some poses of compound 5d interacting with the haem iron via the methoxy group
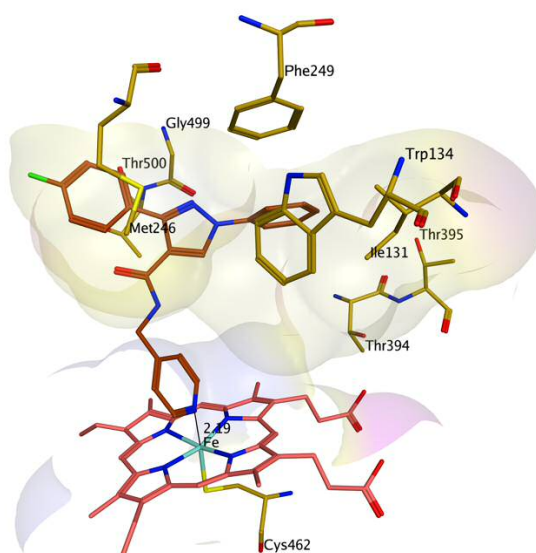
Figure 62: docking data for 5c

cpd	A	Key amino acids making interaction	
		B	**C**
5a	**2.35 Å**	**Glu329 - CONH**	**Met246, Phe249, Ala326, Ala327, Thr330, and Thr500**
5b	**2.87 Å**	**-**	**Ile131, Met246, Phe249, Leu325, Ala326, Glu329 and Thr330**
5c	**2.19 Å**	**-**	**Arg128, Ala327, Glu329, Val391, Thr394, Leu325, Ala326, Val328, Thr330 and Thr500**
5d	**2.33 Å**	**-**	**Arg128, Leu148, Glu329, Val391, Phe393, Thr394, Ala326, Thr330 and Thr500**
5e	**2.34 Å**	**Glu329 - CONH**	**Met246, Phe249, Leu325, Ala326, Ala327, Thr330 and Val391**

Table 32: (A) Distance between N of pyridine and iron of haem, (B) 3D and (C) 2D with binding interaction

3.5.2 Docking studies on the human CYP24A1 model with the development of lead 1 by replacement with imidazole

Inhibitor compounds have been designed by modification of lead 1, introducing the imidazole ring instead of the pyrazole ring and changing the linker to the two carbons. The designed compounds **10a** - **10e** interacted perpendicularly with the haem iron of the human CYP24A1 model with a distance ranging between 2.02 Å and 2.40 Å. All the designed compounds showed hydrophobic interaction with the amino acid residues (Table 33, Figure 63, 64 and 65). Furthermore, **10a**, **10c** and **10e** formed additional hydrogen bonds. However, there were poses for compound **10d**, where the methoxy group bonded perpendicularly with the haem iron with a distance of 2.13 Å. In addition, the amide **10e** interacted perpendicularly with the haem iron (Figure 66).
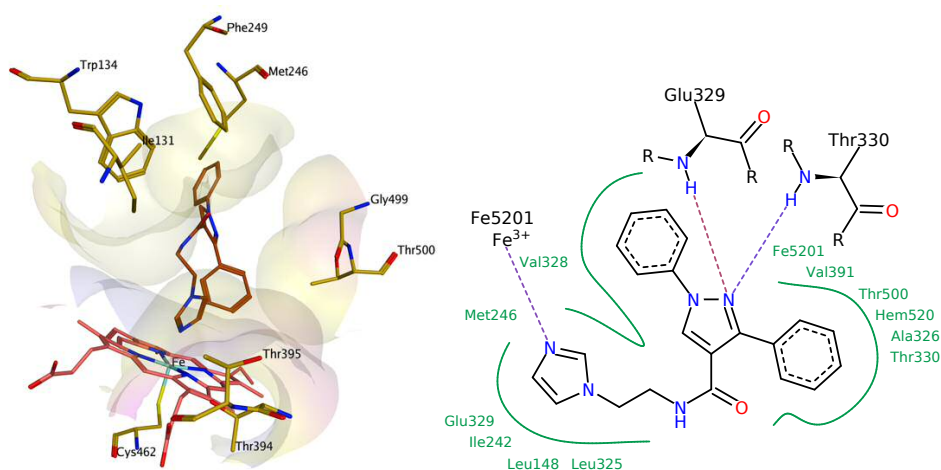
Figure 63: docking data for 10a
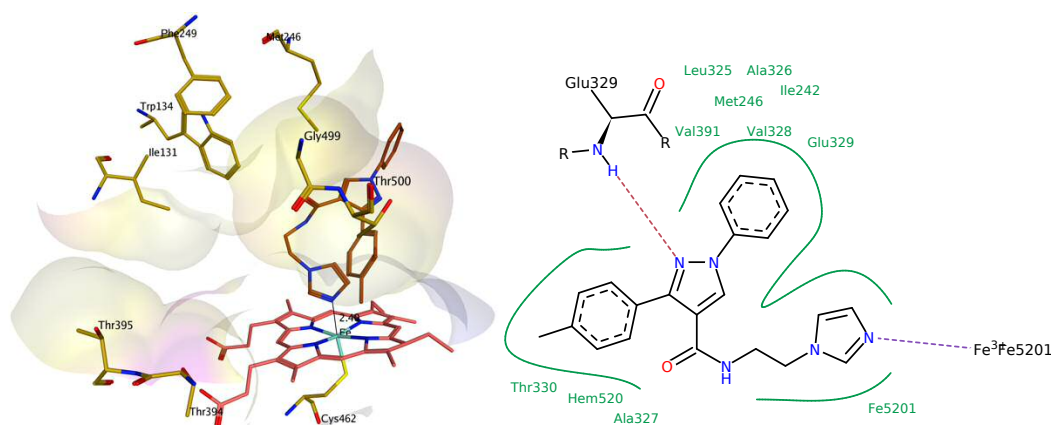
Figure 64: docking data for 10e

| cpd | A | Key amino acids making interaction | |
		B	C
10a	2.02 Å	Glu329 - CONH Thr330 - CONH	Leu148, Ile242, Met246, Leu325, Ala326, Ala327, Val328, Val391 and Thr500
10b	2.33 Å	-	Arg128, Ile131, Leu148, Ala326, Glu329 andThr330
10c	2.27 Å	Val328 - CONH	Phe212, Ile239, Ile242, Met246, Leu325, Ala326, Ala327, Glu329 and Thr330
10d	2.32 Å	-	Arg128, Leu148, Ala326, Thr330, Val391, phe393, Thr394 and Thr500
10e	2.40 Å	Glu329 - pyrazole	Ile242, Leu325, Ala326, Ala327, Val328, Thr330 and Val391

Table 33: (A) Distance between N of imidazole and iron of haem, (B) 3D and (C) 2D with binding interaction
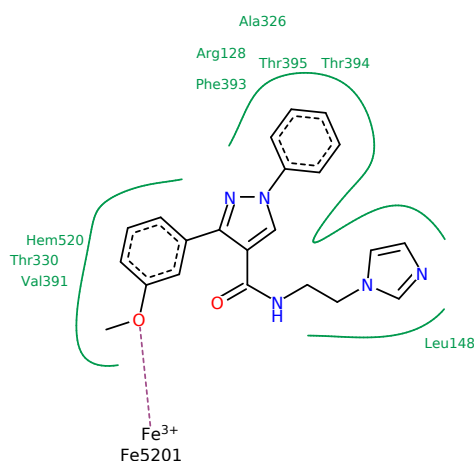
Figure 65: Example of some poses of compound 10d interacting with the haem iron via methoxy group
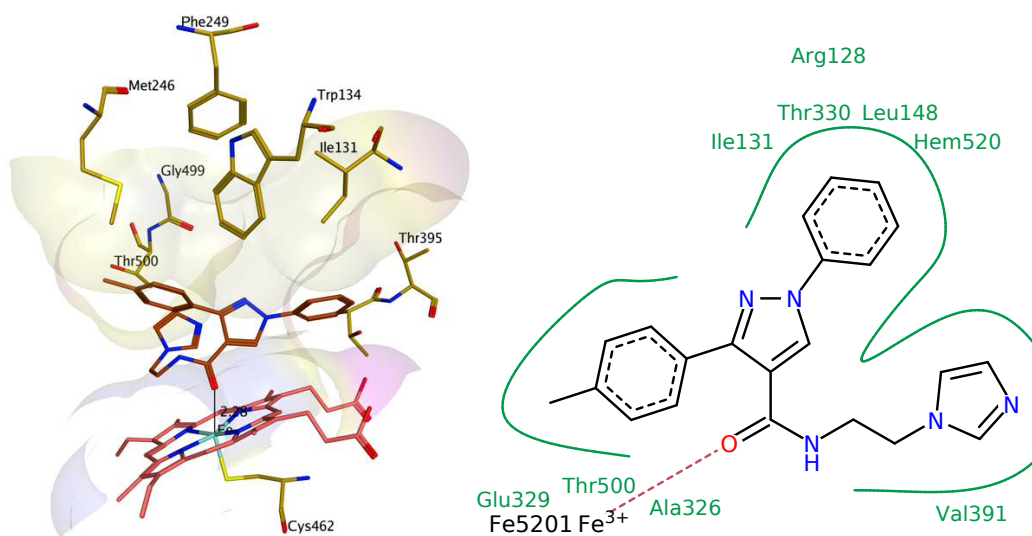
Figure 66: Example of some poses of compound 10e interacting with the haem iron via the carbonyl groups

3.5.3   Docking studies on the human CYP24A1 model with the development of lead 1 by replacement with triazole

The modification of lead 1 was achieved by introducing the triazole ring instead of the pyrazole ring and changing the linker to the two carbons. The designed compound **15e** interacted perpendicularly with the haem iron of human CYP24A1 with a distance of 2.15 Å. **15e** showed hydrophobic interactions with the amino acid residues (Ile242, Met246, Phe249, Ala326, Val328 Glu329 and Thr330, and Thr500) (Figure 67). Hydrogen bonds were observed between the amide group of **15e**, through the nitrogen atom and amino acid Leu325
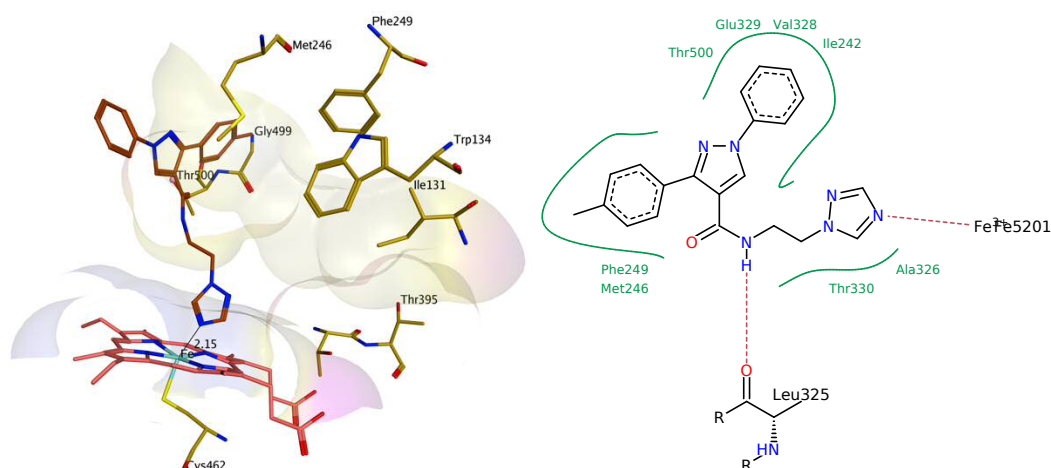
Figure 67: Example of some poses of compound 15e interacting with the haem iron via nitrogen of amide group

3.6 Biological assay

3.6.1 CYP24A1 inhibitor enzymatic assay[279]

All the final compounds **5a - 5e**, **10a - 10e**, **15e** and **16a** were evaluated by enzymatic assay to determine CYP24A1 inhibitory activity. The assay was performed according to the method of Zhu *et al.*[279] in general, the compounds displayed weak inhibition of CYP24A1 activity when compared with the ketoconazole standard, and were less active than lead 1 (IC_{50} 4.1 µM)[222]. The IC_{50} values ranged between 10.2 and 28.4 µM, and the best IC_{50} value was obtained for compound **10b** (10.2 µM). The IC_{50} values are the average (± 10 %) of two independent experiments (n = 2), which followed published paper methods[191,280, 281,282,283] The limit of two experiments is owing to the high cost of enzyme isolation and the appropriate vitamin D substrates.
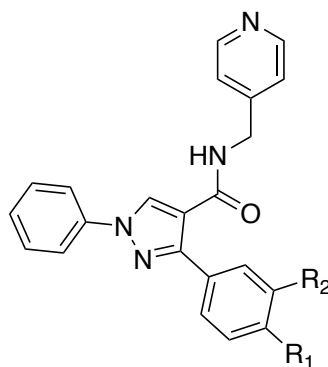
5a = R_1 = H, R_2 = H
5b = R_1 = F, R_2 = H
5c = R_1 = Cl, R_2 = H
5d = R_1 = H, R_2 = OCH_3
5e = R_1 = CH_3, R_2 = H

Figure 68: 3-(substituted/unsubstituted phenyl)-1-phenyl-*N*-(pyridin-4-ylmethyl)-1*H*-pyrazole-4-carboxamide derivatives
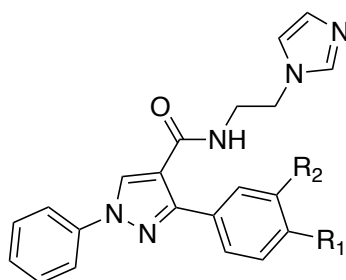
10a = R_1 = H, R_2 = H
10b = R_1 = F, R_2 = H
10c = R_1 = Cl, R_2 = H
10d = R_1 = H, R_2 = OCH_3
10e = R_1 = CH_3, R_2 = H

Figure 69: *N*-(2-(1*H*-imidazol-1-yl) ethyl)-3-(substituted/unsubstituted phenyl)-1-phenyl-1*H*-pyrazole-4-carboxamide derivatives
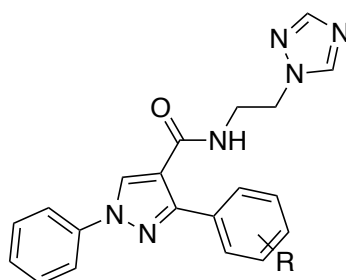
Where R R = H, F, Cl,OCH$_3$ and CH$_3$
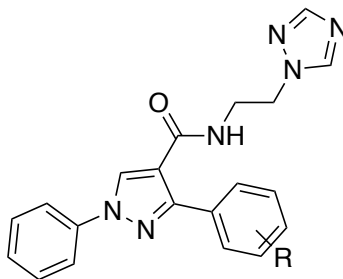
Figure 70: *N*-(2-(1*H*-1,2,4-triazol-1-yl)ethyl)-1-phenyl-3-(substituted/unsubstituted phenyl)-1*H*-pyrazole-4-carboxamide derivatives

The main difference between modified lead 1 compounds (**5a – 5e**), (**10a – 10e**) and **15e** was the variation in the length of the linker with different heterocyclic groups (pyridine, imidazole and triazole), where (**5a – 5e**) have one carbon linker attached to pyridine, (**10a – 10e**) have a two carbon linker to the imidazole group, and **15e** has a two carbon linker attached to the triazole group, to allow the complete filling of the hydrophobic channel of the CYP24A1 active site. The results of all designed compounds were less active than ketoconazole (0.51μM) and lead 1 (4.2 μM) (Figures 68 and 69). The best inhibitory activity was observed for the imidazole-pyrazole series with 4-fluoro substitution on the phenyl ring **10b** (Figure 70 and 71) that might be due to the two carbon linker, which leads to a reduction in the distance between the imidazole group and the haem iron of CYP24A1. In addition, Saberi *et al*.[281] reviewed how dependence on the basicity of the nitrogen heterocycle with inhibitory activity decreased with decreasing basicity (pKa: imidazole 14.5 > triazole 10 > pyridine 5.2), which correlates well with protein affinity (PA) (imidazole, PA = 247 kJmol^{-1} > triazole, PA = 231kJmol^{-1} > pyridine, PA = 206 kJmol^{-1}). Furthermore, Vinh *et al*.[280] showed that the imidazole interacts optimally through a N:-Fe^{III}-haem coordinate link, through the N3 of imidazole, however introducing an additional nitrogen in the heterocyclic ring (triazole) reduces the coordination potential through the N: due to the electron withdrawing effect of the additional electronegative nitrogen, this effect is increased with two additional nitrogens (tetrazole) drawing electron density from both sides of the coordinating nitrogen. Moreover, the inhibitor activity for **10b** was slightly greater than for **5b**; this might be because fluorine is more electronegative and much smaller in size than chlorine and has a greater ability than chlorine to attract electrons. It was found that **5d** (13.1μM) had the best inhibitory activity in the pyridine series, which could be related to computational molecular docking of **5d** in the human CYP24A1 homology model; this would predict some poses interacting with the haem iron via

the methoxy group and enable it to make two additional hydrogen bonds with Ala326 and Glu329.
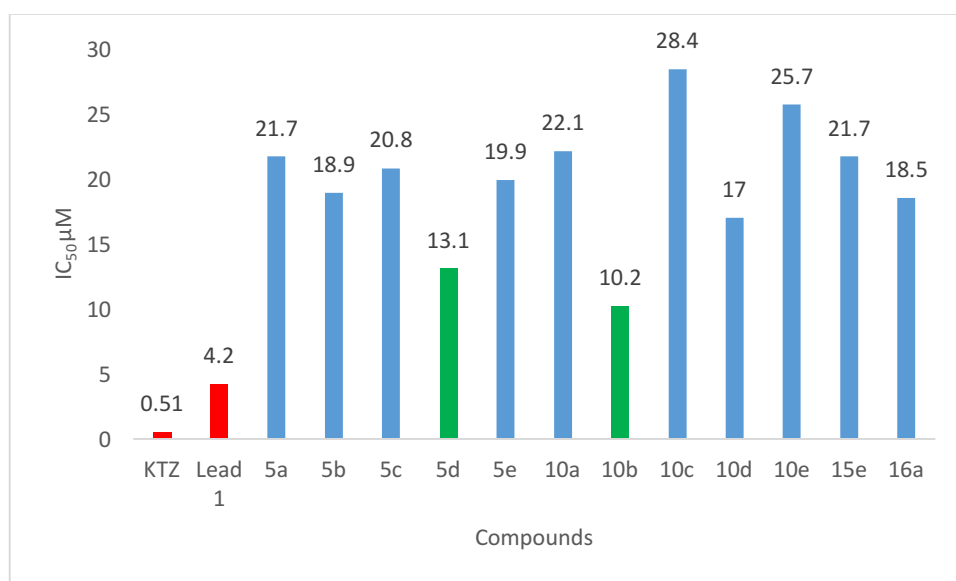
Figure 71: CYP24A1 inhibitor enzymatic assay

3.7   Conclusions

Previous screening for lead 1 from the SPECS database identified some promising CYP24A1 inhibitors with moderate inhibitory activity,

Development of lead 1 by replacement with pyridine and imidazole was synthesised successfully. Replacement with triazole was also synthesised by the same methods, however, intermediate compounds ware produced due to the carboxylic group reacting with CDI rather than with triazolylethylamine salt. All the compounds accessed the vitamin D channel and interacted with the active site of CYP24A1. The compounds exhibited weak potency and IC_{50} ranging between 10.2 to 28.4 μM against CYP24A1. Owing to the low CYP24A1 inhibitory activity the compounds were not evaluated against CYP27B1.

However, computational molecular docking of two exemplar compounds **5d** and **10b** in the CYP27B1 homology model would predict **10b** may have some inhibitory activity of this enzyme. Both compounds were found to be at a distance too far for the imidazole to interact with the haem iron, however the amide nitrogen of **10b** forms a H-bonding interaction with Asp320, one of the amino acids identified as important for CYP27B1 inhibitory activity (Figure 72 and 73).
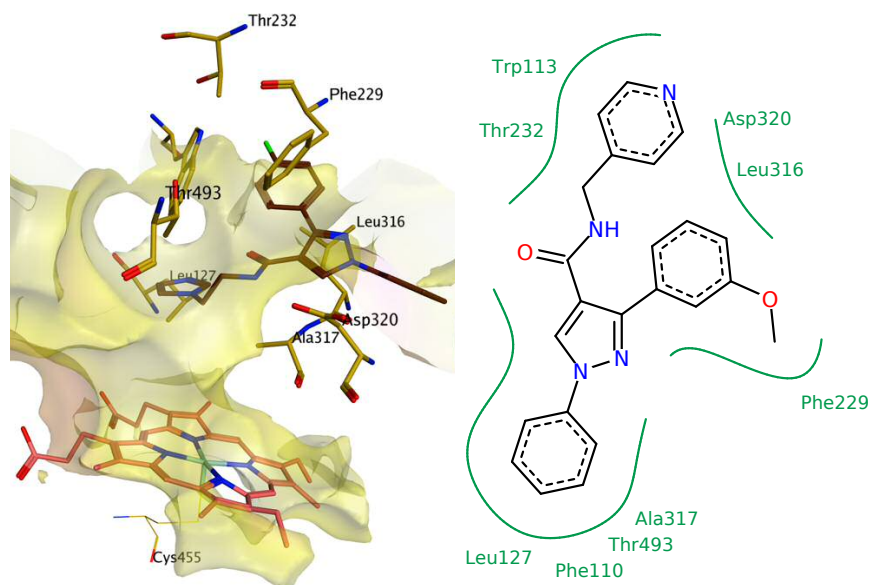
Figure 72: 3D and 2d models showing key binding interactions of 5d with CYP27B1 model
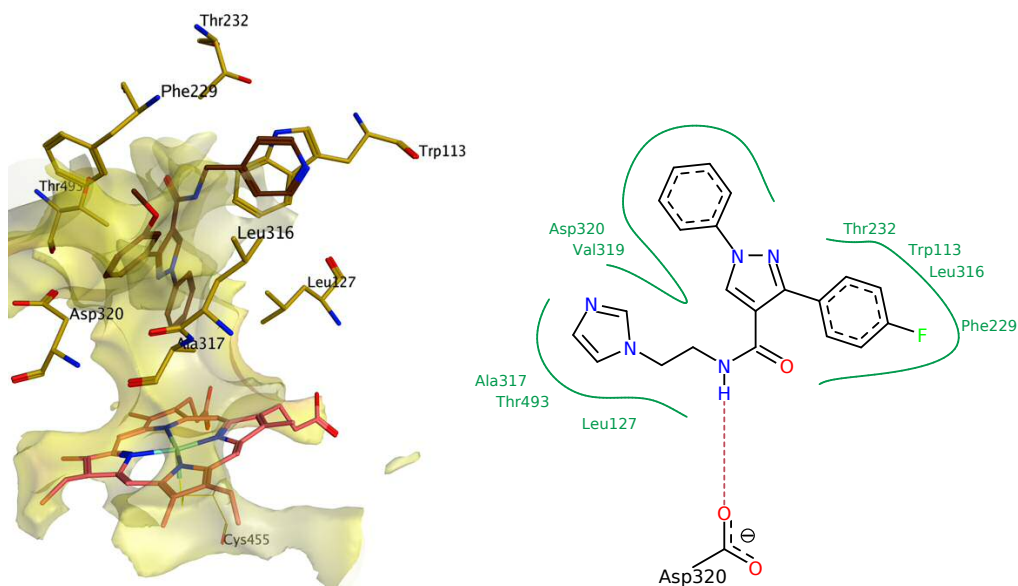
Figure 73: 3D and 2d models showing key binding interactions of 10b with CYP27B1 mode

3.8   Experimental

Chemistry general information

All chemicals, reagents, and solvents were purchased from Sigma-Aldrich and Fisher Scientific and, where required, solvents were dried and stored over 4 Å molecular sieves under nitrogen. Flash column chromatography was performed with silica gel 60 nm (230 - 400) (Merck), and TLC was formed on precoated silica gel plates (Merck Kiesegel 60F$_{254}$) and preparative TLC plates with 254 UV and dimension 20 ×20 cm (Analtech, Inc.). Melting points were determined on an electrothermal instrument (Gallenkamp) and are uncorrected. Compounds were visualised by irradiation with UV light at 254 nm and 366 nm. ^{1}H and ^{13}C NMR spectra were recorded on a Bruker Advance DPX500 spectrometer operating at 500 MHz and 125 MHz respectively and autocalibrated to deuterated solvent reference peak. Chemical shifts are given in δ relative to tetramethylsilane (TMS); the coupling constant (J) is given in Hertz. TMS was used as an internal standard (δ = 0) for ^{1}H NMR, and CDCl$_3$ served as an internal standard (δ = 77.0) for ^{13}C NMR. Multiplicity is denoted as s (singlet), d (doublet), t (triplet), m (multiplet) or combinations. Mass spectra were performed on a Bruker Daltonics microTof-LC, (atmospheric pressure ionisation and electron spray mass spectroscopy) in either positive mode. Mass spectroscopy and microanalysis were performed by Medac Ltd, Alpha 319, Chobham Business Centre, Surrey and EPSRS Swansea.

3.8.1   Molecular modelling

All molecular modelling method information is reported in Chapter 2.

3.8.2   CYP24A1 inhibitor enzymatic assay[279]

All the final compounds **5a - 5e**, **10a - 10e**, **15e** and **16a** were evaluated by enzymatic assay to determine CYP24A1 inhibitory activity. The assay was performed according to the method of Zhu *et al,*[279] and required a buffer solution containing (Adx + AdxR + CYP24A1 + calcitriol + inhibitors + NADPH) [279] with concentrations and volumes detailed in Table 34. The assay was performed in a buffer solution containing 20 mM Tris (pH = 7.6 - 7.7) and 125 mM NaCl. The inhibitor compounds were prepared by serial dilution (control with zero time, control, 0.125 μM, 0.25 μM, 0.5 μM, 1 μM, and 2 μM).

Material	CYP24A1	
	Concentration	Volume
Adx	0.1 μM	0.35 μL
AdxR	0.1 μM	2 μL
CYP24A1	0.1 μM	5.7 μL
Calcitriol	2.5 μM	2 μL
Inhibitor	0 - 2 μM	2 μL
NADPH	0.5 mM	2 μL
Buffer solution	186 μL	
Total volume	200 μL	

Table 34: The concentration and volumes required in the CYP24A1 inhibition assay

The reaction was initiated by the addition of NADPH at a final concentration of 0.5 mM and the mixture kept for 25 min at 37 ℃ to keep calcitriol conversion at less than 25 %. Then the reaction was quenched by adding four volumes of dichloromethane. After centrifugation, the dichloromethane layer was collected and kept overnight to dry. The assay for each compound was performed in duplicate (n =2). The reaction was conducted and analysed by HPLC with an eluent of 15 % isopropanol and 85 % hexane; the reaction mixture was injected into HPLC on the silica column (Waters Sherisorb S5W, 25 cm x 4.6 mm, 5 μm, SUPELCO Analytical) and monitored at 265 nm.

3.8.3   Chemistry

Synthesis of 3-(substituted/unsubstituted phenyl)-1-phenyl-*N*-(pyridin-4-ylmethyl)-1*H*-pyrazole-4-carboxamide derivatives
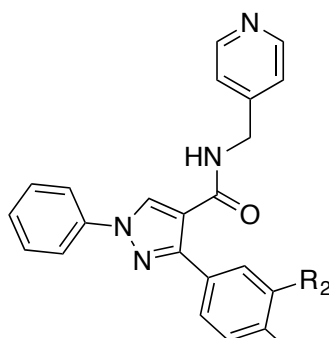
Where R
5a = R_1 = H, R_2 = H
5b = R_1 = F, R_2 = H
5c = R_1 = Cl, R_2 = H
5d = R_1 = H, R_2 = OCH$_3$
5e = R_1 = CH$_3$, R_2 = H

3.8.3.1   (*E*)-1-phenyl-2-(1-phenylethylidene)hydrazine (2a)
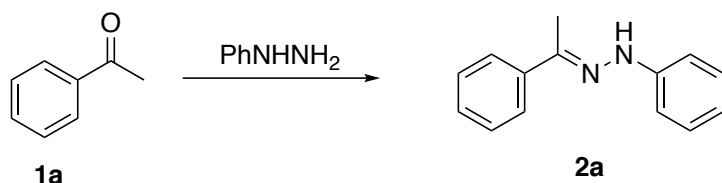
2a
Chemical Formula: $C_{14}H_{14}N_2$
Molecular Weight: 210.28

Method:

Acetophenone **1a** (4.8 g, 40 mmol) was mixed with acetic acid (40 mL), then, phenylhydrazine (4 mL, 40 mmol.) was added slowly with stirring for 15 min. The resulting yellow solid was collected by filtration and washed with cold ethanol to remove acetic acid[263].

TLC. Petroleum ether-EtOAc 4: 1 v/v, $R_f = 0.35$

m. p. = 80 - 82 ℃ (Lit. m. p. 108 ℃)[258]

Yield = 8.46 g (100 %), white solid

3.8.3.2   (*E*)-1-(1-(4-fluorophenyl)ethylidene)-2-phenylhydrazine (2b)
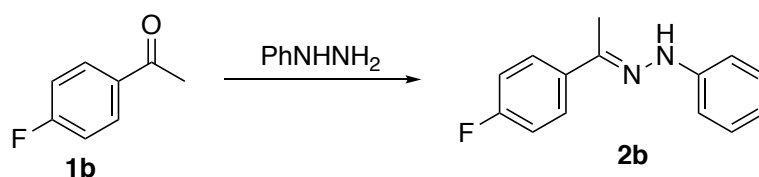
2b
Chemical Formula: $C_{14}H_{13}FN_2$
Molecular Weight: 228.27

Method: See 3.8.3.1

Reagent: 4-Fluoroacetophenone (5.5 g, 40 mmol) **1b**

TLC: Petroleum ether-EtOAc 3:1 v/v, Rf = 0.53

m. p. = 88 - 90 ℃ (Lit. m. p. 134 -136 ℃)[257]

Yield = 1.86 g (20 %), light yellow crystals

3.8.3.3   (*E*)-1-(1-(4-chlorophenyl)ethylidene)-2-phenylhydrazine (2c)
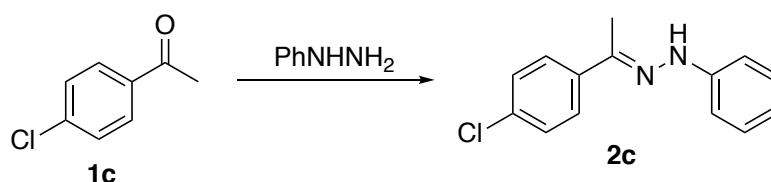
2c
Chemical Formula: $C_{14}H_{13}ClN_2$
Molecular Weight: 244.72

Method: See 3.8.3.1

Reagent: 4-chloroacetophenone (6.2 g, 40 mmol) **1c**

TLC: Petroleum ether-EtOAc 3:1 v/v, R_f = 0.63

m. p. = 109 - 111℃ (Lit. m. p. 102 ℃)[259]

Yield = 8.78 g (89 %), light yellow crystals

3.8.3.4   (*E*)-1-(1-(3-methoxyphenyl)ethylidene)-2-phenylhydrazine (2d)
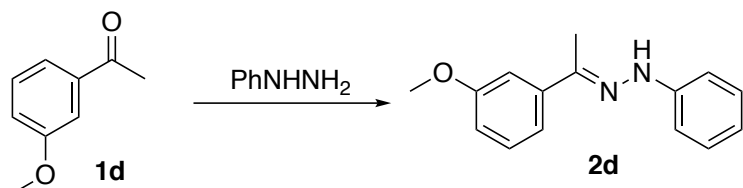
Chemical Formula: $C_{15}H_{16}N_2O$
Molecular Weight: 240.31

Method:

3-Methoxyacetophenone **1d** (6 g, 40 mmol) was mixed with acetic acid (4 mL) then, phenylhydrazine (4 mL) was added slowly with stirring for 15 min. After stirring for 15 min, no precipitate formed. Methanol was added, followed by ice water (100 mL) to give a yellow gum. This was extracted with CH_2Cl_2 (100 mL), and then the organic layer was washed with H_2O (100 mL × 2), dried ($MgSO_4$) and concentrated under reduced pressure to give a thick dark brown syrup. To this syrup was added ethanol (50 mL) and on standing, the product precipitated. The product was collected by vacuum filtration, washed with cold ethanol and dried under vacuum to give a light yellow solid[263].

TLC: Petroleum ether-EtOAc 4:1 v/v, R_f = 0.29

m. p. = 61 - 62 ℃

Yield = 7.5 g (78 %), light yellow solid

3.8.3.5   (*E*)-1-phenyl-2-(1-(*P*-tolyl)ethylidene)hydrazine (2e)
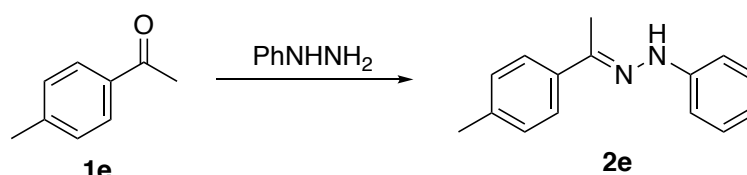
Chemical Formula: $C_{15}H_{16}N_2$
Molecular Weight: 224.31

Method:

Phenylhydrazine (1.08 g, 10 mmol) was mixed with acetic acid (1mL) and a solution of 4-methylacetophenone **1e** (1.34 g, 0.01 mmol) in ethanol (30 mL) added. The reaction mixture was refluxed for 1 h at 83 ℃. Once complete the reaction was cooled and the solvent removed under vacuum. Precipitation of product was achieved in ethanol and the resulting precipitate was filtered and washed with cold ethanol followed by drying under vacuum[257].

TLC: Petroleum ether-EtOAc 4:1 v/v, R_f = 0.48

m. p. = 80 - 82 ℃ (Lit. m. p 80 ℃)[260]

Yield = 2.24 g (100 %), light yellow solid

3.8.3.6   1,3-Diphenyl-1*H*-pyrazole-4-carbaldehyde (3a)

Chemical Formula: $C_{16}H_{12}N_2O$
Molecular Weight: 248.29
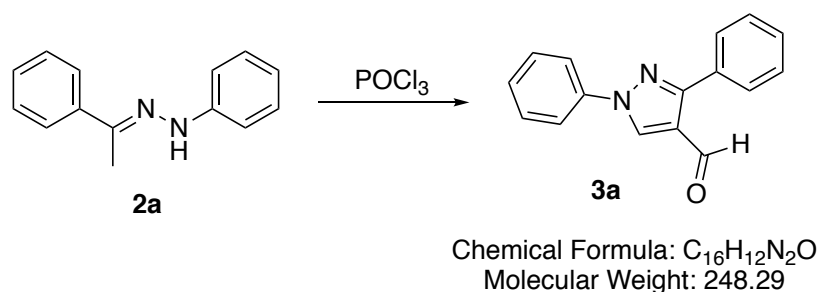
Method:

(*E*)-1-phenyl-2-(1-phenylethylidene) hydrazine **2a** (5.8 g, 28 mmol) was dissolved in dry DMF (15 mL), then $POCl_3$ (8.5 mL, 91.1 mmol) was added slowly dropwise at 0 ℃ and after complete addition of $POCl_3$, the mixture was stirred for 2 h at 90 ℃. The mixture was then poured into ice (50 mL) and 10 % aqueous NaOH solution (10 mL) was added to neutralise the solution. The resulting mixture was extracted with CH_2Cl_2 (2 ×50 mL), washed with water (2 ×50 mL) to remove excess DMF, then organic layer was dried ($MgSO_4$) and evaporated under reduced pressure. To the crude product petroleum ether (10 mL/ mmol) was added and the mixture stirred for 30 min. The resulting solid was collected by filtration and dried[263].

TLC: Petroleum ether-EtOAc 2:1 v/v, R_f = 0.57

m. p. =128 - 130 ℃ (Lit. m. p. 144 -146 ℃)[258]

Yield = 4.5 g (66 %), light yellow solid

^{1}H NMR (CDCl[3]):

δ : 10.08 (s, 1H, CHO), 8.57 (s, 1H, pyrazole), 7.81(m, 4H, Ar), 7.48 (m, 5H, Ar), 7.42 (t, J = 7.5 Hz, 1H, Ar).

3.8.3.7   3-(4-Fluorophenyl)-1-phenyl-1*H*-pyrazole-4-carbaldehyde (3b)
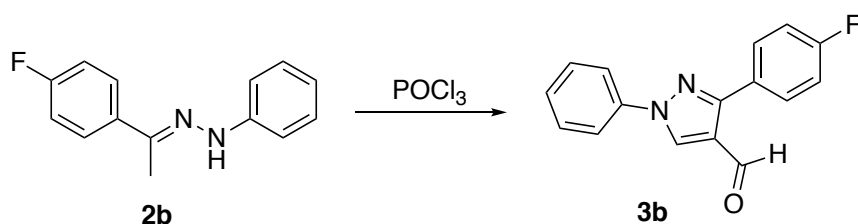
Chemical Formula: $C_{16}H_{11}FN_2O$
Molecular Weight: 266.28

Method: See 3.8.3.6

Reagent: *(E)*-1-(1-(4-fluorophenyl)ethylidene)-2-phenylhydrazine (1.9 g, 8 mmol) **2b**

TLC: Petroleum ether-EtOAc 3:1v/v, R_f = 0.48

m. p. =150 - 154℃ (Lit. m. p. 173 - 175 ℃)[257]

Yield = 0.97 g (44 %), light yellow crystals

¹H NMR (CDCl₃):

 δ : 10.06 (s, 1H, CHO), 8.56 (s, 1H, pyrazole), 7.90 (dd, J = 5.4, 8.9 Hz, 2H, Ar), 7.82 (d, J = 8.1 Hz, 2H, Ar), 7.55 (φt, J = 7.6, 8.1 Hz, 2H, Ar), 7.43 (t, J= 7.5 Hz, 1H, Ar), 7.22 (t, J = 8.5 Hz, 2H, Ar).

3.8.3.8   3-(4-Chlorophenyl)-1-phenyl-1*H*-pyrazole-4-carbaldehyde (3c)
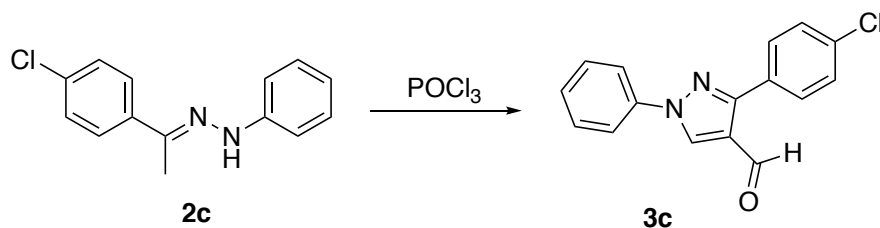
Chemical Formula: $C_{16}H_{11}ClN_2O$
Molecular Weight: 282.73

Method: See 3.8.3.6

Reagent: (*E*)-1-(1-(4-chlorophenyl)ethylidene)-2-phenylhydrazine (2 g, 8 mmol) **2c**

TLC: Petroleum ether-EtOAc 3:1 v/v, R_f = 0.42

m. p. = 139 -142 ℃ (Lit. m. p. 138 - 140 ℃)[263]

Yield = 1.4 g (61 %), light yellow crystals

¹H NMR (CDCl₃):

 δ : 10.06 (s, 1H, CHO), 8.55 (s, 1H, pyrazole), 7.86 (d, J = 8.6 Hz, 2H, Ar), 7.81(d, J = 7.7 Hz, 2H, Ar), 7.55 (φt, J = 8.1, 8.5 Hz, 2H, Ar), 7.5 (d, J = 8.5 Hz, 2H, Ar), 7.43 (t, J = 7.0 Hz, 1H, Ar).

3.8.3.9 3-(3-Methoxyphenyl)-1-phenyl-1*H*-pyrazole-4-carbaldehyde (3d)
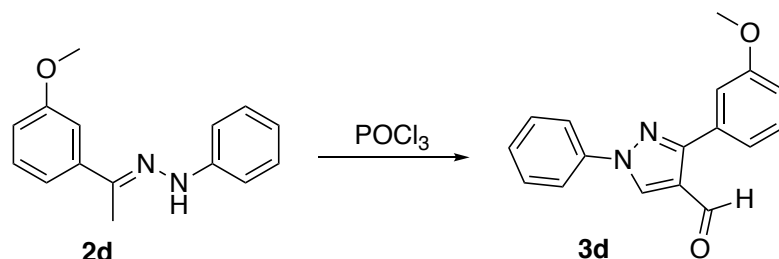
Chemical Formula: $C_{17}H_{14}N_2O_2$
Molecular Weight: 278.31

Method: See 3.8.3.6

Reagent: (*E*)-1-(1-(3-methoxyphenyl)ethylidene)-2-phenylhydrazine (4.3 g, 18 mmol) **2d**

TLC: Petroleum ether-EtOAc 3:1 v/v, R_f = 0.46

m. p. = 70 - 74 ℃ (Lit. m.p 102 ℃)[284,285]

Yield = 3.49 g (69 %), light yellow crystals

¹H NMR (CDCl₃):

δ : 10.09 (s, 1H, CHO), 8.56 (s, 1H, pyrazole), 7.53 (t, J = 7.9 Hz, 2H, Ar), 7.82 (dd, J = 1.1, 8.6 Hz, 2H, Ar), 7.40 (m, 4H, Ar), 7.04 (m, 1H, Ar), 3.91 (s, 3H, OCH₃).

3.8.3.10 1-Phenyl-3-(*p*-tolyl)-1*H*-pyrazole-4-carbaldehyde (3e)
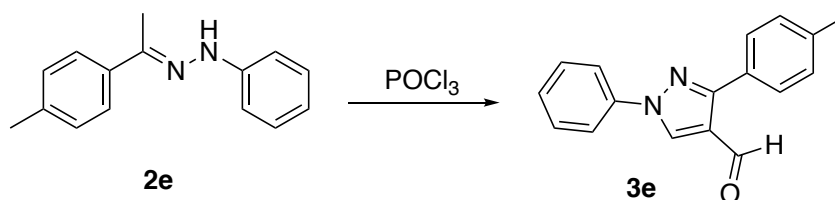
Chemical Formula: $C_{17}H_{14}N_2O$
Molecular Weight: 262.31

Method: See 3.8.3.6

Reagent: (*E*)-1-phenyl-2-(1-(*p*-tolyl)ethylidene)hydrazine (2.24 g, 10 mmol) **2e**

TLC: Petroleum ether-EtOAc 3:1 v/v, R_f = 0.63

m. p. = 125 - 128 ℃ (Lit. m. p. 120 ℃) [286]

Yield = 2.6 g (39 %), light yellow solid

¹H NMR (CDCl₃)

δ : 10.07 (s, 1H, CHO), 8.56 (s, 1H, pyrazole), 7.81 (d, J = 7.6 Hz, 2H, Ar), 7.74 (d, J = 8.1 Hz, 2H, Ar), 7.53 (φt, J = 7.6, 8.4 Hz, 2H, Ar), 7.41 (t, J = 7.4 Hz, 1H, Ar), 7.34 (d, J = 7.9 Hz, 2H, Ar), 2.45 (s, 3H, CH₃).

3.8.3.11 3-Diphenyl-1*H*-pyrazole-4-carboxylic acid (4a)
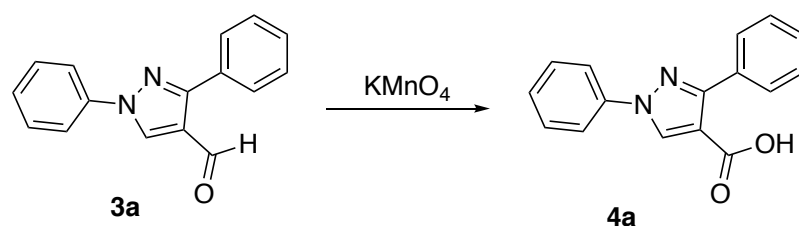
Chemical Formula: $C_{16}H_{12}N_2O_2$
Molecular Weight: 264.28

Method:

1,3-Diphenyl-1*H*-pyrazole-4-carbaldehyde **3a** (1g, 4 mmol) was dissolved in a mixture of *t*-butanol/H$_2$O 1:1 (10 mL/10 mL), then, an aqueous solution of KMnO$_4$ (0.7 g in 20 mL H$_2$O, 4.1 mmol) was added dropwise over 45 min with stirring at 75 ℃. 10 % aqueous KOH solution (15 mL) was then added until alkaline pH. The mixture was filtered and the filtrate was acidified with conc. HCl to pH 2. The precipitated solid was collected by filtration and washed with H$_2$O[258].

TLC: CH$_2$Cl$_2$-CH$_3$OH 9: 1 v/v, R$_f$ = 0.73

m. p. = 198 - 200 ℃ (Lit. m. p. 200 - 202℃)[258]

Yield = 0.91 g (83 %), pale yellow solid recrystallised with methanol

¹H NMR (DMSO-d₆):

δ : 12.59 (s, 1H, COOH), 9.06 (s, 1H, pyrazole), 7.98 (d, J = 7.6 Hz, 2H, Ar), 7.98 (d, J = 8.4 Hz, 2H, Ar), 7.85 (d, J = 7.9 Hz, 2H, Ar), 7.55 (φt, J = 7.0, 9.0 Hz, 2H, Ar), 7.47 (m, 2H, Ar).

3.8.3.12 3-(4-Fluorophenyl)-1-phenyl-1*H*-pyrazole-4-carboxylic acid (4b)
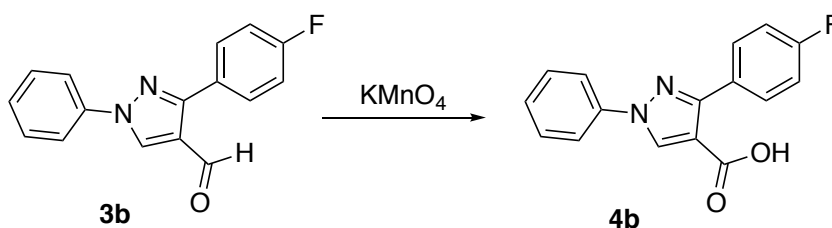
Chemical Formula: $C_{16}H_{11}FN_2O_2$
Molecular Weight: 282.27

Method: See 3.8.3.11

Reagent: 3-(4-Fluorophenyl)-1-phenyl-1*H*-pyrazole-4-carbaldehyde (1 g, 3.8 mmol) **3b**

TLC: CH$_2$Cl$_2$-CH$_3$OH 9: 1 v/v, R$_f$ = 0.53

m. p. = 222 - 223 ℃ (Lit. m. p. 229 - 230 ℃) [276]

Yield = 0.35 g, (37 %), a white crystals recrystallised with methanol

¹H NMR (DMSO-d₆)

δ : 12.60 (s, 1H, COOH), 9.07 (s, 1H, pyrazole), 7.98 (d, J = 7.4 Hz, 2H, Ar), 7.93 (dd, J = 5.6, 88 Hz, 2H, Ar), 7.55 (t, J = 7.8 Hz, 2H, Ar), 7.40 (φt, J = 7.0, 8.5 Hz, 1H, Ar), 7.39 (t, J = 8.5Hz, 2H, Ar)

3.8.3.13   3-(4-Chlorophenyl)-1-phenyl-1*H*-pyrazole-4-carboxylic acid (4c)
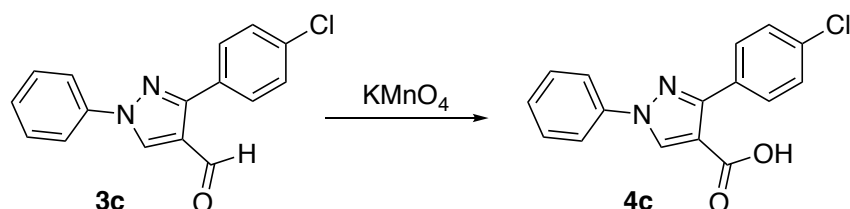
Chemical Formula: $C_{16}H_{11}ClN_2O_2$
Molecular Weight: 298.73

Method: See 3.8.3.11

Reagent: 3-(4-chlorophenyl)-1-phenyl-1*H*-pyrazole-4-carbaldehyde (1g, 3.5mmol) **3c**

TLC: CH₂Cl₂-CH₃OH 9: 1 v/v, R$_f$ = 0.23

m. p. = 238 - 240 ℃ (Lit. m. p. 240 - 242 ℃)[276]

Yield = 0.85 g (80 %), white solid recrystallised with methanol

¹H NMR (DMSO-d₆)

δ : 12.68 (s, 1H, COOH), 9.08 (s, 1H, pyrazole), 7.98 (d, J = 7.9 Hz, 2H, Ar), 7.90 (d, J = 8.4 Hz, 2H, Ar), 7.86 (m, 4H, Ar), 7.40 (t, J = 7.4 Hz, 1H, Ar).

3.8.3.14 3-(3-Methoxyphenyl)-1-phenyl-1*H*-pyrazole-4-carboxylic acid (4d)
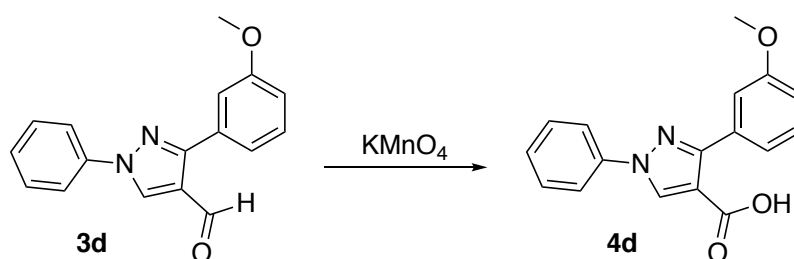
Chemical Formula: $C_{17}H_{14}N_2O_3$
Molecular Weight: 294.31

Method: See 3.8.3.11

Reagent: 3-(3-methoxyphenyl)-1-phenyl-1*H*-pyrazole-4-carbaldehyde (1 g, 3.4 mmol) **3d**

TLC: CH₂Cl₂-CH₃OH 9:1 v/v, R$_f$ = 0.77

m. p. = 139 - 140 ℃

Yield = 0.71 g (70 %), white solid, recrystallised with methanol

¹H NMR (DMSO-d₆):

δ : 12.55 (s, 1H, COOH), 9.06 (s, 1H, pyrazole), 7.98 (d, J = 7.6 Hz, 2H, Ar), 7.55 (t, J = 8.0 Hz, 3H, Ar), 7.35 (m, 4H, Ar), 3.85 (s,1H, OCH₃).

¹³C NMR (DMSO-d₆):

δ : 163.7 (COOH), 158.7, 152.5, 138.8, 113.9, 133.3 (5 × C, Ar), 133.6 (pyrazole), 129.6, 128.8, 127.2, 121.3, 119.2, 119.0, 114.8, 114.0 (9 × CH, Ar), 55.1 (OCH₃).

Microanalysis:

Anal. Calcd for $C_{17}H_{14}N_2O_3$ (294.30): C 69.38 %, H 4.79 %, N 9.51, %. Found C 69.40 %, H 4.66 %, N 9.51 %.

3.8.3.15 1-Phenyl-3-(*p*-tolyl)-1*H*-pyrazole-4-carboxylic acid(4e)

Chemical Formula: $C_{17}H_{14}N_2O_2$
Molecular Weight: 278.31
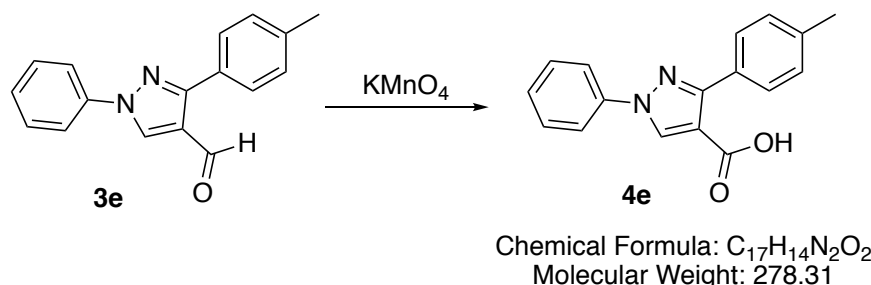
Method: See 3.8.3.11

Reagent: 1-phenyl-3-(*p*-tolyl)-1*H*-pyrazole-4-carbaldehyde (0.8g, 3mmol) **3e**

TLC: CH_2Cl_2-CH_3OH 9:1 v/v, R_f = 0.26

m. p. = 235 - 238 ℃ (Lit. m. p. 191 - 193 ℃)[287]

Yield = 0.47 g, (54 %) white solid

¹H NMR (DMSO-d₆):

δ : 12.64 (s, 1H, COOH), 9.03 (s, 1H, pyrazole), 8.03 (m, 2H, Ar), 7.74 (d, 2H, J = 8.1 Hz, Ar), 7.57 (m, 2H, Ar), 7.43 (m, 1H, Ar), 7.26 (d, J = 8.2 Hz, 2H, Ar), 2.37 (s, 3H, CH₃).

3.8.3.16 1,3-Diphenyl-*N*-(pyridin-4-ylmethyl)-1*H*-pyrazole-4-carboxamide derivatives (5a)
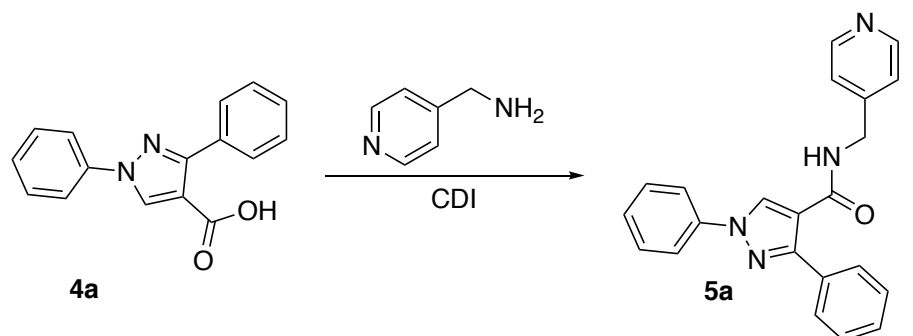
Chemical Formula: $C_{22}H_{18}N_4O$
Molecular Weight: 354.41

Method:

1,3-Diphenyl-1*H*-pyrazole-4-carboxylic acid **4a** (0.3 g, 1.1 mmol) was dissolved in anhydrous DMF (5 mL), then a solution of *N,N′* -carbonyldiimidazole (0.2 g, 1.2 mmol) in dry DMF (3 mL) added and the reaction stirred for 1 h. The reaction was cooled to 0 ℃, and a solution of 4-aminomethylpyridine (0.16 g, 1.5 mmol) in dry DMF (4 mL) was added and the mixture stirred at room temperature for 20 h. Once complete, ice - H_2O (50 mL) was added and the resulting white precipitate collected by filtration and washed with cold water and dried[210].

TLC: CH_2Cl_2-CH_3OH 9:1v/v, $R_f = 0.79$

m. p. = 188 - 190 ℃

Yield = 0.16 g (39 %), white solid, recrystallised with methanol

^{1}H NMR (DMSO-d$_6$):

δ : 9.01 (s, 1H, pyrazole), 8.84 (t, J = 5.8 Hz, 1H, NH), 8.53 (d, J = 5.6 Hz, 2H, pyridine), 7.93 (d, J = 7.7 Hz, 2H, Ar), 7.86 (dd, J = 1.3, 7.6 Hz, 2H, Ar), 7.58 (φt, J = 7.5, 8.3 Hz, 2H), 7.44 (m, 6H, Ar), 4.48 (d, J = 5.9 Hz, 2H, CH$_2$).

^{13}C NMR (DMSO-d$_6$):

δ : 163.0 (CO), 150.9, 148.4, 139.0 (3 × C), 132.2 (CH, pyrazole), 130.3 (C), 129.6, 128.7, 128.3, 127.9, 126.9, 122.2, 118.6 (14 × CH, Ar), 117.4 (C), 41.5 (CH$_2$)

Microanalysis:

Anal. Calcd for $C_{22}H_{18}N_4O$ (354.40): C 74.56 %, H 45.12 %, N 15.80 %. Found C 74.36 %, H 5.04 %, N 15.84 %.

3.8.3.17 3-(4-Fluorophenyl)-1-phenyl-*N*-(pyridin-4-ylmethyl)-1*H*-pyrazole-4-carboxamide (5b)
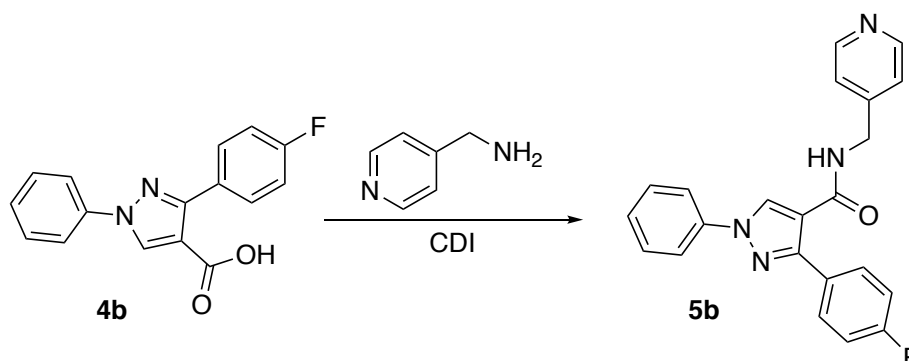
Chemical Formula: $C_{22}H_{17}FN_4O$
Molecular Weight: 372.40

Method: See 3.8.3.16

Reagent: 3-(4-fluorophenyl)-1-phenyl-1*H*-pyrazole-4-carboxylic acid (0.3 g, 1.1 mmol) **4b**

TLC: CH_2Cl_2-CH_3OH 9:1 v/v, R_f = 0.58

m. p. = 199 - 200 ℃

Yield = 0.24 g (58 %), white crystals, recrystallised with methanol

^{1}H NMR (DMSO-d$_6$):

δ : 9.03 (s, 1H, pyrazole), 8.54 (φt, J = 1.5, 4.5 Hz, 1H, NH), 8.54 (dd, 2H, J = 1.5, 4.5 Hz, pyridine), 7.94 (m, 4H, Ar), 7.57 (φt, 2H, J = 8.5, 7.5 Hz, Ar), 7.41 (m, 3H, Ar), 7.25 (t, 2H, J = 9.0 Hz, pyridine), 4.49 (d, 2H, J = 6.0 Hz, CH_2).

^{13}C NMR (DMSO-d$_6$):

δ : 163.2 (CO), 162.9 (F-C), 161.2, 150.2 (2 × CH, Ar), 149.5, 148.4, 138.9, 130.6, 130.5 (5 × C), 130.4 (CH, pyrazole), 130.1, 129.7, 128.8, 128.7, 127.1, 122, 117.1, 118.7, 114.9, 114.8 (11 × CH, Ar), 41.4 (CH_2).

LRMS (ES-TOF)

m/z: 373 [M + H]$^+$

HRMS (ES-TOF)

Calculated mass: 373.1459 [M + H]$^+$, measured mass: 373.1493 [M + H]$^+$

3.8.3.18 3-(4-Chlorophenyl)-1-phenyl-*N*-(pyridin-4-ylmethyl)-1*H*-pyrazole-4-carboxamide (5c)
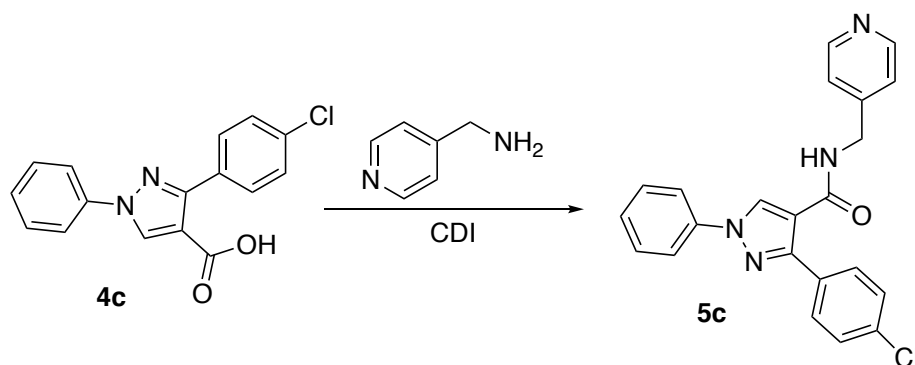
Chemical Formula: $C_{22}H_{17}ClN_4O$
Molecular Weight: 388.86

Method: See 3.8.3.16

Reagent: 3-(4-chlorophenyl)-1-phenyl-1*H*-pyrazole-4-carboxylic acid (0.5 g, 3.3 mmol) **4c**.

TLC: CH_2Cl_2-CH_3OH 9:1 v/v, R_f = 0.58

m. p. = 222 - 223 ℃

Yield = 0.24 g (37 %), white crystals**,** recrystallised with methanol

^{1}H NMR (DMSO-d$_6$):

δ : 9.04 (s, 1H, pyrazole), 8.87 (t, J = 5.6 Hz, 1H, NH), 8.53 (dd , J = 1.4, 4.6 Hz, 2H, pyridine), 7.91 (t, J = 8.7 Hz, 4H, Ar), 7.60 (φt, J = 8.2, 7.5 Hz, 2H, Ar), 7.48 (d, J = 8.6 Hz, 2H, Ar), 7.41 (t , J = 7.3 Hz, 1H, Ar), 7.36 (d, J = 5.7 Hz, 2H, pyridine), 4.48 (d, J = 5.7 Hz, 2H, CH_2).

^{13}C NMR (DMSO-d$_6$):

δ : 162.8 (CO), 149.9, 148.3, 138.9, 133.0, 131.2 (5 × C), 130.48 (CH, pyrazole), 130.1, 129.7, 128.0, 127.1, 122.2, 118.7 (13 × CH, Ar), 117.3 (C), 41.5 (CH_2).

Microanalysis:

Anal. Calcd for $C_{22}H_{17}ClN_4O$ (388.85): C 67.95 %, H 4.41 %, N 14.41 %. Found C 67.87 %, H 4.31 %, N 14.58 %.

3.8.3.19 3-(3-Methoxyphenyl)-1-phenyl-*N*-(pyridin-4-ylmethyl)-1*H*-pyrazole-4-
       carboxamide (5d)
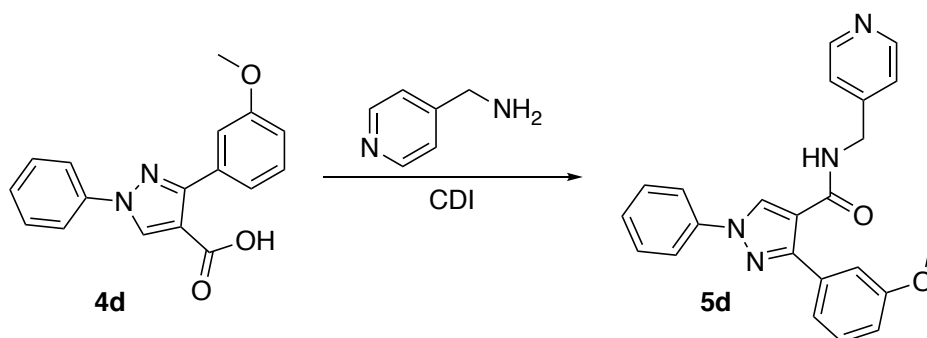
Chemical Formula: $C_{23}H_{20}N_4O_2$
Molecular Weight: 384.44

Method: See 3.8.3.16

Reagent: 3-(3-methoxyphenyl)-1-phenyl-1*H*-pyrazole-4-carboxylic acid (0.5 g, 1.7 mmol) **4d**

TLC: CH_2Cl_2-CH_3OH 9:1 v/v, R_f = 0.67

m. p. = 143 - 144 ℃

Yield = 0.22 g (33 %), white crystals, recrystallised with methanol

¹H NMR (DMSO-d₆):

δ : 8.99 (s, 1H, pyrazole), 8.87 (t, J = 5.9 Hz, 1H, NH), 8.53 (d, J = 5.8 Hz, 2H, pyridine), 7.93 (d, J = 7.8 Hz, 2H, Ar), 7.57 (t, J = 7.9, 2H, Ar), 7.47 (m, 2H, Ar), 7.47 (m, 4H, Ar), 6.98 (dd, J = 2, 8, Hz, 2H, Ar), 4.48 (d, J = 5.9 Hz, 2H, CH₂), 3.77 (s, 3H, OCH₃).

¹³C NMR (DMSO-d₆):

δ : 163.1 (CO), 158.9, 150.6, 148.3, 139.0, 133.5, (5 × C), 130.2 (CH, pyrazole), 129.7, 129.1, 126.9, 122.2, 120.6, 118.7, (11 × CH, Ar), 117.6 (C), 113.8, 113.9 (2 × CH, Ar), 41.5 (CH₂), 54.9 (OCH₃).

Microanalysis:

Anal. Calcd for $C_{23}H_{20}N_4O_2$ (384.43): 71.86 %, H 5.24 %, N 14.57 %. Found C 71.90 %, H 5.12 %, N 14.73 %.

3.8.3.20   1-Phenyl-*N*-(pyridin-4-ylmethyl)-3-(*p*-tolyl)-1*H*-pyrazole-4-carboxamide (5e)

Chemical Formula: $C_{23}H_{20}N_4O$
Molecular Weight: 368.44
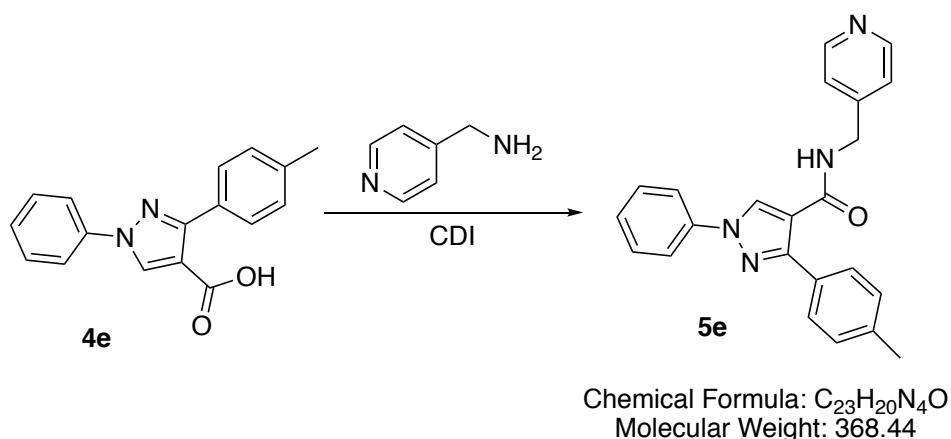
Method: See 3.8.3.16

Reagent: 1-phenyl-3-(*p*-tolyl)-1*H*-pyrazole-4-carboxylic acid (0.47 g, 1.7 mmol) **4e**

TLC: CH_2Cl_2-CH_3OH 9:1 v/v R_f = 0.48

m. p. = 191 - 193 ℃

Yield = 0.026 g (4 %), white solid**,** recrystallised with methanol

^{1}H NMR (DMSO-d$_6$):

δ : 8.97 (s, 1H, pyrazole), 8.80 (t, J = 6 Hz,1H, NH), 8.53 (d, J = 5.6 Hz, 2H, pyridine), 7.91 (d, J = 7.7 Hz, 2H, pyridine), 7.75 (d, J = 8 Hz, 2H, Ar), 7.57 (t, J = 8 Hz, 2H, Ar), 7.40 (m, 3H, Ar), 7.22 (d, J = 7.8 Hz, 2H), 4.47 (d, J = 6 Hz, 2H, CH$_2$), 2.35 (s, 3H, CH$_3$).

^{13}C NMR (DMSO − d$_6$):

δ : 163.1 (CO), 150.9, 148.4, 139.0, 137.6, (4 × C), 131.1 (CH, pyrazole), 131.0, 130.1, 129.7, 128.6, 128.2, 126.9, 122.2, 118.6 (13 × CH, Ar), 117.3 (C), 41.5 (CH$_2$), 20.8 (CH$_3$).

Microanalysis:

Anal. Calcd for $C_{23}H_{20}N_4O \cdot 0.3\ H_2O$ (373.85): C 73.89 %, H 5.47 %, N 14.98 %. Found C 73.72 %, H 5.40 %, N 14.59 %.

3.8.3.21   2-(2-(1*H*-imidazol-1-yl)ethyl)isoindoline-1,3-dione[272] (8)

Chemical Formula: $C_{13}H_{11}N_3O_2$
Molecular Weight: 241.25
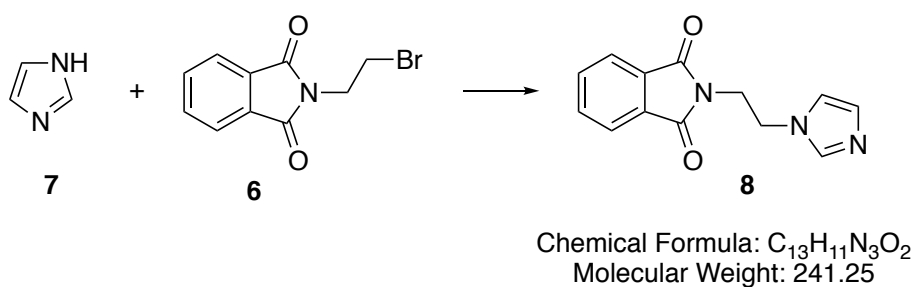
Method:

Potassium iodide (0.2 g, 0.07 mmol) was added to melted imidazole **7** (5.7 g, 84 mmol). Then *N*-(2-bromoethyl)phthalimide **6** (7.1 g, 28 mmol) was added. The mixture was stirred at 100 ℃ for 3 h. Toluene (25 mL) was added, the reaction stirred at 115 ℃ for 20 h. The solvent was reduced under vacuum to give a thick syrup. The syrup was recrystallised with isopropanol[272].

TLC: CH_2Cl_2-CH_3OH 9:1 v/v, R_f = 0.57

m. p. = 126 - 130 ℃ (Lit. m. p. 155 - 157 ℃)[272]

Yield = 3.3 g (49 %), white solid, recrystallised with isopropanol

¹H NMR (DMSO-d₆):

δ : 7.85 (d, J = 1.7 Hz, 4H, Ar), 7.55 (s, 1H, imid), 7.13 (s, H, imid), 6.82 (s, 1H, imid), 4.26 (t, J = 6.1 Hz, 2H, CH_2), 3.92 (t, J = 6.2 Hz, 2H, CH_2)

3.8.3.22 1-(2-Ammonioethyl)-1*H*-imidazol-3-ium chloride (9) [270,288]

Chemical Formula: $C_5H_{11}Cl_2N_3$
Molecular Weight: 184.06
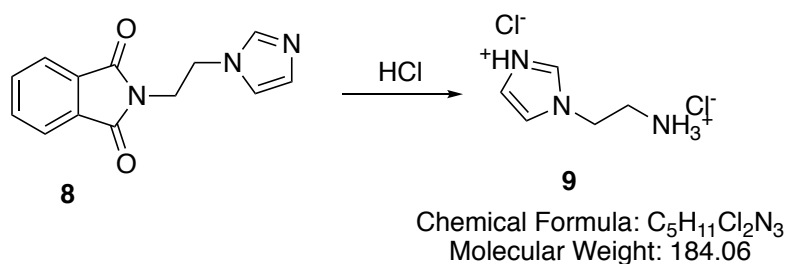
Method:

2-(2-(1*H*-imidazol-1-ylethyl)isoindoline-1,3-dione **8** (2.75 g, 11.4 mmol) and hydrazine monohydrate (1.2 g, 22.8 mmol) dissolved in ethanol (25 mL) was heated under reflux for 4 h. The resulting mixture was cooled to 0 ℃ and filtered, and the filtrate was evaporated to dryness under reduced pressure. The residue was dissolved in aqueous 1 N HCl (50 mL) and filtered, and the solvent was removed under reduced pressure to give a pale yellow solid[270].

TLC: CH_2Cl_2-CH_3OH 9:1 v/v, R_f = 0.00

m. p. = 170 - 175 ℃ (Lit. m. p. 217 - 220 ℃)[288]

Yield = 1.73 g (82 %), pale yellow solid

¹H NMR (D₂O)

δ : 8.88 (s, 1H, imid), 7.60 (s, 1H, imid), 7.54 (s, 1H, imid), 4.63 (t, J = 6.2 Hz, 2H, CH_2), 3.57 (t, J = 6.2 Hz, 2H, CH_2).

3.8.3.23 *N*-(2-(1*H*-imidazol-1-yl)ethyl)-1, 3-diphenyl-1*H*-pyrazole-4-carboxamide (10a)

Chemical Formula: $C_{21}H_{19}N_5O$
Molecular Weight: 357.42
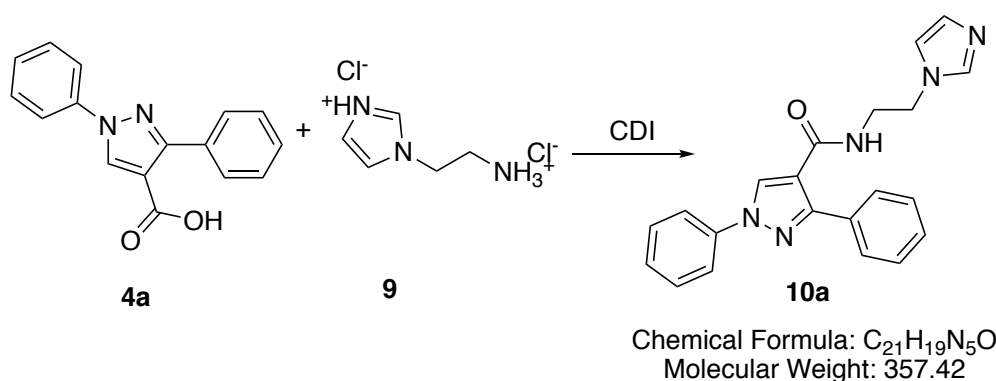
Method:

1,3-Diphenyl-1*H*-pyrazole-4-carboxylic acid **4a** (0.42 g, 1.6 mmol) was dissolved in anhydrous DMF (8 mL), then a solution of *N,N′*-carbonyldiimidazole (0.26 g, 1.6 mmol) in dry DMF (2 mL) added and the reaction stirred for 1 h. The reaction was cooled to 0 ℃, and a mixture of 1-(2-ammonioethyl)-1*H*-imidazol-3-ium chloride **9** (0.3 g, 1.6 mmol) with triethylamine (0.5 mL, 3.2 mmol) in dry DMF (4 mL) was added and the mixture stirred at room temperature for 20 h. Once complete, ice-H_2O (50 mL) was added and the resulting yellow precipitate collected by filtration and washed with cold water and dried. The product was purified by gradient flash column chromatography, product was eluted with EtOAc-CH_3OH 9:1 v/v[210].

TLC: EtOAc-CH_3OH 9:1 v/v R_f = 0.42

m. p. = 136 - 138 ℃

Yield = 0.24 g (40 %), white solid

¹H NMR (DMSO-d₆):

δ : 8.90 (s, 1H, pyrazole), 8.37 (s, 1H, NH), 7.88 (d, J = 7.3 Hz, 2H, Ar), 7.79 (d, J = 6.5 Hz, 2H, Ar), 7.65 (s, 1H, imid), 7.58 (t, J = 6.8 Hz, 2H, Ar), 7.43 (t, J = 8.2 Hz, 4H, Ar), 7.21 (s, 1H, imid), 6.92 (s, 1H, imid), 4.16 (s, 2H, CH₂), 3.57 (d, J = 4.6 Hz, 2H, CH₂)

¹³C NMR (DMSO-d₆):

δ : 162.9 (CO), 150.9, 138.9, 132.2 (3 × C), 129.9 (CH, pyrazole), 129.7, 129.6, 129.1, 128.4, 128.2, 128.2, 128.0, 127.9, 127.7, 126.9, 126.6, 118.8 (13 × CH, Ar), 117.4 (C), 45.3, 40.0 (CH₂).

Microanalysis:

$C_{21}H_{19}N_5O$ (357.42): C 70.57%, H 5.36 %, N 19.59 %. Found: C 70.28 %, H 5.19 %, N 19.29%.

3.8.3.24 *N*-(2-(1*H*-imidazol-1-yl) ethyl)-3-(4-fluorophenyl)-1-phenyl-1*H*-pyrazole-4-
      carboxamide (10b)
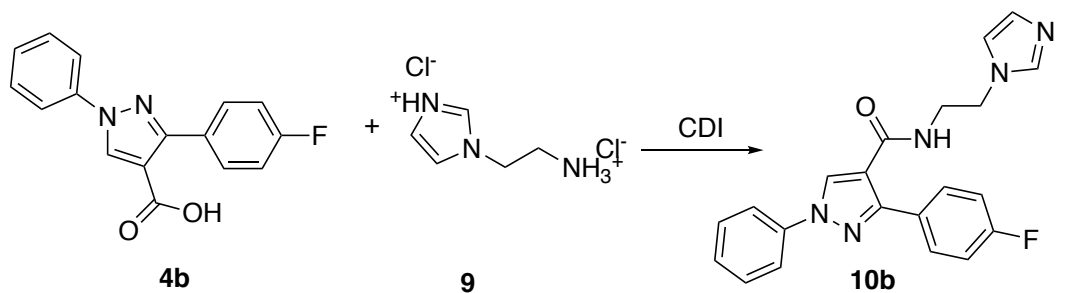
Chemical Formula: $C_{21}H_{18}FN_5O$
Molecular Weight: 375.41

Method: See 3.8.3.23

The product was purified by gradient flash column chromatography; product was eluted with EtOAc- CH_3OH 9:1 v/v.

Reagent: 3-(4-Fluorophenyl)-1-phenyl-1*H*-pyrazole-4-carboxylic acid (0.25 g, 1.4 mmol) **4b**

TLC: EtOAc-CH_3OH 9: 1 v/v, R_f = 0.2

m. p. = 158 -160 ℃

Yield = 0.18 g (29 %), white crystals

^{1}H NMR (CD$_3$OD):

δ : 8.49 (s, 1H, pyrazole), 7.83 (d, J = 7.7 Hz, 2H, Ar), 7.85 (m, 3H, Ar), 7.56 (φt, J = 7.6, 8.4 Hz, 2H, Ar), 7.41 (t, J = 7 Hz, 1H, imid), 7.20 (s, 1H, imid), 7.19 (m, 2H, Ar), 7.05 (s, 1H, imid), 4.28 (t, 2H, J = 6.0 Hz, CH$_2$), 3.72 (t, J = 6.0 Hz, 2H, CH$_2$).

^{13}C NMR (CD$_3$OD):

δ : 166.1 (CO), 165.4 (F-C), 163.5 (C), 152.4 (C), 140.7 (C), 131.8, 131.7, 131.1, 129.9, 130.7, 128.9, 128.5 (13 × CH, Ar), 129.8 (C), 118.1 (C), 47.2 (CH$_2$), 41.4 (CH$_2$).

Microanalysis:

Calculation for $C_{21}H_{18}FN_5O \cdot 0.3\ H_2O$ (380.81): C, 66.60, H, 4.90, N, 18.31. Found: C, 66.57; H, 4.82; N, 17.99.

3.8.3.25 *N*-(2-(1*H*-imidazol-1-yl) ethyl)-3-(4-chlorophenyl)-1-phenyl-1*H*-pyrazole-4-

   carboxamide (10c)
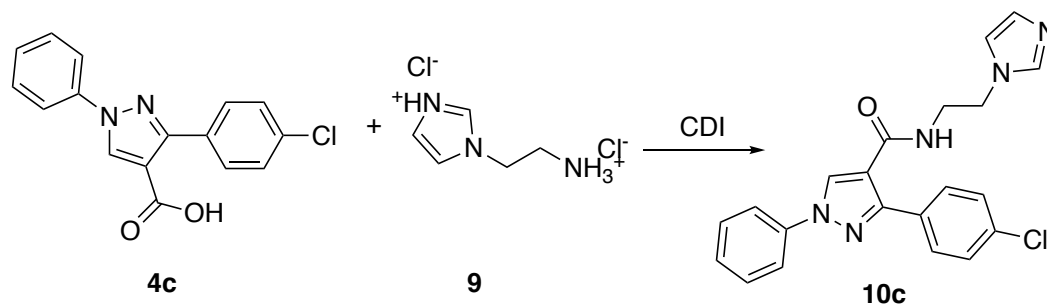
Chemical Formula: $C_{21}H_{18}ClN_5O$
Molecular Weight: 391.86

Method: See 3.8.3.23

Reagent: 3-(4-Chlorophenyl)-1-phenyl-1*H*-pyrazole-4-carboxylic acid (0.42 g, 1.4 mmol) **4c**

TLC: EtOAc-CH$_3$OH 9: 1v/v, R_f = 0.125

m. p. = 184 - 186 ℃

 Yield = 0.12 g (19 %), white crystal**,** recrystallised from acetonitrile

¹H NMR (CD₃OD):

 δ : 8.53 (s, 1H, pyrazole), 7.83 (d, J = 7.7 Hz, 2H, Ar), 7.72 (d, J = 8.5 Hz, 2H, Ar), 7.68 (s, 1H, imid), 7.55 (φt, J = 7.6, 8.4 Hz, 2H, Ar), 7.44 (m, 3H, Ar), 7.18 (s, 1H, imid), 7.03 (s, 1H, imid), 4.25 (t, J = 6.0 Hz, 2H, CH₂), 3.71 (t, J = 6.0 Hz, 2H, CH₂).

¹³C NMR (CD₃OD):

 δ : 166.1 (CO), 152.2 (C), 140.7 (C), 135.6 (C), 132.3 (C), 131.2 (CH, pyrazole), 131.1, 130.8, 129.4, 128.6, 120.5 (12 × CH, Ar), 118.3 (C), 47.1 (CH₂), 41.4 (CH₂).

Microanalysis:

Calculated for $C_{21}H_{18}ClN_5O \cdot 0.1\ H_2O$ (393.66): C, 64.07, H, 4.65, N, 17.79. Found: C, 63.92, H, 4.33, N, 17.76.

3.8.3.26 *N*-(2-(1*H*-imidazol-1-yl) ethyl)-3-(3-methoxyphenyl)-1-phenyl-1*H*-pyrazole-4-carboxamide (10d)

Chemical Formula: $C_{22}H_{21}N_5O_2$
Molecular Weight: 387.44
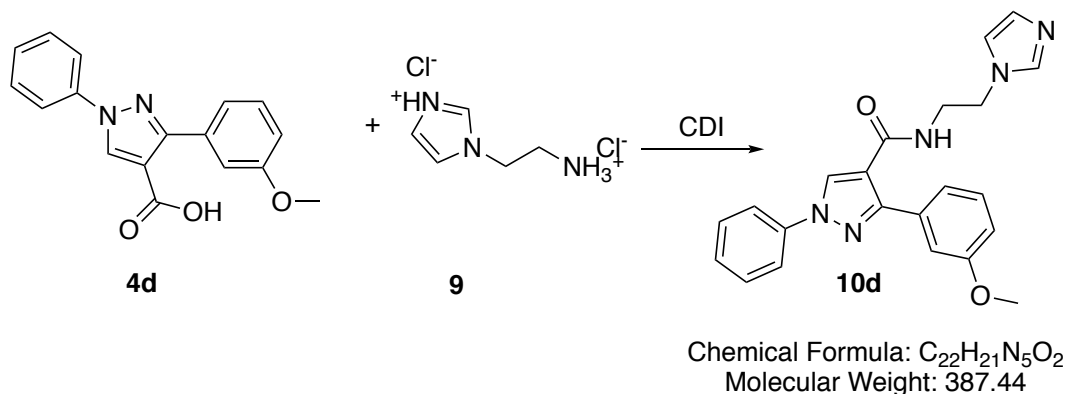
Method: See 3.8.3.23

After 20 h the reaction was incomplete. Additional CDI (about 2 eq.) and 1-(2-ammonioethyl)-1*H*-imidazol-3-ium chloride **9** (1eq.) added and the reaction heated at 60 ℃ overnight. The product was purified by gradient flash column chromatography, product was eluted with EtOAc- CH_3OH 9:1 v/v.

Reagent: 3-(3-Methoxyphenyl)-1-phenyl-1*H*-pyrazole-4-carboxylic acid (0.4 g, 1.4 mmol) **4d**

TLC: EtOAc-CH_3OH 2:1 v/v, R_f = 0.6

m. p. = 108 - 112 ℃

Yield = 0.18 g (32 %), bright yellow crystals

^{1}H NMR (CD$_3$OD):

δ : 8.51 (s, 1H, pyrazole), 7.83 (d, J = 7.7 Hz, 2H, Ar), 7.66 (s, 1H, imid), 7.55 (φt, J = 7.6, 8.4 Hz 2H, Ar), 7.42 (m, 4H, Ar), 7.16 (s, 1H, imid), 7.01(m, 2H, Ar), 4.25 (t, J = 6.0 Hz, 2H, CH$_2$), 3.86 (s, 3H, OCH$_3$), 3.71 (t, J = 6.0 Hz, 2H, CH$_2$).

^{13}C NMR (CD$_3$OD):

δ : 166.3 (CO), 161.1, 152, 9, 140.8, 134.8 (4 × C), 131.2 (CH, pyrazole), 130.7, 130.5, 129.2, 128.5, 122.1, 120.9, 115.4, 115.2 (12 × CH, Ar), 118.5 (C), 55.8 (OCH$_3$), 47.1 (CH$_2$), 41.5 (CH$_2$).

Microanalysis:

Calculated for $C_{22}H_{21}N_5O_2 \cdot 0.2\ H_2O$ (391.04): C, 67.57, H, 5.51, N, 17.91. Found: C, 67.21, H, 5.25, N, 17.56.

3.8.3.27 *N*-(2-(1*H*-imidazol-1-yl)ethyl)-1-phenyl-3-(*p*-tolyl)-1*H*-pyrazole-4-carboxamide

   (10e)
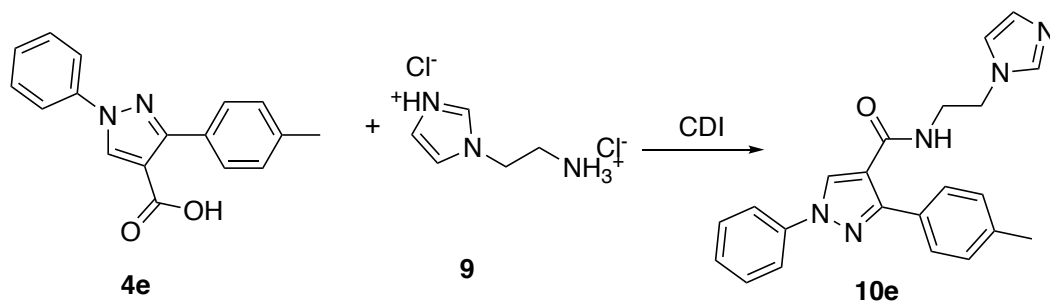
Chemical Formula: C$_{22}$H$_{21}$N$_5$O
Molecular Weight: 371.44

Method: See 3.8.3.23

The product was purified by gradient flash column chromatography, product was eluted with EtOAc- CH$_3$OH 9:1 v/v.

Reagent: 1-phenyl-3-(p-tolyl)-1*H*-pyrazole-4-carboxylic acid (0.47 g, 1.7 mmol) **4e**

TLC: EtOAc-CH$_3$OH 9: 1 v/v, R$_f$ =0.20

m. p. = 76 - 80 ℃

Yield = 0.034 g (6 %), white solid

¹H NMR (CD$_3$OD):

δ : 8.5 (s, 1H, pyrazole), 7.81 (d, J = 7.7 Hz, 2H, Ar), 7.69 (s, 1H, imid), 7.59 (d, J = 8.1 Hz, 2H, Ar), 7.53 (φt, J = 7.7, 8.3 Hz, 2H, Ar), 7.39 (t, J = 7.5 Hz, 1H, Ar), 7.24(d, J = 8 Hz, 2H, Ar), 7.17 (s, 1H, imid), 7.03 (s, 1H, imid), 4.23 (t, 2H, J = 6.0 Hz, CH$_2$), 3.68 (t, J = 6 Hz, 2H, CH$_2$), 2.45 (s, 3H, CH$_3$).

¹³C NMR (CD$_3$OD):

δ : 165.6 (CO), 152.50 (C), 139.98 (C), 139.1 (C), 130.4 (CH, pyrazole), 129.9, 129.2, 128.3, 119.7 (12 × CH, Ar), 129.8 (C), 117.4 (C), 46.4 (CH2), 40.6 (CH2), 20.6 (CH$_3$).

Microanalysis:

Calculation for C$_{22}$H$_{21}$N$_5$O (371.44): C, 71.14; H, 5.70; N, 18.85. Found: C, 70.87, H, 5.74, N, 18.67.

3.8.3.28 2-(2-(1*H*-1, 2,4-triazol-1-yl)ethyl)isoindoline-1,3-dione (12) [272]

6   **11**   **12**

Chemical Formula: $C_{12}H_{10}N_4O_2$
Molecular Weight: 242.24
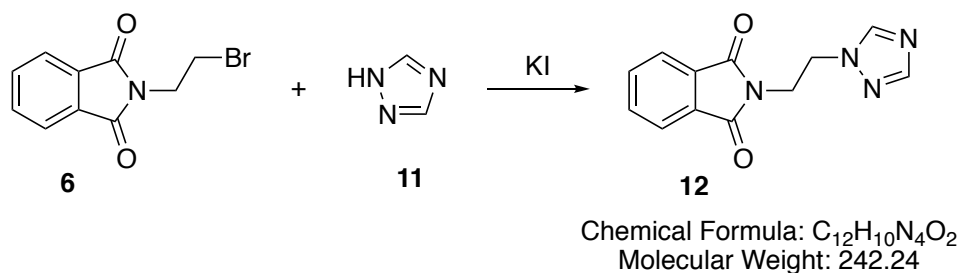
Method:

Potassium iodide (60.3 g, 1.8 mmol) was added to melted triazole **11** (6.5 g, 94 mmol). Then *N*-(2-bromoethyl)phthalimide **6** (6 g, 24 mmol) was added . The mixture was stirred at 100 ℃ for 3 h. Petroleum ether (20 mL) was added to give a waxy orange precipitate that was recrystallised with isopropanol[272].

TLC: CH_2Cl_2-CH_3OH 9.9: 0.1 v/v, R_f = 0.64

m. p. = 152 - 156 ℃ (lit. m. p. 166 - 169 ℃)[272]

Yield = 2.3 g (46 %), yellow crystals

¹H NMR (CD₃OD):

δ : 8.50 (s, 1H, triazole), 7.90 (s, H, triazole), 7.85 (m, 4H, Ar), 4.57 (φt, J = 5.5, 5.9 Hz, 2H, CH_2), 4.12 (t, J = 5.7 Hz, 2H, CH_2)

3.8.3.29 1-(2-Ammonioethyl)-1*H*-1,2,4-triazol-4-ium chloride (13)[272]

12   **13**

Chemical Formula: $C_4H_{10}Cl_2N_4$
Molecular Weight: 185.05
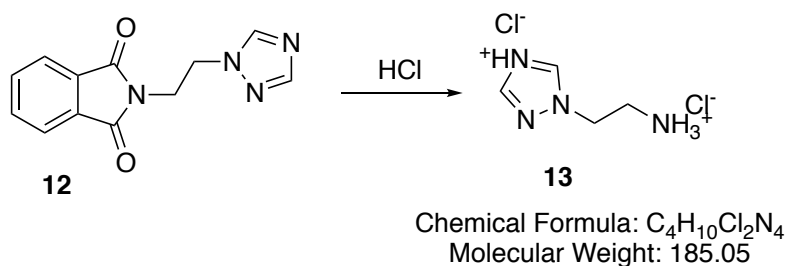
Method: See 3.8.3.22

Reagent: 2-(2-(1*H*-1, 2,4-triazol-1-yl)ethyl)isoindoline-1,3-dione (1.2 g, 5 mmol) **12**

TLC: CH_2Cl_2-CH_3OH 9: 1 v/v, R_f = 0.00

m. p. = 162 -166 ℃ (lit. m. p. 182 - 183 ℃)[272]

Yield = 1.0 g (85 %), pale yellow solid

¹H NMR (DMSO-d₆):

δ : 9.48 (s, 1H, triazole), 8.66 (s, 1H, triazole), 8.56 (br. s, 3H, NH_3^+), 4.65 (t, J = 6 Hz, 2H, CH_2), 3.32 (t, J = 6 Hz, 2H, CH_2).

¹³C NMR (DMSO-d₆):

δ : 167.4, 131.4 (4 × C, Ar), 151.4, 144.3, 134.4, 123.1 (6 × CH, Ar) 46.7, 37.7 (2 × CH₂, CH₂).

3.8.3.30 1-(4-Fluorophenyl)-3-phenyl-1*H*-pyrazole-4-carbonyl chloride (14b)
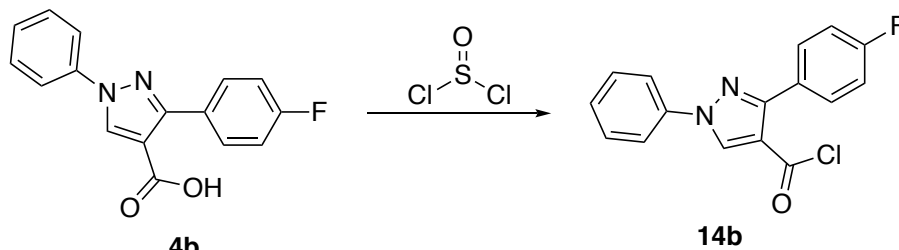
Chemical Formula: $C_{16}H_{10}ClFN_2O$
Molecular Weight: 300.72

Method:

3-(4-Fluorophenyl)-1-phenyl-1*H*-pyrazole-4-carboxylic acid **4b** (0.17 g, 0.58 mmol) was suspended in dry toluene (15 mL) then thionyl chloride (0.13 mL, 1.8 mmol) was added dropwise. The mixture was refluxed for 6 h, then cooled to room temperature. The solvent was removed under reduced pressure to give a solid compound which was washed with petroleum ether to give a white solid[275]

Yield = 0.10 g (57 %), white solid

m. p. = 122 -126 ℃ (lit. m. p. 140 - 141 ℃)[276]

TLC: Petroleum ether-EtOAc 3: 1, R_f = 0.42

¹H NMR (DMSO-d₆):

δ : 9.07 (s, 1H, pyrazole), 7.99 (d, J = 7.7 Hz, 2H, Ar), 7.92 (m, 2H, Ar), 7.55 (t, J = 7.7 Hz, 2H, Ar), 7.39 (t, J = 7.4 Hz, 1H, Ar), 7.29 (t, J = 8.9 Hz, 2H, Ar).

3.8.3.31 3-Phenyl-1-(*p*-tolyl)-1*H*-pyrazole-4-carbonylchloride (14b)
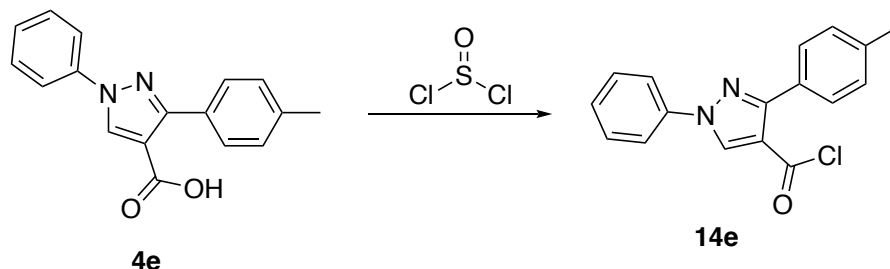
Chemical Formula: $C_{17}H_{13}ClN_2O$
Molecular Weight: 296.75

Method: See 3.8.3.30

Reagent: 1-phenyl-3-(*p*-tolyl)-1*H*-pyrazole-4-carboxylic acid (0.35 g, 1.3 mmol) **4e**

m. p. = 92 - 94 ℃

TLC: Petroleum ether-EtOAc 3: 1, R_f = 0.58

Yield = 0.291 g (78 %), white solid.

¹H NMR (DMSO-d₆):

δ : 9.06 (s, 1H, pyrazole), 7.97 (d, J = 8.0 Hz, 2H, Ar), 7.56 (t, J = 7.5 Hz, 3H, Ar), 7.42 (m, 4H, Ar), 2.33 (s, 3H, CH₃).

3.8.3.32 *N*-(2-(1*H*-1,2,4-triazol-1-yl)ethyl)-1-phenyl-3-(*p*-tolyl)-1*H*-pyrazole-4-carboxamide (15e)
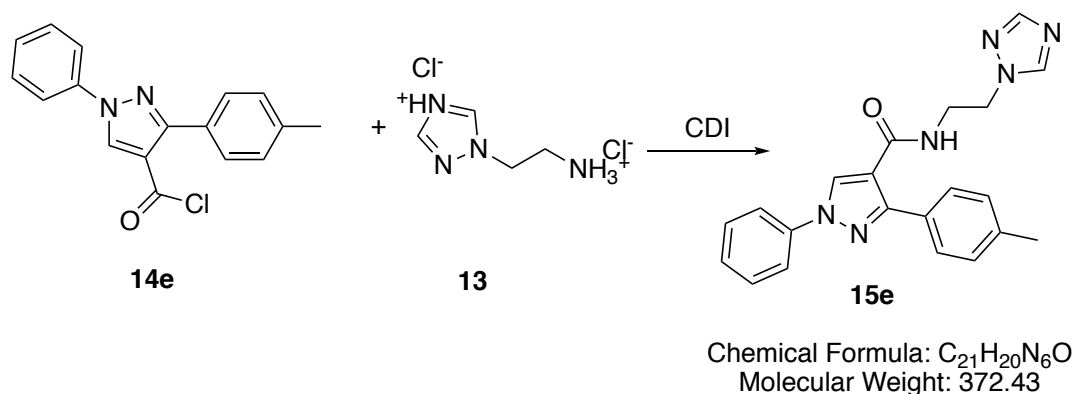
Chemical Formula: C₂₁H₂₀N₆O
Molecular Weight: 372.43

Method: See 3.8.3.23

 The product was purified by gradient flash column chromatography; the product was eluted with EtOAc- CH₃OH 9:1 v/v.

Reagent: 3-phenyl-1-(*p*-tolyl)-1*H*-pyrazole-4-carbonylchloride (0.245 g, 1.3 mmol) **14e**

TLC: EtOAc-CH₃OH 9: 1, R_f = 0.29

m. p. = 142 - 148 ℃

Yield = 0.023 g (6 %)

¹H NMR (CDCl₃):

δ : 8.41 (s, 1H, NH), 7.95 (s, 1H, triazole), 7.80 (s, 1H, triazole), 7.66 (d, J = 7.8 Hz, 2H, Ar), 7.38 (φt, J = 7.7, 8.2 Hz, 3H, Ar), 7.32 (d, J = 7.8 Hz, 3H, Ar), 7.25 (t, J = 7.5, Hz, 1H, Ar), 7.15 (d, J = 7.7, 1H, Ar), 4.25 (t, 2H, J = 5.4, Hz, CH₂), 3.68 (q, J = 5.4 Hz, 2H, CH₂), 2.25 (s, 3H, CH₃).

¹³C NMR (CDCl₃):

δ : 163.2 (CO), 151.1 (C), 139.4 (C), 139.3 (C), 131.1 (CH, pyrazole), 129.7, 129.6, 128.9, 127.4, 119.4 (11 × CH, Ar), 128.9 (C), 117.3 (C), 48.6 (CH₂), 39.0 (CH₂), 21.4 (CH₃).

LRMS (ES-TOF)

m/z: 373 [M + H]$^+$, 319 [M - triazole]$^+$

HRMS (ES-TOF)

Calculated mass: 373.1771 [M + H]$^+$, measured mass: 373.1772 [M + H]$^+$

3.8.3.33 (1,3-Diphenyl-1*H*-pyrazol-4-yl)(1*H*-imidazol-1-yl)methanone (16a)

Chemical Formula: $C_{19}H_{14}N_4O$
Molecular Weight: 314.35
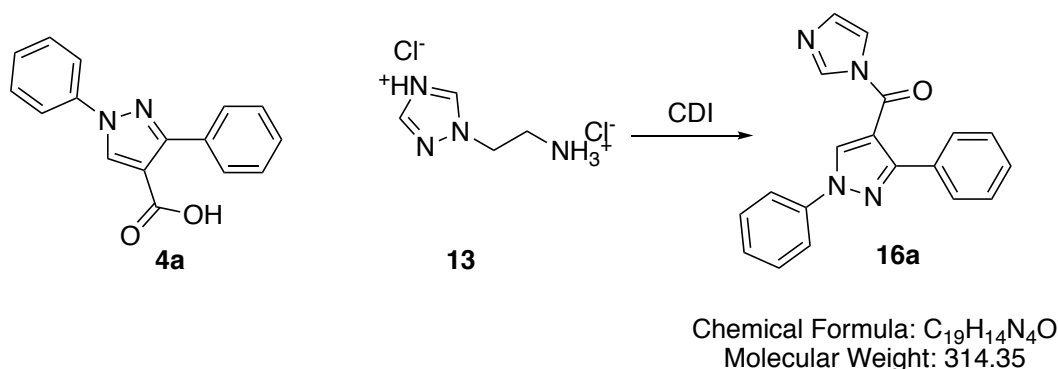
Method: See 3.8.3.23

Reagent: 1,3-diphenyl-1*H*-pyrazole-4-carboxylic acid (0.13 g, 0.7 mmol) **4a**

TLC: Petroleum ether-EtOAc 1:9 v/v, R_f = 61

m. p. = 118 - 120 ℃

Yield = 0.75 g (42 %), white solid

^{1}H NMR (DMSO ‑ d$_6$):

δ : 9.21 (s, 1H, pyrazole), 8.42 (s, 1H, imid), 8.02 (d, J = 8.0 Hz, 3H, 1×imid, 2×Ar), 7.71 (m, 4H, Ar), 7.59 (t, J = 7.5 Hz, 3H, Ar), 7.44 (s, 1H, imid), 7.14 (s, 1H, Ar)

^{13}C NMR (DMSO-d$_6$):

δ : 167.2 (CO), 160.5, 153.2, 138.7, 138.6 (4 × C, Ar), 135.8, 134.3, 133.1, 129.8, 127.5, 120.4 (14 × CH, Ar).

LRMS (ES-TOF)

m/z: 314 [M + H]$^+$

HRMS (ES-TOF)

Calculated mass: 314.1217 [M + H]$^+$, measured mass: 314.1209 [M + H]$^+$

3.8.3.34 (3-(4-Fluorophenyl)-1-phenyl-1*H*-pyrazol-4-yl)(1*H*-imidazol-1-yl) methanone (16b)

Chemical Formula: $C_{19}H_{13}FN_4O$
Molecular Weight: 332.34
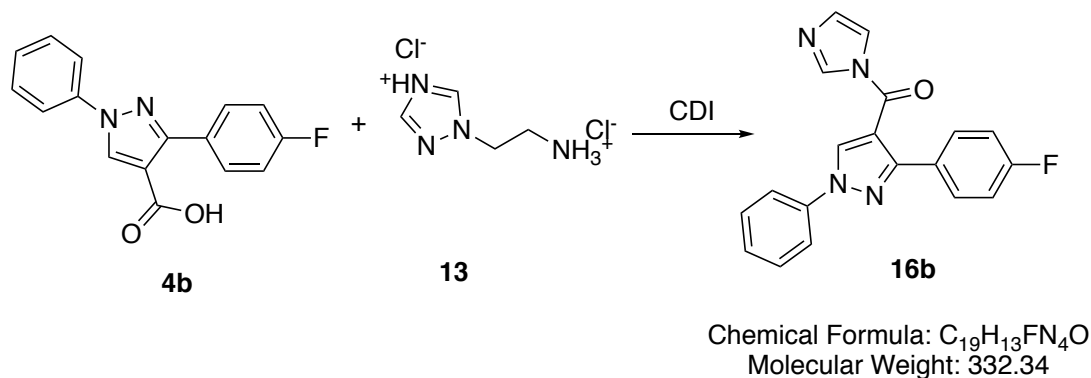
Method: See 3.8.3.23

Reagent: 3-(4-fluorophenyl)-1-phenyl-1*H*-pyrazole-4-carboxylic acid (0.17 g, 0.58 mmol) **4b**

TLC: Petroleum ether-EtOAc 3:1 v/v, R_f = 62

m. p. = 130 - 134 ℃

Yield = 0.80 g (39 %), white solid

^{1}H NMR (DMSO-d$_6$):

δ : 9.24 (s, 1H, pyrazole), 8.45 (s, 1H, Ar), 8.03 (d, J = 7.9 Hz, 2H, Ar), 7.81 (φt, J = 5.8, 7.9 Hz, 3H, Ar), 7.59 (t, J = 7.7 Hz, 2H, Ar), 7.45 (t, J = 7.3 Hz, 1H, Ar), 7.33 (s, 1H, imid) 7.28 (t, J = 8.7 Hz, 1H, imid), 7.17 (s, 1H, imid).

^{13}C NMR (DMSO-d$_6$):

δ : 165.5 (CO), 163.5 (C), 154.2 (C), 140.7 (C), 130.1 (5 × C), 134.4, 132.6, 130.1, 128.8, 120.9, 115.6 (13 × CH, Ar).

LRMS (ES-TOF)

m/z: 333 [M + H]$^+$

HRMS (ES-TOF)

Calculated mass: 333.1152 [M + H]$^+$, measured mass: 333.1146 [M + H]$^+$

3.8.3.35 2-((1*H*-Imidazol-1-yl)methyl)isoindoline-1,3-dione (18) [277]

Chemical Formula: $C_{12}H_9N_3O_2$
Molecular Weight: 227.22
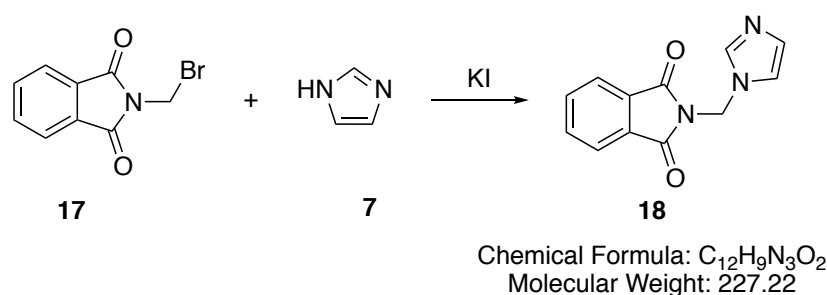
Method:

Potassium iodide (0.4 g, 2.4 mmol) was added to melted imidazole **7** (5.7 g, 83 mmol). Then *N*-(2-bromomethyl)phthalimide **17** (5 g, 21 mmol) was added. The mixture was stirred at 100 ℃ for 3 h. The mixture was diluted with EtOAc (20 mL), washed with brine (2 × 50 mL) Extracted with EtOAc (150) and washed with water (100 mL ×3). The organic layer was dried (MgSO$_4$) and concentrated in *vacuo* to give a white solid which was recrystallised with methanol [272].

Reagent: *N*-(2-bromomethyl)phthalimide (5 g, 20.8 mmol) **17**

TLC: CH$_2$Cl$_2$-CH$_3$OH 9:1 v/v, R$_f$ = 0.96

m. p. = 168 - 172 ℃ (Lit. m. p. 185 - 187 ℃)[277]

Yield = 1.8 g (38 %), white crystals

^{1}H NMR (DMSO-d$_6$):

δ : 7.94 (m, 2H, Ar), 7.89 (m, 2H, Ar), 7.77 (s, 1H, imid), 7.19 (s, 2H, imid), 6.91 (s, 1H, imid), 5.97 (s, 2H, CH$_2$).

3.8.3.36 2-((1*H*-1, 2, 4-triazol-1-yl)methyl)isoindoline-1,3-dione (19)[272]
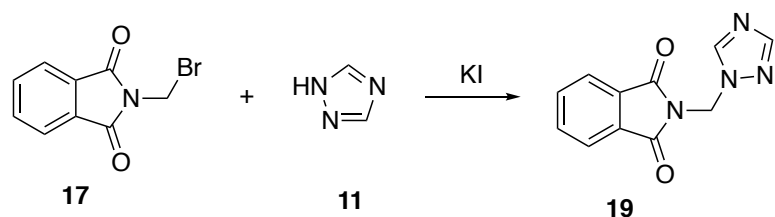
Chemical Formula: C$_{11}$H$_8$N$_4$O$_2$
Molecular Weight: 228.21

Method: See 3.8.3.35

Reagent: *N*-(2-bromomethyl)phthalimide (5 g, 20.8 mmol) **12**

TLC: Petroleum ether-EtOAc 3:1 v/v, R$_f$ = 0.44

m. p. = 164 - 168 ℃ (Lit. m. p. 169 - 170 ℃)[272].

Yield = 2.7 g (57 %), white crystal**,** recrystallised with acetonitrile

^{1}H NMR (DMSO-d$_6$):

δ : 8.72 (s, 1H, triazole), 7.99 (s, 1H, traizole), 7.94 (m, 2H, Ar), 7.90 (m, 2H, Ar), 5.96 (s, 2H, CH$_2$).
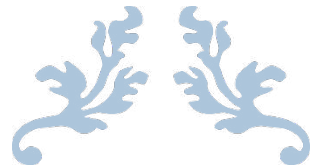
CHAPTER FOUR

Lead 2

Development of lead 2

Previous screening of the SPECS database[221] identified lead 2 with promising CYP24A1 inhibitor activity IC_{50} 5.5 µ M. Lead 2 was able to access the enzyme channel and reach the CYP24A1 active site with one polar head group (pyrazole) interacting perpendicularly with iron haem at a distance of 2.39 Å (Figure 74) . In addition, lead 2 formed hydrogen bonds with amino acid residues Glu329, Thr330 and Gly499 (Table 35). Leu148, Met246, Gln324, Leu325, Val328, Val391 and Thr500 interacted with lead 2 by hydrophobic bonds.
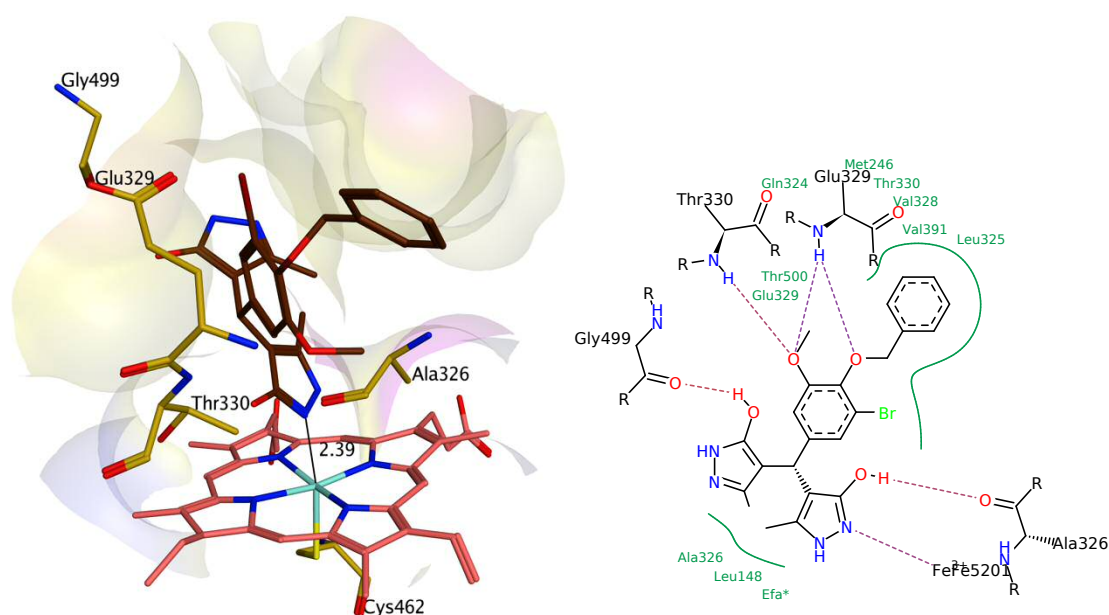
Figure 74: 3D and 2D models showing key binding interactions with lead 2 with CYP24A1

	Distance	Hydrogen bond
1	3.13 Å	Between hydroxyl group of lead 2 and Gly499
2	2.47 Å	Between hydroxyl group of lead 2 and Ala326
3	3.97 Å	Between methoxy group of lead 2 and Thr330
4	2.27 Å	Between ether group of lead 2 and Glu329
5	2.45 Å	Between methoxy group of lead 2 and Glu329

Table 35: Hydrogen bonds between lead 2 and amino acids residues of the CYP24A1 model

Lead 2[222] was modified and developed, specifically through (i) replacement of the phenyl with a nitrogen containing heterocycle to enhance the binding interaction with the haem moiety, (ii) simplifying of the bromomethoxyphenyl with an unsubstituted phenyl ring, (iii) addition of phenyl substituents on the dipyrazole rings or replacement of the dipyrazole rings with a basic heterocycle to allow complete filling in the active site of CYP24A1, and (iv) variation of the ether group position to allow complete filling in of the active site of CYP24A1.

This chapter is divided into five parts as follows:

1. Results and discussion
2. Molecular modelling
3. Biological assay
4. Conclusions
5. Experimental

3.9 Results and discussion

A two steps synthetic pathway was devised and is shown in Scheme 30
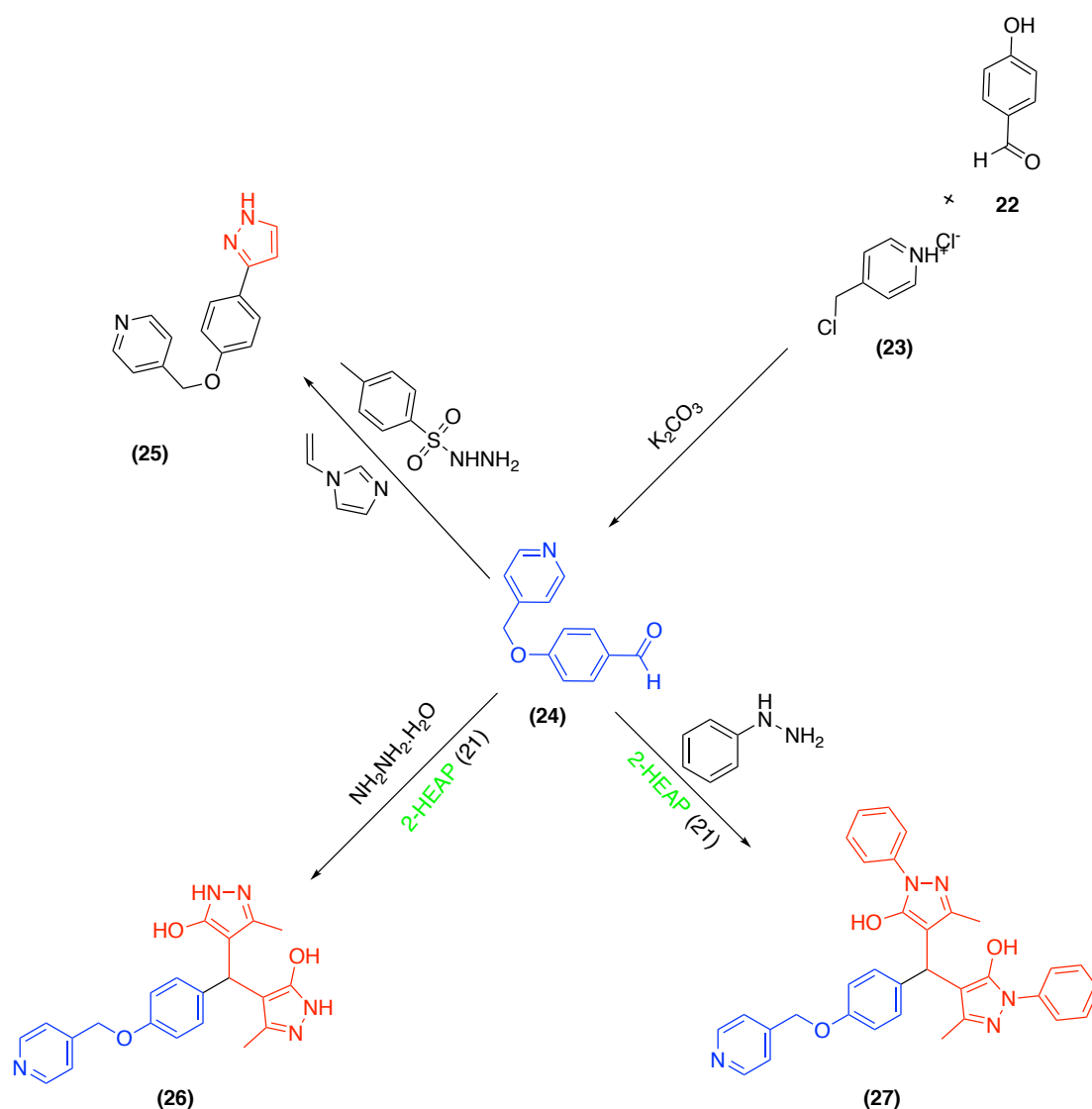
Scheme 30: synthetic pathway of the modified lead 2 compounds

3.9.1 2-Hydroxyethanaminium propionate[289] (2-HEAP) (21)

2-Hydroxy ethylammonium propionate (2-HEAP) was a relatively good catalyst for the synthesis of compounds **26** and **27**. In addition, 2-HEAP can be easily and cheaply synthesised from a simple acid-base neutralisation reaction. Recently, Sobhani *et al.*[290] reported the reaction of aldehydes with 3-methyl-1-phenyl-5-pyrazolone in ethanol in the presence of 2-hydroxy ethylammonium acetate as a recyclable catalyst. Here it was used to help prepare **26** and **27** by starting directly from aldehydes, phenylhydrazine/hydrazine hydrate, and ethyl acetoacetate, and using 2-HEAP as an efficient, cost effective, and recyclable catalyst. The product was a yellow viscous liquid with a yield of 81% (Scheme 31).
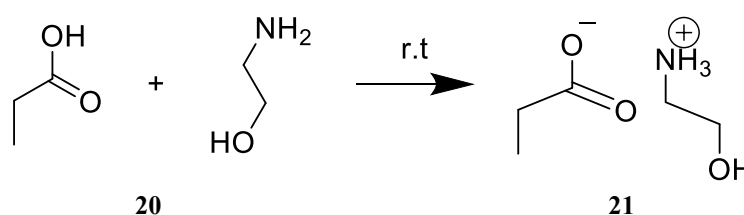
Scheme 31: 2-HEAP

3.9.2 Synthesis of aldehyde derivatives (24b and 24c)

Having determined the method using benzaldehyde **24a** as the model, the required pyridine derivatives, **24b** and **24c** (Scheme 32 and Table 36), were prepared by mixing 4-hydroxylbenzaldehyde **22a** or 3-hydroxylbenzaldehyde **22b** with 4-(chloromethyl)pyridine hydrochloride and K_2CO_3, which was stirred at 80 ℃ for 7 h. The obtained yields were in the range of 55 and 61 % for **24b** and **24c** respectively (Table 2).
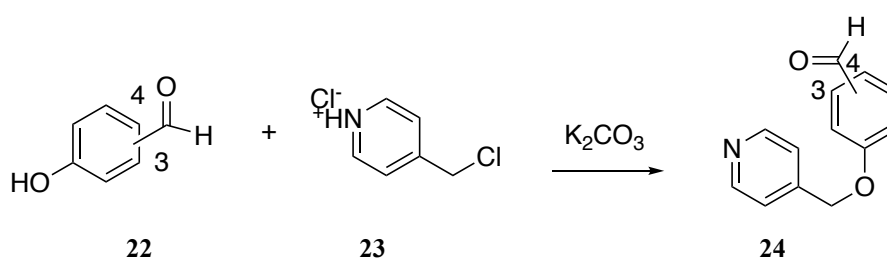
Scheme 32: 4/3-(Pyridin-4-ylmethoxy)benzaldehyde (24b) and (24c)

cpd	Yield %	m.p.		Colour and appearance
		Practical	Lit.	
24a	Sigma-Aldrich			
24b	61	102 - 104℃	57 - 58℃[291]	Tan crystals
24c	55	94 - 96℃	74 - 75℃[291]	White solid

Table 36: Formation of aldehydes 24

3.9.3 Synthesis of 4-((4-(1*H*-pyrazol-3-yl)phenoxy)methyl)pyridine (25)

The synthesis of pyrazoles remains of great interest due to the various applications in the biological and pharmaceutical industry. The best method for the preparation of pyrazoles involves the double condensation of 1,3-diketones with hydrazine or its derivatives.

The method of Varinder *et al.*[292] was followed to prepare **25b** with two head groups (pyridine and pyrazole). Benzaldehyde **24a** and *p*-toluenesulfonyl hydrazide were stirred for 3 h at room temperature in the presence of 5 N aqueous NaOH and finally vinyl imidazole was added, and mixture was stirred at 50 °C for 48 h (Scheme 33).

24a **25a**
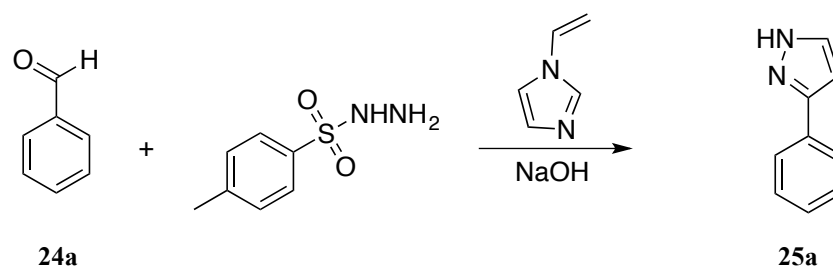
Scheme 33: 3-Phenyl-1*H*-pyrazole[292]

The formation of the diazo compound might be produced *in situ* from aldehydes in a one- pot process. Condensation of tosylhydrazine with benzaldehyde in the presence of an aqueous solution of sodium hydroxide led to the formation of benzaldehyde tosylhydrazone sodium salt, which on warming to 50 °C gave a reddish solution of phenyldiazomethane. Prior to warming the reaction mixture, 1-vinyl-1*H*-imidazole was added (Scheme 34).
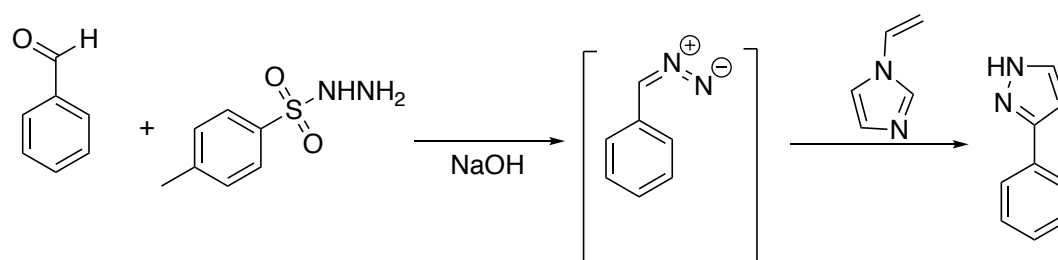
Scheme 34: Formation of 3-phenyl-1*H*-pyrazole[292]

The yield of **25a** was 20 % as a yellow liquid, which was purified by flash column chromatography. **25a** was used as a model to confirm that the method of Aggarwal *et al.*[292] can be used to synthesise **25b** (Scheme 35).
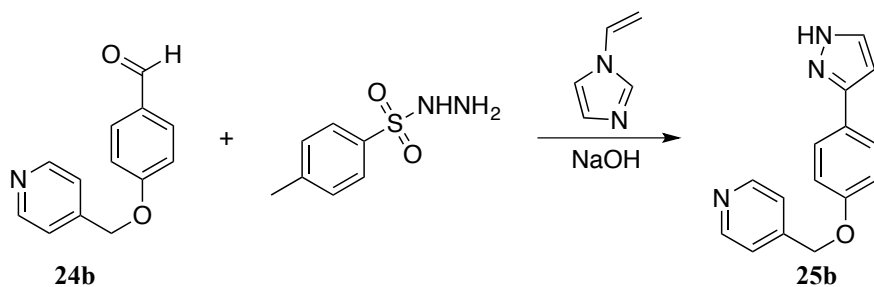
Scheme 35: 4-((4-(1*H*-pyrazol-3-yl)phenoxy)methyl)pyridine

Pyrazole **25b** was obtained in a yield of 28 % as a yellow viscous liquid, produced by using **24b** as starting material and following the procedure of Varinder *et al.*[292] Column chromatography was used for purification (Table 37).

3.9.4 Synthesis of 1*H*-pyrazol-3-ol derivatives (26)
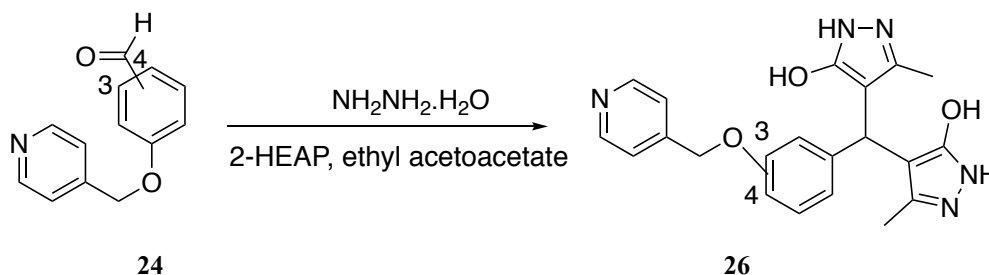
Scheme 36: Synthesis of 1*H*-pyrazol-3-ol derivatives (26)

The method of Zhou *et al.*[293] was used to synthesise compound **26**. In this procedure, aldehydes, phenylhydrazine/hydrazine hydrate, and ethyl acetoacetate were reacted using 2-hydroxy ethylammonium propionate (2-HEAP) as the catalyst.

The products **26a** and **26b** were prepared with hydrazine monohydrate with a yield of 36 % and 25 % respectively. These compounds were purified by recrystallisation from methanol (Scheme 36). ^{1}H NMR confirmed the presence of the aliphatic CH with a peak δ 4.56 for **26a** and δ 4.72 for **26b** as a singlet. ^{13}CNMR spectra confirmed an aliphatic CH at δ 32.9 and two CH$_3$ groups at δ 12.1

The method of Zhou *et al.*[293] was used to synthesise compound **27**. In this procedure, aldehydes, phenylhydrazine/hydrazine hydrate, and ethyl acetoacetate were reacted using 2-hydroxy ethylammonium propionate (2-HEAP) as the catalyst.

Benzaldehyde **24a** was used as a model to confirm that the 2-HEAP reagent can help the reaction of aldehyde with phenylhydrazine (Scheme 37).

24a   **27a**

Scheme 37: 4,4'-(phenylmethylene)bis(3-methyl-1-phenyl-1*H*-pyrazol-5-ol) (27a)
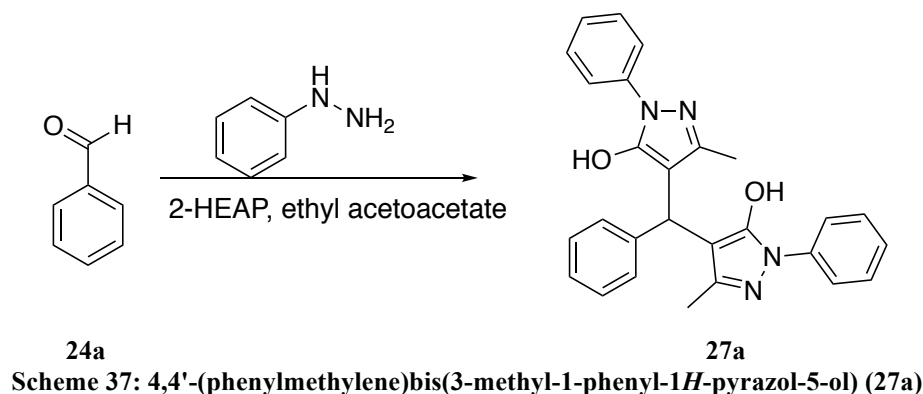
The procedure of Zhou *et al.*[293] had a mistake in the order of the addition of the starting material, as benzaldehyde was used and mixed with phenylhydrazine and ethyl acetoacetate for 40 min and then 2-HEAP was added, which produced an imine compound. As a result, the addition of the starting material was changed by adding phenylhydrazine, ethyl acetoacetate and then adding 2-HEAP; the mixture was refluxed for 40 min. Then benzaldehyde **24a** was added and refluxed further. The product was obtained after recrystallisation with methanol (Scheme 38).

^{1}H NMR confirmed the presence of the aliphatic CH with a peak at δ 4.98 as a singlet and the two CH$_3$ groups as a singlet at δ 2.23.

24   **27**

Scheme 38: 4,4'-((3/4-(pyridin-4-ylmethoxy)phenyl)methylene)bis(3-methyl-1-phenyl-1*H*-pyrazol-5-ol) (27b) and (27c)
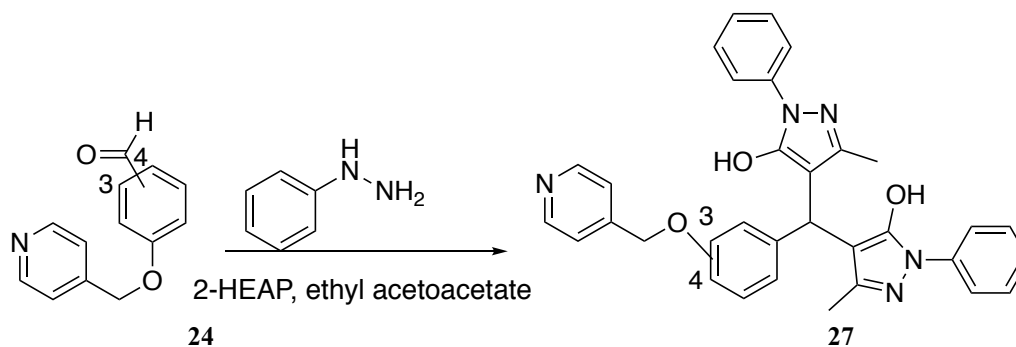
The reaction of the aldehydes **24b** and **24c** with phenylhydrazine, ethyl acetoacetate and 2-HEAP at reflux for 1 h gave compounds **27b** and **27c** in yields of 35 % and 10 % respectively. **27c** required purification by column chromatography using EtOAc as the mobile phase followed by recrystallisation with methanol. **27b** was purified by recrystallisation with methanol (Table 37).

cpd.	Yield %	m.p.		HRMS	Colour and appearance
		Practical	Lit.		
25b	28	-	-	Calculated mass: 252.1145 [M + H]$^+$, measured mass: 252.1155 [M + H]$^+$	Yellow viscous liquid
26a	36	194 - 198 ℃	Novel	Calculated mass: 392.1717 [M + H]$^+$, measured mass: 392.1720 [M + H]$^+$	Tan solid
26b	25	264 - 268℃	Novel	Calculated mass: 392.1717 [M + H]$^+$, measured mass: 392.1707 [M + H]$^+$	Tan solid
27a	55	152 - 154℃	169℃[293]	-	Yellow solid
27b	35	210 - 214℃	Novel	Calculated mass: 544.2343 [M + H]$^+$, measured mass: 544.2348 [M + H]$^+$	Brown crystals
27c	10	180 - 186℃	Novel	Calculated mass: 544.2343 [M + H]$^+$, measured mass: 544.23031 [M + H]$^+$	Brown solid

Table 37: Identification data for 25, 26 and 27

3.10 Molecular modelling
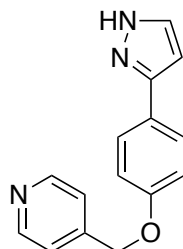
Figure 75: Compound 25b

In this chapter, compounds were designed by taking lead 2 and using different substitutions to explore SAR. **25b** was designed by using a simplified polar head group to one pyrazole group (Figure75). The compounds were docked using the LeadIT 2.1.2 programme, and the results were visualised using MOE (Figure 76). **25b** displayed the ether group perpendicular to the haem iron with a distance of 2.20 Å and hydrophobic interactions with Trp134, Leu148, Glu322, leu325, Ala326, Thr330 and Val391(Table 38).
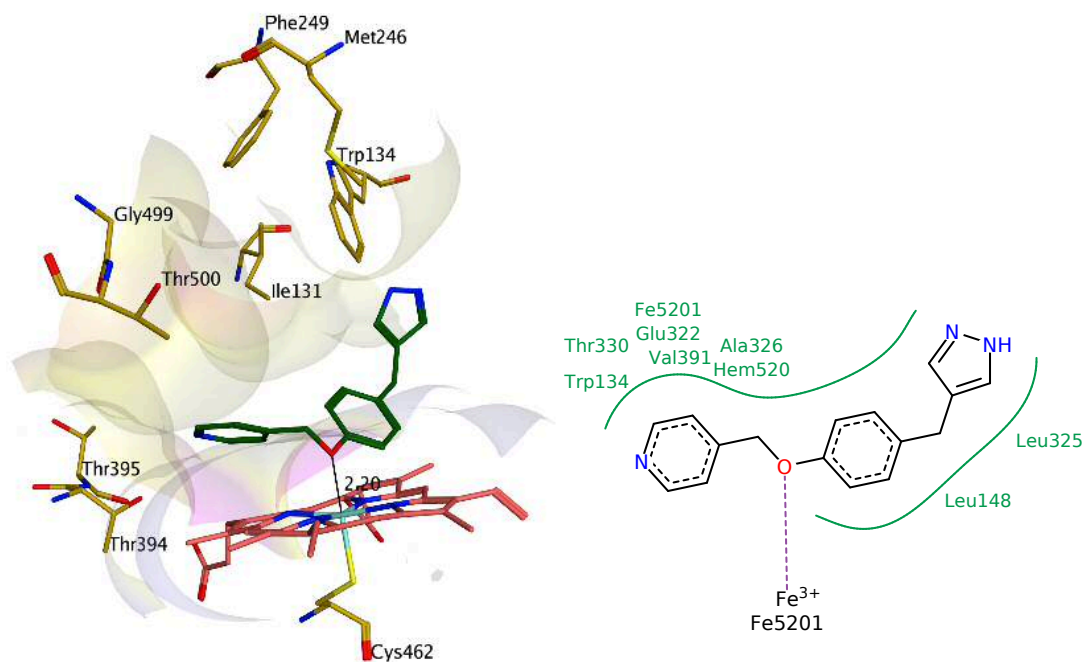
Figure 76: 3D and 2D models showing key binding interactions 25b with CYP24A1 model

cpd	Distance	Key binding interactions	
		Hydrogen bond interaction	**Hydrophobic interaction**
25b	2.20 Å	-	Trp134, Leu148, Glu322, Leu325, Ala326, Thr330 and Val391

Table 38: Key bind interactions between 25b
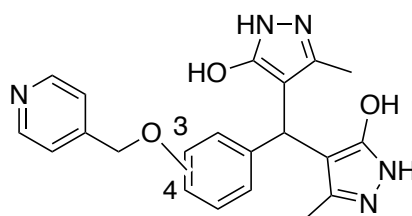
Figure 77: Compound 26

26a and **26b** were designed without a phenyl substitution on bis(3-methyl-1*H*-pyrazol-5-ol) and changing the position of the ether group from the 4 to 3 position (Figure 77). **26a** and **26b** were designed without phenyl substitution on bis(3-methyl-1*H*-pyrazol-5-ol) by changing the position of the ether group from the 4 to the 3 position. The compounds were docked using the LeadIT 2.1.2 programme, and the results were visualized on MOE. **26a** and **26b** were observed making hydrogen bonds between amino acids as shown (Table 39) and the nitrogen atom of pyridine for **26a** and **26b** interacted perpendicularly with the haem iron with a distance of 2.25 Å and 1.89 Å respectively (Figure 78). In addition, the length hydrogen bonds between **26a**

and **26b** and amino acid residues was ranging between 1.60 Å to 2.95 Å, which was slightly shorter than the length hydrogen bonds (2.27 Å to 3.14 Å) between lead 2 and amino acid residues (Table 39).
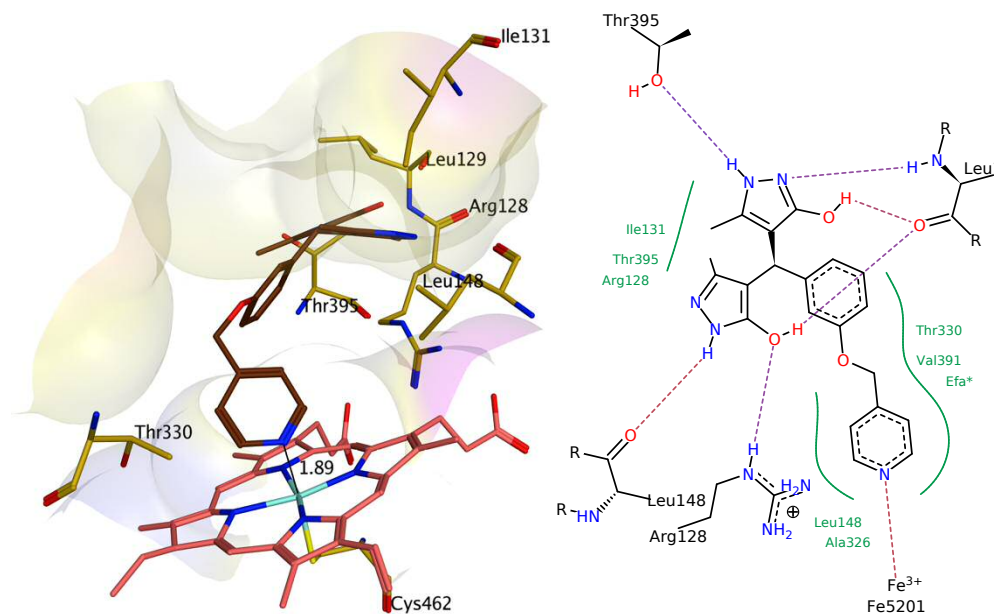
Figure 78: 3D and 2D models showing key binding interactions 26b with CYP24A1 model

cpd	Length HB	Hydrogen bonds
26a	2.31 Å	Between hydroxyl group of 26a and Glu130
	1.65 Å	Between hydroxyl group of 26a and Thr395
	1.85 Å	Between hydroxyl group of 26a and Leu129
26b	1.60 Å	Between hydroxyl group of 26b and Leu129
	2.38 Å	Between hydroxyl group of 26b and Leu129
	2.26 Å	Between pyrazole of 26b and Leu129
	2.95 Å	Between methoxy group of 26b and Arg128
	1.91 Å	Between pyrazole of 26b and Leu148
	2.14 Å	Between pyrazole of l26b and Thr395

Table 39: Hydrogen bond interaction 26a, 26b and amino acid residues of the CYP24A1 model
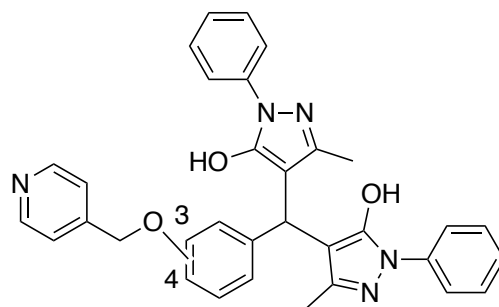
Figure 79: Compound 27

Compounds **27b** and **27c** have two phenyl rings on bis(3-methyl-1*H*-pyrazol-5-ol) (Figure 79); these were modified by changing the position of the ether group from the 4 to the 3 position. For compounds **27b** and **27c** the hydroxyl group interacted perpendicularly with the haem iron with a distance of 2.63 Å and 2.05 Å for **27b** and **27c** respectively rather than interaction through any heterocycle rings present in **27b** and **27c** (Figure 80 and Table 40).
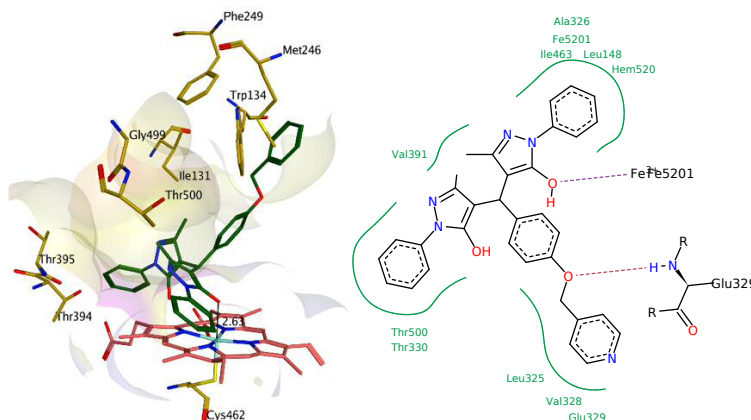
Figure 80: 3D and 2D models showing key binding interactions with 27b on CYP24A1 model

cpd	A	Key binding interactions	
		B	**C**
27b	2.63 Å	Glu329 - ether	Leu148, Leu325, Ala326, Val328, Glu329, Thr330, Val391, Ile463 and Thr500
27c	2.05 Å	Arg128 - ether	Leu148, Met246, Ala327, Val391, Phe393, Thr395 and Thr330

Table 40: (A) Distance hydroxyl group of 27a, 27b and iron of haem, (B) Hydrogen bond interaction (C) hydrophobic key binding interactions

3.10.1 Docking studies of compounds 26a and 26b using a CYP27B1 homology model

Both compounds **26a** and **26b** reached the active site through the access channel and were exposed to multiple hydrophobic residues Phe110, Leu127, Ala317, Thr321, Gly386, Val387 and Thr493 for **26a** (Figure 81), and Phe110, Leu127, Ala317, Thr321, Val387 and Thr493 for

26b (Figure 77). Both **26a** and **26b** formed hydrogen bonds between the nitrogen of pyrazole with Asp320 additionally **26b** formed hydrogen binding interaction with Asn387 (Figure 82). Both these amino acids Asp320 and Asn387 have been identified as important amino acids for CYP27B1 inhibitory activity (see Chapter 2). The nitrogen atom of the pyrazole for both compounds was perpendicular on the haem iron with a distance of 2.20 Å for **26a** and 2.23 Å for **26b.**
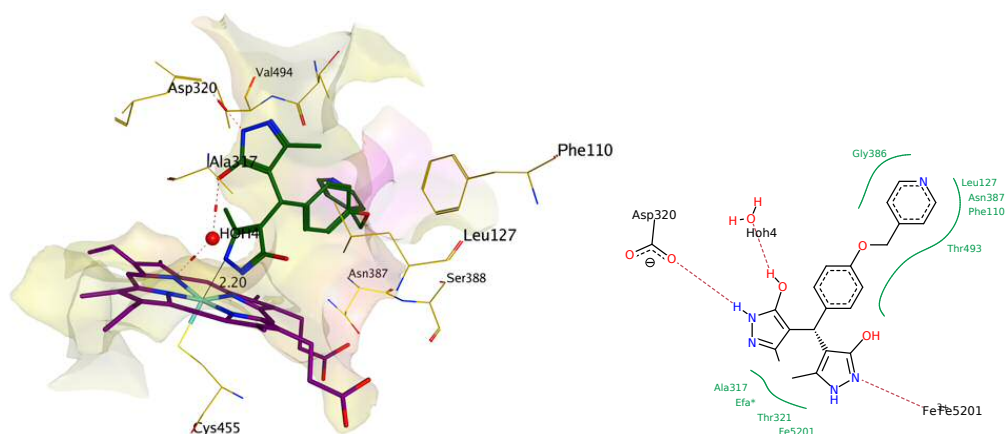
Figure 81: 3D and 2D models showing key binding interactions of 26a with CYP27B1 model
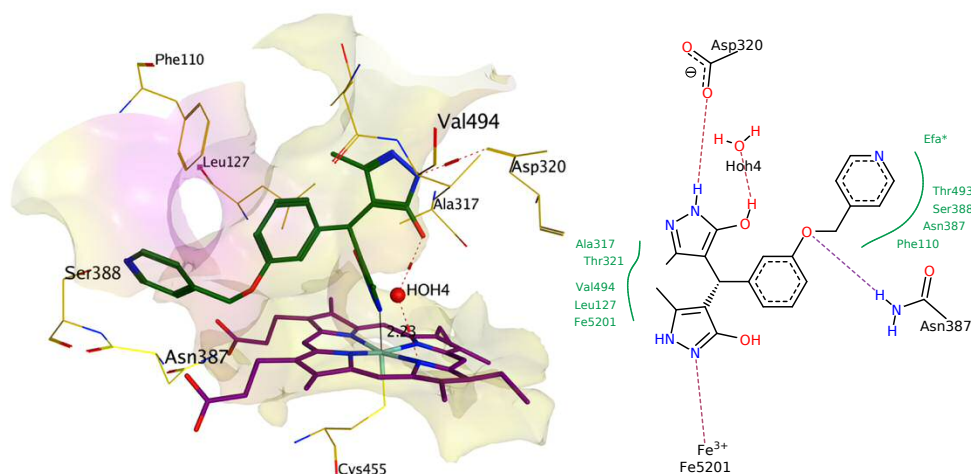
Figure 82: 3D and 2D models showing key binding interactions of 26b with CYP27B1 model

3.11 Biological assay

3.11.1 CYP24A1 inhibitor enzymatic assay

The final compounds **25b, 26a, 26b, 27b** were evaluated by enzymatic assay to determine CYP24A1 inhibitory activity as previously described (see 3.6.1).

Generally, compounds **25b**, **26a**, **26b** and **27b** displayed weak inhibition of CYP24A1 activity when compared with the ketoconazole standard. **26a** and **26b** were more active than lead 2 (IC_{50} 5.5 µM)[191]. The IC_{50} values ranged between 2.5 to 25.5 µM, and the best IC_{50} values were obtained for compounds **26a** and **26b**, which were twice as active as lead 2 (Figure 83).
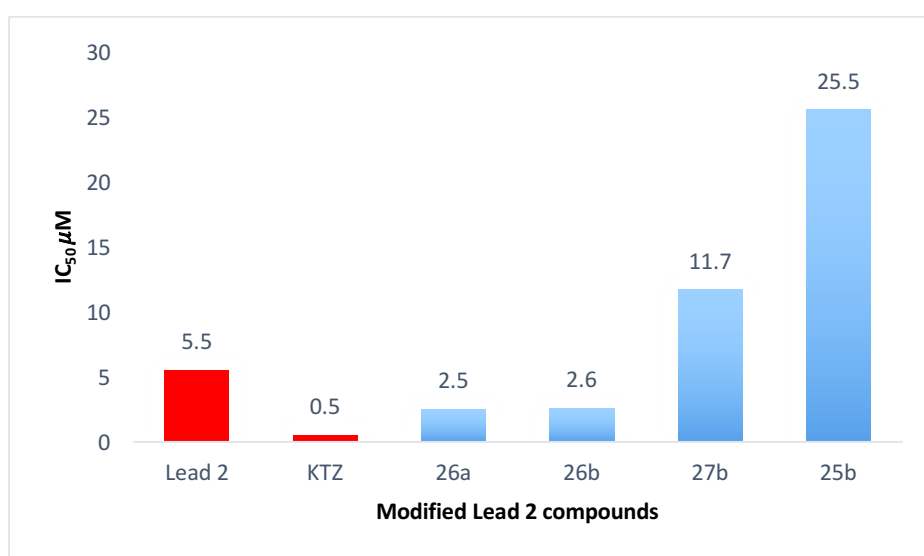
Figure 83: Biological assay for modified lead 2 compounds on CYP24A1

The structure of compound **25b** was different from that of the other compounds. This a compound with a simple pyrazole ring and lacking hydroxyl substituents on the pyrazole ring. The less of inhibitory activity compared with lead 2 might be owing to the structure, which is straight and without branching to give a T shaped or Shaped structure, which are often more efficient at filling the active site and enhancing competitive inhibition. Complete filling of the binding cavity has shown to be important for improved IC_{50}[191].

The main difference between **26a** and **26b** was changing the position of the ether group from the para position to the meta position on the phenyl ring, but it resulted in no notable improvement in the activity. 26a and 26b (IC_{50} = 2.5 µM and 2.6 µM). displayed activity twice as active as lead 2. The activity **26a** and **26b**, may be owing to the presence of a pyridine ring instead of a phenyl ring, which interacted with haem iron leaving the two pyrazole rings free to make hydrogen bonds with amino acid residues. In addition, the polar nature **of 26a** and

26b, which was also supported by a lower Log P of 0.56 compared with **27b** and **27c** where Log P was 4.35. The main difference between **26a** and **26b** was changing the position of the ether group from the para position to the meta position on the phenyl

ring, but this result did not notable an improvement in the inhibitory activity.

Compound 27b displayed poor inhibitory activity (IC_{50} = 11.7 µM) compared with lead 2 (IC_{50} = 5.5 µM). This effect is perhaps due to the presence of two phenyl-ring substituents on two pyrazole rings resulting a very bulky compound preventing the nitrogen of the pyrazole from interacting efficiently with the haem iron

3.11.2 CYP27B1 inhibitor enzymatic assay

Compounds **26a** and **26b** showed inhibitory activity against CYP24A1 that was twice as active as lead 2. So, **26a** and **26b** were subject to further evaluation against CYP27B1. The IC_{50} values are the average (± 10 %) of two independent experiments (n = 2), which followed published paper methods[191,280, 281,282,283] The limit of two experiments is owing to the high cost of enzyme isolation and the appropriate vitamin D substrates. However, both compounds showed inhibition (IC50 = 0.57 µM and 0.41 µM respectively) against CYP27B1 that was greater than that against CYP24A1. As a result, **26a** and **26b** have selectivity for CYP27B1 that is five times greater than CYP24A1. The selectivity of **26a** and **26b** could be related to better fit and binding in the CYP27B1 active site, where the pyrazole ring interacted with the haem iron instead pyridine as in the lead 2. Also, formation of hydrogen bond with Asp320 and Asn387, which are important amino acids in CYP27B1(see Chapter 2) (Figure 84).
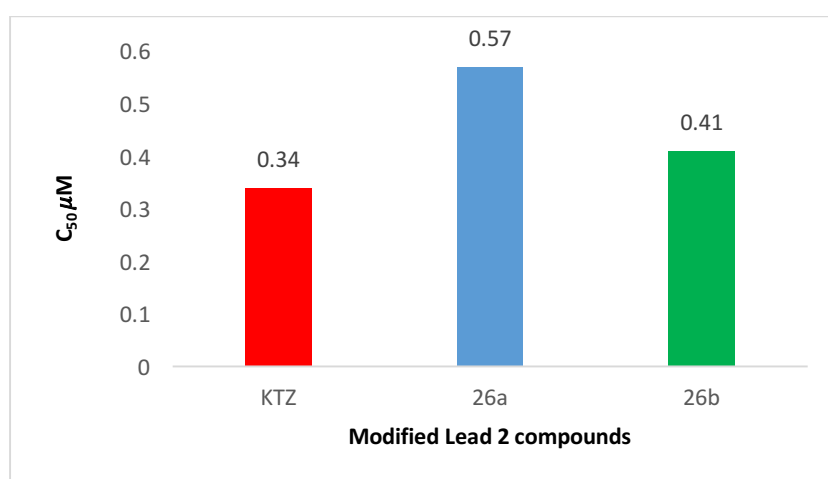
Figure 84: Biological assay for 26a and 26b compounds on CYP27B1

3.12 Conclusion

Lead 2 has promising CYP24A1 inhibitory activity (IC$_{50}$ 5.5 µM) with a pyrazole nitrogen interacting perpendicularly with the iron haem at a distance 2.39 Å. In addition, lead 2 formed hydrogen bonds with amino acid residues Glu329, Thr330 and Gly499. The modified lead 2 compounds **25b**, **26a**, **26b**, **27a**, **27b** and **27c** were all synthesised successfully. **25b** interacted perpendicularly with the haem iron of CYP24A1 via ether oxygen with a distance of 2.20 Å. **26a** and **26b** were designed without phenyl substituent by changing the position of the ether group from the 4 to the 3 position and formed hydrogen bonds between number of amino acids, with the nitrogen atom of pyridine interacting perpendicularly with the haem iron of CYP24A1 with a distance 2.25 Å and 1.89 Å respectively. Compounds **27b** and **27c** interact with the haem iron via a hydroxyl group with a distance of 2.05 and 2.63 Å respectively for CYP24A1. **26a** and **26b** were the most promising CYP24A1 inhibitors (IC$_{50}$ 2.5 µM and 2.6 µM respectively) and so further evaluated against CYP27B1. However, **26a** and **26b** showed enzymatic inhibition (IC$_{50}$ = 0.57 µM and 0.41 µM respectively) against CYP27B1. As a result, both compounds showed a 5- fold selectivity for CYP27B1 confirming the importance of Asp320 in particular and also Asn387 as important amino acids for CYP27B1 inhibitory activity (see Chapter 2).

3.13 Experimental

3.13.1 Molecular modelling

molecular modelling method information as previously described Chapter 2.

3.13.2 CYP24A1 inhibitor enzymatic assay[279]

All CYP24A1 inhibitor enzymatic assay method information as previously described in Chapter 3.

3.13.3 CYP27b1 inhibitor enzymatic assay[279]

Inhibition of CYP27B1 was assayed in a manner similar to that of CYP24A1 except that the buffer contained 20 mM Tris (pH 7.5), 125 mM NaCl, 0.1% CHAPS with (Adx + AdxR + CYP27B1 + 25-hydroxyvitamin D + inhibitors + NADPH)[279] (Table 41). The HPLC mobile phase was isopropanol-hexane 7: 93 v/v. The assay for each compound was performed in duplicate (n = 2).

Material	CYP24A1	
	Concentration	Volume
Adx	2 µM	8 µL
AdxR	0.2 µM	8 µL
CYP27B1	0.1 µM	8 µL
25-Hdroxyvitamin D	2.5 µM	5 µL
Inhibitor	0 - 2 µM	2 µL
NADPH	1 mM	2 µL
Buffer solution	367 µL	

Table 41: The concentration and volume required in the CYP27B1 inhibition assay

3.13.4 Chemistry experimental

3.13.4.1 2-Hydroxyethanaminium propionate (2- HEAP)[289] (21)

Chemical Formula: $C_5H_{13}NO_3$
Molecular Weight: 135.16
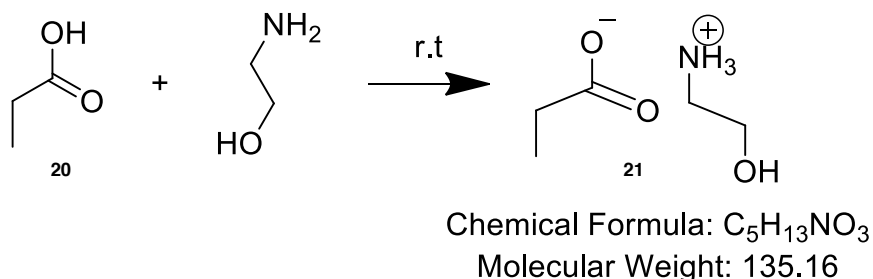
Method:

A solution of propionic acid (3.7 g, 50 mmol) in ethanol (1.5 mL) was added dropwise to a stirring solution of 2-aminoethanol (3.1 g, 50 mmol) in ethanol (1.5 mL) at room temperature over 1 h. The resultant mixture was stirred at room temperature for another 24 h. Ethanol was removed in *vacuo* and the product was dried in a vacuum oven at 40 ℃ for 48 h[289].

Yield = 5.5 g (81 %), a yellow viscous liquid

¹H NMR (CDCl₃):

δ : 7.28 (s, 3H, NH₃), 5.01 (m, 1H, OH), 3.76 (m, 2H, CH₂), 3.11 (m, 2H, CH₂), 2.17 (m, 2H, CH₂), 1.04 (m, 3H, CH₃).

3.13.4.2 4-(Pyridin-4-ylmethoxy)benzaldehyde (24b)[291]

Chemical Formula: $C_{13}H_{11}NO_2$
Molecular Weight: 213.24
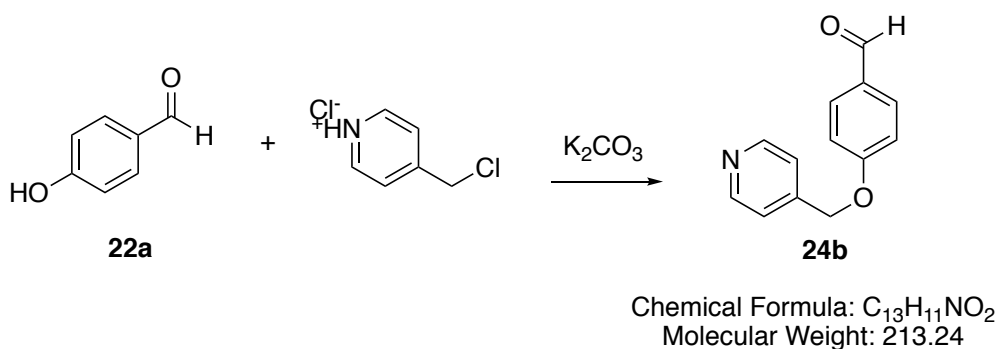
Method:

A mixture of 4-hydroxylbenzaldehyde (1.2 g, 10 mmol), 4-(chloromethyl)pyridine hydrochloride (1.6 g, 10 mmol) and K_2CO_3 (4.2 g, 30 mmol) in dry DMF (12 mL) was stirred at 80 ℃ for 7 h. The cooled mixture was extracted with EtOAc (100 mL). The organic layer was washed with brine (2 × 100 mL), dried (MgSO₄) and concentrated to dryness[291].

TLC: petroleum ether-EtOAc 1: 3 v/v, R_f = 0.24

m. p. = 92 - 94 ℃ (Lit. m. p. 57 - 58 ℃)[291].

Yield = 1.3 g (61 %), tan crystals, recrystallised with methanol.

^{1}H NMR (DMSO-d$_6$):

δ : 9.89 (s, 1H, CHO), 8.60 (dd, J = 1.6, 4.5 Hz, 2H, Ar), 7.91 (m, 2H, Ar), 7.47 (d, J = 6.3 Hz, 2H, Ar), 7.22 (dd, J = 1.8, 7Hz, 2H, Ar), 5.33 (s, 2H, CH$_2$).

3.13.4.3 3-(Pyridin-4-ylmethoxy)benzaldehyde (24c)
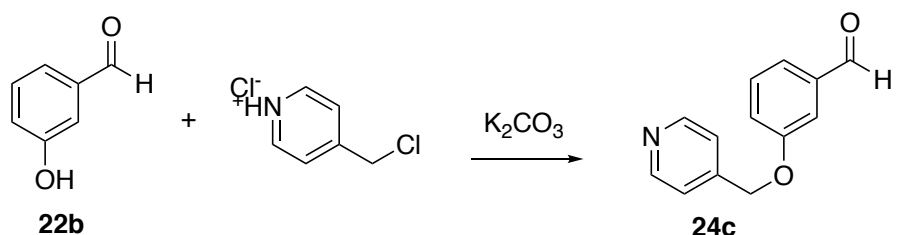
Chemical Formula: C$_{13}$H$_{11}$NO$_2$
Molecular Weight: 213.24

Method: See 3.13.4.2

The crude product was purified by gradient flash column chromatography, the product was eluted with EtOAc-CH$_3$OH 9:1v/v.

Reagent: 3-Hydroxylbenzaldehyde (1.22 g, 10 mmol) **22b**

TLC: EtOAc-CH$_3$OH 95: 5 v/v, R$_f$ = 0.4

m. p. = 94 - 96 ℃ (Lit. m. p. 74 - 75 ℃)[291]

Yield = 1.5 g (55 %), white solid

^{1}H NMR (CDCl$_3$):

δ : 10.01 (s, 1H, CHO), 8.70 (d, J = 6 Hz, 2H, Ar), 7.54 (m, 3H, Ar), 7.30 (m, 1H, Ar), 7.22 (dd, J = 1.8, 7.0 Hz, 2H, Ar), 5.31 (s, 2H, CH$_2$).

3.13.4.4 3-Phenyl-1*H*-pyrazole[294]
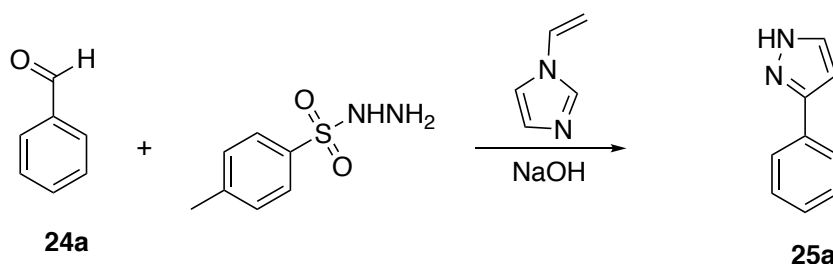
Chemical Formula: C$_9$H$_8$N$_2$
Molecular Weight: 144.18

Benzaldehyde (0.3 g, 3 mmol) was added to a solution of *p*-toluenesulfonyl hydrazide (0.5 g, 3 mmol) in dry acetonitrile (15 mL). After the mixture was stirred for 3 h at room temperature, a solution 5 N aqueous NaOH (10 mL) was added and the mixture was stirred for a further 20

min. Vinyl imidazole (1.4 g, 15 mmol) was added, and the mixture was stirred at 50 ° C for 48 h. The mixture was evaporated under reduced pressure, and the residue was dissolved in a 1:1 mixture of water- EtOAc (70 mL). The organic layer was separated and dried over $MgSO_4$. After filtration and removal of the solvent under reduced pressure, the crude material was purified by gradient flash column chromatography, product was eluted with petroleum ether-EtOAc 1:1 v/v [292].

TLC: petroleum ether-EtOAc 1: 1 v/v, $R_f = 0.42$

Yield = 0.08 g (20 %), yellow liquid.

¹H NMR (CDCl₃):

δ : 9.62 (s, 1H, NH), 7.71 (d, J = 7.1 Hz, 2H, Ar), 7.54 (s, 1H, Ar), 7.31 (t, J = 7.6 Hz, 2H, Ar), 7.25 (d, J = 7.5 Hz, 1H, Ar), 6.54 (s, 1H, Ar).

3.13.4.5 4-((4-(1*H*-Pyrazol-3-yl)phenoxy)methyl)pyridine

24b   **25b**

Chemical Formula: $C_{15}H_{13}N_3O$
Molecular Weight: 251.29
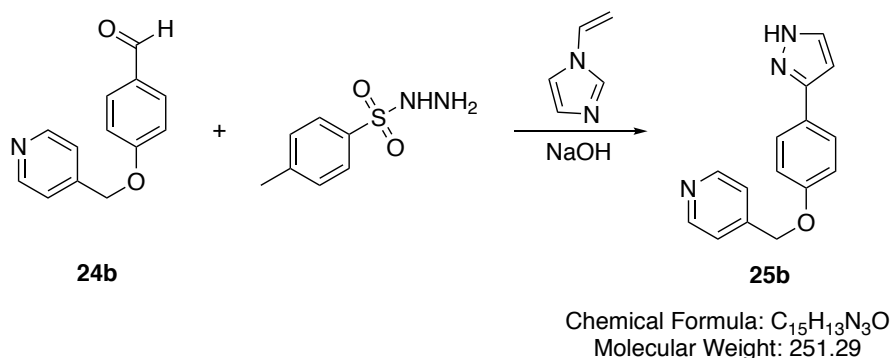
Method: See 3.13.4.4

The product was purified by gradient flash column chromatography, product was eluted with EtOAc-CH₃OH 9.5: 0.5 v/v

Reagent: 4-(Pyridin-4-ylmethoxy)benzaldehyde (0.5 g, 2.4 mmol) **24b**

TLC: EtOAc-CH₃OH 9.5: 0.5 v/v, $R_f = 0.40$

Yield = 0.17 g (28 %), yellow viscous liquid

¹H NMR (CDCl₃):

δ : 10.01 (s, 1H, NH), 8.53 (dd, J = 1.4, 4.5 Hz, 2H, Ar), 7.66 (d, J = 2.2 Hz, 1H, Ar), 7.52 (m, 2H, Ar), 7.45 (t, J = 1.7 Hz, 1H, Ar), 7.39 (d, J = 7.8 Hz, 1H, Ar), 7.05 (t, J = 7.8 Hz, 1H, Ar), 6.98 (dd, J = 1.3, 8.0 Hz, 1H), 6.66 (d, J = 2.2 Hz, 1H, Ar), 5.2 (s, 2H, CH₂).

¹³C NMR (DMSO-d₆):

δ : 157.9 (C), 148.5 (CH, Ar), 149.5, 146.5 (2 × C), 129.2, 129.1 (2 × CH, Ar) 125.4 (C) 111.2, 110.9, 100.4 (7 × CH, Ar), 66.63 (CH$_2$).

LRMS (ES-TOF)

m/z: 252 [M + H]$^+$

HRMS (ES-TOF)

Calculated mass: 252.1145 [M + H]$^+$, measured mass: 252.1175 [M + H]$^+$

3.13.4.6 4,4'-((4-(Pyridin-4-ylmethoxy)phenyl)methylene)bis(3-methyl-1*H*-pyrazol-5-ol) (26a)
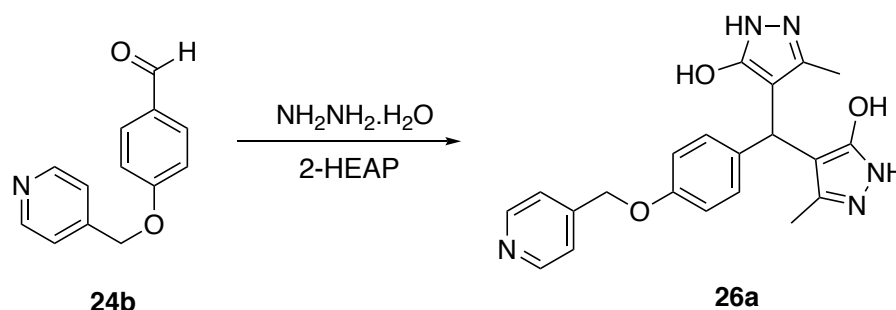
Chemical Formula: C$_{21}$H$_{21}$N$_5$O$_3$
Molecular Weight: 391.43

Method: See 4.5.4.8

Reagent: 4-(pyridin-4-ylmethoxy)benzaldehyde (0.30 g, 1.7 mmol) **24b**

TLC: CH$_2$Cl$_2$-CH$_3$OH 9: 1 v/v, R$_f$ = 0.34

m. p. = 194 -198 ℃

Yield = 0.20 g (36 %), tan solid, recrystallised with methanol

¹H NMR (CDCl₃):

δ : 8.69 (d, J = 6.0, 2H, Ar), 7.41 (d, J = 6 Hz, 2H, Ar), 7.16 (t, J = 8.0 Hz, 2H, Ar), 6.76 (m, 2H, Ar), 5.08 (s, 2H, CH$_2$), 4.47 (s, 1H, CH), 2.06 (s, 6H, 2CH$_3$)

¹³C NMR (CDCl₃):

δ : 158.2 (C), 150.1 (CH, Ar), 146.7, 145.8, 146.3 (8 × C), 129.3, 122.4, 121.0, 115.3, 123.4, 111.4 (6 × CH, Ar), 102.4 (CH, Ar), 68.0 (CH$_2$), 35.4 (CH), 10.8 (2 × CH$_3$)

LRMS (ES-TOF)

m/z: 392 [M + H]$^+$

HRMS (ES-TOF)

Calculated mass: 392.1717 [M + H]$^+$, measured mass: 392.1720 [M + H]$^+$

3.13.4.7 4,4'-((3-(pyridin-4-ylmethoxy)phenyl)methylene)bis(3-methyl-1*H*-pyrazol-5-ol) (26b)
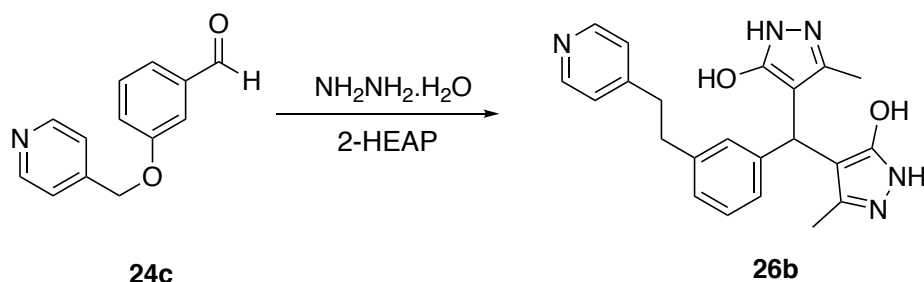
Chemical Formula: $C_{22}H_{23}N_5O_2$
Molecular Weight: 389.46

Method: See 4.5.4.8

Reagent: 4-(Pyridin-3-ylmethoxy)benzaldehyde (0.40 g, 1.9 mmol) **24c**

TLC: EtOAc-CH$_3$OH 6: 1 v/v, R$_f$ = 0.75

m. p. = 264 - 268 ℃

Yield = 0.18 g (25 %), tan solid, recrystallised with methanol.

¹H NMR (CDCl₃):

δ : 8.55 (d, J = 5.7 Hz, 2H, Ar), 7.40 (d, J = 5.8 Hz, 2H, Ar), 7.15 (t, J = 8.3 Hz, 1H, Ar), 6.75 (m, 3H, Ar), 5.08 (s, 2H, CH₂), 4.72 (s, 1H, CH), 2.06 (s, 6H, 2CH₃)

¹³C NMR (DMSO-d₆):

δ : 158.2, 156.2 (2 × C), 150.7, 145.8 (2 × CH, Ar), 145.9, 141.3. 129.2, 128.3, 122.42 (6 × CH, Ar), 121.0, 115.3, 111.4 (7 × C), 67.9 (CH₂), 33.2 (CH), 11.2 (2 × CH₃).

LRMS (ES-TOF)

m/z: 392 [M + H]⁺

HRMS (ES-TOF)

Calculated mass: 392.1717 [M + H]⁺, measured mass: 392.1707 [M + H]⁺

3.13.4.8 4,4'-(Phenylmethylene)bis(3-methyl-1-phenyl-1*H*-pyrazol-5-ol) (27a)
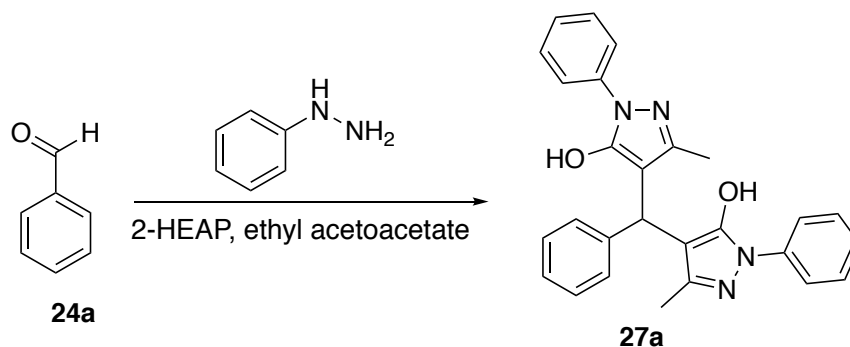
Chemical Formula: $C_{27}H_{24}N_4O_2$
Molecular Weight: 436.52

Method:

Phenylhydrazine (0.5 mL, 5 mmol) was mixed with ethyl acetoacetate (1.3 mL, 10 mmol). Then 2-hydroxy ethylammonium propionate (2-HEAP) (0.07 g, 0.5 mmol) was stirred under solvent free conditions for 40 min. Then, benzaldehyde (0.53 g, 5 mmol) was added and the reaction mixture heated at 90 ℃ for 1 h. After completion, the reaction was cooled to room temperature, where upon it solidified. The pure product was obtained from this solid by recrystallisation with methanol[293].

TLC: petroleum ether- EtOAc 1: 3 v/v, R_f = 0.41

m. p. = 152 - 154 ℃ (Lit. m. p. 169 ℃)[295]

Yield = 1.2 g (55 %), yellow solid, recrystallised with methanol

^{1}H NMR (DMSO-d₆):

δ : 13.96 (s, 2H, 2 × OH), 7.73 (m, 4H, Ar), 7.29 (m, 6H, Ar), 7.18 (m, 5H, Ar), 4.98 (s, 1H, CH), 2.23 (s, 6H, 2 × CH₃).

3.13.4.9 4,4'-((4-(Pyridin-4-ylmethoxy)phenyl)methylene)bis(3-methyl-1-phenyl-1*H*-pyrazol-5-ol) (27b)

Chemical Formula: $C_{33}H_{29}N_5O_3$
Molecular Weight: 543.63
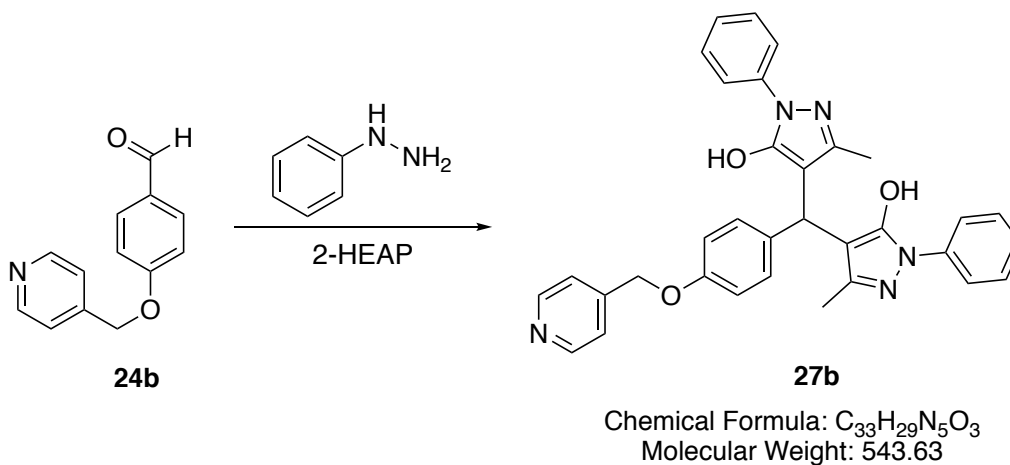
Method: See 4.5.4.8

Reagent: 4-(pyridin-4-ylmethoxy)benzaldehyde (0.53 g, 5 mmol) **24b**.

 TLC: EtOAc-CH$_3$OH 4:1v/v, R$_f$ = 0.26

m. p. = 210 - 214 ℃

Yield = 0.96 g (35 %), brown crystals, recrystallised with methanol.

^{1}H NMR (DMSO-d$_6$):

 δ :14.00 (s, 1H, OH), 13.12 (s, 1H, OH), 7.53 (dd, J = 1.5, 4.5, 2H, Ar), 7.71 (d, J = 7.7 Hz, 4H, Ar), 7.45 (m, 6H, Ar), 7.32 (t, J = 7.4 Hz, 2H, Ar) 7.18 (d, J = 8.5 Hz, 2H, Ar), 6.93 (m, 2H, Ar), 5.14 (s, 2H, CH$_2$), 4.91 (s, 1H, CH), 2.30 (s, 6H, 2 × CH$_3$)

^{13}C NMR (DMSO-d$_6$):

 δ : 156.2 (C), 149.6 (CH, Ar), 146.5, 146.1, 134.8 (10 × C), 128.9, 128.3, 125.5, 121.8, 120.5, 114.9 (17 × CH, Ar), 67.9 (CH$_2$), 32.9 (CH), 12.1 (2 × CH$_3$)

LRMS (ES-TOF)

m/z: 544 [M + H]$^+$

HRMS (ES-TOF)

Calculated mass: 544.2343 [M + H]$^+$, measured mass: 544.2348 [M + H]$^+$

3.13.4.10   4,4'-((3-(Pyridin-4-ylmethoxy)phenyl)methylene)bis(3-methyl-1-phenyl-1*H*-pyrazol-5-ol) (27c)
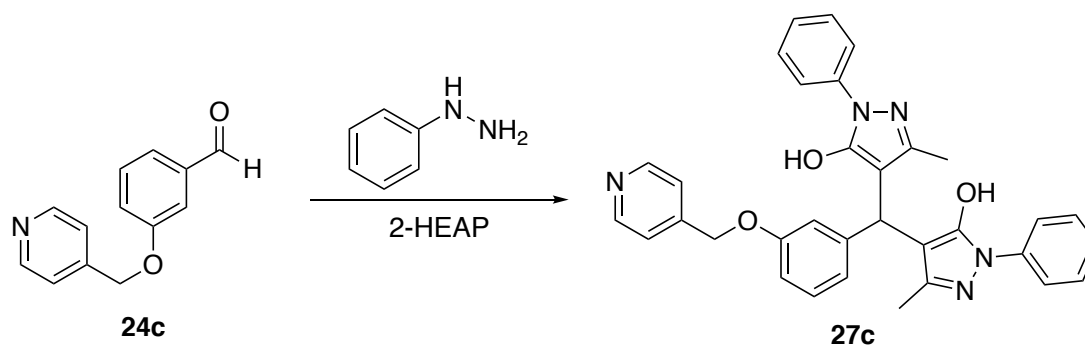
Chemical Formula: $C_{33}H_{29}N_5O_3$
Molecular Weight: 543.63

Method: See 4.5.4.8

The crude product was purified by preparative TLC EtOAc-CH_3OH 9: 1 v/v

Reagent: 3-(Pyridin-4-ylmethoxy)benzaldehyde (0.30 g, 1.7 mmol) **24c**

TLC: EtOAc-CH_3OH 9: 1 v/v, R_f = 0.27

m. p. = 180 -186 ℃

Yield = 0.07 g (10 %), brown solid

^{1}H NMR (CDCl$_3$):

δ : 8.51 (d, J = 5.6 Hz, 2H, Ar), 7.94 (d, J = 7.5 Hz, 2H, Ar), 7.42 (d, J = 6.0 Hz, 2H, Ar), 7.33 (t, J = 7.5 Hz, 2H, Ar), 7.11 (t, J = 8.0 Hz, 2H, Ar), 7.05 (m, 4H, Ar), 6.99 (d, J = 8.0 Hz, 2H, Ar), 6.87 (d, J = 8.0 Hz, 2H, Ar), 5.05 (s, 2H, CH_2), 4.93 (s, 1H, CH), 2.03 (s, 6H, 2 × CH_3)

^{13}C NMR (CDCl$_3$):

δ : 158.2 (C), 157.7, 150.1, 149.2 (3 × CH, Ar), 146.7, 146.3, 141.2(10 × C), 128.8, 123.3, 122.5, 120.9, 119.5, 114.9, 110.9, 102.4 (15 × CH, Ar), 67.9 (CH_2), 35.5 (CH), 13.5 (2 × CH_3)

LRMS (ES-TOF)

m/z: 544 [M + H]$^+$

HRMS (ES-TOF)

Calculated mass: 544.2343 [M + H]$^+$, measured mass: 544.2307 [M + H]$^+$
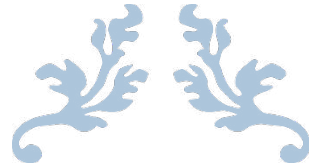
CHAPTER FIVE

Lead 3

4   Development of Lead 3

The docking study for lead 3 compound[191,296]showed that the pair electron of the imidazole nitrogen was perpendicular to the haem iron of the CYP24A1 model at a distance of 2.28 Å. Furthermore, hydrogen bonds between the dimethoxy groups and Arg128 and Ile131 as well as several hydrophobic interactions with Leu129, Glue 130, Leu148, Ile149, Ala326, Glu329, Thr330 and Val391 (Figure 85) were observed. In addition, the validation of the accuracy of Leadit 2.1.2 was done by docking the known CYP24A1 inhibitor (*R*)-VID 400 (IC_{50} 15nM)[297], which showed interaction between the nitrogen of imidazole and the iron of the haem. Also, there were hydrophobic interactions with amino acid residues in the active site of the CYP24A1 model[191] (Leu148, Met246, Phe249, Thr330 and Ala326).
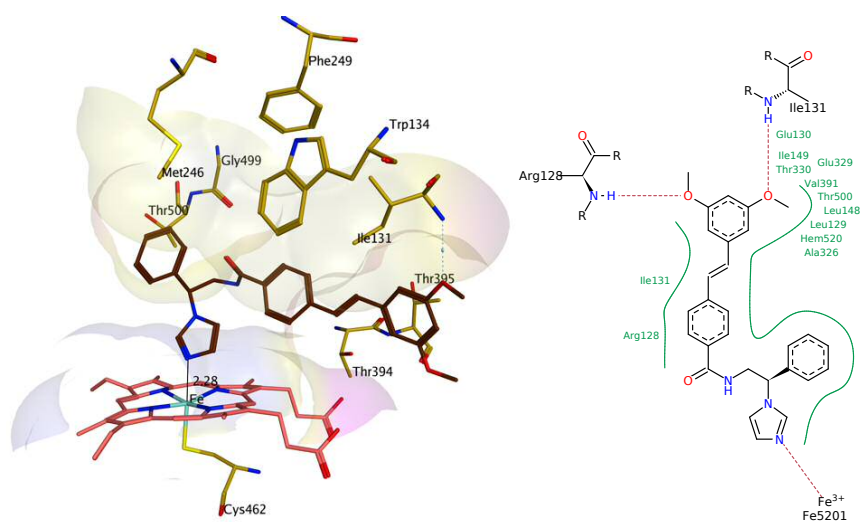
Figure 85: 3D and 2D for lead 3
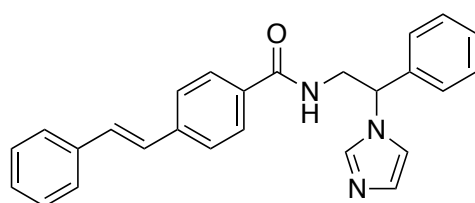
IC_{50} 0.40 μ M

Figure 86: lead 3 compound[191]

Lead 3 (Figure 86) was modified and developed, specifically through (i) substitution of the phenyl ring on the imidazole side to explore structure activity-relationships, (ii) substitution of the phenyl ring of styrene to explore structure activity-relationships, and (iii) variation of the alkene position to allow the complete filling in the active site of t CYP24A1 (Figure 87).
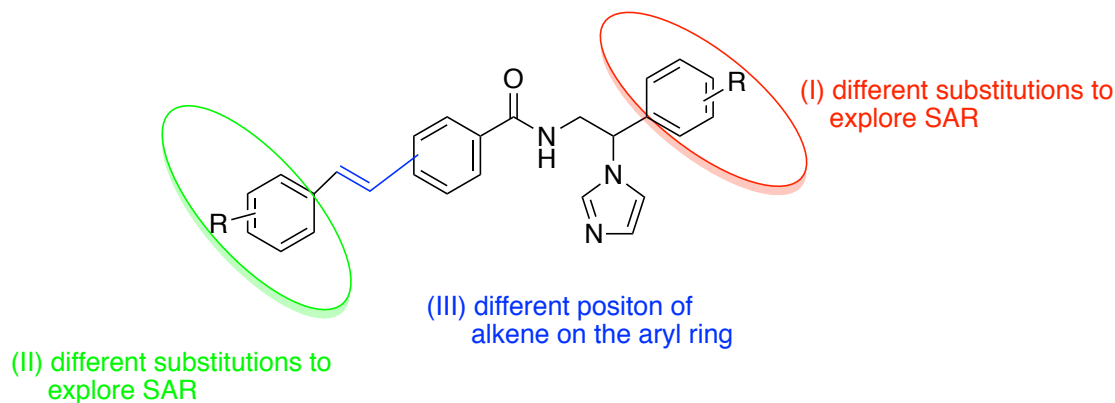
Figure 87: Modification of lead 3 compounds

This chapter is divided into six parts as follows:

1. Synthesis of (*E*)-*N*-(2-(1*H*-imidazol-1-yl)-2-(substituted/unsubstituted phenyl)ethyl)-**4**-(substituted/unsubstituted styryl)benzamides.

2. Synthesis of (*E*)-*N*-(2-(1*H*-imidazol-1-yl)-2-(substituted/unsubstituted phenyl)ethyl)-**3**-(substituted/unsubstituted styryl)benzamides

3. Molecular modelling

4. Biological assay

5. Conclusions

6. Experimental

4.1   Synthetic pathway of (*E*)-*N*-(2-(1*H*-imidazol-1-yl)-2-(substituted/unsubstituted phenyl)ethyl)-4-(substituted/unsubstituted styryl)benzamides
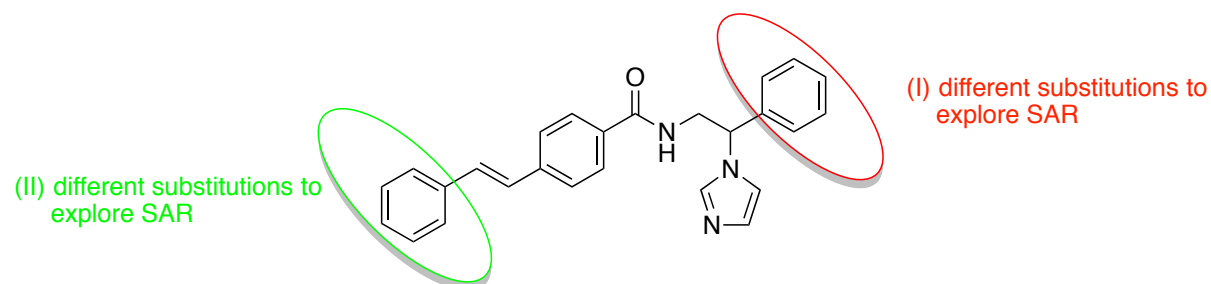
The synthetic pathway is illustrated in Scheme 39.
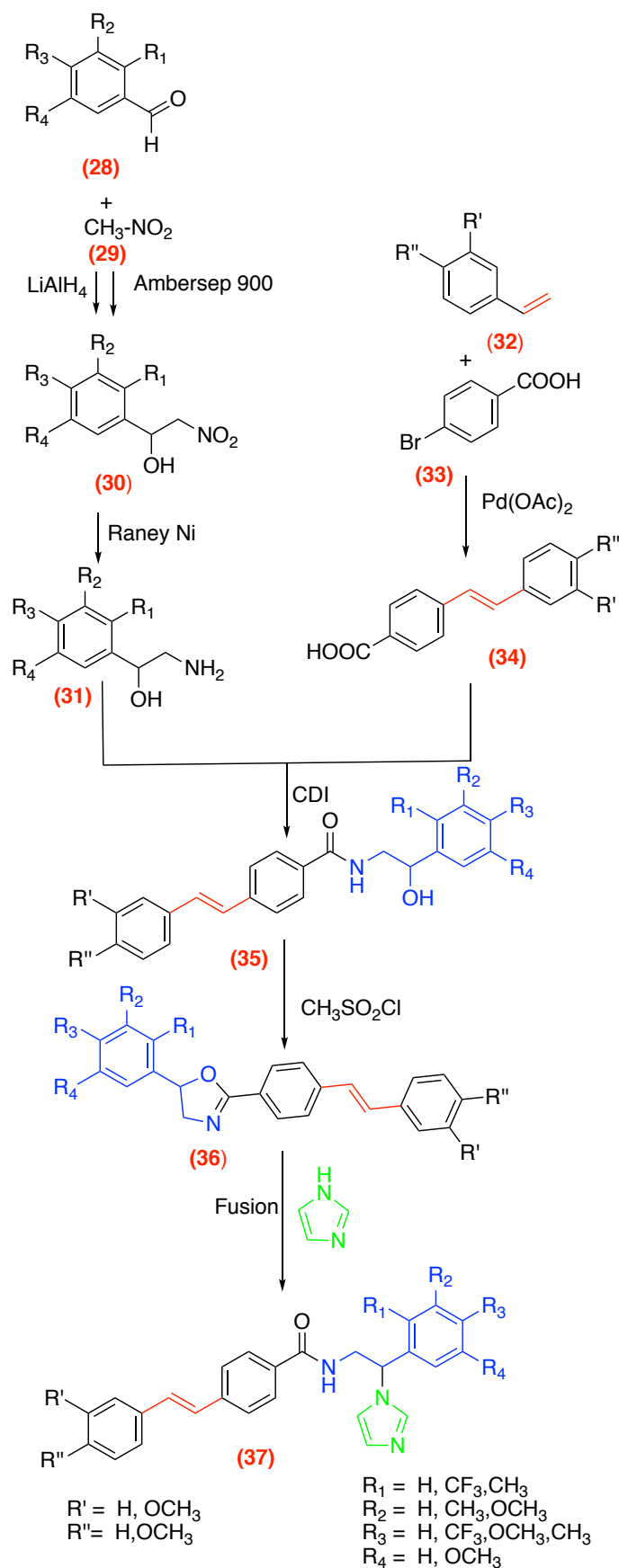
Scheme 39: Synthetic pathway of (*E*)-*N*-(2-(1*H*-imidazol-1-yl)-2-(substituted/unsubstituted phenyl)ethyl)-4-(substituted/unsubstituted styryl)benzamides

R' = H, OCH$_3$
R"= H, OCH$_3$

R$_1$ = H, CF$_3$, CH$_3$
R$_2$ = H, CH$_3$, OCH$_3$
R$_3$ = H, CF$_3$, OCH$_3$, CH$_3$
R$_4$ = H, OCH$_3$

4.1.1   Synthesis of substituted 2-nitro-1-phenyl-ethanol derivatives

The Henry reaction of carbonyl compounds with alkyl nitro compounds bearing α-hydrogen atoms is one of the most fundamental and widely utilised methods for the construction of carbon-carbon bonds that lead to the formation of β-nitroalcohols[298,299].

The Henry reaction (nitroaldol) is an ideal, atom economical, and powerful method for stereo-selective carbon-carbon bond formation, which is a nucleophilic addition of nitroalkanes to carbonyl compounds, the resulting chiral adducts, β-nitro alcohols, can be easily transformed into a variety of valuable synthetic intermediates such as β-amino alcohols[300], α-hydroxy carboxylic acids, aziridines, and other complex target molecules that are highly useful as a framework for the synthesis of bioactive natural products and pharmaceutical agents[299] (e.g. chloramphenicol, ephedrine, norephedrine, (*S*)-propanolol, (*S*)-pindolol and antibiotics)[301,302,303,304].

The β-nitroalcohols are generally obtained in good yield by the reaction of an aldehyde with nitroalkanes in the presence of a catalytic amount of base[305]. The choice of reaction conditions is important to stop the reaction at the stage of β-nitroalcohols[306]. So, the reaction is generally conducted at room temperature in the presence of around 10 % of base to give β-nitroalcohols in good yield. The most popular bases and solvents employed in the Henry reaction are NaOH, KOH, K_2CO_3, triethylamine and alkoxides in water or alcohols[300].

In addition, a more effective catalyst for the Henry reaction is a polymer base, such as amberlyst A-21, amberlite IRA-420 (OH) and DOWEX-1(OH) without a solvent[300].

Many methods have been attempted to synthesise substituted 2-nitro-1-phenyl-ethanol derivatives (**30a - 30h**).

The first method followed the procedure of Langer e*t al.*[307] In this method, the β-nitroaldol reaction between benzaldehydes and nitromethane in ice-cooled methanol occurs in the presence of NaOH as a base catalyst to form the corresponding β-nitroalcohols **30a** and **30d** (Scheme 40).
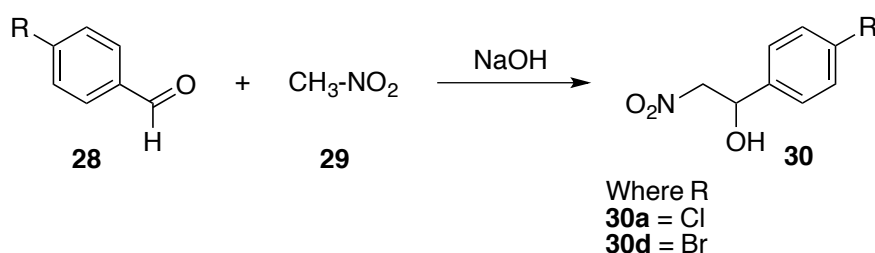
Scheme 40

Overall, aromatic aldehydes bearing strong electron-withdrawing substituents in the para position were easily converted in the presence of NaOH into the corresponding β-nitroalcohols; for example, **30a** and **30d**, gave excellent yields of 72 % and 92 % respectively. Compound **30a** was purified using flash chromatography; in contrast, compound **30d** was used for further reaction without purification (Scheme 41).

Where R:
a = R_1 = OH, R_2 = H
b = R_1 = H, R_2 = CH_3
c = R_1 = H, R_2 = C_2H_5
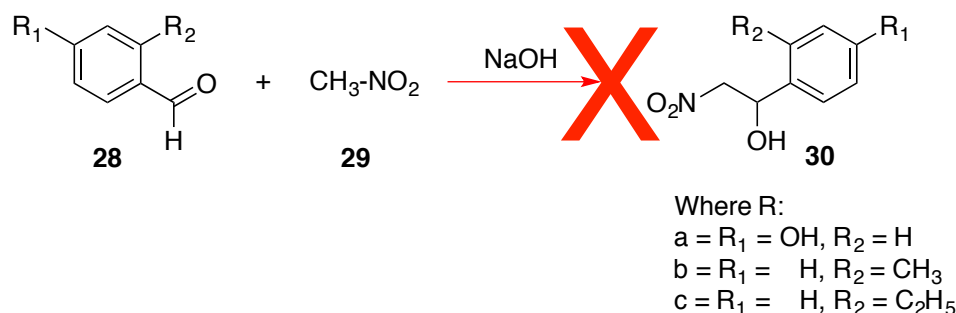
Scheme 41

However, the aromatic aldehydes bearing electron-donating substituents produced very thick brown syrups that contained only trace amounts of the expected product (less than 5 %) As the method of Langer *et al.*[307] was unsuccessful for aromatic aldehydes bearing electron-donating substituents, which may be due to the use of the strong base NaOH as a catalyst, a second method followed the procedure of Bhabak and Arenz[308], using triethylamine rather than NaOH; however, only one compound **30f**, prepared and purified by column chromatography, gave a good yield of 85 % as a yellow liquid (Scheme 42).
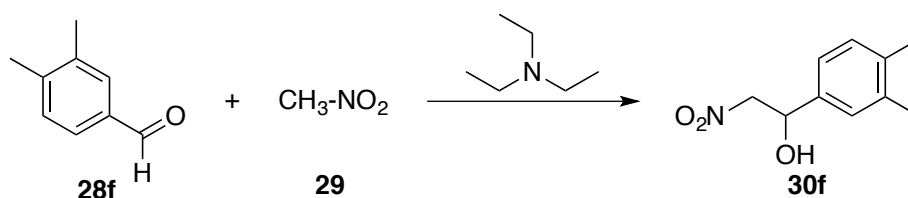
Scheme 42

A third method followed the procedure of Won *et al.*[309] Using this method, the β-nitroaldol was produced by the reaction of benzaldehydes and nitromethane in ice-cooled dry THF in the presence of a slurry of lithium aluminium hydride (10 mol %) in tetrahydrofuran as a base catalyst to form the corresponding *β*-nitroalcohols **30a**, **30b**, **30d**, **30e**, 30g and **30h** with the isolated yields ranging from 71% to 92 % (Table 42 and Scheme 43)

Where R:
30a = R_1 = H R_2 = H, R_3 = Cl, R_4 = H
30b = R_1 = H, R_2 = H , R_3 = CF$_3$, R_4 = H
30d = R_1 = H, R_2 = H , R_3 = Br, R_4 = H
30e = R_1 = CH$_3$, R_2 = H, R_3 = H, R_4 = H
30g = R_1 = H, R_2 = H, R_3 = OCH$_3$, R_4 = H
30h = R_1 = H, R_2 = OCH$_3$, R_3 = H, R_4 = OCH$_3$
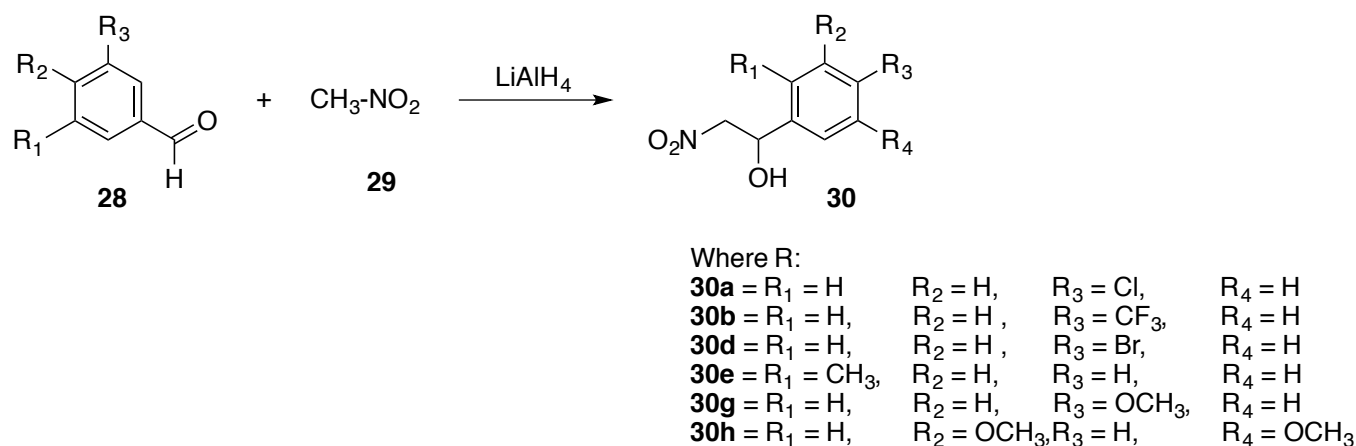
Scheme 43

The fourth method followed the procedure of Lodh *et al.*[310] This method begins with the condensation of benzaldehyde with nitromethane in the presence of 10 wt % of Ambersep 900 (OH) under solvent-free conditions at room temperature (a further increase in the amount of catalyst did not improve the yield significantly). The corresponding β-nitroalcohols were obtained in yields ranging from 51 % to 86 % for compounds **30a**, **30b**, **30c**, **30g** and **30h** (Scheme 44). These compounds were obtained as a yellow liquid or oil and were used for further reaction without purification.

Where R:
30a = R_1 = H R_2 = Cl, R_3 = H
30b = R_1 = H, R_2 = CF$_3$, R_3 = H
30c = R_1 = CF$_3$, R_2 = H, R_3 = H
30g = R_1 = H, R_2 = OCH$_3$, R_3 = H,
30h = R_1 = OCH$_3$, R_2 = H, R_3 = OCH$_3$
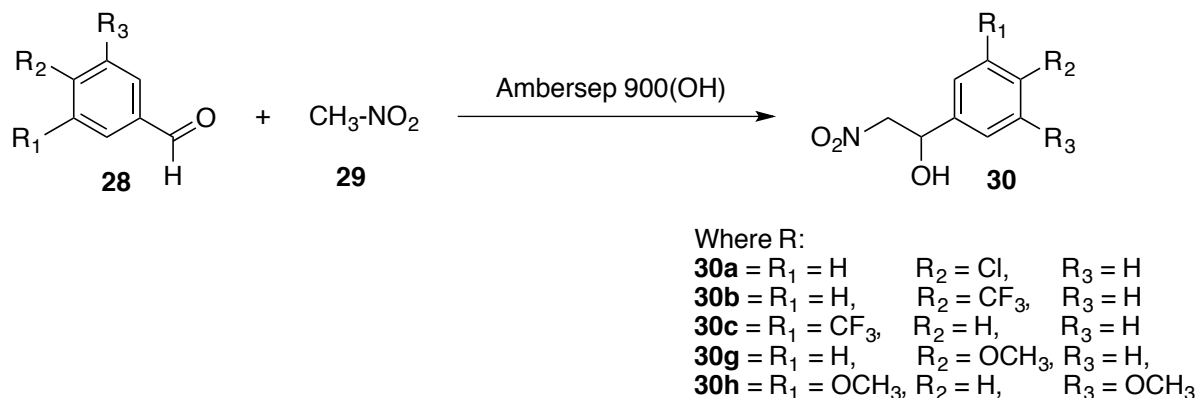
Scheme 44

The method of Won *et al.*[309] and Lodh *et al.*[310] was found to be the optimal option for the synthesis of β-nitroalcohol derivatives.

^{1}H NMR confirmed the formation of the substituted 2-nitro-1-phenyl-ethanol derivatives by observation of the hydroxyl group with a peak at approximately $\delta \cong 5.90$, and an aliphatic (CH) group was observed with a peak at approximately at $\delta \cong 5.40$ for **30a - 30h**. A peak for the aldehyde group of the starting material was absent, confirming complete reaction.

cpd	% Yield Method 1	% Yield Method 2	% Yield Method 4	% Yield Method 5	Colour and appearance
30a	72	-	90	76	Yellow liquid
30b	-	-	92	85	Yellow liquid
30c	-	-	-	78	Yellow oil
30d	92	-	-	-	Brown oil
30e	-	-	55	-	Brown oil
30f	-	85	-	-	Brownish yellow liquid
30g	-	-	86	20	Yellow oil
30h	-	-	63	85	Yellow oil

Table 42: Yield % and colour and appearance of β-nitroalcohols for each method

4.1.2   Synthesis of 2-amino-1-(substituted phenyl)ethan-1-ol derivatives

The amino alcohols were prepared by catalytic hydrogenation.
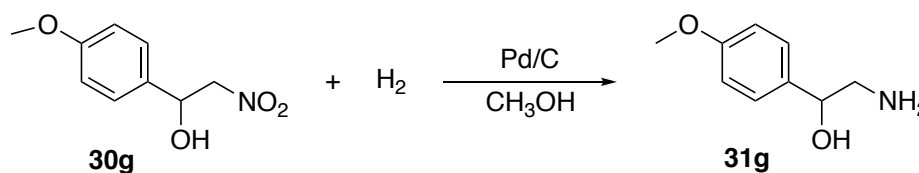
Scheme 45

The first method followed the procedure of Lee *et al.*[311]. In this method (1-(4-methoxyphenyl)-2-nitroethan-1-ol) **30g** was reduced using hydrogenation at 45 psi with palladium/carbon and methanol for 6 h to produce 2-amino-1-(4-methoxyphenyl)ethan-1-ol **31g** in a 42 % yield (Scheme 45).

Where R:
31a = R_1 = H, R_2 = H, R_3 = Cl, R_4 = H
31b = R_1 = H, R_2 = H, R_3 = CF_3, R_4 = H
31c = R_1 = CF_3, R_2 = H, R_3 = H, R_4 = H
31e = R_1 = CH_3 R_2 = H, R_3 = H, R_4 = H
31f   = R_1 = H, R_2 = CH_3, R_3 = CH_3, R_4 = H
31g = R_1 = H, R_2 = H, R_3 = OCH_3, R_4 = H
31h = R_1 = H, R_2 = OCH_3, R_3 = H, R_4 = OCH_3
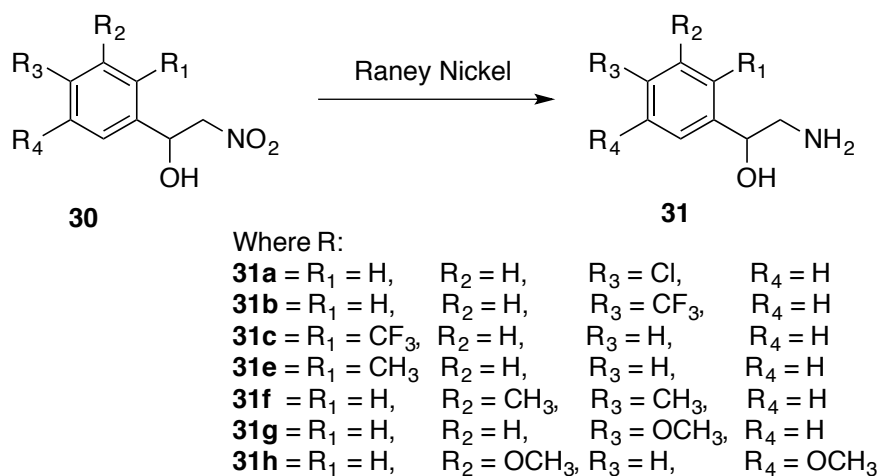
Scheme 46

The second method followed the procedure by Gowda *et al.*[312] In this method, the *β*-nitroalcohols were reduced to the corresponding amine derivatives using a slurry of Raney nickel and formic acid under H_2 atmosphere at room temperature for 6 h. The yields obtained ranged from 17 % to 84 % for **31a**, **31b**, **31c**, **31e**, **31f**, **31g** and **31h** (Scheme 46). All products were characterised by a comparison of their TLC, melting points, and ^{1}H NMR with corresponding literature compounds (Table 43). ^{1}H NMR confirmed the formation of the substituted 2-amino-1-phenylethan-1-ol by observation of an aliphatic hydroxyl and amine group as a broad singlet at approximately $\delta \cong 3.00$.

cpd.	Yield %	m.p.		Colour and appearance
		Practical	Lit.	
31a	84	106 - 110℃	94 - 95℃ [313]	Pale yellow solid
31b	53	60 - 64℃	Unrecorded	White solid
31c	67	80 - 86℃	Unrecorded	White solid
31e	57	-	-	Amber oil
31f	63	64 - 68℃	Unrecorded	Pale yellow solid
31g	47	46 - 50 ℃	70℃ [314]	Yellow solid
31h	17	-	-	Yellow oil

Table 43: Identification data for 2-amino-1-(substituted phenyl)ethan-1-ol derivatives

4.1.3 Substituted/unsubstituted (*E*)-4-styrylbenzoic acids

More than four decades ago, Mizorokil[315] and Heck[316] discovered the palladium-catalysed arylation and vinylation of olefins. The Heck reaction is the vinylation of aryl/vinyl halides in the presence of a base and catalysed by Pd(0) complexes, resulting in the formation of a carbon-carbon bond.

The catalytic cycle for the Heck reaction involves three fundamental steps: the catalytic cycle with the oxidative addition of an aryl/alkenyl halide, the carbometalation reaction via the complex, and the *β*-hydride elimination[317]. The method of Aboraia *et al.*[210] was used to synthesise compounds **34a** and **34b** (Scheme 47).

Where R:
34a = R_1 = H, R_2 = H
34b = R_1 = OCH_3, R_2 = OCH_3
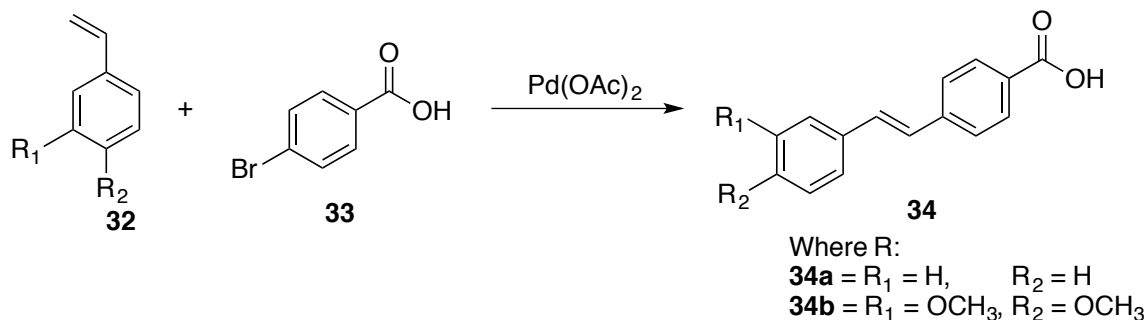
Scheme 47

4-Bromobenzoic acid **33** reacted with alkenes **32** in the presence of 0.01 equivalents of palladium acetate; 0.05 equivalents of tri-*o*-tolylphosphine, and 2.5 equivalents of triethylamine were mixed in a sealed tube at 100 ℃ overnight to form unsubstituted/substituted (*E*)-4-styrylbenzoic acid **34a** and **34b** in yields of 51 % and 82 % respectively (Table 44).

Cpd	Yield %	m.p.		Microanalysis	Colour and appearance
		Practical	Lit.		
24a	**51**	**240 - 242℃**	**257℃**[318]	-	**Yellow crystals**
34b	**59**	**244 - 248℃**	**Novel**	**Anal. Calcd for $C_{17}H_{16}O_4 \cdot 0.1H_2O$ (286.1): C 71.37 %, H 5.71 %. Found C71.29 %, H 5.47 %.**	**Yellow crystals**

Table 44: Analytical data for unsubstituted/substituted (*E*)-4-styrylbenzoic acids

4.1.4   (*E*)-*N*-(-2-hydroxy-2-(substituted phenyl)ethyl)-4-(unsubstituted/substituted styryl)benzamides (35)
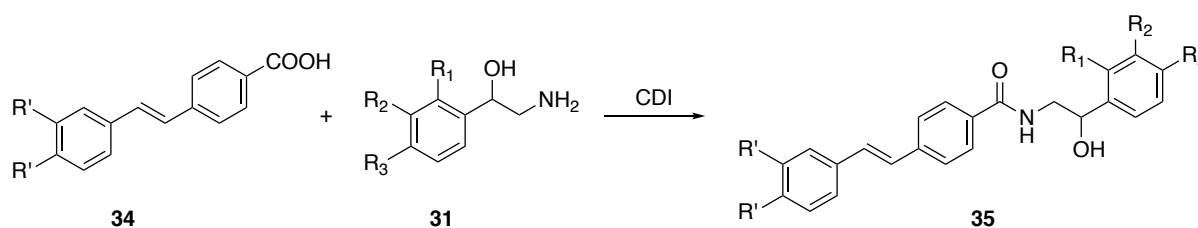
Where R:
35a = R_1= H, R_2 = H, R_3 = Cl,   R' = H
35b = R_1= H , R_2 = H, R_3 =CF_3,   R' = H
35c = R_1= CF_3, R_2 = H, R_3 = H,   R' = H
35d = R_1= H, R_2 = CH_3, R_3 = CH_3,   R' = H
35e = R_1= H, R_2 = H, R_3 = OCH_3, R' = H
35f = R_1= H, R_2 = H, R_3 = Cl,   R' = OCH_3

Scheme 48

The substituted/unsubstituted (*E*)-4-styrylbenzoic acids **34** were activated by CDI, and then intermediate compounds were reacted with substituted-2-amino-1-phenylethanol **31** at 0 ℃ to produce the desired compounds **35a - 35f**. The obtained yields ranged from 35 % to 69 % (Table 45 and Scheme 48).

cpd	Yield %	m.p.	Microanalysis/ HRMS	Colour and appearance
35a	67	258 - 260℃	Anal. Calcd for $C_{23}H_{20}ClNO_2 \cdot 0.3H_2O$ (382.52): C 72.08 %, H 5.42 %, N 3.65 %. Found C72.20 %, H 5.26 %, N 3.86 %.	White crystals
35b	35	220 - 224℃	Anal. Calcd for $C_{24}H_{20}F_3NO_2$ (411.42): C 70.07 %, H 4.90 %, N 3.40 %. Found C 70.39 %, H 4.79 %, N 3.47 %	White crystals
35c	58	160 - 166℃	Anal. Calcd for $C_{24}H_{20}F_3NO_2$ (411.42): C 70.07 %, H 4.90 %, N 3.40 %. Found C 70.22 %, H 4.92 %, N 3.38 %	White solid
35d	60	150 - 154℃	Anal. Calcd for $C_{25}H_{25}NO_2$ (371.48): C 80.83 %, H 6.78 %, N 3.77 %. Found C 81.10 %, H 6.78 %, N 3.88 %	White solid
35e	35	218 - 220℃	Anal. Calcd for $C_{24}H_{23}NO_3$ (373.45): C 77.19 %, H 6.21 %, N 3.75 %. Found C 77.32 %, H 6.02 %, N 3.70 %	White solid
35f	69	168 - 172℃	Calculated mass: 438.1472 $[M + H]^+$, measured mass: 438.1463 $[M + H]^+$	White solid

Table 45: Anylitical data for (*E*)-*N*-(-2-hydroxy-2-(substituted phenyl)ethyl)-4-(unsubstituted/substituted styryl)benzamides (35)

4.1.5 Synthesis of (*E*)-5-(substituted phenyl)-2-(4-(unsubstituted/substituted styryl)phenyl)-4,5-dihydrooxazole derivatives (36)

The dihydrooxazoles were prepared following the procedure of Aboraia e*t al.*[210] The method involved the formation of the oxazole ring by reacting (*E*)-*N*-(-2-hydroxy-2-(substituted phenyl)ethyl)-4-(unsubstituted/substituted styryl)benzamides **35a - 35f** with methansulfonyl chloride and triethylamine in dry THF (Scheme 49).

Where R:
36a = R_1 = H, R_2 = H, R_3 = Cl, R' = H
36b = R_1 = H, R_2 = H, R_3 = CF_3, R' = H
36c = R_1 = CF_3, R_2 = H, R_3 = H, R' = H
36d = R_1 = H, R_2 = CH_3, R_3 = CH_3, R' = H
36e = R_1 = H, R_2 = H, R_3 = OCH_3, R' = H
36f = R_1 = H, R_2 = H, R_3 = Cl, R' = OCH_3
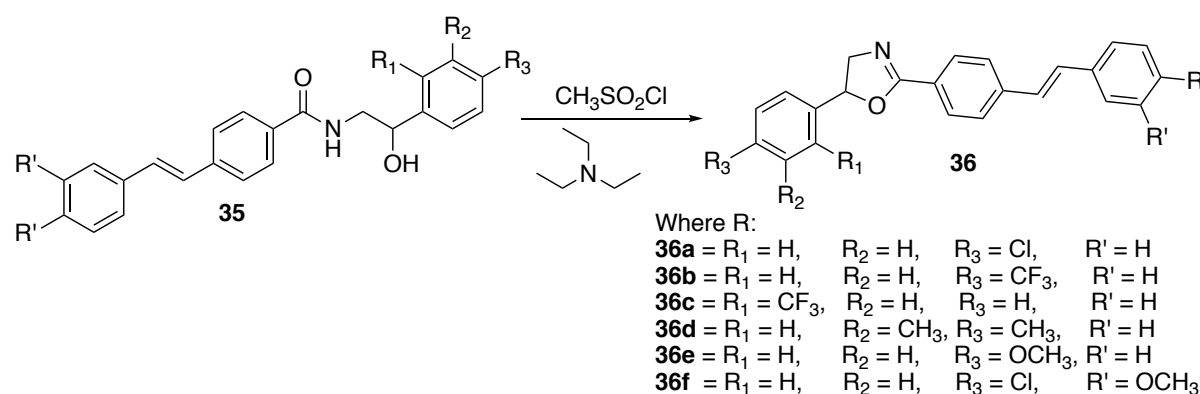
Scheme 49

Generally, the preparation of 4,5-diydrooxazole compounds **36a - 36f** gave good yields ranging from 40 - 90 %, and these were used in the next step without further purification except for compound **36a**, which was recrystallised with methanol.

4,5-diydrooxazole compounds was found to be unstable with the rearrangement leading to opening of the oxazole ring. TLC showed a mixture of two spots (3:1), one major and one minor. The ^{1}H NMR spectra showed that one was the dihydrooxazole and the other was an unknown compound with an amide group as a triplet at approximately $\delta \cong 8.9$.

4.1.6 Synthesis of (*E*)-N-(2-(1*H*-imidazol-1-yl)-2-(substituted phenyl)ethyl)-4-(unsubstituted/substituted styryl)benzamide derivatives

The procedure of Schuster *et al.*[319] was used in the final step, and achieved refluxing oxazole compounds **36** in the presence of excess imidazole for 48 h at 125 ℃. The products were purified by recrystallisation with EtOAc or acetonitrile. The yields ranged between 12 % to 35 % for **37a** - 37f. The low yield resulted from the impure oxazole starting material **36**. Column chromatography, rather than recrystallisation may have resulted in isolation of the product **37** at high yields (Scheme 50).

Where R:
37a = R_1 = H, R_2 = H, R_3 = Cl,   R' = H
37b = R_1 = H, R_2 = H, R_3 = CF_3,   R' = H
37c = R_1 = CF_3, R_2 = H, R_3 = H,   R' = H
37d = R_1 = H, R_2 = CH_3, R_3 = CH_3,   R' = H
37e = R_1 = H, R_2 = H, R_3 = OCH_3, R' = H
37f = R_1 = H, R_2 = H, R_3 = Cl,   R' = OCH_3
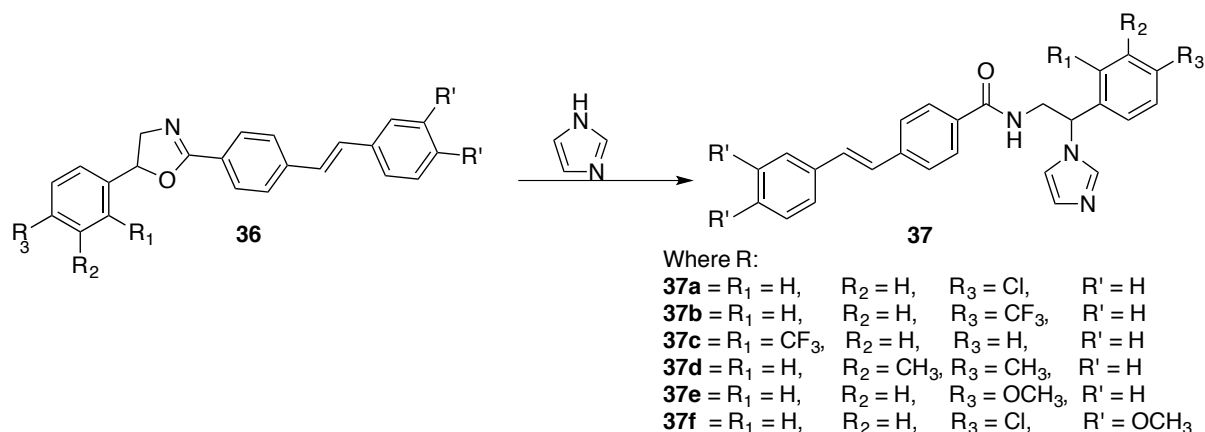
Scheme 50

The use of imidazole as both a reactant and a solvent improved the yields compared with the use of isopropyl acetate as a solvent[191,210,219](Table 46).

cpd	Yield %	m.p.	Microanalysis/ HRMS	Colour and appearance
37a	12	238 - 240℃	Calculated mass: 428.1523 [M + H]$^+$, measured mass: 428.1524 [M + H]$^+$	White crystals
37b	33	208 - 210℃	Anal. Calcd for $C_{27}H_{22}F_3N_3O \cdot 0.15\ H_2O$: (463.87), C 69.86 %, H 4.84 %, N 9.05 %. Found C 69.56 %, H 4.79 %, N 8.98 %.	Creamy solid
37c	35	174 - 178℃	Anal. Calcd for $C_{27}H_{22}F_3N_3O \cdot 0.1H_2O$ (463.29): C 70.00 %, H 4.83 %, N 9.07 %. Found C 69.64 %, H 4.84 %, N 9.07 %.	Creamy solid
37d	27	134 - 136℃	Calculated mass: 422.225 [M + H]$^+$, measured mass: 422.2232 [M + H]$^+$	Yellow solid
37e	32	218 - 222℃	Calculated mass: 424.2020 [M + H]$^+$, measured mass: 424.2016 [M + H]$^+$	White solid
37f	35	204 - 208℃	Calculated mass: 488.1743 [M + H]$^+$, measured mass: 488.174 [M + H]$^+$	White crystals

Table 46: Analytical data for (*E*)-*N*-(2-(1*H*-imidazol-1-yl)-2-(substituted phenyl)ethyl)-4-(unsubstituted/substituted styryl)benzamides

4.2   Synthesis of (*E*)-*N*-(2-(1*H*-imidazol-1-yl)-2-(substituted phenyl)ethyl)-3-(unsubstituted/substituted styryl)benzamide derivatives
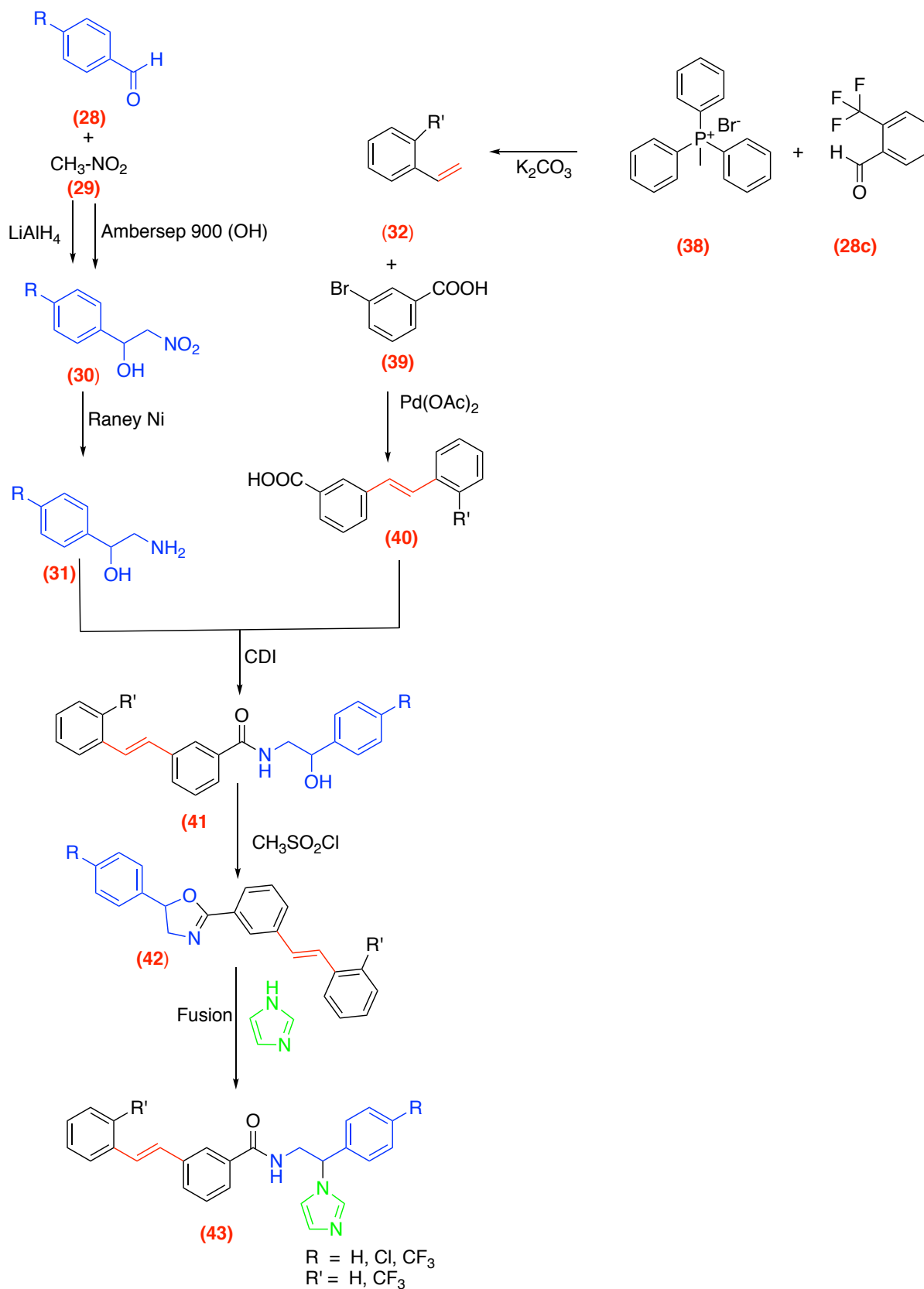
Scheme 51: Synthesis of (*E*)-*N*-(2-(1*H*-imidazol-1-yl)-2-(substituted/unsubstituted) ethyl)-3-(substituted/unsubstituted styryl)benzamides

4.2.1   1-(Trifluoromethyl)-2-vinylbenzene (32c)

The Wittig reaction, discovered in 1954 by Georg Wittig[320], is one of the most common techniques used for the stereoselective preparation of alkenes[321]; the reaction allows for the formation of an alkene product and a triphenylphosphine oxide side product from the reaction of an aldehyde and triphenylphosphonium ylide. The key step of the mechanism was the nucleophilic addition of the ylide to the electrophilic carbonyl group of an aldehyde or ketone, forming a four-membered ring that dissociates into the product molecule.

The method of Zhang and Tang[322] was used to synthesise compound **32c**. In this procedure, 2-(trifluoromethyl)benzaldehyde **28c** was reacted with methyltriphenylphosphonium bromide **38** and potassium carbonate in dry THF under reflux for 10 h to give 1-(trifluoromethyl)-2-vinylbenzene **32** in a yield of 67 % as a colourless liquid (Scheme 52).

28c   **38**   **32c**
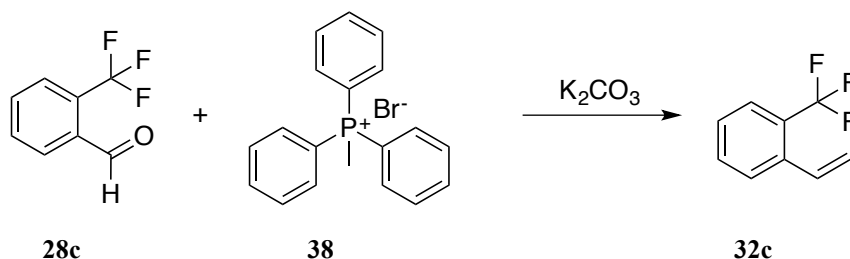
Scheme 52

^{1}H NMR confirmed the presence of the CH of the alkene group with a peak at δ = 7.00 as a doublet of doublet of doublets (ddd) with J values (2.5, 11, and 17.3 Hz). The CH$_2$ of the alkene group was observed as two peaks; one was observed at δ = 5.92 as a doublet with J value 17.3 Hz and the other proton was observed at δ = 5.50 as a doublet of doublets with J value 0.95 and 11.05 Hz. The aldehyde group of the starting materials was absent, confirming the complete reaction. Other vinylbenzenes were purchased from Sigma Aldrich.

4.2.2   (*E*)-3-styrylbenzoic acid (41)

32   **39**   **40**

Where R:
40a = R = H
40b = R = CF$_3$
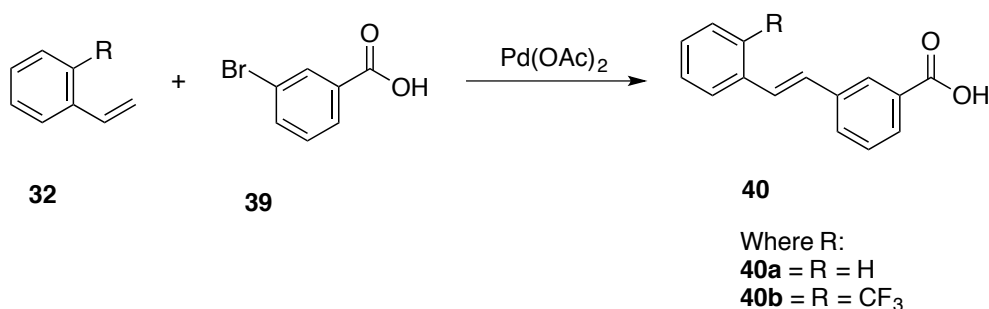
Scheme 53

3-Bromobenzoic acid **39** reacted with alkenes **32** in the presence of 0.01 equivalents of palladium acetate, 0.05 equivalents of tri-*o*-tolylphosphine and 2.5 equivalent of triethylamine in a sealed tube at 100 ℃ overnight to form (*E*)-3-styrylbenzoic acid **40** (Scheme 53). The products were obtained in yields of 73 % and 82 % for **40a** and **40b** respectively (Table 47).

cpd	Yield %	m.p.		Microanalysis	Colour and appearance
		Practical	Lit.		
40a	73	188 - 192℃	197 - 198℃[323]	-	**Brown crystals**
40b	82	162 – 164℃	Novel	**Anal. Calcd for C$_{16}$H$_{11}$F$_3$O$_2$ (292.26): C 65.76 %, H 3.79 %, N 0.00 %. Found C 65.63 %, H 3.81 %, N <0.10 %.**	**creamy crystals**

Table 47: Analytical data for substituted/substituted (*E*)-3-styrylbenzoic acids

4.2.3   Synthesis of (*E*)-*N*-(2-(unsubstituted/substituted phenyl)-2-hydroxyethyl)-3-(unsubstituted/substituted styryl)benzamides (41)

Where:
41a = R' = H,   R = H
41b = R' = H,   R = Cl
41c = R' = H,   R = CF$_3$
41d = R' = CF$_3$, R = H
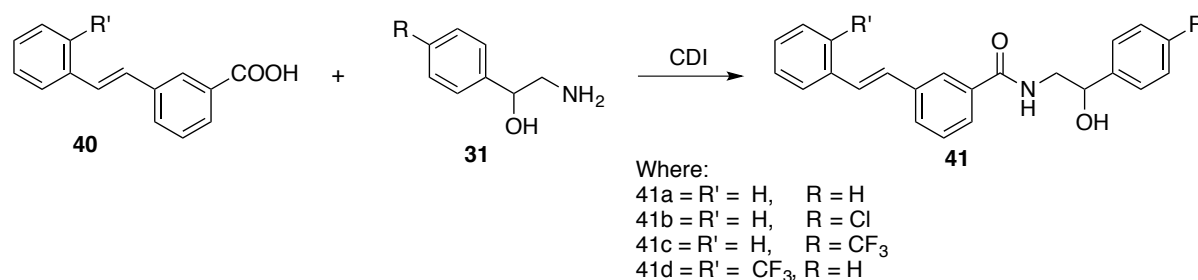
Scheme 54

The (*E*)-3-styrylbenzoic acids (**40**) were activated by CDI, and then intermediate compounds were reacted with substituted-2-amino-1-phenylethanol derivatives (**31**) at 0 ℃ to produce the desired compounds **41a - 41f** (Scheme 54). The desired compounds were obtained in yields ranging from 31 % to 75 % (Table 48).

cpd	Yield %	m.p.	Microanalysis/ HRMS	Colour and appearance
41a	60	128- 132 ℃	Anal. Calcd for $C_{23}H_{21}NO_2 \cdot 0.4\ H_2O$ (350.36): C 78.79 %, H 6.27 %, N 3.99 %. Found C 78.35 %, H 6.56 %, N 3.83 %.	White solid
41b	50	138 - 142 ℃	Anal. Calcd for $C_{24}H_{20}ClNO_2 \cdot 0.2\ H_2O$ (381.47): C 72.42 %, H 5.39 %, N 3.67 %. Found C 72.11 %, H 5.36 %, N 3.77 %.	creamy solid
41c	31	184 - 186 ℃	Anal. Calcd for $C_{24}H_{20}F_3NO_2 \cdot 0.1 H_2O$ (413.23): C 69.76 %, H 4.93 %, N 3.39 %. Found C 69.51%, H 4.94 %, N 3.42 %.	White crystals
41d	75	88 - 90 ℃	Anal. Calcd for $C_{24}H_{20}F_3NO_2$ (411.42): C 70.07%, H 4.90 %, N 3.40 %. Found C 69.99 %, H 5.05 %, N 3.53 %.	White solid

Table 48: Analytical data for (*E*)-*N*-(2-(unsubstituted/substituted phenyl)-2-hydroxyethyl)-3-(unsubstituted/substituted styryl)benzamides

4.2.4 Synthesis of (*E*)-*N*-(2-(unsubstituted/substituted phenyl)-2-hydroxyethyl)-3-(unsubstituted/substituted styryl)phenyl-4,5-dihydrooxazoles (42)

Where:
42a = R' = H,   R = H
42b = R' = H,   R = Cl
42c = R' = H,   R = CF₃
42d = R' = CF₃, R = H
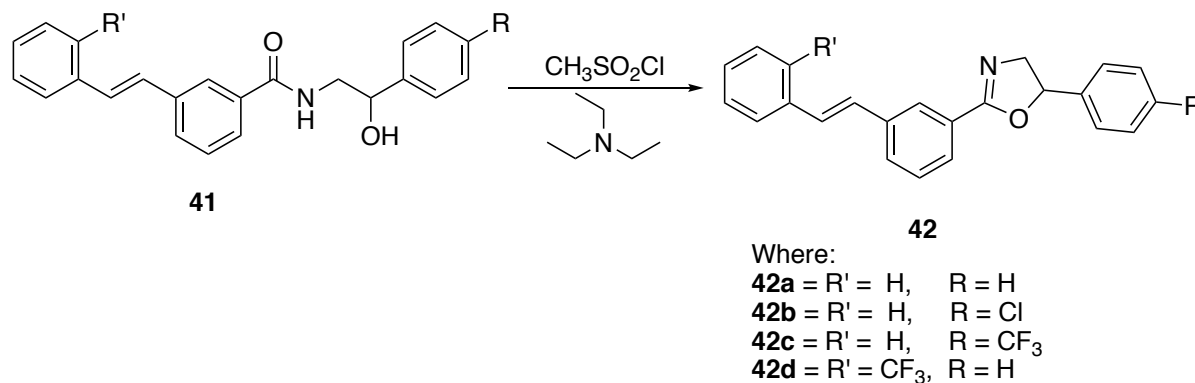
Scheme 55

Following the previously described method in (5.1.5). Compounds **42a** - **42d** were obtained in yields ranging from 40 % - 90 % (Scheme 55).

4.2.5 Synthesis (*E*)-*N*-(2-(1*H*-imidazol-1-yl)-2-(unsubstituted/substituted phenyl)ethyl)-3-(substituted/unsubstituted styryl)benzamides
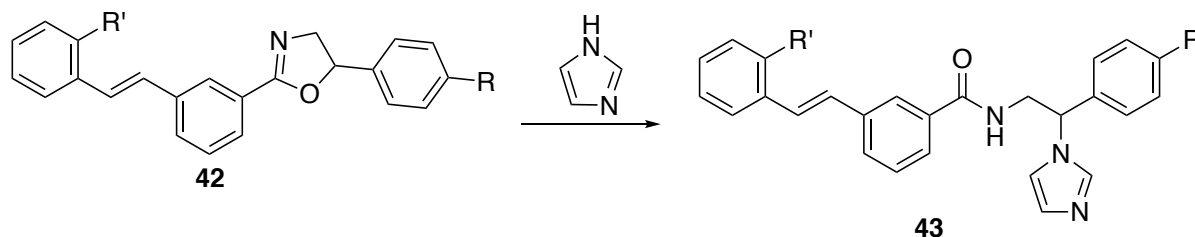
Scheme 56

Following the previously described method in (5.1.6). Reaction of oxazole (42) with excess imidazole gave **43a - 43d** in yields ranging from 32 % - 938 % (Scheme 56 and table 49).
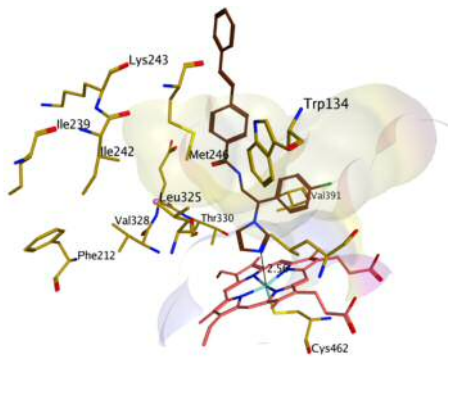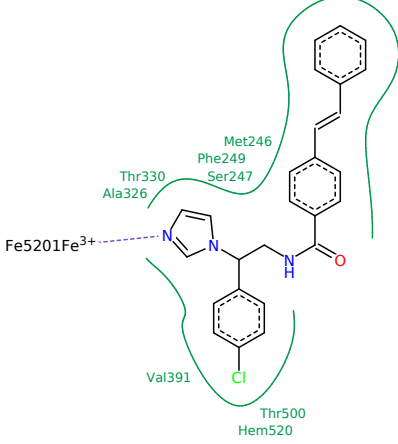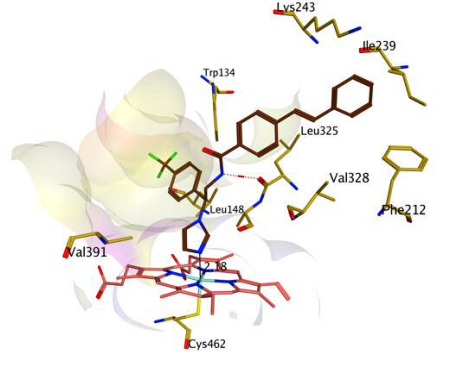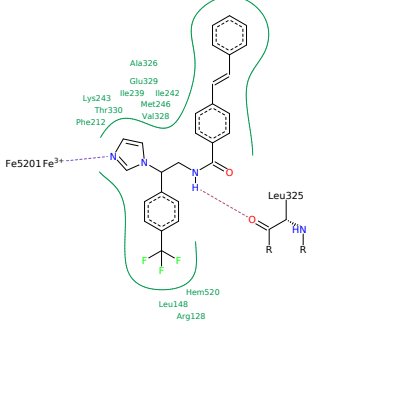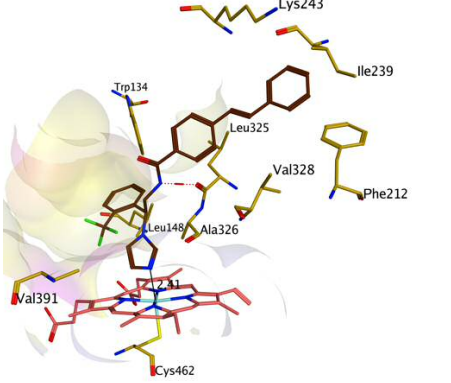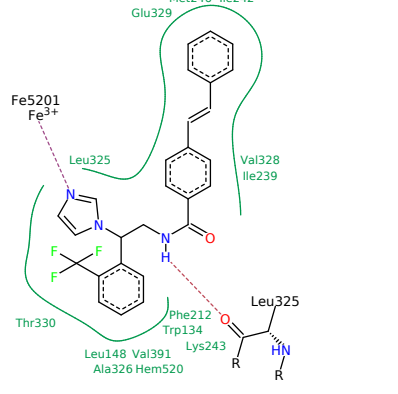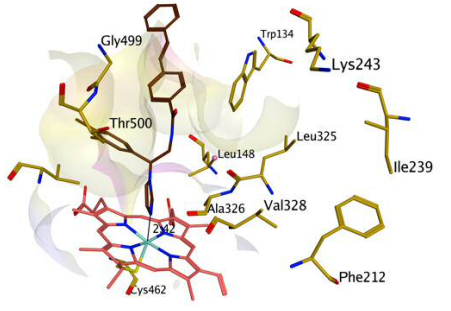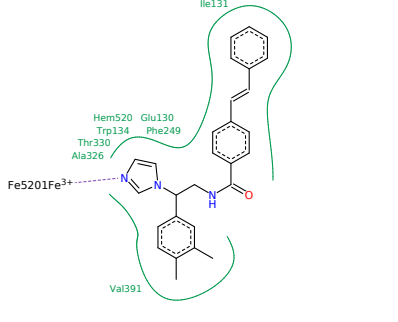
cpd	Yield %	m.p.	Microanalysis/ HRMS	Colour and appearance
43a	38	158 - 160℃	Anal. Calcd for $C_{26}H_{23}N_3O \cdot 0.25\ H_2O$ (397.99): C 78.47 %, H 5.95 %, N 10.56 %. Found C 78.17 %, H 5.95 %, N 10.56.	White solid
43b	32	148 - 152℃	Anal. Calcd for $C_{26}H_{22}ClN_3O$ (427.93): C 72.98 %, H 5.18 %, N 9.81 %. Found C 72.77 %, H 5.36 %, N 8.40 %.	White solid
43c	48	126 - 130℃	Calculated mass 462.1793 $[M + H]^+$, measured mass: 462.1799 $[M + H]^+$	White solid
43d	33	110 - 114℃	Calculated mass 462.1793 $[M + H]^+$, measured mass: 462.1795 $[M + H]^+$	White solid

Table 49: Analytical data for (*E*)-*N*-(2-(1*H*-imidazol-1-yl)-2-(unsubstituted/substituted phenyl)ethyl)-3-(unsubstituted/substituted styryl)benzamides

4.3   Molecular modelling

Ferla *et al.*[191] reported that the styrylphenyl ring was important to the activity and that the imidazole was essential for metal-ligand interaction with the haem group of the enzyme. Introduction of substituents on the styrylphenyl ring resulted in an improvement in the activity by up to four times, as the introduction of methoxy groups in positions 3 and 5 led to an increase in CYP24A1inhibitory activity.

In this chapter, compounds were designed by taking lead 3 and using different substitutions to explore SAR. Compounds **37a** - **37f** have electron withdrawing and electron donating (4-chloro, 4-trifluoromethyl, 2-trifluoromethyl, 3,4-dimethyl and 4-methoxy groups) actions on the phenyl ring. All compounds were designed without substitution on the styrene group except compound **37f**, which has a 4-Cl on the phenyl ring and a 3,4-dimethoxy substitution on the styrene group. All the compounds reached the active site through the vitamin D access tunnel and were exposed to multiple hydrophobic residues (Arg128, Glu130, Ile131, Trp134, Leu148, Asn208, Phe212, Ile239, Ile242, Lys243, Met246, Ser247, Phe249, Ala326, Val328, Glu329, The330, Val391 and Thr500). Compounds **37b** - **37d** formed hydrogen bonds between the nitrogen of the amide group with Leu325. For compound **37e,** an additional hydrogen bond between the methoxy group and Arg128 was observed. The distance between the imidazole ring and the haem iron was between 2.18 Å and 2.58 Å (Table 50).

cpd.	A	B	C
37a	2.56 Å		
37b	2.18 Å		
37c	2.41 Å		
37d	2.42 Å		
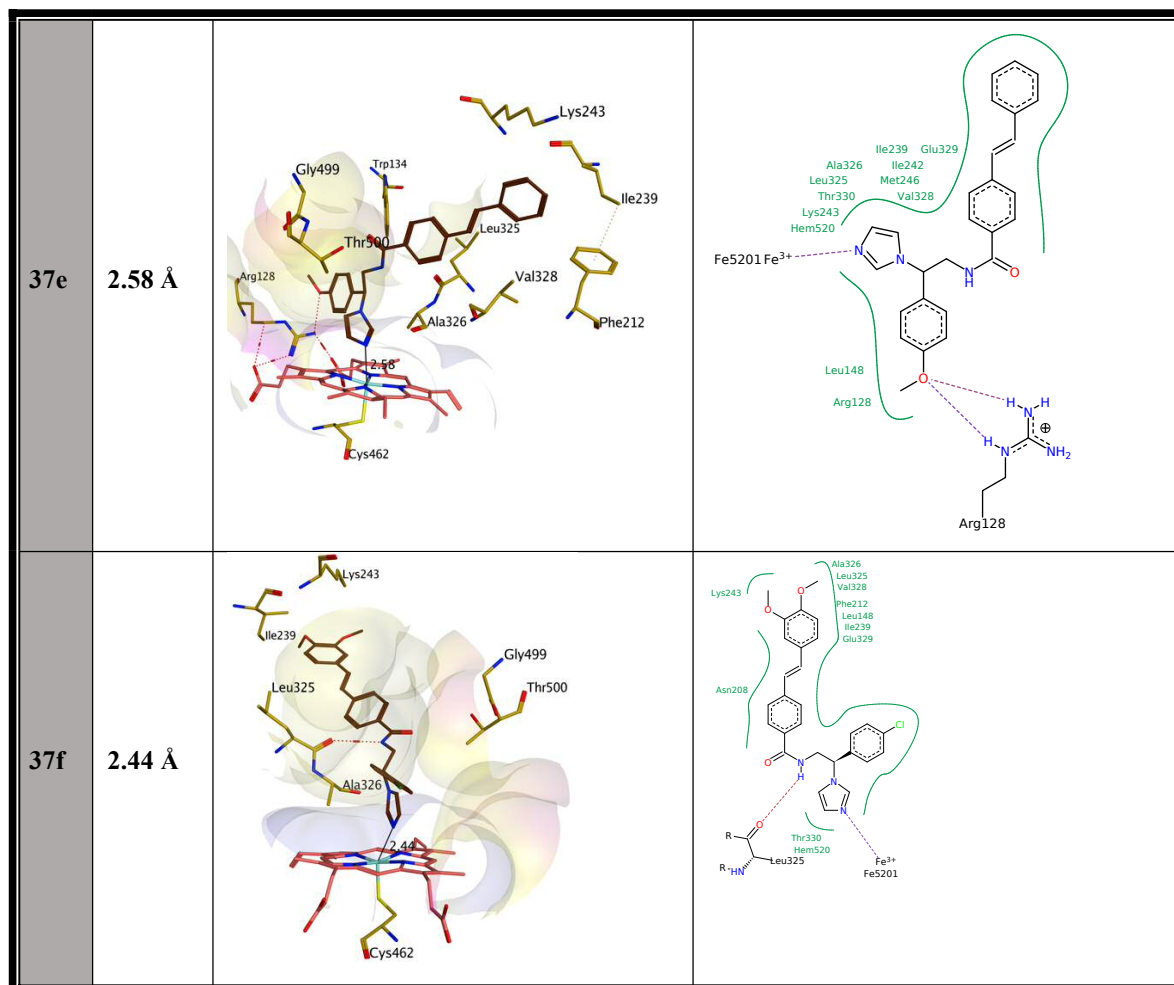
Table 50: (A) Distance between N of heterocycle and iron of haem, (B) 3D and (C) 2D structure with binding interactions

However, there are some poses of compounds **37c** and **37e** that form different interactions with the haem. The carbonyl of the amide group **37c** interacts with the iron of the haem (distance 2.28 Å), while **37e** interacts with the iron of the haem via the methoxy group (distance 2.19 Å) (Figure 88).
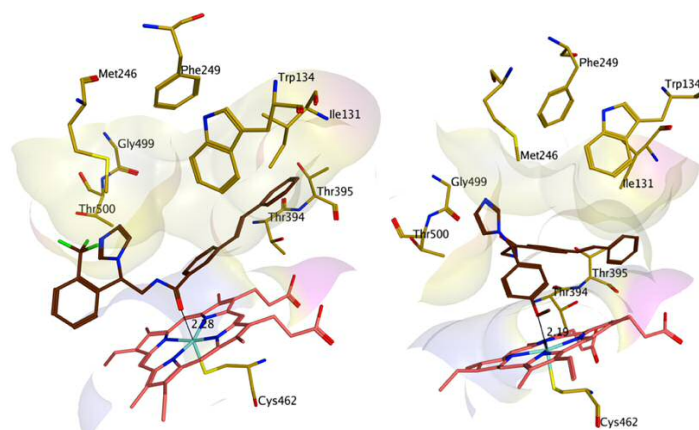
Figure 88: Example of some poses of compounds 37c and 37e interacting with the haem iron via carbonyl and methoxy groups

4.3.1 **Docking studies of (*E*)-*N*-(2-(1*H*-imidazol-1-yl)-2-(unsubstituted/substituted phenyl)ethyl) -3-(unsubstituted/substituted styryl)benzamides using a CYP24A1 homology model**[191]

Compounds **43a** - **43d** were modified by changing the position of the alkene group from the 4 to the 3 position.

The compounds were docked using the LeadIT 2.1.2 programme, and the results were visualised on MOE. All compounds showed good interaction with the active site and interaction between the imidazole nitrogen and the iron of the haem with distances ranging between 2.04 Å and 2.29 Å. Hydrogen bonds were observed between the amide group, through the C=O and/or NH, and amino acids Glu329, Thr330 and Leu325 (Table 51).

cpd.	A	B	C
43a	2.04 Å		
43b	2.29 Å		

43c	2.22 Å		
43d	2.28 Å		
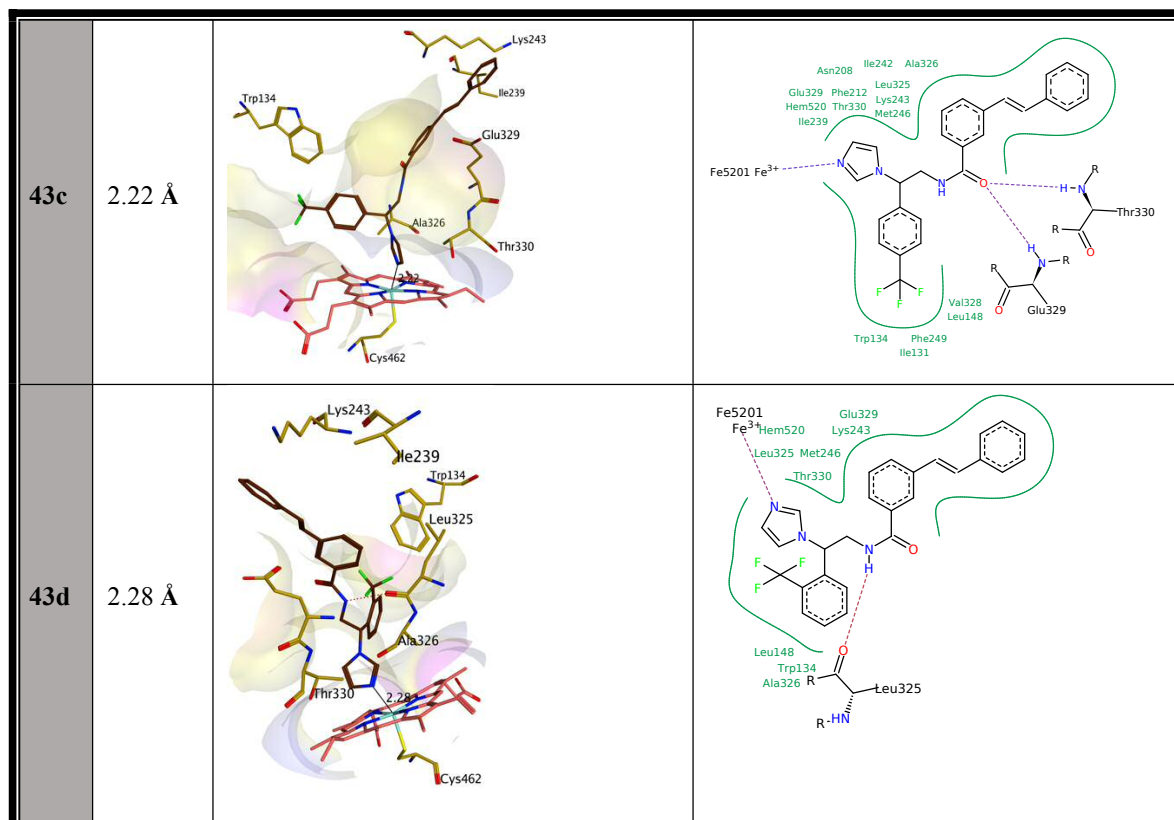
Table 51: (A) Distance between N of heterocycle and iron of haem, (B) 3D and (C) 2D models showing key binding interactions

4.4 CYP24A1 inhibitor enzymatic assay[279]

All the final compounds **37a** - **37f** and **43a** - **43d** were evaluated by enzymatic assay to determine CYP24A1 inhibitory activity (see 3.6.1).

In general, the compounds displayed potent inhibition of CYP24A1 activity when compared with the ketoconazole standard and comparable with or more active than lead 3 (IC_{50} 0.40 µM)[191].

The IC_{50} values ranged between 11 and 35 µM, and the best IC_{50} value was obtained for compound **37e** (0.11µM) (Figure 89 and 90).

All of the imidazole styrylbenzamide derivatives exhibited significant activity, but the compound with methoxy substitution in the phenyl ring was noted as having optimal activity (0.11 µM). Altering the position of the alkene double bond from position 4 to 3 was not beneficial in terms of the activity. However, a slight difference in the inhibitory effect was recorded, with compounds having different substituents in the phenyl ring where **43b**, **43c** and **43d** were proved to be better than **37a**, **37b** and **37c**. Moreover, 4, 5-dimethoxy substitution on the styrene ring (compound **37f)** and methoxy substitution on the phenyl ring (compound **37e**) was better than electron withdrawing substituents. For example, compound **37f** was more active than the compound with trifluoromethyl substitution in the styrene ring (**43d**). Interestingly, the unsubstituted phenyl ring (compound **43a**) was more active than the unsubstituted phenyl ring for lead 3.

Where R:
37a = R_1 = H, R_2 = H, R_3 = Cl, R' = H
37b = R_1 = H, R_2 = H, R_3 = CF_3, R' = H
37c = R_1 = CF_3, R_2 = H, R_3 = H, R' = H
37d = R_1 = H, R_2 = CH_3, R_3 = CH_3, R' = H
37e = R_1 = H, R_2 = H, R_3 = OCH_3, R' = H
37f = R_1 = H, R_2 = H, R_3 = Cl, R' = OCH_3

Where R:
43a = R' = H, R = H
43b = R' = H, R = Cl
43c = R' = H, R = CF_3
43d = R' = CF_3, R = H
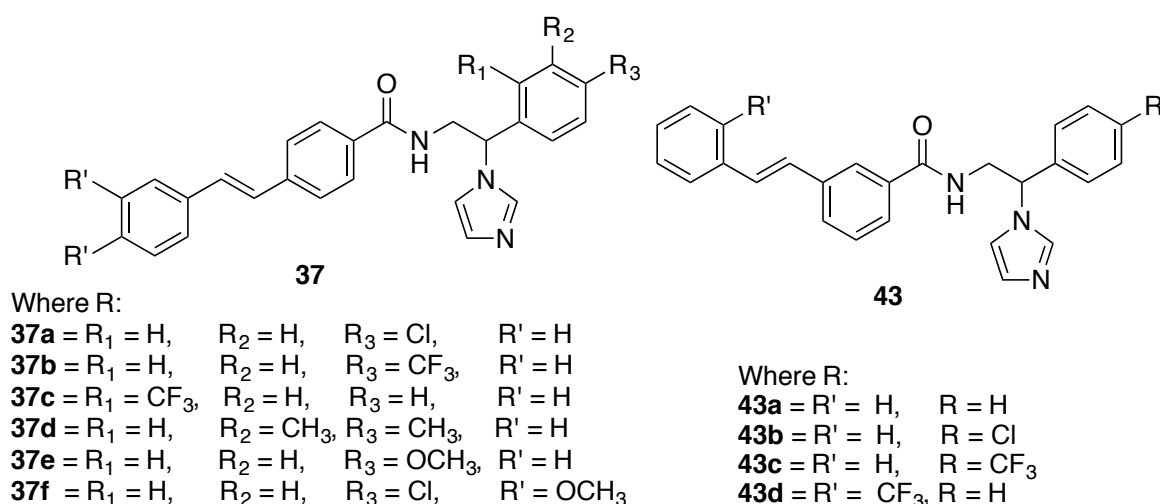
Figure 89: Chemical structure compounds 37a - 37f and 43a - 43d
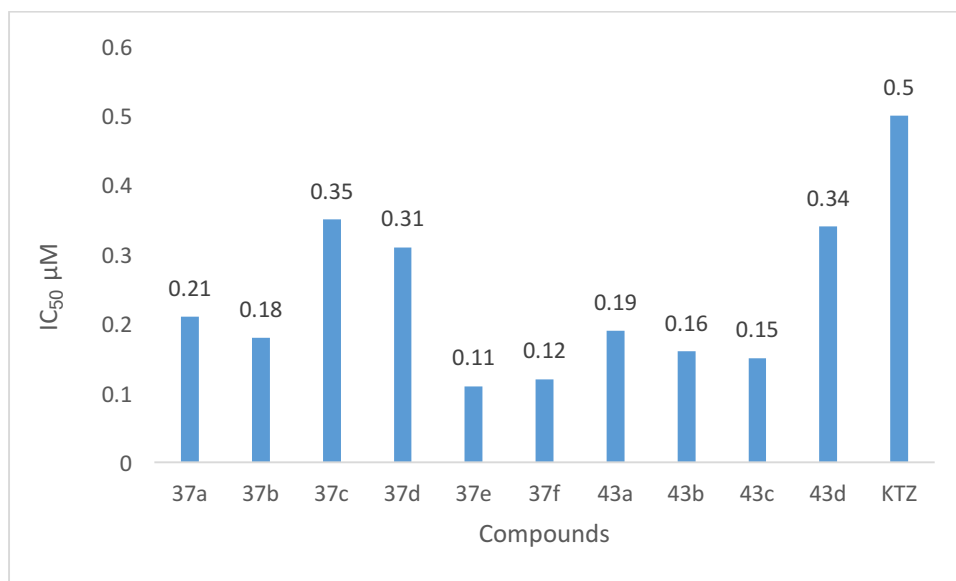
Figure 90: CYP24A1 inhibitor enzymatic assay

In general, binding energies (Figure 91) and IC_{50} showed a good correlation with the exception of compounds **11b** and **17c**. Substitution of these compounds with the more bulky trifluoromethyl group in the para position of the phenyl ring results in a slightly less favourable conformer energy compared with the other inhibitors, which affects the overall binding energy.
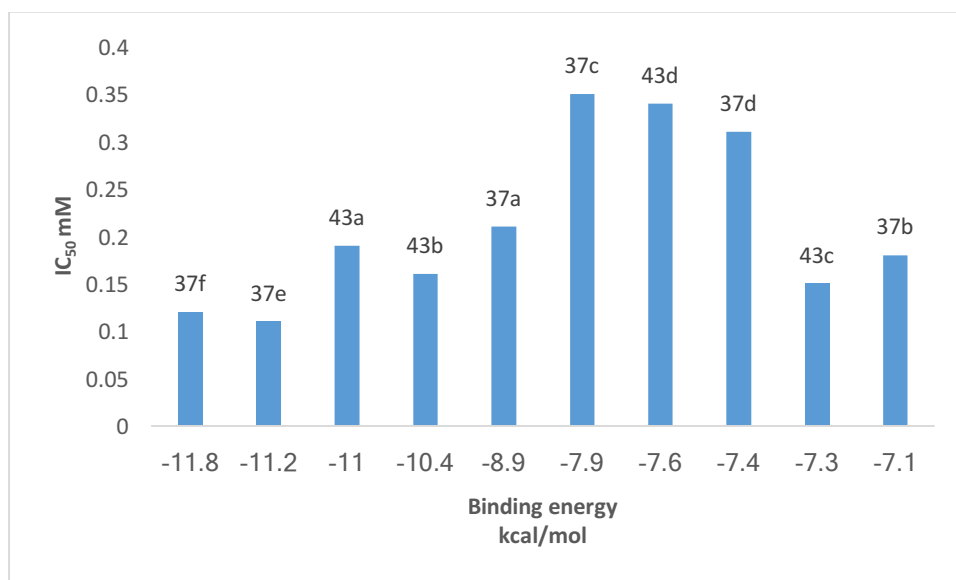
Figure 91: Correlation between CYP24A1 IC_{50} and binding energy for imidazole derivatives 37 and 43

Computational molecular docking of two exemplar compounds **37e** and **37f** in the CYP27B1 homology model would predict some inhibitory activity of this enzyme. Both compounds were found to interact with the haem iron via the amide carbonyl, however the imidazole nitrogen forms H-bonding interaction with Asn387, one of the amino acids identified as important for

CYP27B1 inhibitory activity. Whether just one H-bonding interaction with Asn387, rather than interaction with all three of the identified amino acids (Arg107, Asp320, Asn387), would produce significant or low inhibition would need to be determined experimentally (Figure 92 and 93).
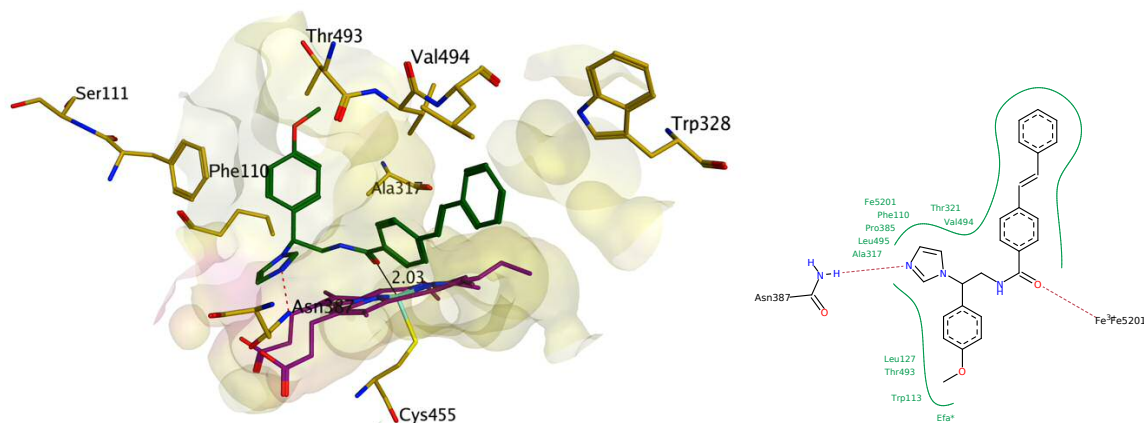
Figure 92: 3D and 2D models showing key binding interactions of 37e with CYP27B1 model
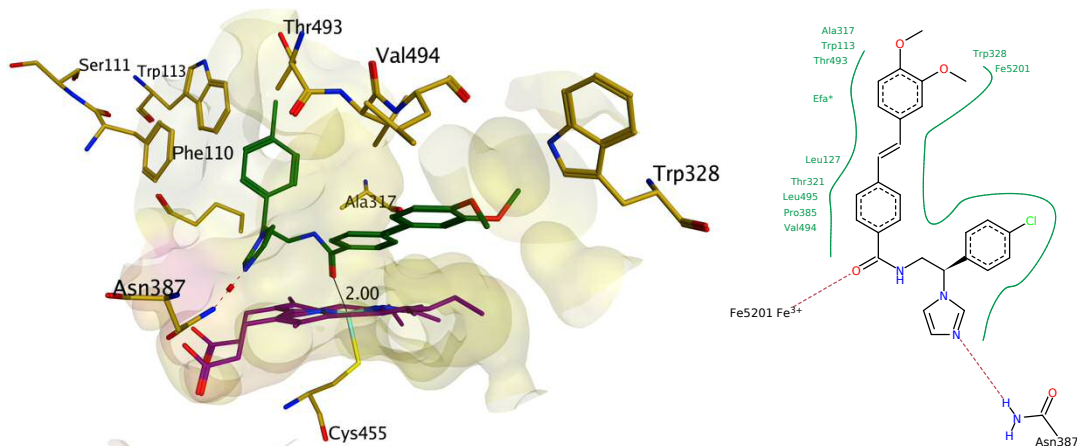
Figure 93: 3D and 2D models showing key binding interactions of 37f with CYP27B1 model

4.5   Conclusion

The aim of current chapter was to develop potential CYP24A1 inhibitors that could be used in combination with calcitriol for the treatment of various diseases. The compounds were prepared by the modification of lead 3, specifically through substitution of the phenyl ring on the imidazole side, substitution of the phenyl ring of styrene, and variation of the alkene double bond. Imidazole styrylbenzamide derivatives **37a - 37f** and **43a - 43d** were prepared from various aldehydes comprising six steps: aldehydes $\longrightarrow$ β-nitroalcohols $\longrightarrow$ amino alcohols $\longrightarrow$ styrylbenzamides $\longrightarrow$ dihydrooxazoles $\longrightarrow$ imidazole styrylbenzamides. Synthesis of β-nitroalcohols involves five different methods. Ambersep 900 (OH) was used as a catalyst, which is considered as environmentally friendly. Amino alcohols were prepared by catalytic hydrogenation employing a slurry of Raney nickel as a catalyst. (*E*)-substituted and unsubstituted styrylbenzoic acids were prepared by Heck reaction and then coupled with amino alcohols to give styrylbenzamides. Dihydrooxazoles were prepared from methansulfonylchloride, which were used as the crude product without further purification. Excess imidazole was used as reactant and solvent for the reaction of imidazole and styrylbenzamides and gave impressive yields. Docking studies revealed that all compounds access the active site of CYP24A1, occupying the same hydrophobic tunnel and with interacting amino acid residues as the known inhibitor. The hydrogen bond formed between the methoxy group of compounds **37e** and Arg128 stabilises the docked compound in a favourable conformation. All the synthesised compounds were tested for their ability to inhibit CYP24A1 demonstrating significant activity *in vitro*. Compounds **37e** and **37f** emerged as potential inhibitors displaying pronounced activity IC_{50} 0.11 µ M and 0.12 µ M respectively comparable with the CYP inhibitor ketoconazole (IC_{50} 0.50 µ M).

However, although collaboration at delivery the University of Wisconsin sent CYP27B1 enzyme on two different occasions, the enzyme was denatured (owing to customs holdup) on both deliveries. Owing to the time in enzyme preparation, extraction and the costs involved there was no further attempts to send compounds.

4.6   Experimental

4.6.1   Molecular modelling

molecular modelling method information as previously described Chapter 2.

4.6.2   CYP24A1 inhibitor enzymatic assay[279]

All CYP24A1 inhibitor enzymatic assay method information as previously described in Chapter 3.

4.6.3   Chemistry

4.6.3.1   1-(4-Chlorophenyl)-2-nitroethan-1-ol (30a)[307]
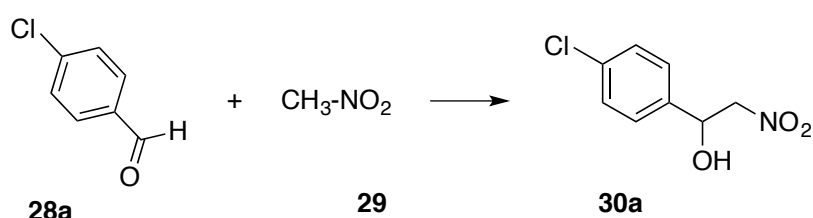
Chemical Formula: C8H8ClNO3
Molecular Weight: 201.61

Method 1	Method 4
To a solution of 4-chlorobenzaldehyde **28a** (5 g, 35.4 mmol) in methanol (20 mL), cooled to 0 ° C, nitromethane **29** (3.8 mL, 71 mmol) and aqueous NaOH (10 M, 14 mL) were added and the resulting solution was stirred at 0 ° C for 24 h. After addition of aqueous acetic acid (2 %, v/v, 10 mL) the reaction mixture was stirred at room temperature for 1 h, the methanol was removed under vacuum and the resulting solution extracted with dichloromethane (100 mL). The organic layer was washed with brine (2 × 100 mL), dried (MgSO$_4$) concentrated and purified by gradient flash column chromatography, product eluted with petroleum ether- EtOAc 1:1 v/v[307].	To a solution of 4-chlorobenzaldehyde **28a** (3 g, 21.4 mmol) in nitromethane **29** (10 mL, 183.3 mmol) was added Ambersep 900 (OH) (0.1 eq./1 mmol). The solution was stirred overnight and progress of the reaction was monitored by TLC. The Ambersep 900 was removed by filtration. The crude product was extracted with EtOAc (100 mL) and washed with brine (2× 100 mL), dried (Mg$_2$SO$_4$) and concentrated under vaccum to dryness[310].
Yield = 5.1 g (72 %), yellow liquid	Yield = 3.3 g (76 %), yellow liquid
Method 3	
To a slurry of LiAlH$_4$ (2 mmol, 5 mL), was added to nitromethane **29** (10 mL, 183.3 mmol) and the reaction stirred for 30 min at 0 °C. Then, 4-chlorobenzaldehyde **28a** (3 g, 21.4 mmol) was added and the mixture stirred	

overnight and then quenched with 1N aqueous HCl (20 mL). Then extracted with EtOAc (100 mL), washed with brine (2 × 100 mL), dried (Mg_2SO_4) and concentrated under vaccum[309].

Yield = 3.8 g (90 %), yellow liquid
TLC: petroleum ether-EtOAc 1:1 v/v, R_f = 0.38
^{1}H NMR (CD₃OD):
δ : 7.45 (d, J = 8.4 Hz, 2H, Ar), 7.38 (m, 2H, Ar), 5.41 (dd, J = 3.5, 9.7 Hz, 1H, C<u>H</u>-OH), 4.72 (dd, J = 3.5, 12.6 Hz, 1H, CH₂), 4.61 (dd, J = 9.7, 12.6 Hz, 1H, CH₂).

4.6.3.2   2-Nitro-1-(4-(trifluoromethyl)phenyl)ethan-1-ol (30b)

28b   **29**   **30b**
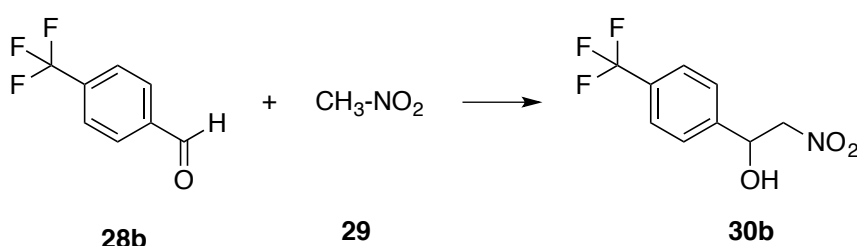
Chemical Formula: $C_9H_8F_3NO_3$
Molecular Weight: 235.16

Method 3	Method 4
Method 3: See 4.6.3.1	**Method 2:** See 4.6.3.1
Reagent: 4-(trifluoromethyl)benzaldehyde (0.75 g, 4.3 mmol) **28b**	**Reagent**: 4-(trifluoromethyl)benzaldehyde (1.1g, 7.3 mmol) **28b**
Yield = 1.1 g (92 %), yellow liquid	Yield = 1.5 g (85 %), yellow liquid
TLC: CH₂Cl₂: CH₃OH 9:1 v/v, R_f = 0.5	
^{1}H NMR (DMSO-d₆):	
δ : 7.76 (d, J = 8.3 Hz, 2H, Ar), 7.69 (d, J = 8.3 Hz, 2H, Ar), 6.31 (d, J = 4.7 Hz, 1H, OH), 5.41 (m, 1H, C<u>H</u>-OH), 4.94 (dd, J = 3.0, 12.3 Hz, 1H, CH₂), 4.64 (dd, J = 10.1, 12.7 Hz, 1H, CH₂).	

4.6.3.3   2-Nitro-1-(2-(trifluoromethyl)phenyl)ethan-1-ol (30c)

28c   **29**   **30c**
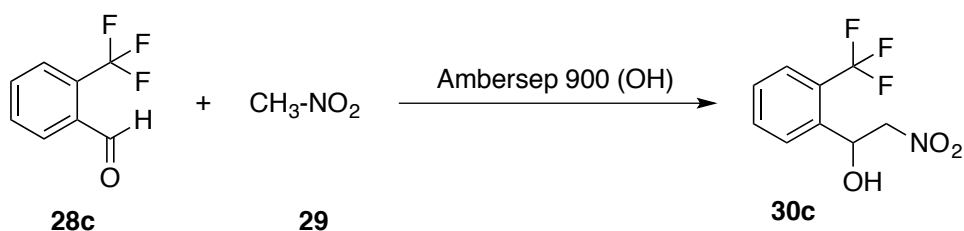
Chemical Formula: $C_9H_8F_3NO_3$
Molecular Weight: 235.16

Method 4: See 4.6.3.1

Reagent: 2-(trifluoromethyl)benzaldehyde (2 g, 11.5 mmol) **28c**

TLC: petroleum ether-EtOAc 4:1 v/v, $R_f = 0.50$

Yield = 2.1 g (78 %), yellow oil

^{1}H NMR (DMSO－d$_6$):

δ : 7.9 (d, J = 8.0 Hz, 1H, Ar), 7.77 (t, J = 7.5 Hz, 2H, Ar), 7.58 (t, J = 7.5 Hz, 1H, Ar), 6.43 (dd, 1.0, 4.7 Hz, 1H, OH), 5.64 (t, J = 5.0 Hz 1H, C**H**-OH), 4.75 (dd, J =1.0, 2.7 Hz, 1H, CH$_2$), 4.64 (dd, J = 10.1, 12.7 Hz, 1H, CH$_2$).

4.6.3.4   1-(4-Bromophenyl)-2-nitroethan-1-ol (30d)

Chemical Formula: C$_8$H$_8$BrNO$_3$
Molecular Weight: 246.06
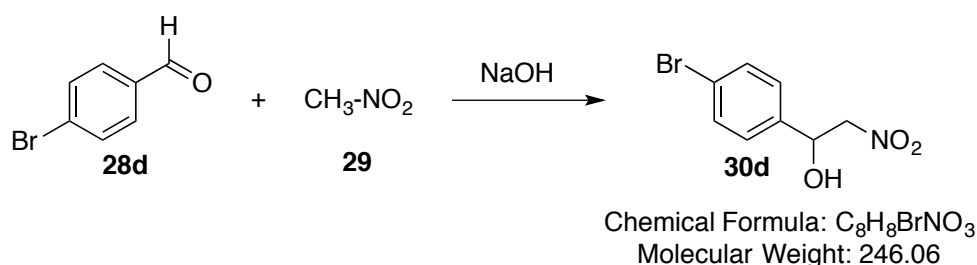
Method 1: See 4.6.3.1

Reagent: 4-Bromobenzaldehyde (3 g, 16.2 mmol) **28d**

TLC: CH$_2$Cl$_2$-CH$_3$OH 9: 1 v/v, $R_f = 0.36$

Yield = 3.6 g (92 %), brown oil

^{1}H-NMR (DMSO－d$_6$):

δ : 7.58 (dd, J = 1.8, 6.6 Hz, 2H, Ar), 7.43 (dd, J = 2.2, 10.5 Hz, 2H, Ar), 6.19 (d, J = 4.3 Hz, 1H, OH), 5.29 (dd, J = 3.8, 5.6 Hz, 1H, C**H**-OH), 4.87 (dd, J = 3.5, 12.6 Hz, 1H, CH$_2$), 4.60 (dd, J = 9.7, 12.6 Hz, 1H, CH$_2$).

4.6.3.5   2-Nitro-1-(*o*-tolyl)ethan-1-ol (30e)

Chemical Formula: C$_9$H$_{11}$NO$_3$
Molecular Weight: 181.19
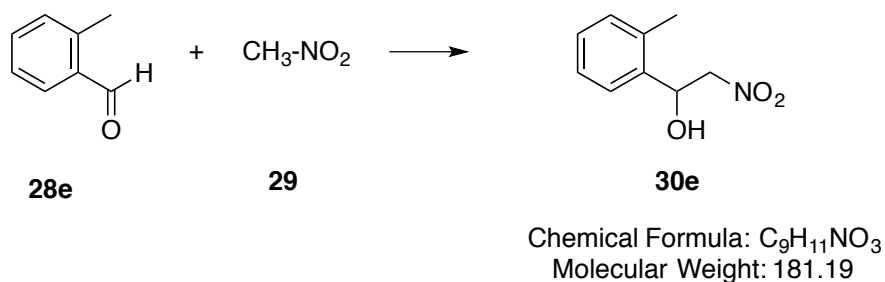
Method 3: See 4.6.3.1

Reagent: 2- methylbenzaldehyde **28e** (1 g, 0.83 mmol) **28d**

TLC: hexane-EtOAc 5:1 v/v, R_f = 0.12

Yield = Yield = 1.6 g (55 %), brown oil

4.6.3.6   1-(3,5-Dimethylphenyl)-2-nitroethan-1-ol (30f)
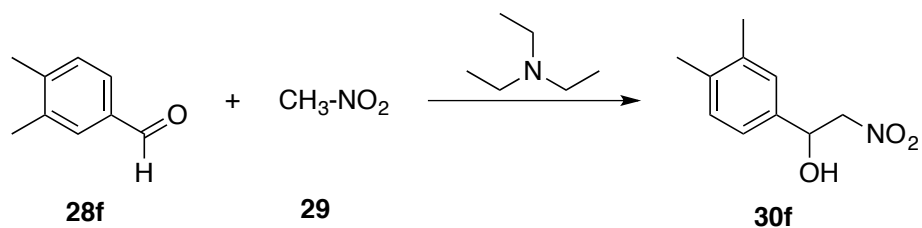
Chemical Formula: $C_{10}H_{13}NO_3$
Molecular Weight: 195.22

Method:

To a stirred solution of 3,5-dimethylbenzaldehyde **38f** (0.5 g, 3.7 mmol,) in nitromethane **29** (2.1g, 37 mmol) was added triethylamine (5 mL) and the resulting solution was stirred at room temperature until consumption of the aldehyde was indicated by TLC. The solution was diluted with EtOAc (100 mL), washed with sodium bicarbonate (2 × 50 mL), brine (2 × 50 mL) and water (2 × 50 mL). The organic layer was dried (MgSO₄) and concentrated in *vacuo*. The crude product was purified by gradient flash column chromatography; the product was eluted with petroleum ether-EtOAc 3:1 v/v[308].

TLC: petroleum ether-EtOAc 3:1 v/v, R_f = 0.57

m. p. = 54 - 56 ° C

Yield = 0.67 g (85 %), brownish yellow solid.

¹H NMR (DMSO-d₆):

δ : 7.32 (s, 1H, Ar), 7.10 (m, 2H, Ar), 5.94 (dd, J = 1.1, 4.8 Hz, 1H, OH), 5.44 (m, 1H, C<u>H</u>-OH), 4.79 (dd, J = 1.1, 3.0 Hz, 1H, CH₂), 4.47 (dd, J = 10.0, 12.6 Hz, 1H, CH₂), 2.30 (s, 3H, CH₃), 2.28 (s, 3H, CH₃).

4.6.3.7   1-(4-Methoxyphenyl)-2-nitroethan-1-ol (30g)
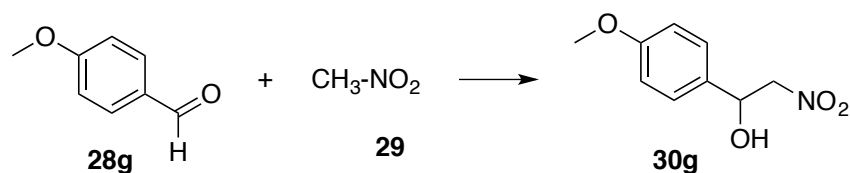
Chemical Formula: $C_9H_{11}NO_4$
Molecular Weight: 197.19

Method 3	Method 2
Method 3: See 4.6.3.1 **Reagent:** 4-methoxybenzaldehyde (2 g, 14.7 mmol) **28g** Purified by gradient flash column chromatography, product was eluted with petroleum ether- EtOAc 4:1 v/v.	**Method 2:** See 4.6.3.1 **Reagent:** 4-methoxybenzaldehyde (1.4 g, 10 mmol) **28g** Purified by gradient flash column chromatography, product was eluted with petroleum ether- EtOAc 4:1 v/v.
Yield = 2.5 g (86 %), yellow oil	Yield = 0.4 g (20 %), yellow oil
TLC: petroleum ether-EtOAc 4:1 v/v, R_f = 0.4	
^{1}H NMR (DMSO-d$_6$): δ : 7.36 (d, J = 8.6 Hz, 2H, Ar), 6.94 (d, J = 11.6 Hz, 2H, Ar), 5.98 (dd, J = 0.8, 5.0 Hz, 1H, OH), 5.23 (m, 1H, C$\underline{H}$-OH), 4.80 (dd, J = 2.8, 12.5 Hz, 1H, CH$_2$), 4.57 (dd, J =10.1, 12.7 Hz, 1H, CH$_2$), 3.75 (s, 3H, OCH$_3$).	

4.6.3.8   1-(3,5-Dimethoxyphenyl)-2-nitroethan-1-ol
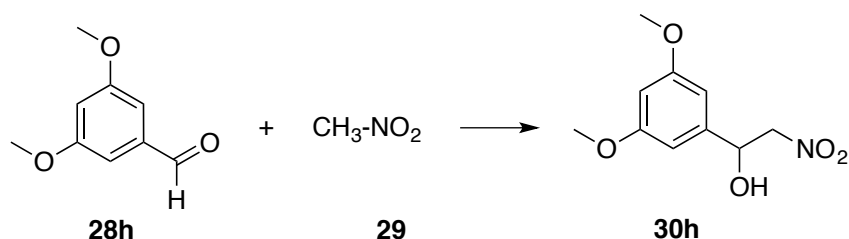
Chemical Formula: C$_{10}$H$_{13}$NO$_5$
Molecular Weight: 227.22

Method 4	Method 2
Method 4: See 4.6.3.5 **Reagent:** 3,5-dimethoxybenzaldehyde (3 g, 18 mmol) **28h** Purified by gradient flash column chromatography, product was eluted with petroleum ether-EtOAc 3:1 v/v.	**Method 2:** See 4.6.3.1 **Reagent:** 3,5-dimethoxybenzaldehyde (3 g, 18 mmol) **28h**
Yield = 2.5 g (63 %), yellow oil	Yield = 3.3 g (85 %), yellow oil
TLC: petroleum ether-EtOAc 4:1 v/v, R_f = 0.6	
^{1}H NMR (DMSO ˗ d$_6$): δ : 6.62 (d, J = 2.3 Hz, 2H, Ar), 6.43 (t, J = 2.3 Hz, 1H, Ar), 6.07 (d, J = 5 Hz, 1H, OH), 5.23 (m, 1H, C$\underline{H}$-OH), 4.86 (dd, J = 3.2, 12.5 Hz, 1H, CH$_2$), 4.56 (dd, J = 10.1, 12.5 Hz, 1H, CH$_2$), 3.74 (s, 6H, OCH$_3$).	

4.6.3.9   2-Amino-1-(4-chlorophenyl)ethan-1-ol (31a)

Chemical Formula: $C_8H_{10}ClNO$
Molecular Weight: 171.62
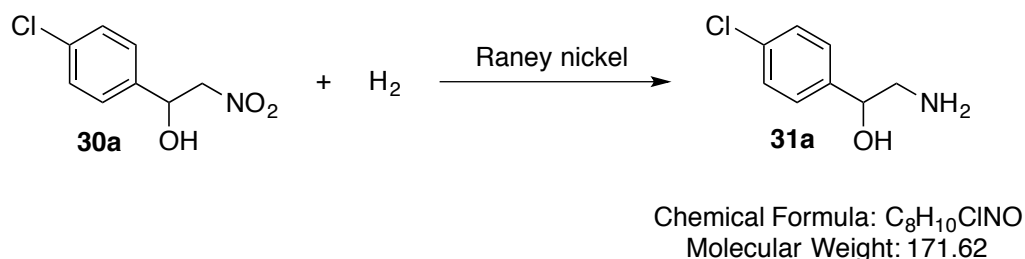
Method:

Raney nickel (50 % slurry in H_2O, 3 mL) was added to a solution of 1-(4-chlorophenyl)-2-nitroethan-1-ol **30a** (1.5 g, 7.5 mmol) in methanol (40 mL) and aqueous formic acid (50 % v/v, 8 mL). The reaction flask was then degassed and a hydrogen balloon was used until all starting material had been consumed. The reaction mixture was filtered, and the methanol was removed under vacuum. The aqueous residue was made alkaline with NH_4OH and extracted with EtOAc (100 mL) and washed with brine (2 × 100 mL), dried ($MgSO_4$), filtered and reduced under vacuum to give yellow solid[312].

TLC: CH_2Cl_2-CH_3OH 9:1 v/v, $R_f = 0.20$

m. p. = 106 - 110 ° C (Lit. m. p. 94 - 95 ° C)[313]

Yield = 1.28 g (84 %), pale a yellow solid

^{1}H NMR (CD$_3$OD):

δ : 7.38 (m, 4H, Ar), 4.53 (m, 1H, C$\underline{H}$-OH), 3.41 (br. s, 3H, OH, NH_2), 2.73 (dd, J = 3.8, 12.9 Hz, 1H, CH_2), 2.61 (dd, J = 7.9, 12.9 Hz, 1H, CH_2).

4.6.3.10 2-Amino-1-(4-(trifluoromethyl)phenyl)ethan-1-ol (31b)

Chemical Formula: $C_9H_{10}F_3NO$
Molecular Weight: 205.18
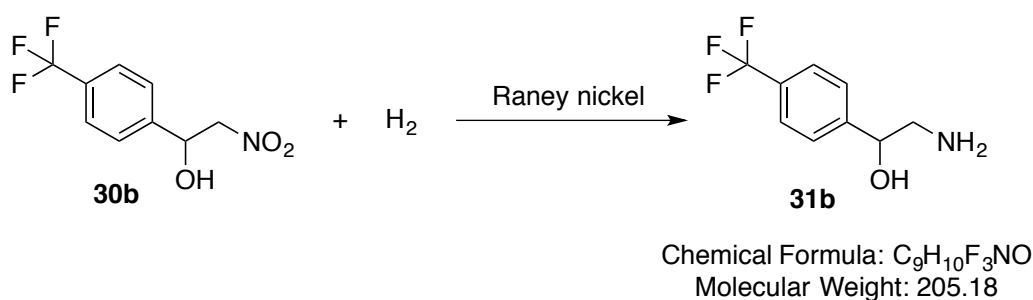
Method:

Raney nickel (50 % slurry in H_2O, 3 mL) was added to a solution of 2-nitro-1-(4-(trifluoromethyl)phenyl)ethan-1-ol **30b** (1 g, 4.25 mmol) in methanol (40 mL) and aqueous

formic acid (50 % v/v, 8 mL). The suspension was subject to hydrogenation at 45 psi for 6 h. The reaction mixture was filtered, and the methanol was removed under vacuum. The aqueous residue was made alkaline with NH_4OH and extracted with EtOAc (100 mL), washed with brine (2 × 100 mL), dried ($MgSO_4$), filtered and reduced under vacuum to give a white solid[312]. TLC: CH_2Cl_2-CH_3OH 9:1 v/v, R_f = 0.30

m. p. = 60 - 64 ° C

Yield = 0.46 g (53 %), white solid

^{1}H NMR (DMSO-d_6):

δ : 7.68 (d, J = 8.1 Hz, 2H, Ar), 7.56 (d, J = 8.1 Hz, 2H, Ar), 4.56 (φt, J = 4.2, 6.6 Hz, 1H, C$\underline{H}$-OH), 3.14 (br. s, 3H, OH, NH$_2$), 2.73 (d, J = 3.3 Hz, 1H, CH$_2$), 2.62 (m, 1H, CH$_2$).

4.6.3.11 2-Amino-1-(2-(trifluoromethyl)phenyl)ethan-1-ol (31c)
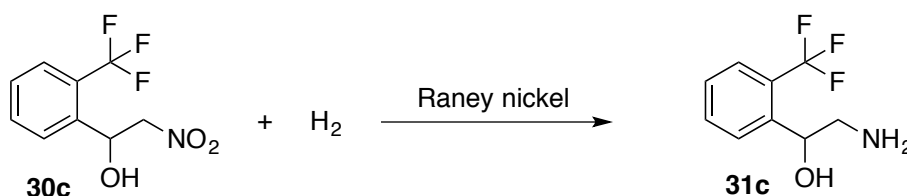
Chemical Formula: $C_9H_{10}F_3NO$
Molecular Weight: 205.18

Method: See 4.6.3.10

Reagent: 2-nitro-1-(2-(trifluoromethyl)phenyl)ethan-1-ol (1 g, 4.5 mmol) **31c**.

TLC: CH_2Cl_2-CH_3OH 9:1 v/v, R_f = 0.60

m. p. = 80 - 86 ° C

Yield = 0.60 g (67 %), white solid

^{1}H NMR (DMSO-d_6):

δ : 7.77 (d, J = 7.8 Hz, 1H, Ar), 7.69 (m, 2H, Ar), 7.47 (t, J = 7.6 Hz,1H, Ar), 4.80 (m, 1H, C$\underline{H}$-OH), 3.01 (br. s, 3H, OH, NH$_2$), 2.67 (d, J = 3.3 Hz, 1H, CH$_2$), 2.55 (m, 1H, CH$_2$).

4.6.4 2-Amino-1-(*o*-tolyl)ethan-1-ol (31e)
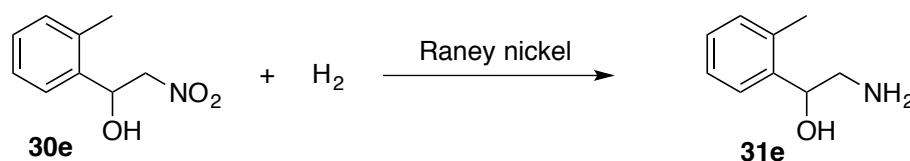
Chemical Formula: $C_9H_{13}NO$
Molecular Weight: 151.21

Method: See 4.6.3.10

Reagent: 2-nitro-1-(*o*-tolyl)ethan-1-ol (1 g, 5.5 mmol) **31e**

TLC: CH_2Cl_2-CH_3OH 9:1 v/v, $R_f = 0.6$

Yield = 0.46 g (57 %), amber oil. Purified by gradient flash column chromatography, product was eluted with CH_2Cl_2-CH_3OH 9:1 v/v.

¹H NMR (CDCl₃):

δ : 7.50 (d, J = 8.6 Hz, 1H, Ar), 7.25 (m, 3H, Ar), 5.08 (dd, J = 3.0, 8.4 Hz, 1H, C$\underline{H}$-OH), 3.77 (m, 1H, CH₂), 3.24 (m, 1H, CH₂), 3.15 (br. s, 3H, OH, NH₂), 2.36 (s, 3H, CH₃).

4.6.4.1   2-Amino-1-(3,4-dimethylphenyl)ethan-1-ol (31f)

Chemical Formula: $C_{10}H_{15}NO$
Molecular Weight: 165.24
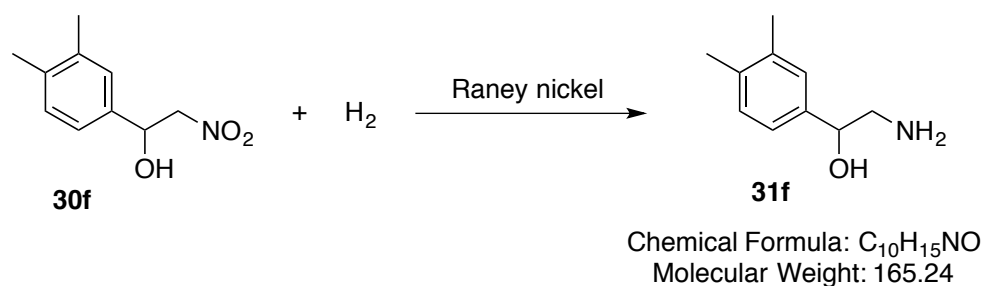
Method: See 4.6.3.10

Reagent: 1-(3,4-dimethylphenyl)-2-nitroethan-1-ol (0.67 g, 3.5 mmol) **31f**

TLC: CH_2Cl_2-CH_3OH 9:1 v/v, $R_f = 0.1$

m. p. = 64 - 68 ° C

Yield = 0.35 g (63 %), pale yellow solid

¹H NMR (DMSO-d₆):

δ : 7.21 (s, 1H, Ar), 6.99 (d, J = 7.6 Hz, 2H, Ar), 4.62 (m, 1H, C$\underline{H}$-OH), 3.38 (br. s, 3H, OH, NH₂), 2.63 (dd, J = 3.8, 12.9 Hz, 1H, CH₂), 2.57 (dd, J = 7.9, 12.9 Hz, 1H, CH₂), 2.25 (s, 3H, CH₃), 2.22 (s, 3H, CH₃).

4.6.4.2   2-Amino-1-(4-methoxyphenyl)ethan-1-ol (31g)

Chemical Formula: $C_9H_{13}NO_2$
Molecular Weight: 167.21

Method 1	Method 2
Method 1: See 4.6.3.10 **Reagent**: 1-(4-methoxyphenyl)-2-nitroethan-1-ol (1 g, 5 mmol) **30g**	**Method 2:** Pd/C (100 mg) was added to a solution of 1-(4-methoxyphenyl)-2-nitroethan-1-ol **30g** (1 g, 5 mmol) in methanol (20 mL) and subject to hydrogenation 45 psi for 6 h. The reaction mixture was filtered, and the methanol was removed under vacuum. The residue was made alkaline with NH_4OH and extracted with EtOAc (100 mL) and washed with brine (2 $\times$ 100 mL), dried over anhydrous ($MgSO_4$), filtered and reduced under vacuum. The product was purified by gradient flash column chromatography, product eluted with CH_2Cl_2-CH_3OH 9:1 v/v to give a yellow solid[311].
Yield = 0.40 g (47 %), yellow solid	Yield = 0.36 g (42 %), yellow solid
m. p. = 46 - 50 ° C (Lit. 70° C[314])	
TLC: CH_2Cl_2-CH_3OH 9:1 v/v, R_f = 0.6	
¹H NMR (DMSO-d₆): δ : 7.28 (d, J = 8.6 Hz, 2H, Ar), 6.90 (d, J = 8.6 Hz, 2H, Ar), 4.61 (m, 1H, C$\underline{H}$-OH), 3.81 (s, 3H, OCH_3), 3.93 (d, J = 3.3 Hz, 1H, CH_2), 3.60 (m, 1H, CH_2), 2.29 (br. s, 3H, OH, NH_2).	

4.6.4.3   2-Amino-1-(3,5-dimethoxyphenyl)ethan-1-ol (31h)
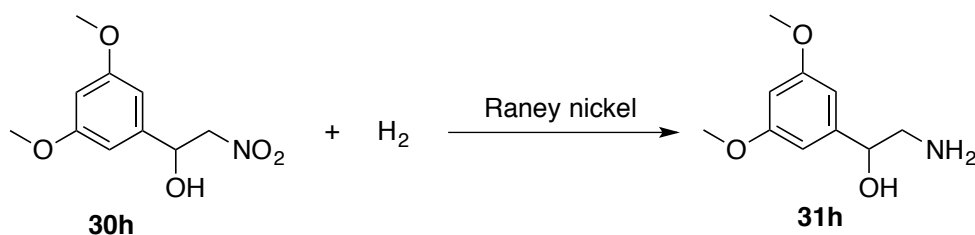
Chemical Formula: $C_{10}H_{15}NO_3$
Molecular Weight: 197.23

Method: See 4.6.3.10

The product was purified by gradient flash column chromatography, product was eluted with CH_2Cl_2-CH_3OH 9:1 v/v.

Reagent: 1-(3,5-dimethoxyphenyl)-2-nitroethan-1-ol (3.5 g, 15.4 mmol) **30h**

TLC: CH_2Cl_2-CH_3OH 9:1 v/v, R_f = 0.76

Yield = 0.5 g (17 %), yellow oil

¹H NMR (DMSO-d₆):

δ : 6.52 (d, J = 2.3 Hz, 2H, Ar), 6.38 (t, J = 2.3 Hz, 1H, Ar), 4.56 (m, 1H, <u>CH</u>-OH), 3.73 (s, 6H, 2 × OCH₃), 3.07 (br.s, 3H, OH & NH₂), 2.46 (m, 1H, CH₂), 2.18 (m, 1H, CH₂).

4.6.4.4   *(E)*-4-styrylbenzoic acid (34a)

32a   **33**   **34a**

Chemical Formula: C₁₅H₁₂O₂
Molecular Weight: 224.26
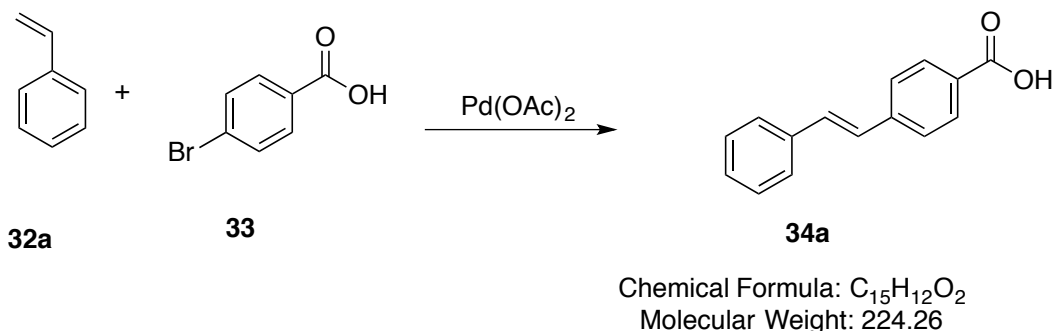
Method:

Styrene **32a** (3.2 g, 31.1 mmol), 4-bromobenzoic acid **33** (5 g, 24.9 mmol) and triethylamine (69 mL, 77.7 mmol) were heated in the presence of tri(*o*-tolyphosphine) (0.3 g, 0.99 mmol) and Pd(OAc)₂ (50 mg, 0.27 mmol) in a sealed glass tube at 100 ˚ C overnight. After the reaction was complete, a white-gray precipitate formed. Then cold aqueous 1M HCl (15 mL) was added and the mixture was extracted with EtOAc (100 mL) and washed with brine (2 × 100 mL), dried (MgSO₄), filtered and reduced under vacuum.

TLC: petroleum ether-EtOAc 1:1 v/v, R_f= 0.63

m. p. = 240 - 242 ˚ C (Lit. 257 ℃[318])

Yield = 3.5 g (51 %), yellow crystals, recrystallised with ethanol

¹H NMR (DMSO-d₆):

δ : 12.91 (s, 1H, COOH), 7.95 (d, J = 8.4 Hz, 2H, Ar), 7.73 (d, J = 8.4 Hz, 2H, Ar), 7.65 (d, J = 7.4 Hz, 2H, Ar), 7.35 (m, 5H, Ar).

4.6.4.5   *(E)*-4-(3,4-dimethoxystyryl)benzoic acid (34b)

32b   **33**   **34b**

Chemical Formula: C₁₇H₁₆O₄
Molecular Weight: 284.31
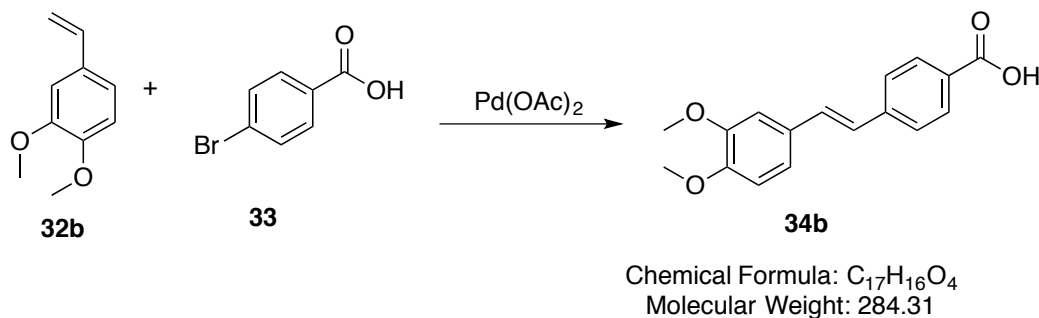
Method: See 4.6.4.4

Reagent: 1,2-dimethoxy-4-vinylbenzene (1 g, 6 mmol) **32b**

TLC: petroleum ether-EtOAc 1:3 v/v, R_f= 0.22

m. p. = 244 - 248 ° C

Yield = 1 g (59 %), yellow crystals, recrystallised with ethanol.

^{1}H NMR (DMSO-d$_6$):

δ : 12.88 (s, 1H, COOH), 7.94 (d, J = 8.4 Hz, 2H, Ar), 7.69 (d, J = 8.4 Hz, 2H, Ar), 7.36 (d, J = 16.4 Hz, 1H, alkene), 7.24 (d, J = 16.4 Hz, 1H, alkene), 7.16 (dd, J = 1.9, 8.4 Hz, 2H), 6.98 (d, J = 8.4 Hz, 1H, Ar), 3.83 (s, 3H, OCH$_3$), 3.78 (s, 3H, OCH$_3$).

^{13}C NMR (DMSO-d$_6$):

δ : 167.6 (CO), 149.6, 149.4, 142.3 (3 × C), 131.5, 130.3 (2 × CH, Ar), 130.0, 129.4 (2 × C), 126.5, 125.6, 121.1, 112.2, 109.8 (7 × CH, Ar), 55.9 (2 × OCH$_3$, Ar).

Microanalysis

Anal. Calcd for C$_{17}$H$_{16}$O$_4$· 0.1H$_2$O (286.1): C 71.37 %, H 5.71 %. Found C71.29 %, H 5.47 %.

4.6.4.6   (*E*)-*N*-(2-(4-chlorophenyl)-2-hydroxyethyl)-4-styrylbenzamide (35a)

Chemical Formula: C$_{23}$H$_{20}$ClNO$_2$
Molecular Weight: 377.87
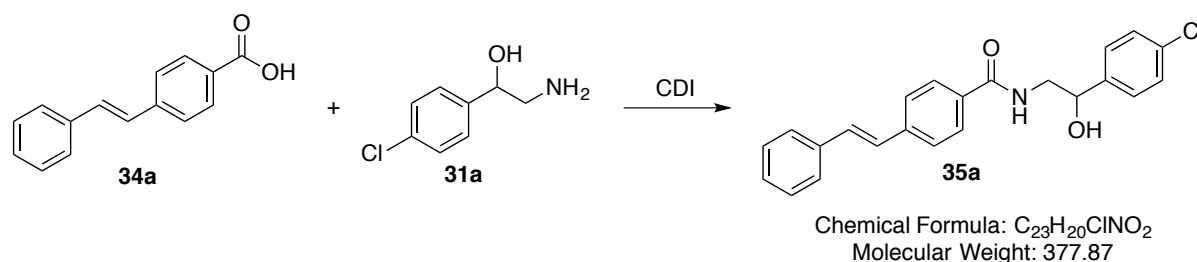
Method:

A suspension of (*E*)-4-styrylbenzoic acid **34a** (0.9 g, 4.1 mmol) in dry DMF (16 mL) was combined with CDI (0.7 g, 4.5 mmol). The reaction was stirred for 1 h at room temperature under nitrogen. The mixture was cooled to 0 ° C then added to a solution of 2-Amino-1-(4-chlorophenyl)ethan-1-ol **31a** (0.7 g, 4.1 mmol) in dry DMF (5 mL). The resulting mixture was stirred at room temperature overnight. On completion, ice was added into the flask and the resulting white solid collected by filtration, washed with ice-cold water and dried[210].

TLC: CH$_2$Cl$_2$-CH$_3$OH 9:1 v/v, R_f= 0.86

m. p. = 258 - 260 ° C

Yield = 1 g (67 %), white crystals, recrystallised with methanol

¹H NMR (DMSO-d₆):

δ : 8.52 (t, J = 5.3 Hz, 1H, NH), 7.85 (d, J = 8.2 Hz, 2H, Ar), 7.73 (d, J = 8.4 Hz, 2H, Ar), 7.74 (d, J = 8.2 Hz, 2H, Ar), 7.42 (m, 5H, Ar) 7.24 (m, 4H, Ar), 5.64 (s, 1H, OH), 4.80 (m, 1H, C$\underline{H}$OH), 3.49 (m,1H, CH₂), 3.40 (m, 1H, CH₂).

¹³C NMR (DMSO-d₆):

δ : 167.6 (CO), 140.9, 137.5, 135.2, 133.6, 133.2 (5 × C), 129.4, 128.5, 128.1, 127.3, 127.2, 127.1, 126.9 (15 × CH, Ar), 72.2 (CH), 47.1 (CH₂)

Microanalysis

Anal. Calcd for C₂₃H₂₀ClNO₂· 0.3H₂O (382.52): C 72.08 %, H 5.42 %, N 3.65 %. Found C72.20 %, H 5.26 %, N 3.86 %.

4.6.4.7   (*E*)-*N*-(2-hydroxy-2-(4-(trifluoromethyl)phenyl)ethyl)-4-styrylbenzamide (35b)

Chemical Formula: C₂₄H₂₀F₃NO₂
Molecular Weight: 411.42
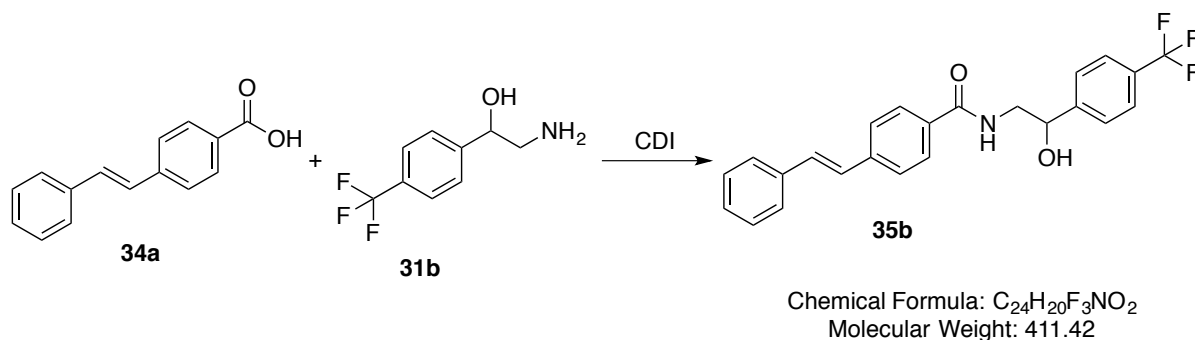
Method: See 4.6.4.6

Reagent: (*E*)-4-styrylbenzoic acid (0.4g, 2 mmol) **34a**

TLC: petroleum ether-EtOAc 3:1 v/v, R$_f$= 0.75

m. p. = 220 - 224 ° C

Yield = 0.35 g (35 %), white crystals, recrystallised with methanol.

¹H NMR (DMSO-d₆):

δ : 8.58 (t, J = 5.7 Hz, 1H, NH), 7.84 (d, J = 8.4 Hz, 2H, Ar), 7.72 (φ t, J = 8.4, 10.5 Hz, 4H, Ar), 7.65 (m, 4H, Ar), 7.42 (m, 3H, Ar) 7.33 (m, 2H, Ar), 5.77 (d, J = 4.5 Hz, 1H, OH), 4.89 (t, J = 5.5 Hz, 1H, C$\underline{H}$OH), 3.53 (m,1H, CH₂), 3.43 (m, 1H, CH₂).

¹³C NMR (DMSO-d₆):

δ : 166.6 (CO), 149.0, 140.3, 137.2, 133.6 (4 × C), 129.2, 128.5 (2 × CH, Ar), 128.3, 128.0 (2 × C), 127.9, 127.3, 127.2, 127.1, 126.7, 125.4 (13 × CH, Ar), 71.2 (CH), 47.9 (CH₂)

Microanalysis

Anal. Calcd for C₂₄H₂₀F₃NO₂ (411.42): C 70.07 %, H 4.90 %, N 3.40 %. Found C 70.39 %, H 4.79 %, N 3.47 %.

4.6.4.8   (*E*)-*N*-(2-hydroxy-2-(2-(trifluoromethyl)phenyl)ethyl)-4-styrylbenzamide (35c)
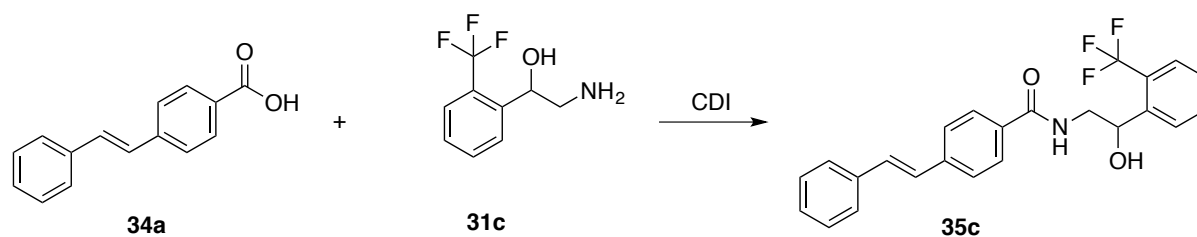
Chemical Formula: $C_{24}H_{20}F_3NO_2$
Molecular Weight: 411.42

Method: See 4.6.4.6

Reagent: (*E*)-4-styrylbenzoic acid (0.7 g, 3 mmol) **34a**

TLC: petroleum ether-EtOAc 3:1 v/v, $R_f = 0.40$

m. p. = 160 - 166 ° C

Yield = 0.7 g (58 %), white solid, recrystallised with methanol.

^{1}H NMR (DMSO-d$_6$):

δ : 8.58 (t, J = 6 Hz, 1H, NH), 7.87 (d, J = 8.5 Hz, 3H, Ar), 7.74 (m, 4H, Ar), 7.68 (d, J = 15.5 Hz, 2H, Ar), 7.51 (t, J = 7.7 Hz, 1H, Ar), 7.42 (m, 2H, Ar) 7.33 (m, 3H, Ar), 5.81 (d, J = 4.0 Hz, 1H, OH), 5.14 (dd, J = 5.1, 11.9 Hz, 1H, C<u>H</u>OH), 3.51 (m, 2H, CH$_2$).

^{13}C NMR (DMSO-d$_6$):

δ : 169.6 (CO), 141 (C), 140.3, 131.0 (CH),128.8 (C), 128.2, 128.1, 127.8, 127.3, 127.0, 126.3, 126.6, 125.1, 126.7, 125.4 (14 × CH, Ar), 124.3, 123.2 (5 × C), 77.2 (CH), 48.3 (CH$_2$)

Microanalysis

Anal. Calcd for $C_{24}H_{20}F_3NO_2$ (411.42): C 70.07 %, H 4.90 %, N 3.40 %. Found C 70.22 %, H 4.92 %, N 3.38 %.

4.6.4.9   (*E*)-*N*-(2-(3,4-dimethylphenyl)-2-hydroxyethyl)-4-styrylbenzamide (35d)
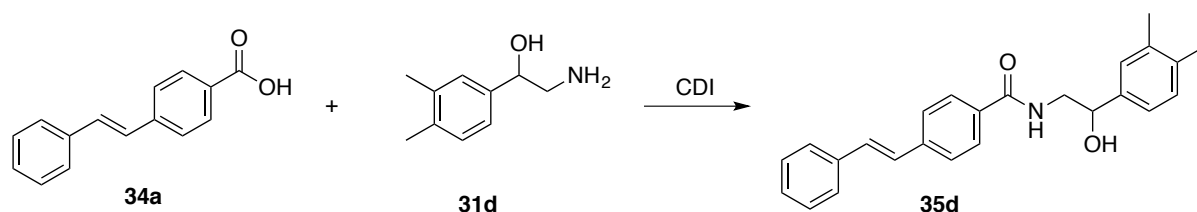
Chemical Formula: $C_{25}H_{25}NO_2$
Molecular Weight: 371.48

Method: See 4.6.4.6

Reagent: 2-amino-1-(3,4-dimethylphenyl)ethan-1-ol (0.50 g, 3 mmol) **31d**

TLC: CH$_2$Cl$_2$- CH$_3$OH 9.5:0.5 v/v, $R_f = 0.80$

m. p. = 150 - 154° C

Yield: 0.70 g (60 %), white solid, recrystallised with ethanol

^{1}H NMR (CDCl$_3$):

δ : 8.08 (s, 1H, Ar), 8.63 (d, J = 8.0 Hz, 1H, Ar), 7.57 (d, J = 7.5 Hz, 2H, Ar), 7.42 (t, J = 7.5 Hz, 2H, Ar), 7.33 (t, J = 7.5 Hz, 2H, Ar), 7.28 (s, 1H, Ar), 7.26 (s, 1H, Ar) 7.19 (d, J = 4.5 Hz, 2H, Ar), 7.15 (m, 3H, Ar), 5.88 (t, J = 10.0 Hz, 1H, OH), 4.56 (dd, J = 10.0, 15.0 Hz, 1H, C<u>H</u>OH), 4.17 (m, 1H, CH$_2$), 3.93 (dd, J = 8.5, 14.5 Hz, 1H, CH$_2$), 3.5 (s, 6H, 2CH$_3$).

^{13}C NMR (CDCl$_3$):

δ : 166.5 (CO), 142.1, 140.1, 137.3, 134.9, 133.7, 131.6 (6 × C), 130.6, 130.3, 129.2, 128.4, 128.2, 128.0, 127.8, 127.2, 126.7 (14× C, Ar), 68.6 (CH), 47.4 (CH$_2$), 21.35, 18.71 (2 × CH$_3$).

Microanalysis

Anal. Calcd for C$_{25}$H$_{25}$NO$_2$ (371.48): C 80.83 %, H 6.78 %, N 3.77 %. Found C 81.10 %, H 6.78 %, N 3.88 %

4.6.4.10 (*E*)-*N*-(2-hydroxy-2-(4-methoxyphenyl)ethyl)-4-styrylbenzamide (35e)

Chemical Formula: C$_{24}$H$_{23}$NO$_3$
Molecular Weight: 373.45
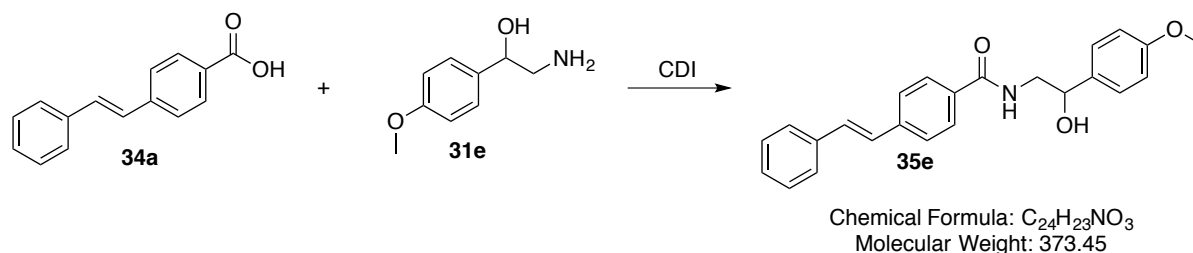
Method: See 4.6.4.6

Reagent: (*E*)-4-styrylbenzoic acid (0.6 g, 2 mmol) **34a**

TLC: petroleum ether-EtOAc 1:3 v/v, R$_f$ = 0.70

m. p. = 218 - 220 ° C

Yield = 0.35 g (35 %), white solid, recrystallised with methanol.

^{1}H NMR (DMSO-d$_6$):

δ : 8.50 (t, J = 5.5 Hz, 1H, NH), 7.87 (d, J = 8.3 Hz, 2H, Ar), 7.70 (d, J = 8.3 Hz, 4H, Ar), 7.65 (q, J = 7.6 Hz, 3H, Ar), 7.33 (m, 2H, Ar), 7.33 (m, 2H, Ar), 6.92 (d, J = 8.3 Hz, 2H), 5.43 (d, J = 4.5 Hz, 1H, OH), 4.76 (m, 1H, C<u>H</u>OH), 3.74 (s, 3H, OCH$_3$), 3.50 (m,1H, CH$_2$), 3.34 (m, 1H, CH$_2$).

^{13}C NMR (DMSO-d$_6$):

δ : 166.5 (CO), 158.8, 140.2, 137.3, 136.3, 133.8 (5 × C), 130.6, 129.2, 128.5, 128.1, 127.6, 127.2, 1114.3 (15 × CH, Ar), 71.2 (CH), 55.4 (OCH$_3$) 48.2 (CH$_2$)

Microanalysis

Anal. Calcd for $C_{24}H_{23}NO_3$ (373.45): C 77.19 %, H 6.21 %, N 3.75 %. Found C 77.32 %, H 6.02 %, N 3.70 %.

4.6.4.11 (*E*)-*N*-(2-(4-chlorophenyl)-2-hydroxyethyl)-4-(3,4-dimethoxystyryl)benzamide (35f)

Chemical Formula: $C_{25}H_{24}ClNO_4$
Molecular Weight: 437.92
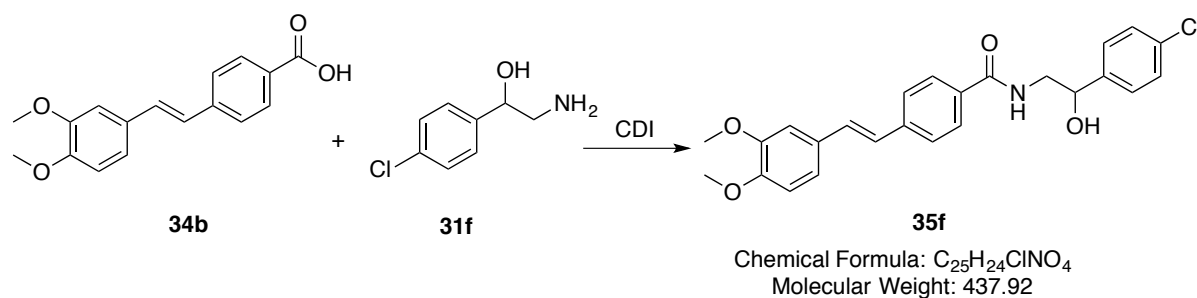
Method: See 4.6.4.6

Reagent: (*E*)-4-(3,4-dimethoxystyryl)benzoic acid (1 g, 3.5 mmol) **34b**

TLC: petroleum ether-EtOAc 1:1 v/v, $R_f = 0.2$

m. p. = 168 - 172 ° C

Yield = 0.9 g (69 %), white solid, recrystallised with acetonitrile

^{1}H NMR (DMSO-d$_6$):

δ : 8.53 (t, J = 6.0 Hz, 1H, NH), 7.84 (d, J = 8.0 Hz, 2H, Ar), 7.65 (d, J = 8.5 Hz, 2H, Ar), 7.40 (s, 2H, Ar), 7.36 (m, 2H, Ar), 7.21 (m, 2H, Ar) 7.00 (m, 3H, Ar), 5.66 (d, J = 4.5 Hz, 1H, OH), 4.81 (m, 1H, CHOH), 3.87 (s, 6H, 2 × OCH$_3$), 3.49 (m, 2H, CH$_2$).

^{13}C NMR (DMSO-d$_6$):

δ : 166.5 (CO), 149.5, 149.4, 143.3, 133.2, 131.9, 128.2 (6 × C), 130.7 (CH, Ar), 130.2 (C),128.4, 128.3, 128.2, 126.3, 125.8, 120.7, 112.3, 109.7 (12 × CH, Ar), 71.0 (CH), 56.3 (2 × OCH$_3$), 47.3 (CH$_2$).

LRMS (ES-TOF)

M/Z: 440 [M^{37Cl} + H]$^+$, 438 [M^{35Cl} + H]$^+$

HRMS (ES-TOF)

Calculated mass: 438.1472 [M + H]$^+$, measured mass: 438.1463 [M + H]$^+$

4.6.4.12 *(E)*-5-(4-chlorophenyl)-2-(4-styrylphenyl)-4,5-dihydrooxazole (36a)

Chemical Formula: $C_{23}H_{18}ClNO$
Molecular Weight: 359.85
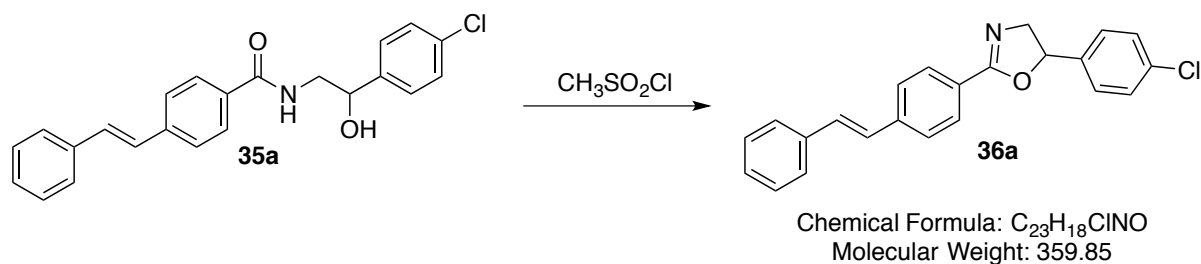
Method:

A solution of *(E)*-*N*-(2-(4-chlorophenyl)-2-hydroxyethyl)-4-styrylbenzamide **35a** (1.3 g, 3.4 mmol) in dry THF (30 mL) was cooled to 0 ° C. Then methansulfonylchloride (2.2 mL, 27 mmol) was added and the resulting mixture stirred at 0 ° C for 3 h. Triethylamine (6.2 mL, 40.8 mmol) was added dropwise and the solution was stirred overnight at room temperature. The mixture was quenched by the addition of NH_4OH (28 %, 3 mL) and the reaction stirred at room temperature for 30 min. Then THF was removed under reduce pressure and the residue was extracted by EtOAc (100mL) and water (2 × 100 mL). The organic layer was collected, dried ($MgSO_4$) and concentrated under vaccum[191].

TLC: CH_2Cl_2-CH_3OH 9:1 v/v, $R_f = 0.47$

m. p. = 128 - 130 ° C

Yield: 0.6 g (40 %), tan crystals, recystallised with methanol

^{1}H NMR (DMSO-d6):

δ : 7.94 (d, J = 8.3 Hz, 2H, Ar), 7.74 (d, J = 8.3 Hz, 2H, Ar), 7.66 (d, J = 7.4 Hz, 2H, Ar), 7.48 (d, J = 8.4 Hz, 2H, Ar), 7.42 (m, 5H, Ar), 7.32 (dd, J = 2.6, 7.3 Hz, 2H, Ar), 5.82 (dd, J = 3.0, 10.0 Hz, 1H, CH), 4,48 (dd, J = 10, 14.9 Hz, 1H, CH_2), 3.85 (dd, J = 7.4, 15.0 Hz,1H, CH_2).

4.6.4.13 *(E)*-2-(4-styrylphenyl)-5-(4-(trifluoromethyl)phenyl)-4,5-dihydrooxazole (36b)
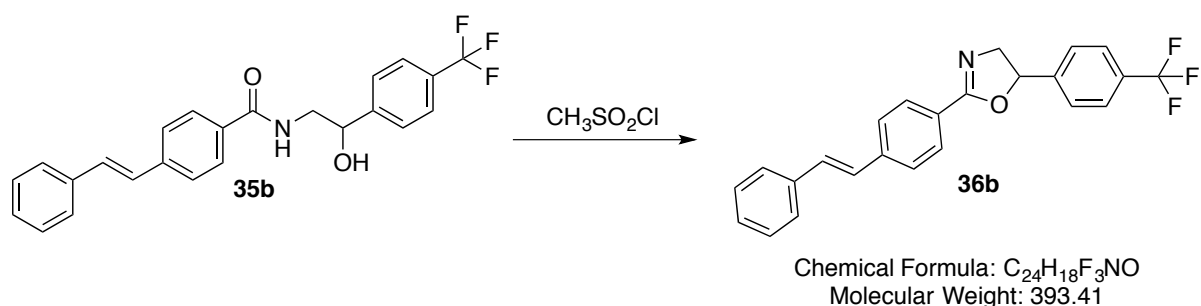
Chemical Formula: $C_{24}H_{18}F_3NO$
Molecular Weight: 393.41

Method: See 4.6.4.12

Reagent: (*E*)-*N*-(2-hydroxy-2-(4-(trifluoromethyl)phenyl)ethyl)-4-styrylbenzamide (0.30 g, 0.73 mmol) **35b**

TLC: petroleum ether-EtOAc 1:1 v/v, $R_f = 0.70$

Yield: 0.29 g (90 %), yellow solid

^{1}H NMR indicated a mixture of oxazole product and an apparent amide in approximately 2: 1 ratio. The oxazole signals are as described below:

^{1}H NMR (DMSO-d$_6$):

δ : 7.97 (d, J = 8.3 Hz, 2H, Ar), 7.80 (m, 4H, Ar), 7.65 (d, J = 7.4 Hz, 4H, Ar), 7.61 (d, J = 8.3 Hz, 2H, Ar), 7.34 (m, 3H, Ar), 5.93 (dd, J = 7.4, 10 Hz, 1H, CH), 4,53 (dd, J = 10, 15 Hz, 1H, CH$_2$), 3.87 (dd, J = 7.2, 10 Hz, 1H, CH$_2$).

4.6.4.14 (*E*)-2-(4-styrylphenyl)-5-(2-(trifluoromethyl)phenyl)-4,5-dihydrooxazole (36c)

Chemical Formula: C$_{24}$H$_{18}$F$_3$NO
Molecular Weight: 393.41
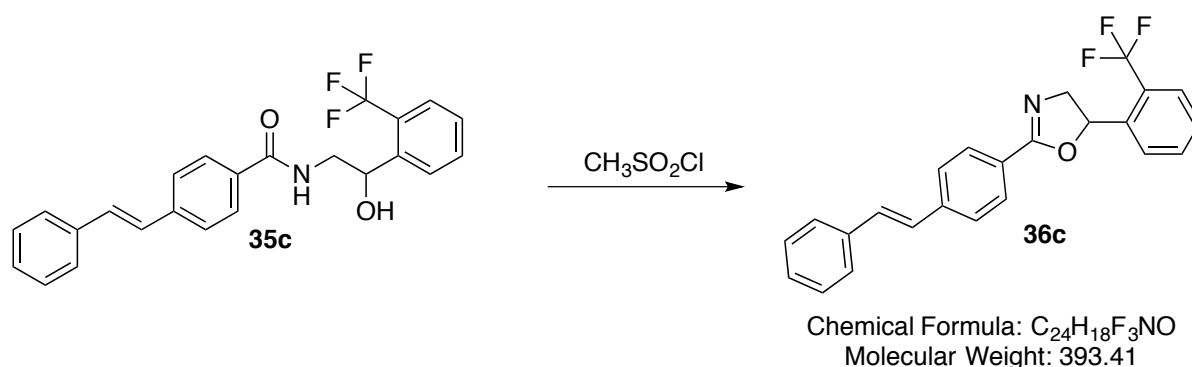
Method: See 4.6.4.12

Reagent: (*E*)-*N*-(2-hydroxy-2-(2-(trifluoromethyl)phenyl)ethyl)-4-styrylbenzamide (0.6 g, 1.5 mmol) **35c**

TLC: petroleum ether-EtOAc 1:1 v/v, $R_f = 0.65$

m. p. = 112 - 118 ° C

Yield: 0.4 g (70 %), yellow solid

^{1}H NMR (DMSO-d$_6$):

δ : 8.1 (m, 4H, Ar), 7.89(m, 3H, Ar), 7.85 (m, 4H, Ar), 7.82 (d, J = 16.2 Hz, H, alkene), 7.59 (m, 3H, Ar), 5.71 (dd, J = 8.0, 10.1 Hz, 1H, CH), 4.51 (dd, J = 10.3, 15.0 Hz, 1H, CH$_2$), 4.01 (dd, J = 8.0, 15.0 Hz, 1H, CH$_2$).

4.6.4.15 (*E*)-5-(3,4-dimethylphenyl)-2-(4-styrylphenyl)-4,5-dihydrooxazole (36d)

Chemical Formula: $C_{25}H_{23}NO$
Molecular Weight: 353.47
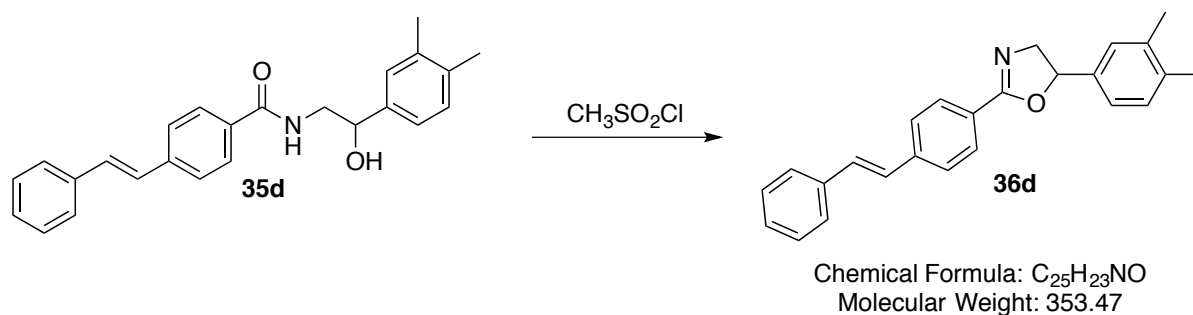
Method: See 4.6.4.12

Reagent: (*E*)-*N*-(2-(3,4-dimethylphenyl)-2-hydroxyethyl)-4-styrylbenzamide (0.70 g, 2.1 mmol) **35d**

TLC: petroleum ether-EtOAc 1:1 v/v, $R_f = 0.40$

Yield: 0.5 g (75 % crude yield), tan solid.

^{1}H NMR indicated a mixture of oxazole product and an apparent amide in approximately 2:1 ratio. The oxazole signals are as described below:

^{1}H NMR (DMSO-d$_6$):

δ : 7.97 (d, J = 8.3 Hz, 2H, Ar), 7.76 (d, J = 8.3 Hz, 2H, Ar), 7.66 (d, J = 7.4 Hz, 2H, Ar), 7.42 (t, J = 7.4 Hz, 3H, Ar), 7.36 (s, 1H, Ar), 7.33 (t, J = 7.4 Hz, 2H, Ar), 7.13 (d, J = 7.4 Hz, 2H, Ar), 5.92 (dd, J = 8.2, 10.1 Hz, 1H, CH), 4.52 (dd, J = 10.3, 14.9 Hz, 1H, CH$_2$), 3.73 (dd, J = 8.0, 14.9 Hz, 1H, CH$_2$), 2.26 (s, 1H, CH$_3$), 2.24 (s, 1H, CH$_3$).

4.6.4.16 (*E*)-5-(4-methoxyphenyl)-2-(4-styrylphenyl)-4,5-dihydrooxazole (36e)

Chemical Formula: $C_{24}H_{21}NO_2$
Molecular Weight: 355.44
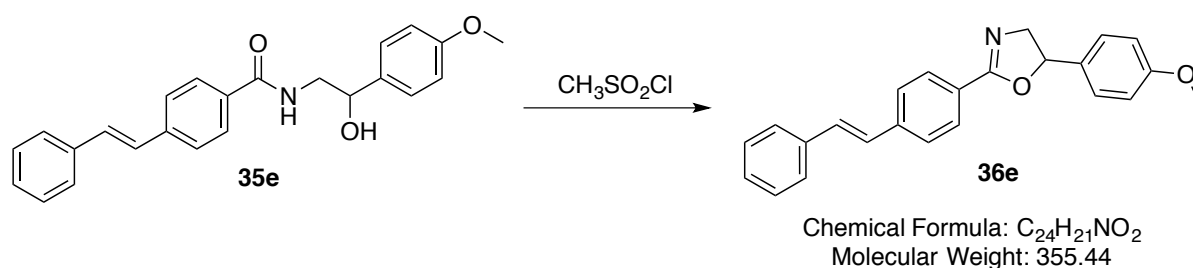
Method: See 4.6.4.12

Reagent: (*E*)-*N*-(2-hydroxy-2-(4-methoxyphenyl)ethyl)-4-styrylbenzamide (0.3 g, 0.8 mmol) **35e**

TLC: petroleum ether-EtOAc 1:1 v/v, $R_f = 0.55$

m. p. = 144 - 146 ° C

Yield: 0.27 g (90 %), tan solid

^{1}H NMR indicated a mixture of oxazole product and an apparent amide in approximately 2:1 ratio. The oxazole signals are as described below:

^{1}H NMR (DMSO-d$_6$):

δ : 7.92 (d, J = 8.3 Hz, 2H, Ar), 7.73 (d, J = 8.3 Hz, 2H, Ar), 7.65 (d, J = 7.5 Hz, 2H, Ar), 7.42 (m, 2H, Ar), 7.34 (m, 5H, Ar), 6.98 (d, J = 8.3 Hz, 2H, Ar), 5.74 (Φ t, J = 7.8, 9.8 Hz, 1H, CH), 4.26 (m, 1H, CH$_2$), 4.03 (m, 1H, CH$_2$), 3.76 (s, 3H, OCH$_3$).

4.6.4.17 (*E*)-5-(3-chlorophenyl)-2-(3-(3,4-dimethoxystyryl)phenyl)-4,5-dihydrooxazole (36f)
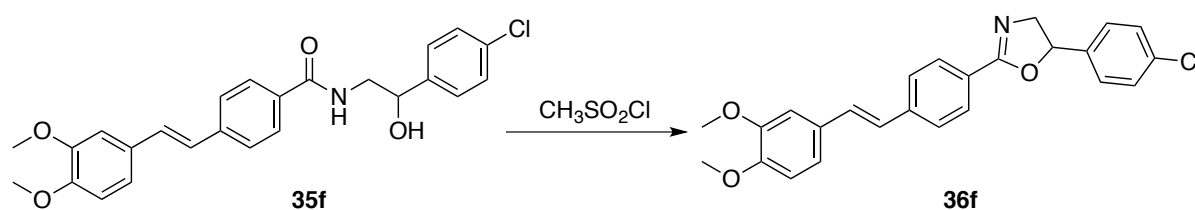
Chemical Formula: C$_{25}$H$_{22}$ClNO$_3$
Molecular Weight: 419.91

Method: See 4.6.4.12

Reagent: (*E*)-*N*-(2-(4-chlorophenyl)-2-hydroxyethyl)-4-(3,4-dimethoxystyryl)benzamide
(1g, 2.5 mmol) **35f**

TLC: petroleum ether-EtOAc 1:1 v/v, R$_f$ = 0.71

Yield: 0.6 g (63 %), tan solid

^{1}H NMR indicated a mixture of oxazole product and an apparent amide in approximately 2:1 ratio. The oxazole signals are as described below:

^{1}H NMR (DMSO-d$_6$):

δ : 7.59 (d, J = 8.4 Hz, 3H, Ar), 7.43 (d, J = 7.5 Hz, 2H, Ar), 7.17 (m, 2H, Ar), 7.15 (m, 3H, Ar), 6.73 (m, 3H, Ar), 5.68 (m, 1H, CH), 4.52 (m, 1H, CH$_2$), 4.1 (m, 1H, CH$_2$), 3.86 (s, 3H, OCH$_3$), 3.72 (s, 3H, OCH$_3$).

4.6.4.18 (*E*)-*N*-(2-(4-chlorophenyl)-2-(1*H*-imidazol-1-yl)ethyl)-4-styrylbenzamide (37a)
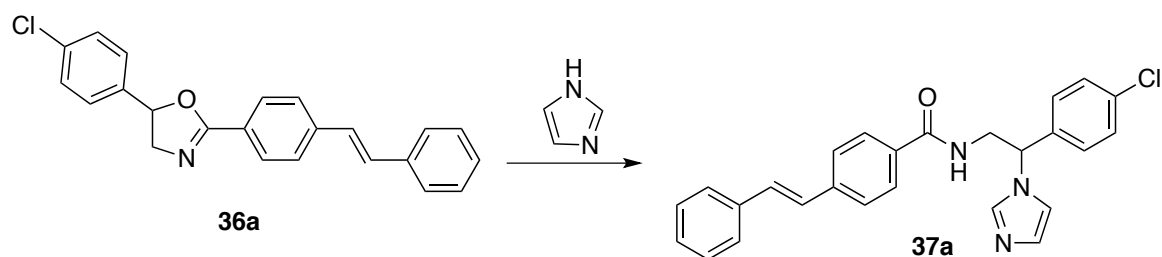
Chemical Formula: $C_{26}H_{22}ClN_3O$
Molecular Weight: 427.93

Method:

A mixture of *(E)*-5-(4-chlorophenyl)-2-(4-styrylphenyl)-4,5-dihydrooxazole (**36a**) (1.2 g, 2.7 mmol) and imidazole (7.3 g, 108 mmol) was refluxed at 125 ° C for 48 h. On completion, the mixture was extracted between EtOAc (100 mL) and brine (2 × 100 mL). The organic layer was dried (MgSO$_4$) and concentrated under vaccum[319].

TLC: CH_2Cl_2-CH_3OH 9:1 v/v, R$_f$ = 0.85

m. p. = 238 - 240° C

Yield: 0.15 g (12 %), white solid, recrystallised with EtOAc

^{1}H NMR (DMSO-d$_6$):

δ : 8.73 (t, J = 5.2 Hz, 1H, NH), 7.86 (s, 1H, imid), 7.77 (d, J = 8.2 Hz, 4H, Ar), 7.68 (d, J = 8.2 Hz, 3H, Ar), 7.64 (d, J = 7.5 Hz, 1H, imid), 7.46 (m, 8H, Ar), 6.92 (s, 1H, imid), 5.70 (dd, J = 6.5, 8.2 Hz, 1H, CH), 4.06 (m,1H, CH$_2$), 3.44 (m, 1H, CH).

^{13}C NMR (DMSO-d$_6$):

δ : 166.8 (CO), 140.5, 138.7,133.2, 133.1 (5 × C), 137.2, 130.7, 129.3, 129.2, 129.1, 128.5, 127.9,127.1, 126.7, 118.7 (18 × CH, Ar), 59.1 (CH), 43.7 (CH$_2$).

LRMS (ES-TOF)

m/z: 430 [M^{37Cl}+ H]$^+$, 428 [M^{35Cl} + H]$^+$, 362 [M - imid]$^+$

HRMS (ES-TOF)

Calculated mass: 428.1523 [M + H]$^+$, measured mass: 428.1524 [M + H]$^+$

4.6.4.19 (*E*)-*N*-(2-(1*H*-imidazol-1-yl)-2-(4-(trifluoromethyl)phenyl)ethyl)-4-

styrylbenzamide (37b)
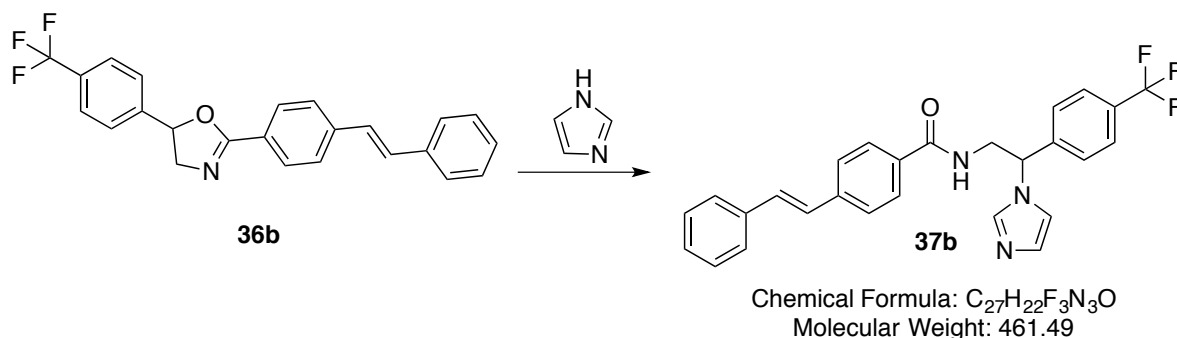
Chemical Formula: $C_{27}H_{22}F_3N_3O$
Molecular Weight: 461.49

Method: See 4.6.4.18

Reagent: (*E*)-2-(4-styrylphenyl)-5-(4-(trifluoromethyl)phenyl)-4,5-dihydrooxazole (1.6 g, 4.1 mmol) **37b**

TLC: CH_2Cl_2-CH_3OH 9:1 v/v, $R_f = 0.32$

m. p. = 208 - 210 ° C

Yield: 0.6 g (33 %), creamy solid, recrystallised with EtOAc

^{1}H NMR (DMSO-d$_6$):

δ : 8.80 (t, J = 5.0 Hz, 1H, NH), 7.91 (s, 1H, imid), 7.78 (dd, J = 3.0, 8.5 Hz, 4H, Ar), 7.69 (d, J = 8.5 Hz, 2H, Ar), 7.64 (d, J = 7.5 Hz, 2H, Ar), 7.60 (s, 1H, imid), 7.42 (m, 4H, Ar), 7.32 (m, 3H, Ar), 6.95 (s, 1H, imid), 5.83 (t, J = 7.5 Hz, 1H, CH), 4.13 (m, 12 Hz, 2H, CH$_2$).

^{13}C NMR (DMSO-d$_6$):

δ : 166.8 (CO), 144.4, 140.5,137.4, 137.1, 135.4, 133.1 (6 × C), 130.8, 129.2, 128.5, 128.2, 128.1, 127.9, 127.1,126.7, 126.1, 118.9 (18 × CH, Ar), 59.3 (CH), 43.7 (CH$_2$).

Microanalysis

Anal. Calcd for $C_{27}H_{22}F_3N_3O \cdot 0.15H_2O$ (463.87): C 69.86 %, H 4.84 %, N 9.05 %. Found C 69.56 %, H 4.79 %, N 8.98 %

4.6.4.20 (*E*)-*N*-(2-(1H-imidazol-1-yl)-2-(2-(trifluoromethyl)phenyl)ethyl)-4

styrylbenzamide (37c)
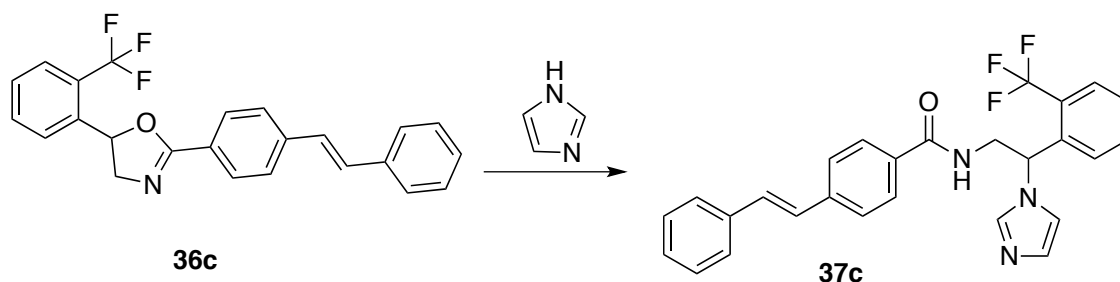
Chemical Formula: $C_{27}H_{22}F_3N_3O$
Molecular Weight: 461.49

Method: See 4.6.4.18

Reagent:(*E*)-2-(4-styrylphenyl)-5-(2-(trifluoromethyl)phenyl)-4,5-dihydrooxazole (1.5 g, 3.8 mmol) **37c**

TLC: CH_2Cl_2-CH_3OH 9:1 v/v, $R_f = 0.21$

m. p. = 174 -178 ° C

Yield: 0.64 g (35 %), creamy solid, recrystallised with EtOAc

^{1}H NMR (DMSO-d$_6$):

δ 8.79 (t, J = 5.0 Hz, 1H, NH), 7.5 (d, J = 8.0 Hz, 1H, imid), 7.80 (m, 5H, Ar), 7.68 (d, J = 8.5 Hz, 2H, Ar), 7.64 (d, J = 7.5 Hz, 2H, Ar), 7.61 (t, J = 7.5 Hz, 1H, imid), 7.41 (m, 3H, Ar), 7.32 (m, 3H, Ar), 6.90 (t, J = 1.0 Hz, 1H, imid), 6.01 (dd, J = 6.0, 9.0 Hz, 1H, CH), 4.33 (m, 2H, CH_2)

^{13}C NMR (DMSO-d$_6$):

δ : 166.8 (CO), 140.5, 137.2, 136.8 (3 × C), 133.1, 131.9 (2 × CH, Ar), 135.2, 134.7 (2 × C), 129.7, 129.5, 129.3, 128.9, 128.8, 128.5, 127.9, 127.7,126.4, 126.7, 125.7, 118.9 (16 × CH, Ar), 59.9 (CH), 44.1 (CH_2).

Microanalysis

Anal. Calcd for $C_{27}H_{22}F_3N_3O \cdot 0.1H_2O$ (463.29): C 70.00 %, H 4.83 %, N 9.07 %. Found C 69.64 %, H 4.84 %, N 9.07 %.

4.6.4.21 (*E*)-*N*-(2-(3,4-dimethylphenyl)-2-(1*H*-imidazol-1-yl)ethyl)-4-styrylbenzamide (37d)
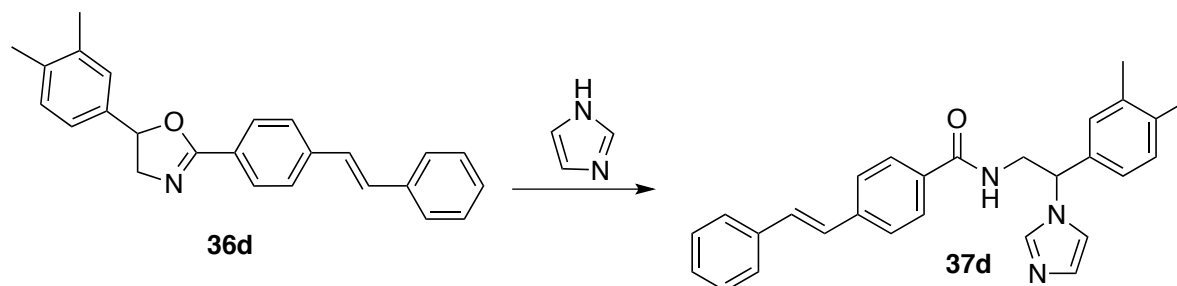
Chemical Formula: $C_{28}H_{27}N_3O$
Molecular Weight: 421.54

Method: See 4.6.4.18

Reagent: (*E*)-5-(3,4-dimethylphenyl)-2-(4-styrylphenyl)-4,5-dihydrooxazole (1.1 g, 3.1 mmol) **37d**

TLC: CH_2Cl_2-CH_3OH 9:1 v/v, $R_f = 0.65$

m. p. = 134 -136 ° C

Yield: 0.35 g (27 %), yellow solid, recrystallised with EtOAc

^{1}H NMR (DMSO-d_6):

δ : 8.73 (t, J = 5.5 Hz, 1H, NH), 7.82 (s, 1H, imid), 7.78 (d, J = 8.5 Hz, 2H, Ar), 7.69 (m, 2H, Ar), 7.41 (m, 2H, Ar), 7.33 (m, 5H, Ar), 7.18 (s,1H, imid), 7.14 (m, 2H, Ar), 7.02 (s, 1H, imid), 6.89 (s, 1H, Ar), 5.59 (dd, J = 5.5, 9.0 Hz, 1H, CH), 4.09 (m,1H, CH_2), 3.94 (m, 1H, CH_2), 2.18 (s, 6H, $2CH_3$).

^{13}C NMR (DMSO-d_6):

δ : 167.8 (CO), 157.5, 140.9, 138.7, 137.5, 136.7, 133.4 (6 × C), 133.2, 130.7, 129.3, 129.2, 129.1, 128.5, 127.9, 127.1, 126.7, 118.7 (17 × CH, Ar), 59.9 (CH), 43.7 (CH_2), 25.7 (2 × CH_3).

LRMS (ES-TOF)

m/z: 422 $[M + H]^+$, 214 $[M - C_6H_5CH=CH-C_6H_5C=O]^+$

HRMS(ES-TOF)

Calculated mass: 422.2251 $[M + H]^+$, measured mass: 422.2232 $[M + H]^+$

4.6.4.22 (*E*)-*N*-(2-(1*H*-imidazol-1-yl)-2-(4-methoxyphenyl)ethyl)-4-styrylbenzamide (37g)

Chemical Formula: $C_{27}H_{25}N_3O_2$
Molecular Weight: 423.52
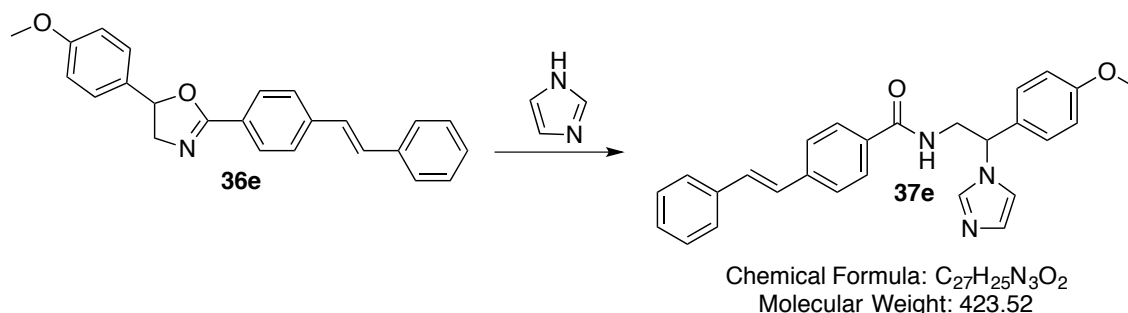
Method: See 4.6.4.18

Reagent: (*E*)-5-(4-methoxyphenyl)-2-(4-styrylphenyl)-4,5-dihydrooxazole (0.27 g, 0.8 mmol) **36g**

TLC: CH_2Cl_2-CH_3OH 9:1 v/v, $R_f = 0.41$

m. p. = 218 - 222° C

Yield: 0.3 g (32 %), white solid, recrystallised with EtOAc

^{1}H NMR (CDCl$_3$):

δ : 8.06 (s, 1H, imid), 7.78 (d, J = 7.7 Hz, 2H, Ar), 7.52 (d, J = 7.5 Hz, 2H, Ar), 7.36 (t, J = 7.0 Hz, 2H, Ar), 7.31 (m, 5H, Ar), 7.24 (d, J = 8 Hz, 2H, Ar), 717 (m, 2H, Ar), 6.94 (d, J = 8.0 Hz, 2H, Ar), 5.70 (dd, J = 4.0, 9.5 Hz, 1H, CH), 4.34 (m, 1H, CH$_2$), 4.04 (m, 1H, CH), 3.81 (s, 3H, OCH$_3$).

^{13}C NMR (DMSO-d$_6$):

δ : 167.8 (CO), 157.5, 140.9, 138.7, 137.5, 136.7, 133.4 (6 × C), 133.2, 130.7, 129.3, 129.2, 129.1, 128.5, 127.9, 127.1, 126.7, 118.7 (18 × CH, Ar), 59.9 (CH), 55.1 (s, 3H, OCH$_3$), 43.7 (CH$_2$).

LRMS (ES-TOF)

m/z: 424 [M + H]$^+$, 356 [M - imid]$^+$

HRMS (ES-TOF)

Calculated mass: 424.2020 [M + H]$^+$, measured mass: 424.2016 [M + H]$^+$

4.6.4.23 (*E*)-*N*-(2-(4-chlorophenyl)-2-(1*H*-imidazol-1-yl)ethyl)-4-(3,4-dimethoxystyryl) benzamide (37f)
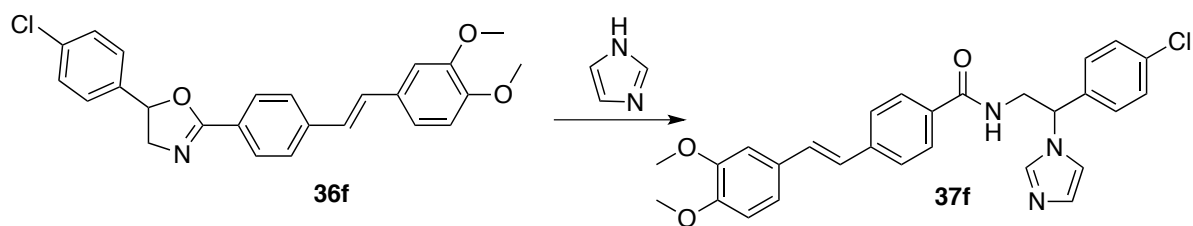
Chemical Formula: $C_{28}H_{26}ClN_3O_3$
Molecular Weight: 487.98

Method: See 4.6.4.18

Reagent: (*E*)-5-(4-chlorophenyl)-2-(4-(3,4-dimethoxystyryl)phenyl)-4,5-dihydrooxazole (1.4 g, 3.6 mmol) **36e**

TLC: CH_2Cl_2-CH_3OH 9:1 v/v, R_f = 0.66

m. p. = 204 - 208° C

Yield: 0.6 g (35 %), white crystals, recrystallised with acetonitrile

¹H NMR (DMSO-d₆):

δ : 8.74 (t, J = 5.4 Hz, 1H, NH), 7.86 (s, 1H, imid), 7.75 (d, J = 8.4 Hz, 2H, Ar), 7.64 (d, J = 8.4 Hz, 2H, Ar), 7.46 (m, 2H, Ar), 7.37 (s, 1H, imid), 7.32 (s, 2H, Ar), 7.29 (d, J = 5.1 Hz, 2H, Ar), 7.17 (s, 1H, imid), 7.14 (dd, J = 1.8, 8.4 Hz, 1H, Ar), 6.98 (d, J = 8.4 Hz, 2H, Ar), 6.92 (s, 1H, Ar), 5.71 (dd, J = 6.3, 8.7 Hz, 1H, CH), 4.08 (m, 2H, CH₂), 3.83 (s, 3H, OCH₃), 3.78 (s, 3H, OCH₃).

¹³C NMR (DMSO-d₆)

δ : 166.8 (CO), 149.5, 149.4, 140.9, 138.8 (4 × C), 137.3 (CH, Ar), 133.2, 132.6 (2×C), 130.8 (CH, Ar), 130.1 (C), 129.3, 129.2, 129.1, 128.1, 126.3, 120.8, 118.7, 112.1, 109.6 (14 × CH, Ar), 59.2 (CH), 55.8 (2 × OCH₃), 43.7 (CH₂).

LRMS (ES-TOF)

m/z: 490 [M^{37Cl} + H]⁺, 488 [M^{35Cl} + H]⁺

HRMS (ES-TOF)

Calculated mass 488.1743 [M + H]⁺, measured mass: 488.1741[M + H]⁺

4.6.4.24 1-(Trifluoromethyl)-2-vinylbenzene (32c)

Chemical Formula: $C_9H_7F_3$
Molecular Weight: 172.15
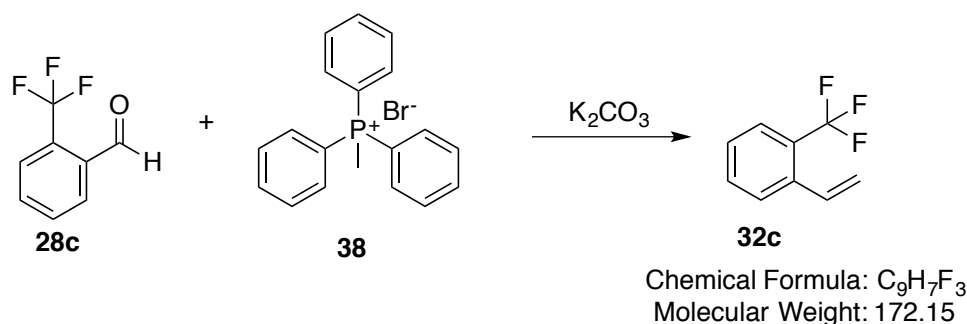
method:

2-(Trifluoromethyl)benzaldehyde **28c** (3g, 17.2 mmol) was added to a solution of methyltriphenylphosphonium bromide **38** (7.4 g, 20.6 mmol) and K_2CO_3 (4g, 29 mmol) in dry THF (30 mL). The mixture was refluxed at 75 ° C for 10 h. THF was removed and the residue diluted, filtered through celite and concentrated under vaccum. The crude product was purified using gradient flash column chromatography, the product was eluted with petroleum ether-EtOAc 3:1 v/v[322].

TLC: petroleum ether-EtOAc 3:1 v/v, R_f= 0.81

Yield = 2 g (67 %), colourless liquid.

^{1}H NMR (DMSO-d$_6$):

δ : 7.94 (d, J = 7.8 Hz, 1H, Ar), 7.69 (m, 2H, Ar), 7.50 (t, J = 7.7 Hz, 1H, Ar), 7.00 (m, 1H, CH), 5.92 (d, J = 17.3 Hz, 1H, CH_2), 5.50 (dd, J = 0.95, 11.05 Hz, 1H, CH_2).

4.6.4.25 (*E*)-3-styrylbenzoic acid (40a)

Chemical Formula: $C_{15}H_{12}O_2$
Molecular Weight: 224.26
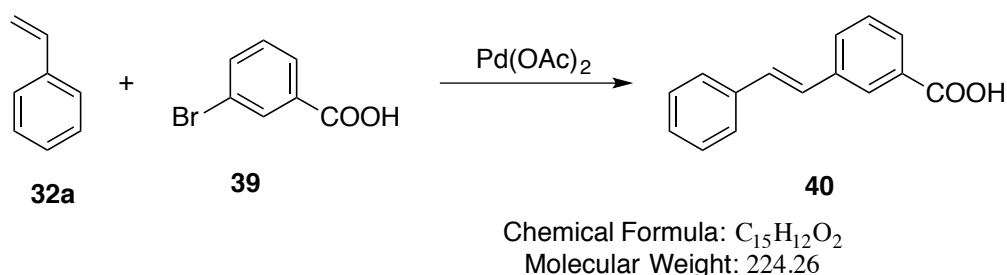
Method: See 4.6.4.4

Reagent: styrene (2.5 g, 24.0 mmol) **32a**

TLC: petroleum ether-EtOAc 1:1 v/v, R_f= 0.7

m. p. = 188 -192 ° C (Lit. 197 - 198 ° C[323])

Yield = 4.0 g (73 %), brown crystals, recrystallised with acetonitrile

^{1}H NMR (DMSO-d$_6$):

δ : 13.11 (s, 1H, COOH), 8.17 (s, 1H, Ar), 7.88 (dd, J = 7.5, 12.0 Hz, 2H, Ar), 7.66 (d, J = 7.5 Hz, 2H, Ar), 7.52 (t, J = 8.0 Hz, 1H, Ar), 7.41 (m, 4H, Ar), 7.31 (t, J = 7.5 Hz, 1H, Ar).

4.6.4.26 (*E*)-3-(2-(trifluoromethyl)styryl)benzoic acid (40b)

Chemical Formula: $C_{16}H_{11}F_3O_2$
Molecular Weight: 292.26
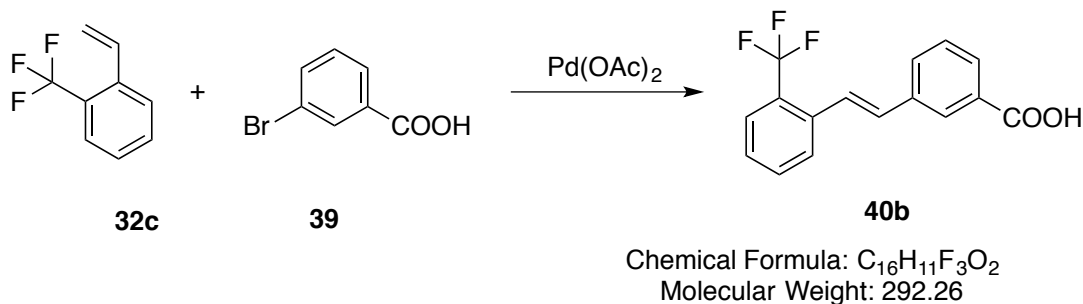
Method: See 4.6.4.4

Reagent: 1-(trifluoromethyl)-2-vinylbenzene (1 g, 6 mmol) **32c**

TLC: petroleum ether-EtOAc 1:1 v/v, R$_f$= 0.74

m. p. = 162 -164 ° C

Yield = 0.9 g (82 %), creamy crystals, recrystallised with acetonitrile

^{1}H NMR (CDCl$_3$):

δ : 8.27 (s, 1H, Ar), 8.09 (d, J = 7.7 Hz, 1H, Ar), 7.84 (t, J = 7.3 Hz, 2H, Ar), 7.72 (d, J = 7.8 Hz, 3H, Ar), 7.61 (m, 1H, Ar),7.43 (t, J = 7.6 Hz, 2H, Ar).

^{13}C NMR (DMSO-d$_6$):

δ :167.6 (CO), 137.2, 135.7 (2 × C), 133.3, 132.8 (2 × CH, Ar), 132.2 (C), 131.5, 131.2, 124.0, 12.6 (8 × CH, Ar).

Microanalysis

Anal. Calcd for $C_{16}H_{11}F_3O_2$ (292.26): C 65.76%, H 3.79 %, N 0.00 %. Found C 65.63 %, H 3.81 %, N <0.10 %.

4.6.4.27 (*E*)-*N*-(2-hydroxy-2-phenylethyl)-3-styrylbenzamide (41a)

Chemical Formula: $C_{23}H_{21}NO_2$
Molecular Weight: 343.43
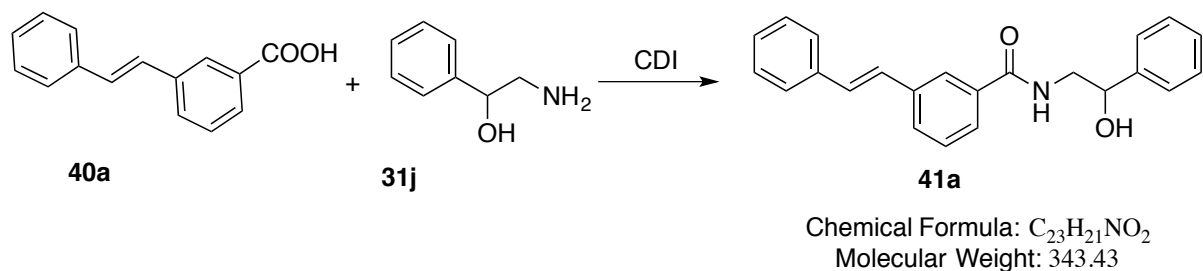
Method: See 4.6.4.6

Reagent: (*E*)-3-styrylbenzoic acid (1 g, 4.5mmol) **40a**

TLC: CH$_2$Cl$_2$-CH$_3$OH 9:1 v/v, R$_f$ = 0.68

m. p. = 128 - 132 ° C

Yield = 0.9 g (60 %), white sold, recrystallised with methanol

^{1}H NMR (DMSO-d$_6$):

δ : 8.64 (t, J = 6.0 Hz, 1H, NH), 8.11 (s, 1H, Ar), 7.73 (d, J = 8.0 Hz, 2H, Ar), 7.65 (d, J = 7.5 Hz, 3H, Ar), 7.49 (t, J = 8.0 Hz, 3H, Ar) 7.42 (t, J = 7.5 Hz, 3H, Ar), 7.37 (m, 4H, Ar), 5.64 (s, 1H, OH), 4.80 (m, 1H, CHOH), 3.49 (m, 1H, CH$_2$), 3.40 (m, 1H, CH$_2$).

^{13}C NMR (DMSO‑d$_6$):

δ : 166.8 (CO), 144.3, 137.5, 137.3, 135.5 (4 × C), 129.8, 129.7, 129.3, 129.1, 127.9, 128.5, 128.4, 128.3, 127.5, 127.0, 126.9, 126.5, (16 × CH, Ar), 71.6 (CH), 48.2 (CH$_2$).

Microanalysis

Anal. Calcd for C$_{23}$H$_{21}$NO$_2$ · 0.4 H$_2$O (350.36): C 78.79 %, H 6.27 %, N 3.99 %. Found C 78.35 %, H 6.56 %, N 3.83 %.

4.6.4.28 (*E*)-*N*-(2-(4-chlorophenyl)-2-hydroxyethyl)-3-styrylbenzamide (41b)
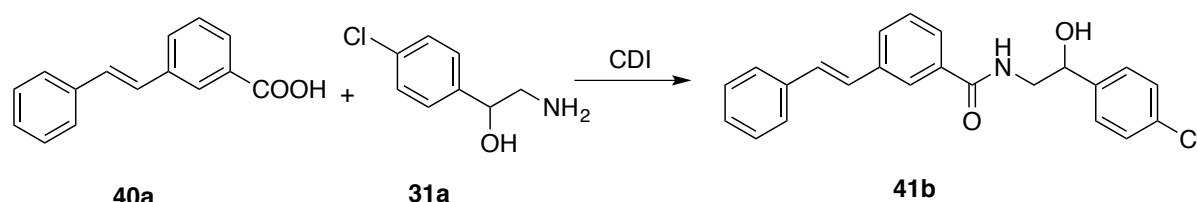
Chemical Formula: C$_{23}$H$_{20}$ClNO$_2$
Molecular Weight: 377.87

Method: See 4.6.4.6

Reagent: (*E*)-3-styrylbenzoic acid (0.6 g, 2.7 mmol) **40a**

TLC: petroleum ether-EtOAc 2:1 v/v, R$_f$ = 0.44

m. p. = 138 - 142 ° C

Yield = 0.6 g (50 %), creamy solid, recrystallised with methanol.

^{1}H NMR (DMSO-d$_6$):

δ : 8.63 (t, J = 5.0 Hz, 1H, NH), 8.09 (s, 1H, Ar), 7.63 (d, J = 7.5 Hz, 4H, Ar), 7.48 (t, J = 8.0 Hz, 4H, Ar), 7.42 (t, J = 7.5 Hz, 3H, Ar) 7.36 (m, 3H, Ar), 5.69 (d, J = 4.0 Hz, 1H, OH), 4.83 (m, 1H, CHOH), 3.51 (m, 1H, CH$_2$), 3.39 (m, 1H, CH$_2$).

^{13}C NMR (DMSO-d$_6$):

δ : 166.9 (CO), 138.6 137.5, 135.8, 134.2, 133.2 (5 × C), 131.9, 128.7,128.6, 127.9, 127.3, 127.4,127.1, 126.9, 126.7,123.4 (15 × CH, Ar), 72.2 (CH), 48.9 (CH$_2$)

Microanalysis

Anal. Calcd for C$_{24}$H$_{20}$ClNO$_2$· 0.2 H$_2$O (381.47): C 72.42 %, H 5.39 %, N 3.67 %. Found C 72.11 %, H 5.36 %, N 3.77 %.

4.6.4.29 (*E*)-*N*-(2-hydroxy-2-(4-(trifluoromethyl)phenyl)ethyl)-3-styrylbenzamide (41c)
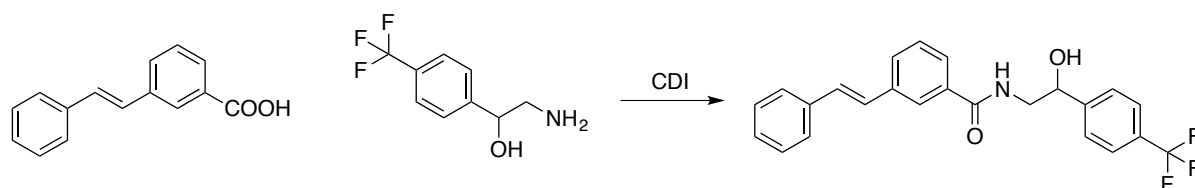
Method: see 4.6.4.6

Reagent: (*E*)-3-styrylbenzoic acid (0.8 g, 3.6 mmol) **40a**

TLC: petroleum ether-EtOAc 2:1 v/v, R$_f$= 0.52

m. p. = 184 - 186 ° C

Yield = 0.46 g (31 %), white crystals, recrystallised with acetonitrile.

^{1}H NMR (DMSO-d$_6$):

δ : 8.66 (t, J = 5.6 Hz, 1H, NH), 8.08 (s, 1H, Ar), 7.74 (φ t, J = 6.6, 7.7 Hz, 4H, Ar), 7.64 (φ t, J = 8.3, 10.0 Hz, 4H, Ar), 7.49 (t, J = 7.7 Hz, 1H, Ar), 7.42 (t, J = 7.6 Hz, 2H, Ar) 7.33 (m, 3H, Ar), 5.80 (d, J = 4.5 Hz, 1H, OH), 4.93 (dd, J = 5.1, 11.9 Hz, 1H, C<u>H</u>OH), 3.54 (m,1H, CH$_2$), 3.44 (m, 1H, CH$_2$).

^{13}C NMR (DMSO-d$_6$):

δ : 166.9 (CO), 149.0, 137.5, 137.2, 135.4 (4 × C), 129.8, 129.7, 129,2, 129.1 (4 × CH, Ar), 128.3, 128.0 (2 × C), 127.7, 127.3, 127.2,127.1, 126.8, 125.9 (11 × CH, Ar), 71.2 (CH), 47.9 (CH$_2$).

Microanalysis

Anal. Calcd for C$_{24}$H$_{20}$F$_3$NO$_2$ · 0.1H$_2$O (413.23): C 69.76 %, H 4.93 %, N 3.39 %. Found C 69.51%, H 4.94 %, N 3.42 %.

4.6.4.30 (*E*)-*N*-(2-hydroxy-2-phenylethyl)-3-(2-(trifluoromethyl)styryl)benzamide (41d)
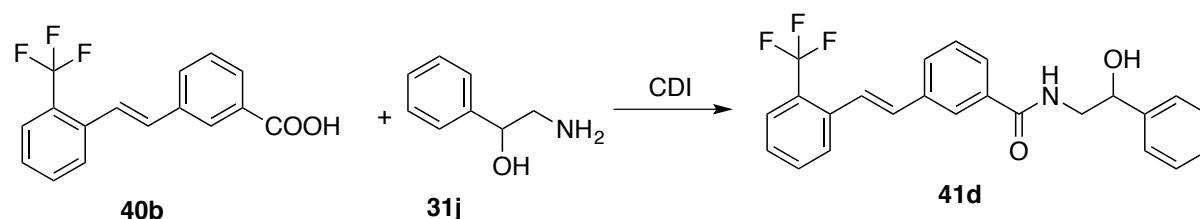
Chemical Formula: $C_{24}H_{20}F_3NO_2$
Molecular Weight: 411.42

Method: See 4.6.4.6

Reagent: (*E*)-3-(2-(trifluoromethyl)styryl)benzoic acid (1 g, 3.4mmol) **40b**

TLC: petroleum ether-EtOAc 1:1 v/v, $R_f = 0.7$

m. p. = 88 - 90 ° C

Yield = 1.2 g (75 %), white solid, purified by gradient flash column chromatography, product was eluted with petroleum ether-EtOAc 1:1 v/v.

^{1}H NMR (CDCl$_3$):

δ : 7.89 (s, 1H, Ar), 7.75 (d, J = 7.7 Hz, 1H, Ar), 7.68 (m, 3H, Ar), 7.56 (t, J = 7.7 Hz, 2H, Ar), 7.50 (m, 5H, Ar), 7.41 (t, J = 8 Hz, 1H, Ar), 7.36 (t, J = 7.7 Hz, 1H, Ar) 7.29 (m, 1H, Ar), 4.97 (dd, J = 3.2, 8.1 Hz, 1H, C<u>H</u>OH), 3.93 (m, 1H, CH$_2$), 3.55 (m, 1H, CH$_2$).

^{13}C NMR (CDCl$_3$):

δ : 167.5 (CO), 141.5, 137.3, 136.3 (3 ×C), 133.6, 129.1, 128.7, 128.4, 127.9, 127.6, 125.7 (14 × CH, Ar), 122.6, 122.2 (2× C), 114.3 (CH, Ar), 71.2 (CH), 48.2 (CH$_2$).

Microanalysis

Anal. Calcd for $C_{24}H_{20}F_3NO_2$ (411.42): C 70.07%, H 4.90 %, N 3.40 %. Found C 69.99 %, H 5.05 %, N 3.53 %.

4.6.4.31 (*E*)-5-phenyl-2-(3-styrylphenyl)-4,5-dihydrooxazole (42a)
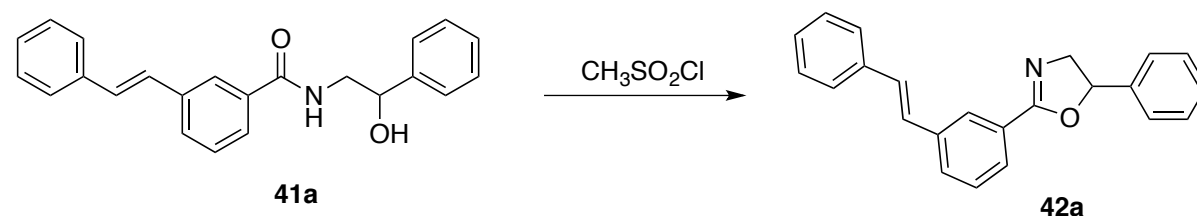
Chemical Formula: $C_{23}H_{19}NO$
Molecular Weight: 325.41

Method: See 4.6.4.12

Reagent: (*E*)-*N*-(2-hydroxy-2-phenylethyl)-3-styrylbenzamide (1.5 g, 4.4 mmol) **41a**

TLC: petroleum ether-EtOAc 3:1 v/v, $R_f = 0.55$

Yield: 1.2 g (85 %), creamy solid

^{1}H NMR indicated a mixture of oxazole product and an apparent amide in approximately 2:1 ratio. The oxazole signals are as described below:

^{1}H NMR (DMSO-d$_6$):

δ : 8.01 (d, J = 7.3 Hz, 2H, Ar), 7.87 (m, 5H, Ar), 7.52 (d, J = 7.3 Hz, 2H, Ar), 7.44 (m, 5H, Ar), 7.38 (d, 7.3 Hz, 2H, Ar), 5.66 (dd, J = 3.0, 9.7 Hz, 1H, CH), 4.56 (dd, J = 9.7, 15.0 Hz, 1H, CH$_2$), 4.51 (dd, J = 7.3, 15.0 Hz,1H, CH$_2$).

4.6.4.32 (*E*)-5-(4-chlorophenyl)-2-(3-styrylphenyl)-4,5-dihydrooxazole (42b)
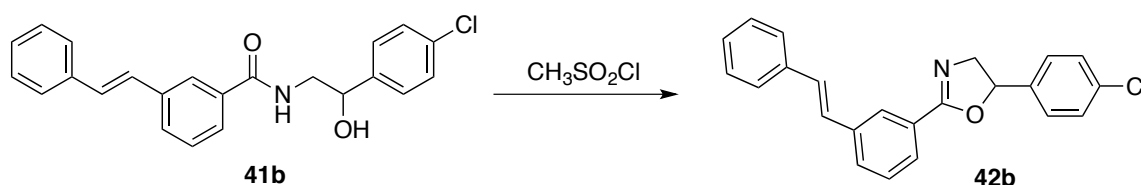
Chemical Formula: $C_{23}H_{18}ClNO$
Molecular Weight: 359.85

Method: see 4.6.4.12

Reagent: (*E*)-*N*-(2-(4-chlorophenyl)-2-hydroxyethyl)-3-styrylbenzamide (0.8 g, 2.1 mmol) **41b**

TLC: petroleum ether-EtOAc 1:1 v/v, $R_f = 0.40$

Yield: 0.6 g (80 %), creamy solid

^{1}H NMR indicated a mixture of oxazole product and an apparent amide in approximately 2:1 ratio. The oxazole signals are as described below:

^{1}H NMR (DMSO-d$_6$):

δ : 8.19 (d, J = 8.5 Hz, 2H, Ar), 7.99 (d, 8.5 Hz, 2H, Ar), 7.50 (m, 2H, Ar), 7.41 (m, 4H, Ar), 7.32 (m, 3H, Ar) 7.18 (m, 3H, Ar), 5.79 (dd, J = 8.2, 10.2 Hz, 1H, CH), 4.50 (dd, J = 10.2, 15.3 Hz, 1H, CH$_2$), 4.31 (dd, J = 8.2, 15.3 Hz,1H, CH$_2$).

4.6.4.33 (*E*)-2-(3-styrylphenyl)-5-(4-(trifluoromethyl)phenyl)-4,5-dihydrooxazole (42c)
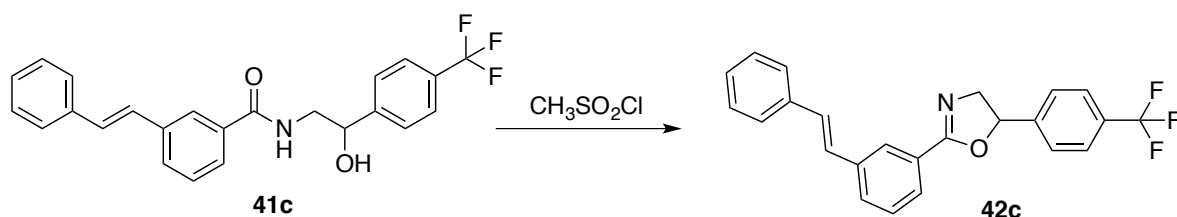
Chemical Formula: $C_{24}H_{18}F_3NO$
Molecular Weight: 393.41

Method: See 4.6.4.12

Reagent: (*E*)-*N*-(2-hydroxy-2-(4-(trifluoromethyl)phenyl)ethyl)-3-styrylbenzamide (0.4 g, 0.9 mmol) **41c**

TLC: petroleum ether-EtOAc 1:1 v/v, $R_f = 0.57$

Yield: 0.35 g (92 %), tan solid

^{1}H NMR indicated a mixture of oxazole product and an apparent amide in approximately 2:1 ratio. The oxazole signals are as described below:

^{1}H NMR (DMSO-d$_6$):

δ : 8.02 (d, J = 8.5 Hz, 2H, Ar), 7.56 (d, 8.5 Hz, 2H, Ar), 7.36 (m, 5H, Ar), 7.17 (m, 3H, Ar), 7.08 (m, 2H, Ar) 7.97 (m, 1H, Ar), 5.51 (dd, J = 10.1, 15.0 Hz, 1H, CH), 4.09 (dd, J = 8.5, 15.0 Hz, 1H, CH$_2$), 3.99 (dd, J = 8.2, 15.3 Hz,1H, CH$_2$).

4.6.4.34 (*E*)-5-phenyl-2-(3-(2-(trifluoromethyl)styryl)phenyl)-4,5-dihydrooxazole (42d)
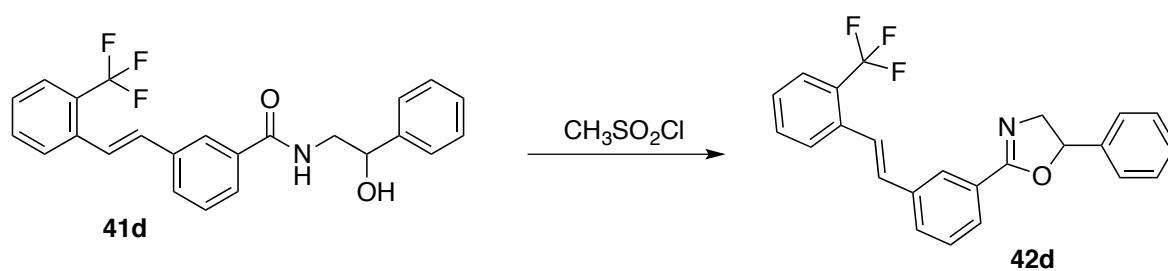
Chemical Formula: $C_{24}H_{18}F_3NO$
Molecular Weight: 393.41

Method: See 4.6.4.12

Reagent: ((*E*)-*N*-(2-hydroxy-2-phenylethyl)-3-(2-(trifluoromethyl)styryl)benzamide (1.3 g, 3.2 mmol) **41d**

TLC: petroleum ether-EtOAc 1:1 v/v, $R_f = 0.60$

Yield: 0.7 g (56 %), creamy solid

^{1}H NMR indicated a mixture of oxazole product and an apparent amide in approximately 2:1 ratio. The oxazole signals are as described below:

¹H NMR (DMSO-d₆):

δ : 7.95 (d, J = 8.3 Hz, 2H, Ar), 7.66 (d, J = 8.3 Hz, 2H, Ar), 7.58 (d, J = 8.3 Hz, 2H, Ar), 7.52 (d, J = 8.3 Hz, 2H, Ar), 7.32 (m, 7H, Ar), 5.80 (dd, J = 7.7, 10.1 Hz, 1H, CH), 4.45 (dd, J = 10.1, 14.9 Hz, 1H, CH₂), 3.89 (dd, J = 7.5, 14.9 Hz,1H, CH₂).

4.6.4.35 (*E*)-*N*-(2-(1*H*-imidazol-1-yl)-2-phenylethyl)-3-styrylbenzamide (43a)
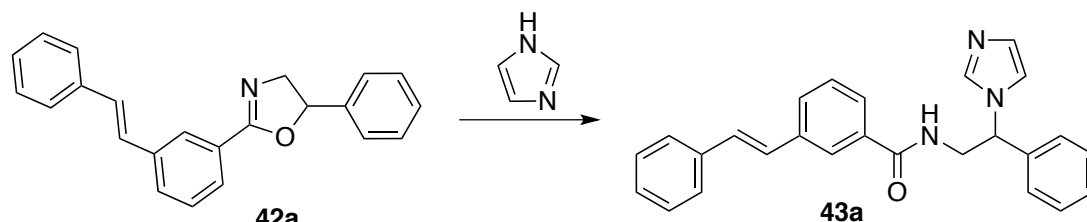
Chemical Formula: $C_{26}H_{23}N_3O$
Molecular Weight: 393.49

Method: See 4.6.4.18

Reagent: (*E*)-5-phenyl-2-(3-styrylphenyl)-4,5-dihydrooxazole (1.4 g, 4.2 mmol**) 42a**

TLC: CH_2Cl_2-CH_3OH 9:1 v/v, R_f = 0.27

m. p. = 158 -160 ° C

Yield: 0.62 g (38 %), white solid, recrystallised with EtOAc

¹H NMR (DMSO-d₆):

δ : 8.82 (t, J = 5.7 Hz, 1H, NH), 7.97 (s, 1H, Ar), 7.75 (d, J = 8.0 Hz, 1H, Ar), 7.64 (d, J = 8.0 Hz, 4H, Ar), 7.47 (s, 1H, Ar), 7.42 (m, 7H, Ar), 7.35 (m, 4H, Ar), 6.92 (s,1H, imid), 5.71 (dd, J = 6.0, 9.5 Hz, 1H, CH), 4.13 (m,1H, CH₂), 4.02 (m, 1H, CH₂).

¹³C NMR (DMSO-d₆):

δ : 167.2 (CO), 139.7, 137.6 (2 × C), 137.3 (CH, Ar), 137.2, 135.2 (2 × C), 129.9, 129.8, 129.6, 129.2, 128.5, 128.3, 128.1, 127.7, 127.4,126.7, 126.3, 125.5, 118.9 (18 × CH, Ar), 59.9 (CH), 43.9 (CH₂).

Microanalysis

Anal. Calcd for $C_{26}H_{23}N_3O$ · 0.25 H_2O (397.99): C 78.47 %, H 5.95 %, N 10.56 %. Found C 78.17 %, H 5.95 %, N 10.56.

4.6.4.36   (*E*)-*N*-(2-(4-chlorophenyl)-2-(1*H*-imidazol-1-yl)ethyl)-3-styrylbenzamide (43b)

Chemical Formula: $C_{26}H_{22}ClN_3O$
Molecular Weight: 427.93
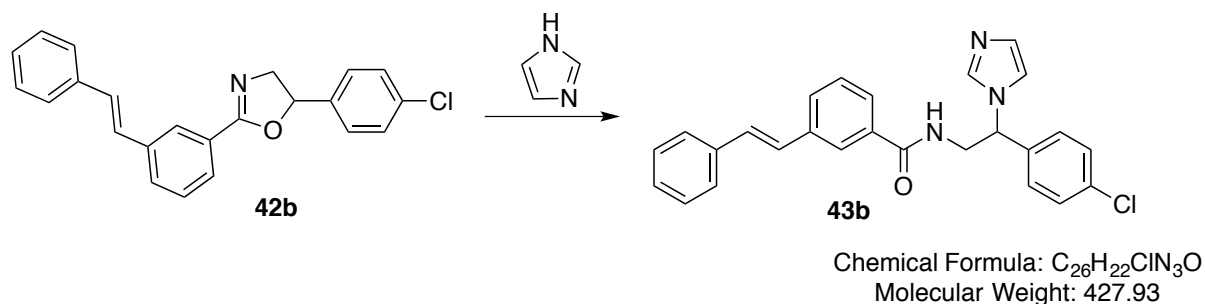
Method: See 4.6.4.18

Reagent: (*E*)-5-(4-chlorophenyl)-2-(3-styrylphenyl)-4,5-dihydrooxazole (0.9 g, 2.4 mmol) **42b**

m. p. = 148 - 152 ° C

TLC: CH_2Cl_2-CH_3OH 9:1 v/v, $R_f = 0.8$

Yield: 0.3 g (32 %), white solid, recrystallised with EtOAc

^{1}H NMR (DMSO-d$_6$):

δ : 8.82 (t, J = 5.5 Hz, 1H, NH), 7.95 (s, 1H, imid), 7.88 (s, 1H, Ar), 7.75 (d, J = 7.5 Hz, 2H, Ar), 7.47 (m, 5H, Ar), 7.31 (m, 8H, Ar), 6.93 (s, 1H, imid), 5.71 (dd, J = 6.0, 8.5 Hz, 1H, CH), 4.11 (m, 1H, CH), 3.91 (m,1H, CH$_2$).

^{13}C NMR (DMSO-d$_6$):

δ : 167.2 (CO), 138.7, 137.6 (2 × C), 137.2 (CH, Ar), 137.1, 135.1, 133.2 (3 × C), 129.9, 129.8, 129.4, 192.2, 129.1, 129.0, 128.4, 128.4,128.1, 127.1, 126.7, 125.5, 118.8 (17 × CH, Ar), 59.1 (CH), 43.7 (CH$_2$).

Microanalysis

Anal. Calcd for $C_{26}H_{22}ClN_3O$ (427.93): C 72.98 %, H 5.18 %, N 9.81 %. Found C 72.77 %, H 5.36 %, N 9.40

4.6.4.37 (*E*)-*N*-(2-(1*H*-imidazol-1-yl)-2-(2-(trifluoromethyl)phenyl)ethyl)-3-styrylbenzamide (43c)
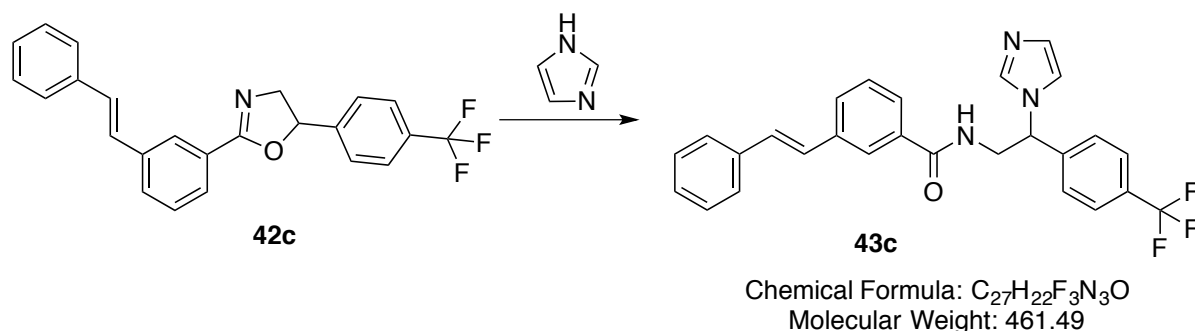
Chemical Formula: C$_{27}$H$_{22}$F$_3$N$_3$O
Molecular Weight: 461.49

Method: See 4.6.4.18

Reagent: (*E*)-2-(3-styrylphenyl)-5-(2-(trifluoromethyl)phenyl)-4,5-dihydrooxazole (0.35 g, 0.9 mmol) **42c**

TLC: CH$_2$Cl$_2$-CH$_3$OH 9:1 v/v, R$_f$ = 0.60

m. p. = 126 -130 ° C

Yield: 0.12 g (48 %), white solid, recrystallised with EtOAc

^{1}H NMR (DMSO-d$_6$):

δ : 8.84 (t, J = 5.5 Hz, 1H, NH), 7.96 (m, 2H, Ar), 7.78 (m, 4H, Ar), 7.64 (m, 5H, Ar), 7.49 (m, 4H, Ar), 7.33 (m, 2H, Ar), 6.96 (s,1H, imid) 5.84 (m, 1H, CH), 4.15 (m, 2H, CH$_2$).

^{13}C NMR (DMSO-d$_6$):

δ : 166.9 (CO), 149.0, 144.4, 137.6, 137.5, 135.4, 135.1, 134.9 (7 × C), 129.9, 129.8, 129.7, 129.2, 129.1, 128.4, 128.3, 128.2, 128.1, 127.3, 127.0, 126.1, 125.5, 125.4, 118.9 (18 × CH, Ar), 59.3 (CH), 43.7 (CH$_2$).

LRMS (ES-TOF)

m/z: 462 [M + H]$^+$

HRMS (ES-TOF)

Calculated mass: 462.1793 [M + H]$^+$, measured mass: 462.1799 [M + H]$^+$

4.6.4.38 *(E)*-*N*-(2-(1*H*-imidazol-1-yl)-2-phenylethyl)-3-(2-(trifluoromethyl)styryl)

     benzamide (43d)
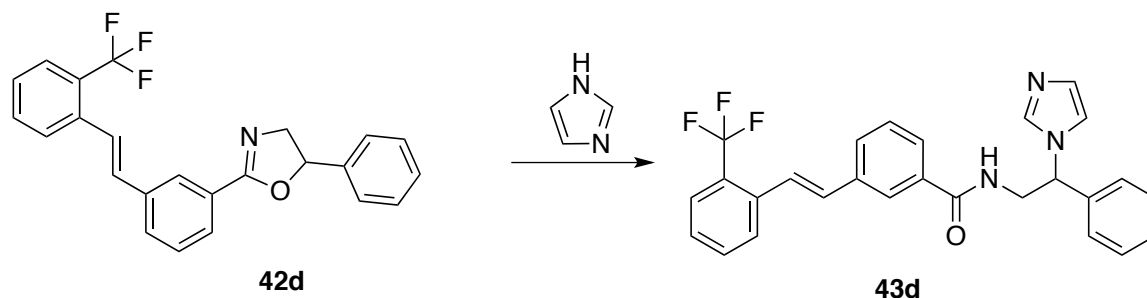
Chemical Formula: $C_{27}H_{22}F_3N_3O$
Molecular Weight: 461.49

Method: See 4.6.4.18

Reagent: (*E*)-2-(3-styrylphenyl)-5-(2-(trifluoromethyl)phenyl)-4,5-dihydrooxazole(0.7 g, 1.8 mmol) **42d**

TLC: CH_2Cl_2-CH_3OH 9:1 v/v, $R_f = 0.5$

m. p. = 110 -114 °C

Yield: 0.27 g (33 %), white solid, recrystallised with EtOAc

^{1}H NMR (DMSO-d_6):

δ : 8.87 (t, J = 5.5 Hz, 1H, NH), 8.02 (d, J = 7.5 Hz, 2H, Ar), 7.86 (s, 1H, imid), 7.78 (m, 4H, Ar), 7.54 (m, 5H, Ar), 7.40 (m, 5H, Ar), 6.91 (s,1H, Ar), 5.71 (dd, J = 6.0, 9.0 Hz, 1H, CH), 4.12 (m, 2H, CH_2).

^{13}C NMR (DMSO-d_6):

δ : 167.9 (CO), 149.0, 144.4, 138.6, 138.5, 136.4, 134.9 (6 × C), 129.9, 129.8, 129.7, 129.2, 129.1, 128.4, 128.3, 128.2, 128.1, 127.3, 127.0, 126.1, 125.5, 125.4, 12.4 (18 × CH, Ar), 59.3 (CH), 43.7 (CH_2).

LRMS (ES-TOF)

m/z: 462 [M + H]$^+$, 394 [M - imid]$^+$

HRMS (ES-TOF)

Calculated mass: 462.1793 [M + H]$^+$, measured mass: 462.1795 [M + H]$^+$
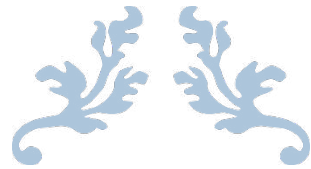
CHAPTER SIX

Conclusions

5   Conclusions

Vitamin D is synthesised from skin by exposure to ultra violet β radiation and undergoes hydroxylation to produce the biologically active metabolite calcitriol. Calcitriol has been shown to exhibit anticancer activity. However, therapy using calcitriol is limited owing to the short duration of action resulting from metabolism by 24-hydroxyvitamin D-24-hydroxylase (CYP24A1).
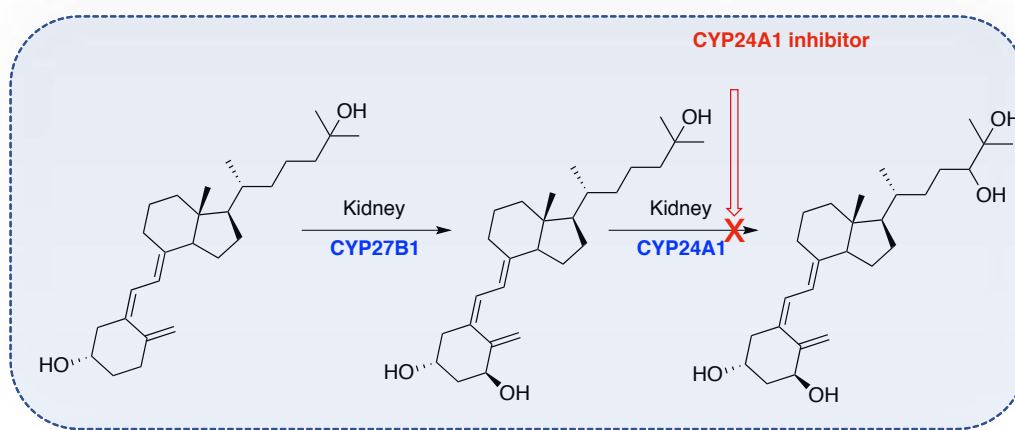
Figure 94: Site of of CYP24A1 inhibitor

Currently, the aim of this work is to develop a CYP27B1 homology model as a tool in the design of a selective inhibitor of vitamin D metabolism, specifically to aid in the design of chemical compounds with a selective inhibition of CYP24A1 and not the inhibition of CYP27B1, which inactivates the active form of vitamin D, calcitriol (Figure 94). A model of CYP24A1 using the rat CYP24A1 crystal structure as a template has previously been described by our group. To assist in the design of a selective CYP24A1 inhibitor, a CYP27B1 homology model was required. This required the generation of a homology modeling for CYP27B1 in order to analyse any differences in active site architecture and binding interactions. was built using Molecular Operating Environment (MOE) in order to try and understand the requirements of the enzyme active site binding where CYP24A1 has been previously developed and published.

CYP27B1 homology model was subject to validation, with further optimisation of the active site architecture achieved by molecular dynamics simulations. Understanding protein-ligand interactions is essential for designing more selective and potent CYP24A1 inhibitors. Monitoring RMSD during simulations indicated that it is a structurally stable homology model. Docking results for CYP27B1 showed amino acids Arg107, Asn387 and Asp320 have an

important role in binding interaction to form hydrogen bonds with inhibitors. Asp320 was part of the α I helix for the CYP27B1 model, which covers the haem binding site and contains SRS-4, and plays a key role in orientating the ligand at the active site by electrostatic interactions.

 The main strategy that can be used to build selective inhibitor CYP24A1 over CYP27B1, is to design compound unable to form hydrogen bonding interactions with CYP27B1 especially with Arg107, Asn387 and Asp320.

Using the data from modelling a lead compound, identified through screening of the SPECS database. The docking studies and synthesis of the modified lead compounds were described in (Figure 95, 96 and 97). Two of these compounds were selected as lead compounds (lead 1 and lead 2) for further development. In addition, lead 3 was synthesised in our laboratory and showed potent CYP24A1 inhibitory activity.
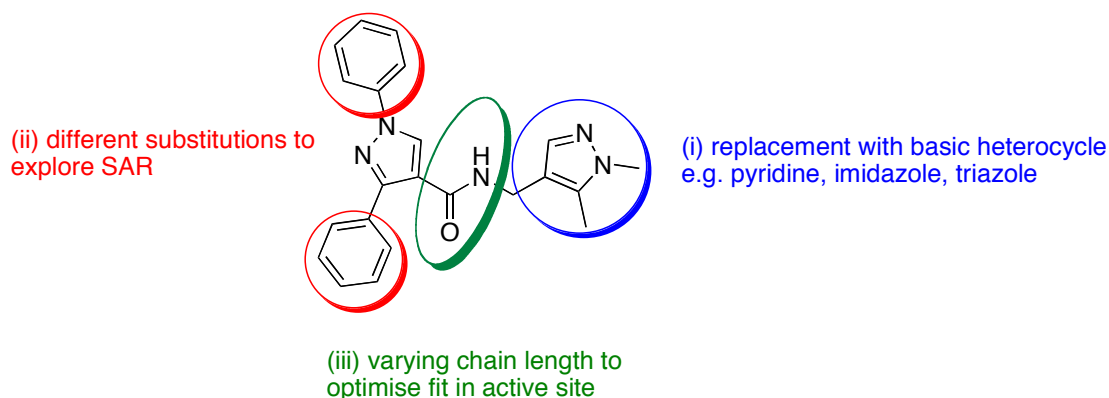
Figure 95: Modifications of lead 1 compound

Development of lead 1 by replacement with pyridine and imidazole was synthesised successfully. Replacement with triazole was also synthesised by the same methods. All the compounds accessed the vitamin D channel and interacted with the active site of CYP24A1. The compounds exhibited weak potency and IC_{50} ranging between 10.2 to 28.4 µM against CYP24A1 (Figure 95).
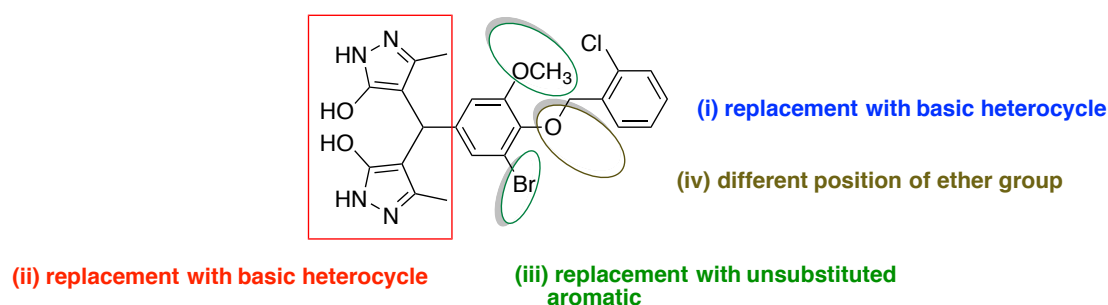
Figure 96: Modifications of lead 2 compound

The modified lead 2 compounds **25b**, **26a**, **26b**, **27a**, **27b** and **27c** were all synthesised successfully. **25b** interacted perpendicularly with the haem iron of CYP24A1 via ether oxygen with a distance of 2.20 Å. **26a** and **26b** were designed without phenyl substituent by changing the position of the ether group from the 4 to the 3 position and formed hydrogen bonds between number of amino acids, with the nitrogen atom of pyridine interacting perpendicularly with the haem iron of CYP24A1 with a distance 2.63 Å and 2.05 Å respectively. However, **26a** and **26b** showed enzymatic inhibition ($IC_{50} = 0.57$ µM and 0.41 µM respectively) against CYP27B1. As a result, both compounds have inhibitor selectivity for CYP27B1 that is five times greater than CYP24A1 owing to Asp320 and Asn387 have been identified as important amino acids for CYP27B1 inhibitory activity (Figure 96).
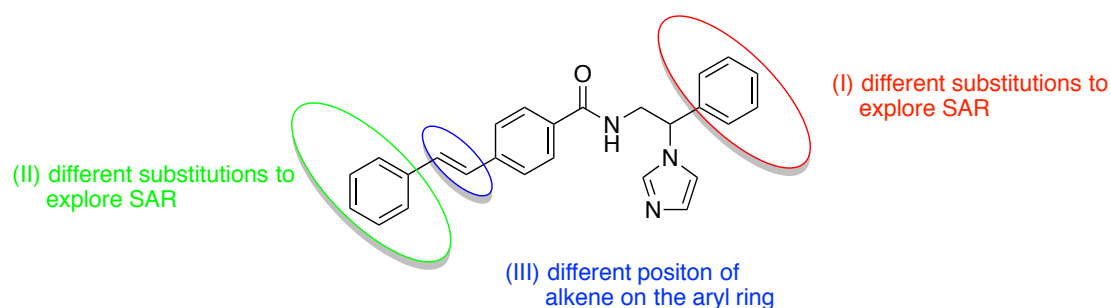
Figure 97: Modifications of lead 2 compound

A series of 3- and 4-styrylbenzamide imidazole derivatives have been prepared using an efficient synthetic route (Figure 97). All the derivatives showed very good inhibitory activity against CYP24A1 and, although there were some small differences in IC_{50} values depending on substituents, overall both 3- and 4-styrylbenzamide imidazoles and a range of substituents were very well tolerated without any significant loss of inhibitory activity. This inhibitory data would agree with the molecular docking where all the compounds fit well within the active site and showed a good fill of the hydrophobic channel of the CYP24A1 active site as well as transition metal interaction between the iron of the haem and the imidazole ring of the derivatives. However, although collaboration at delivery the University of Wisconsin sent CYP27B1 enzyme on two different occasions, the enzyme was denatured (owing to customs holdup) on both deliveries. Owing to the time in enzyme preparation, extraction and the costs involved we were unable to perform CYP27B1 enzyme inhibition assay.

6   References

(1)   Baker, C. P.; Kulkarni, B.; Radhakrishna, K. V; Charyulu, M. S.; Gregson, J.; Matsuzaki, M.; Taylor, A. E.; Prabhakaran, D.; Mamidi, R. S.; Wells, J.; Wilkinson, I.; McEniery, C.; Yasmin; Davey Smith, G.; Ben-Shlomo, Y.; Kuper, H.; Kinra, S. Is the Association between Vitamin D and Cardiovascular Disease Risk Confounded by Obesity? Evidence from the Andhra Pradesh Children and Parents Study (APCAPS). *PLoS One* **2015**, *10* (6), 1–11.

(2)   Fotsing, L.; Fillet, M.; Bechet, I.; Hubert, P.; Crommen, J. Determination of Six Water-Soluble Vitamins in a Pharmaceutical Formulation by Capillary Electrophoresis. *J. Pharm. Biomed. Anal.* **1997**, *15* (8), 1113–1123.

(3)   Mccollum, E. V.; Davis, M. Observations on the Isolation of the Substance in Butter Fat Which Exerts A Stimulating Influence on Growth. *J. Biol. Chem.* **1914**, *19* (2), 245–250.

(4)   Kulie, T.; Groff, A.; Redmer, J.; Hounshell, J.; Schrager, S. Vitamin D: An Evidence-Based Review. *J. Am. Board Fam. Med.* **2009**, *22* (6), 698–706.

(5)   Sadat-Ali, M.; Bubshait, D. A.; Al-Turki, H. A.; Al-Dakheel, D. A.; Al-Olayani, W. S. Topical Delivery of Vitamin D3: A Randomized Controlled Pilot Study. *Int. J. Biomed. Sci.* **2014**, *10* (1), 21–24.

(6)   Guzel, R.; Kozanoglu, E.; Guler-Uysal, F.; Soyupak, S.; Sarpel, T. Vitamin D Status and Bone Mineral Density of Veiled and Unveiled Turkish Women. *J. Womens. Health Gend. Based. Med.* **2001**, *10* (8), 765–770.

(7)   Windaus, A.; Grundmann, W. Über Die Konstitution Des Vitamins D2. II. *Justus Liebig's Ann. der Chemie* **1936**, *524* (1), 295–299.

(8)   Holick, M. F. Resurrection of Vitamin D Deficiency and Rickets. *J. Clin. Invest.* **2006**, *116* (8), 2062–2072.

(9)   Rajakumar, K. Vitamin D, Cod-Liver Oil, Sunlight, and Rickets: A Historical Perspective. *Pediatrics* **2003**, *112* (2), e132 LP-e135.

(10)   De Luca, G. Glycoprotein IIb-IIIa Inhibitors. *Cardiovasc. Ther.* **2012**, *30* (5), e242-54.

(11)   Wolf, G. The Discovery of Vitamin D: The Contribution of Adolf Windaus. *J. Nutr.* **2004**, *134* (6), 1299–1302.

(12)   O'Riordan, J. L. H.; Bijvoet, O. L. M. Rickets before the Discovery of Vitamin D. *Bonekey Rep.* **2014**, *3*, 478.

(13)   Nair, R.; Maseeh, A. Vitamin D: The "sunshine" Vitamin. *J. Pharmacol. Pharmacother.* **2012**, *3* (2), 118–126.

(14)   Imawari, M.; Kida, K.; Goodman, D. S. The Transport of Vitamin D and Its 25-Hydroxy

Metabolite in Human Plasma. Isolation and Partial Characterization of Vitamin D and 25-Hydroxyvitamin D Binding Protein. *J. Clin. Invest.* **1976**, *58* (2), 514‑523.

(15)　Haddad, J. G.; Jennings, A. S.; Choon AW, T. Vitamin D Uptake and Metabolism by Perfused Rat Liver: Influences of Carrier Proteins. *Endocrinology* **1988**, *123* (1), 498‑504.

(16)　Speeckaert, M.; Huang, G.; Delanghe, J. R.; Taes, Y. E. C. Biological and Clinical Aspects of the Vitamin D Binding Protein (Gc-Globulin) and Its Polymorphism. *Clin. Chim. Acta* **2006**, *372* (1), 33‑42.

(17)　Anic, G. M.; Weinstein, S. J.; Mondul, A. M.; Männistö, S.; Albanes, D. Serum Vitamin D, Vitamin D Binding Protein, and Risk of Colorectal Cancer. *PLoS One* **2014**, *9* (7), e102966.

(18)　Powe, C. E.; Ricciardi, C.; Berg, A. H.; Erdenesanaa, D.; Collerone, G.; Ankers, E.; Wenger, J.; Karumanchi, S. A.; Thadhani, R.; Bhan, I. Vitamin D‑Binding Protein Modifies the Vitamin D‑Bone Mineral Density Relationship. *J. Bone Miner. Res.* **2011**, *26* (7), 1609‑1616.

(19)　Ying, H.-Q.; Sun, H.-L.; He, B.-S.; Pan, Y.-Q.; Wang, F.; Deng, Q.-W.; Chen, J.; Liu, X.; Wang, S.-K. Circulating Vitamin D Binding Protein, Total, Free and Bioavailable 25-Hydroxyvitamin D and Risk of Colorectal Cancer. *Sci. Rep.* **2015**, *5*, 7956.

(20)　Tieu, E. W.; Tang, E. K. Y.; Tuckey, R. C. Kinetic Analysis of Human CYP24A1 Metabolism of Vitamin D via the C24-Oxidation Pathway. *FEBS J.* **2014**, *281* (14), 3280‑3296.

(21)　Razzaque, M. S. The FGF23‑Klotho Axis: Endocrine Regulation of Phosphate Homeostasis. *Nat. Rev. Endocrinol.* **2009**, *5* (11), 611‑619.

(22)　Naeem, Z. Vitamin D Deficiency- An Ignored Epidemic. *Int. J. Health Sci. (Qassim).* **2010**, *4* (1), V‑VI.

(23)　Guessous, I. Role of Vitamin D Deficiency in Extraskeletal Complications: Predictor of Health Outcome or Marker of Health Status? *Biomed Res. Int.* **2015**, *2015*, 563403.

(24)　Fleet, J. C.; Schoch, R. D. Molecular Mechanisms for Regulation of Intestinal Calcium Absorption by Vitamin D and Other Factors. *Crit. Rev. Clin. Lab. Sci.* **2010**, *47* (4), 181‑195.

(25)　Christakos, S.; Dhawan, P.; Porta, A.; Mady, L. J.; Seth, T. Vitamin D and Intestinal Calcium Absorption. *Mol. Cell. Endocrinol.* **2011**, *347* (1‑2), 25‑29.

(26)　Moe, S. M. Disorders Involving Calcium, Phosphorus, and Magnesium. *Prim. Care* **2008**, *35* (2), 215‑237.

(27)　Brito Galvao, J. F.; Nagode, L. A.; Schenck, P. A.; Chew, D. J. Calcitriol, Calcidiol,

Parathyroid Hormone, and Fibroblast Growth Factor-23 Interactions in Chronic Kidney Disease. *J. Vet. Emerg. Crit. Care* **2013**, *23* (2), 134－162.

(28) DeLuca, H. F. Overview of General Physiologic Features and Functions of Vitamin D. *Am J Clin Nutr* **2004**, *80* (6), 1689－1696.

(29) Bouillon, R.; Carmeliet, G.; Verlinden, L.; van Etten, E.; Verstuyf, A.; Luderer, H. F.; Lieben, L.; Mathieu, C.; Demay, M. Vitamin D and Human Health: Lessons from Vitamin D Receptor Null Mice. *Endocr. Rev.* **2008**, *29* (6), 726－776.

(30) Proszkowiec-Weglarz, M.; Angel, R. Calcium and Phosphorus Metabolism in Broilers: Effect of Homeostatic Mechanism on Calcium and Phosphorus digestibility1 . *J. Appl. Poult. Res.* **2013**, *22* (3), 609－627.

(31) Melamed, M. L.; Manson, J. E. Osteoporosis: Pathophysiology, Prevention, Diagnosis, and Treatment. *Disease-a-Month* **1993**, *39* (11), 794－867.

(32) Riccardi, D.; Martin, D. The Role of the Calcium-Sensing Receptor in the Pathophysiology of Secondary Hyperparathyroidism. *NDT Plus* **2008**, *1* (1), i7－i11.

(33) Malloy, P. J.; Feldman, D. Genetic Disorders and Defects in Vitamin D Action. *Endocrinol. Metab. Clin. North Am.* **2010**, *39* (2), 333－346.

(34) Sahay, M.; Sahay, R. Rickets－vitamin D Deficiency and Dependency. *Indian J. Endocrinol. Metab.* **2012**, *16* (2), 164－176.

(35) Mitsnefes, M.; Flynn, J.; Cohn, S.; Samuels, J.; Blydt-Hansen, T.; Saland, J.; Kimball, T.; Furth, S.; Warady, B.; Group, for the Ck. S. Masked Hypertension Associates with Left Ventricular Hypertrophy in Children with CKD. *J. Am. Soc. Nephrol.* **2010**, *21* (1), 137－144.

(36) Kumar, J.; McDermott, K.; Abraham, A. G.; Friedman, L. A.; Johnson, V. L.; Kaskel, F. J.; Furth, S. L.; Warady, B. A.; Portale, A. A.; Melamed, M. L. Prevalence and Correlates of 25-Hydroxyvitamin D Deficiency in the Chronic Kidney Disease in Children (CKiD) Cohort. *Pediatr. Nephrol.* **2016**, *31* (1), 121－129.

(37) Nikodimopoulou, M.; Liakos, S. Secondary Hyperparathyroidism and Target Organs in Chronic Kidney Disease. *Hippokratia* **2011**, *15* (1), 33－38.

(38) Al-Badr, W.; Martin, K. J. Vitamin D and Kidney Disease. *Clin. J. Am. Soc. Nephrol.* **2008**, *3* (5), 1555－1560.

(39) Martin, K. J.; Olgaard, K.; Coburn, J. W.; Coen, G. M.; Fukagawa, M.; Langman, C.; Malluche, H. H.; McCarthy, J. T.; Massry, S. G.; Mehls, O.; Salusky, I. B.; Silver, J. M.; Smogorzewski, M. T.; Slatopolsky, E. M.; McCann, L. Diagnosis, Assessment, and

Treatment of Bone Turnover Abnormalities in Renal Osteodystrophy. *Am. J. Kidney Dis.* **2004**, *43* (3), 558–565.

(40)   Plum, L. A.; DeLuca, H. F. Vitamin D, Disease and Therapeutic Opportunities. *Nat Rev Drug Discov* **2010**, *9* (12), 941–955.

(41)   Thadhani, R. Is Calcitriol Life-Protective for Patients with Chronic Kidney Disease? *J. Am. Soc. Nephrol.* **2009**, *20* (11), 2285–2290.

(42)   Judd, S. E.; Tangpricha, V. Vitamin D Deficiency and Risk for Cardiovascular Disease. *Am. J. Med. Sci.* **2009**, *338* (1), 40–44.

(43)   Mozos, I.; Marginean, O. Links between Vitamin D Deficiency and Cardiovascular Diseases. *Biomed Res. Int.* **2015**, *2015*, 109275.

(44)   Ullah, M. I.; Uwaifo, G. I.; Nicholas, C. W.; Koch, A. C. Does Vitamin D Deficiency Cause Hypertension? Current Evidence from Clinical Studies and Potential Mechanisms. *Int. J. Endocrinol.* **2010**, *2010*.

(45)   Chaudhuri, J. R.; Mridula, K. R.; Alladi, S.; Anamika, A.; Umamahesh, M.; Balaraju, B.; Swath, A.; Bandaru, V. C. S. S. Serum 25-Hydroxyvitamin D Deficiency in Ischemic Stroke and Subtypes in Indian Patients. *J. Stroke* **2014**, *16* (1), 44–50.

(46)   Brøndum-Jacobsen, P.; Nordestgaard, B. G.; Schnohr, P.; Benn, M. 25-Hydroxyvitamin D and Symptomatic Ischemic Stroke: An Original Study and Meta-Analysis. *Ann. Neurol.* **2013**, *73* (1), 38–47.

(47)   Pilz, S.; Dobnig, H.; Fischer, J. E.; Wellnitz, B.; Seelhorst, U.; Boehm, B. O.; März, W. Low Vitamin D Levels Predict Stroke in Patients Referred to Coronary Angiography. *Stroke* **2008**, *39* (9), 2611-2613.

(48)   Sarafian, G.; Afshar, M.; Mansouri, P.; Asgarpanah, J.; Raoufinejad, K.; Rajabi, M. Topical Turmeric Microemulgel in the Management of Plaque Psoriasis; A Clinical Evaluation. *Iran. J. Pharm. Res. IJPR* **2015**, *14* (3), 865–876.

(49)   Degitz, K.; Ochsendorf, F. Pharmacotherapy of Acne. *Expert Opin. Pharmacother.* **2008**, *9* (6), 955–971.

(50)   Trémezaygues, L.; Reichrath, J. Vitamin D Analogs in the Treatment of Psoriasis: Where Are We Standing and Where Will We Be Going? *Dermatoendocrinol.* **2011**, *3* (3), 180–186.

(51)   Kim, G. K. The Rationale Behind Topical Vitamin D Analogs in the Treatment of Psoriasis: Where Does Topical Calcitriol Fit In? *J. Clin. Aesthet. Dermatol.* **2010**, *3* (8), 46–53.

(52)   Antal, A. S.; Dombrowski, Y.; Koglin, S.; Ruzicka, T.; Schauber, J. Impact of Vitamin D3

on Cutaneous Immunity and Antimicrobial Peptide Expression. *Dermatoendocrinol.* **2011**, *3* (1), 18 – 22.

(53) Cai, Y.; Fleming, C.; Yan, J. New Insights of T Cells in the Pathogenesis of Psoriasis. *Cell. Mol. Immunol.* **2012**, *9* (4), 302 – 309.

(54) Mostafa, W. Z.; Hegazy, R. A. Vitamin D and the Skin: Focus on a Complex Relationship: A Review. *J. Adv. Res.* **2015**, *6* (6), 793 – 804.

(55) Tang, J.; Zhou, R.; Luger, D.; Zhu, W.; Silver, P. B.; Grajewski, R. S.; Su, S.-B.; Chan, C.-C.; Adorini, L.; Caspi, R. R. Calcitriol Suppresses Antiretinal Autoimmunity through Inhibitory Effects on the Th17 Effector Response. *J. Immunol.* **2009**, *182* (8), 4624 – 4632.

(56) Kim, B. J.; Rho, Y. K.; Lee, H. I.; Jeong, M. S.; Li, K.; Seo, S. J.; Kim, M. N.; Hong, C. K. The Effect of Calcipotriol on the Expression of Human β Defensin-2 and LL-37 in Cultured Human Keratinocytes. *Clin. Dev. Immunol.* **2009**, *2009*, 645898.

(57) http://www.medicinenet.com/image-collection/psoriasis_vulgaris_soles_picture/ picture.htm.

(58) DeLuca, H. F.; Cantorna, M. T. Vitamin D: Its Role and Uses in Immunology. *FASEB J.* **2001**, *15* (14), 2579 – 2585.

(59) Smolders, J.; Damoiseaux, J.; Menheere, P.; Hupperts, R. Vitamin D as an Immune Modulator in Multiple Sclerosis, a Review. *J. Neuroimmunol.* **2008**, *194* (1), 7 – 17.

(60) Merlino, L. A.; Curtis, J.; Mikuls, T. R.; Cerhan, J. R.; Criswell, L. A.; Saag, K. G. Vitamin D Intake Is Inversely Associated with Rheumatoid Arthritis: Results from the Iowa Women's Health Study. *Arthritis Rheum.* **2004**, *50* (1), 72 – 77.

(61) Hewison, M. Vitamin D and the Immune System: New Perspectives on an Old Theme. *Endocrinol. Metab. Clin. North Am.* **2010**, *39* (2), 365 – 379.

(62) Aranow, C. Vitamin D and the Immune System. *J. Investig. Med.* **2011**, *59* (6), 881 – 886.

(63) Di Rosa, M.; Malaguarnera, M.; Nicoletti, F.; Malaguarnera, L. Vitamin D3: A Helpful Immuno-Modulator. *Immunology* **2011**, *134* (2), 123 – 139.

(64) Harandi, A. A.; Harandi, A. A.; Pakdaman, H.; Sahraian, M. A. Vitamin D and Multiple Sclerosis. *Iran. J. Neurol.* **2014**, *13* (1), 1 – 6.

(65) Toro, J.; Cárdenas, S.; Fernando Martínez, C.; Urrutia, J.; Díaz, C. Multiple Sclerosis in Colombia and Other Latin American Countries. *Mult. Scler. Relat. Disord.* **2013**, *2* (2), 80 – 89.

(66) Maahs, D. M.; West, N. A.; Lawrence, J. M.; Mayer-Davis, E. J. Epidemiology of Type 1 Diabetes. *Endocrinol. Metab. Clin. North Am.* **2010**, *39* (3), 481 – 497.

(67)   Mandarino, N. R.; Júnior, F. das C. M.; Salgado, J. V. L.; Lages, J. S.; Filho, N. S. Is Vitamin D Deficiency a New Risk Factor for Cardiovascular Disease? *Open Cardiovasc. Med. J.* **2015**, *9*, 40–49.

(68)   Prietl, B.; Treiber, G.; Pieber, T. R.; Amrein, K. Vitamin D and Immune Function. *Nutrients* **2013**, *5* (7), 2502–2521.

(69)   Gröber, U.; Spitz, J.; Reichrath, J.; Kisters, K.; Holick, M. F. Vitamin D: Update 2013: From Rickets Prophylaxis to General Preventive Healthcare. *Dermatoendocrinol.* **2013**, *5* (3), 331–347.

(70)   Melamed, M. L.; Kumar, J. Low Levels of 25-Hydroxyvitamin D in the Pediatric Populations: Prevalence and Clinical Outcomes. *Ped. Health* **2010**, *4* (1), 89–97.

(71)   Driver, J. P.; Foreman, O.; Mathieu, C.; Van Etten, E.; Serreze, D. V. Comparative Therapeutic Effects of Orally Administered 1,25-Dihydroxyvitamin D3 and 1alpha-Hydroxyvitamin D3 on Type-1 Diabetes in Non-Obese Diabetic Mice Fed a Normal-Calcaemic Diet. *Clin. Exp. Immunol.* **2008**, *151* (1), 76–85.

(72)   Mackawy, A. M. H.; Badawi, M. E. H. Association of Vitamin D and Vitamin D Receptor Gene Polymorphisms with Chronic Inflammation, Insulin Resistance and Metabolic Syndrome Components in Type 2 Diabetic Egyptian Patients. *Meta Gene* **2014**, *2*, 540–556.

(73)   Bailey, R.; Cooper, J. D.; Zeitels, L.; Smyth, D. J.; Yang, J. H. M.; Walker, N. M.; Hyppönen, E.; Dunger, D. B.; Ramos-Lopez, E.; Badenhoop, K.; Nejentsev, S.; Todd, J. A. Association of the Vitamin D Metabolism Gene CYP27B1 with Type 1 Diabetes. *Diabetes* **2007**, *56* (10), 2616–2621.

(74)   Mansouri, R.; Moogooei, M.; Moogooei, M.; Razavi, N.; Mansourabadi, A. H. The Role of Vitamin D3 and Vitamin B9 (Folic Acid) in Immune System. *Int. J. Epidemiol. Res.* **2016**, *3* (1), 69–85.

(75)   Maxwell, C. S.; Wood, R. J. Update on Vitamin D and Type 2 Diabetes. *Nutr. Rev.* **2011**, *69* (5), 291–295.

(76)   Wilcox, G. Insulin and Insulin Resistance. *Clin. Biochem. Rev.* **2005**, *26* (2), 19–39.

(77)   Al-Shoumer, K. A. S.; Al-Essa, T. M. Is There a Relationship between Vitamin D with Insulin Resistance and Diabetes Mellitus? *World J. Diabetes* **2015**, *6* (8), 1057–1064.

(78)   Palomer, X.; González-Clemente, J. M.; Blanco-Vaca, F.; Mauricio, D. Role of Vitamin D in the Pathogenesis of Type 2 Diabetes Mellitus. *Diabetes, Obes. Metab.* **2008**, *10* (3), 185–197.

(79) Pittas, A. G.; Lau, J.; Hu, F.; Dawson-Hughes, B. The Role of Vitamin D and Calcium in Type 2 Diabetes. A Systematic Review and Meta-Analysis. *J. Clin. Endocrinol. Metab.* **2007**, *92* (6), 2017 – 2029.

(80) Aly, Y. E.; Abdou, A. S.; Rashad, M. M.; Nassef, M. M. Effect of Exercise on Serum Vitamin D and Tissue Vitamin D Receptors in Experimentally Induced Type 2 Diabetes Mellitus. *J. Adv. Res.* **2016**, *7* (5), 671 – 679.

(81) Fetahu, I. S.; Höbaus, J.; Kállay, E. Vitamin D and the Epigenome. *Front. Physiol.* **2014**, *5* (164), 1 – 12.

(82) Adams, J. M.; Cory, S. The Bcl-2 Apoptotic Switch in Cancer Development and Therapy. *Oncogene* **2007**, *26* (9), 1324 – 1337.

(83) Huang, Z.; Bao, S.-D. Roles of Main pro- and Anti-Angiogenic Factors in Tumor Angiogenesis. *World J. Gastroenterol.* **2004**, *10* (4), 463 – 470.

(84) Pećina-Šlaus, N. Tumor Suppressor Gene E-Cadherin and Its Role in Normal and Malignant Cells. *Cancer Cell Int.* **2003**, *3*, 17.

(85) Pálmer, H. G.; González-Sancho, J. M.; Espada, J.; Berciano, M. T.; Puig, I.; Baulida, J.; Quintanilla, M.; Cano, A.; de Herreros, A. G.; Lafarga, M.; Muñoz, A. Vitamin D3 Promotes the Differentiation of Colon Carcinoma Cells by the Induction of E-Cadherin and the Inhibition of β -Catenin Signaling. *J. Cell Biol.* **2001**, *154* (2), 369 – 388.

(86) Chakraborti, C. K. Vitamin D as a Promising Anticancer Agent. *Indian J. Pharmacol.* **2011**, *43* (2), 113 – 120.

(87) Colston, K. A. Y.; Colston, M. J.; Feldman, D. 1,25-Dihydroxyvitamin D3 And Malignant Melanoma: The Presence Of Receptors And Inhibition Of Cell Growth In Culture. *Endocrinology* **1981**, *108* (3), 1083 – 1086.

(88) Moukayed, M.; Grant, W. B. Molecular Link between Vitamin D and Cancer Prevention. *Nutrients* **2013**, *5* (10), 3993 – 4021.

(89) Brawer, M. K. Recent Progress in the Treatment of Advanced Prostate Cancer With Intermittent Dose-Intense Calcitriol (DN-101). *Rev. Urol.* **2007**, *9* (1), 1 – 8.

(90) Fleet, J. C.; Desmet, M.; Johnson, R.; Li, Y. Vitamin D and Cancer: A Review of Molecular Mechanisms. *Biochem. J.* **2012**, *441* (1), 61 – 76.

(91) Díaz, L.; Díaz-Muñoz, M.; García-Gaytán, A. C.; Méndez, I. Mechanistic Effects of Calcitriol in Cancer Biology. *Nutrients* **2015**, *7* (6), 5020 – 5050.

(92) Guraya, S. Y. Chemopreventive Role of Vitamin D in Colorectal Carcinoma. *J. Microsc. Ultrastruct.* **2014**, *2* (1), 1 – 6.

(93)   Vuolo, L.; Di Somma, C.; Faggiano, A.; Colao, A. Vitamin D and Cancer. *Front. Endocrinol. (Lausanne).* **2012**, *3*, 58.

(94)   Kim, H. J.; Lee, Y. M.; Ko, B. S.; Lee, J. W.; Yu, J. H.; Son, B. H.; Gong, G.-Y.; Kim, S. B.; Ahn, S. H. Vitamin D Deficiency Is Correlated with Poor Outcomes in Patients with Luminal-Type Breast Cancer. *Ann. Surg. Oncol.* **2011**, *18* (7), 1830–1836.

(95)   Waltman, N. L.; Ott, C. D.; Twiss, J. J.; Gross, G. J.; Lindsey, A. M. Vitamin D Insufficiency and Musculoskeletal Symptoms In Breast Cancer Survivors on Aromatase Inhibitor Therapy. *Cancer Nurs.* **2009**, *32* (2), 143–150.

(96)   Wijngaarden, T. V.; Pols, H. A. P.; Buurman, C. J.; van den Bemd, G. J. C. M.; Dorssers, L. C. J.; Birkenhäger, J. C.; van Leeuwen, J. P. T. M. Inhibition of Breast Cancer Cell Growth by Combined Treatment with Vitamin D Analogues and Tamoxifen. *Cancer Res.* **1994**, *54* (21), 5711 LP-5717.

(97)   Krishnan, A. V; Swami, S.; Feldman, D. The Potential Therapeutic Benefits of Vitamin D in the Treatment of Estrogen Receptor Positive Breast Cancer. *Steroids* **2012**, *77* (11), 1107–1112.

(98)   Masuda, S.; Jones, G. Promise of Vitamin D Analogues in the Treatment of Hyperproliferative Conditions. *Mol. Cancer Ther.* **2006**, *5* (4), 797–808.

(99)   Parsons, J. K. Benign Prostatic Hyperplasia and Male Lower Urinary Tract Symptoms: Epidemiology and Risk Factors. *Curr. Bladder Dysfunct. Rep.* **2010**, *5* (4), 212–218.

(100) Benbrahim-Tallaa, L.; Waalkes, M. Inorganic Arsenic and Human Prostate Cancer. *CiÃ\textordfemeninencia & SaÃ\textordmasculinede Coletiva* **2009**, *14*, 307–318.

(101) Lepor, H. Pathophysiology of Benign Prostatic Hyperplasia in the Aging Male Population. *Rev. Urol.* **2005**, *7* (4), 3–12.

(102) Keum, N.; Giovannucci, E. Vitamin D Supplements and Cancer Incidence and Mortality: A Meta-Analysis. *Br. J. Cancer* **2014**, *111* (5), 976–980.

(103) Luk, J.; Torrealday, S.; Neal Perry, G.; Pal, L. Relevance of Vitamin D in Reproduction. *Hum. Reprod.* **2012**, *27* (10), 3015–3027.

(104) Maj, E.; Papiernik, D.; Wietrzyk, J. Antiangiogenic Cancer Treatment: The Great Discovery and Greater Complexity (Review). *Int. J. Oncol.* **2016**, *49* (5), 1773–1784.

(105) Krishnan, A. V; Swami, S.; Feldman, D. Equivalent Anticancer Activities of Dietary Vitamin D and Calcitriol in an Animal Model of Breast Cancer: Importance of Mammary CYP27B1 for Treatment and Prevention. *J. Steroid Biochem. Mol. Biol.* **2013**, *136*, 289–295.

(106) Ben-Eltriki, M.; Deb, S.; Guns, E. S. T. Calcitriol in Combination Therapy for Prostate Cancer: Pharmacokinetic and Pharmacodynamic Interactions. *J. Cancer* **2016**, *7* (4), 391 – 407.

(107) Okamoto, R.; Delansorne, R.; Wakimoto, N.; Doan, N. B.; Akagi, T.; Shen, M.; Ho, Q. H.; Said, J. W.; Koeffler, H. P. Inecalcitol, an Analog of 1 α ,25(OH)(2)D(3), Induces Growth Arrest of Androgen-Dependent Prostate Cancer Cells. *Int. J. Cancer* **2012**, *130* (10), 2464 – 2473.

(108) Kaeding, J.; Bélanger, J.; Caron, P.; Verreault, M.; Bélanger, A.; Barbier, O. Calcitrol (1 α ,25-Dihydroxyvitamin D Inhibits Androgen Glucuronidation in Prostate Cancer Cells. *Mol. Cancer Ther.* **2008**, *7* (2), 380 – 390.

(109) Mattar, M. C.; Lough, D.; Pishvaian, M. J.; Charabaty, A. Current Management of Inflammatory Bowel Disease and Colorectal Cancer. *Gastrointest. Cancer Res.* **2011**, *4* (2), 53 – 61.

(110) Ma, Y.; Zhang, P.; Wang, F.; Yang, J.; Liu, Z.; Qin, H. Association Between Vitamin D and Risk of Colorectal Cancer: A Systematic Review of Prospective Studies. *J. Clin. Oncol.* **2011**, *29* (28), 3775 – 3782.

(111) Klampfer, L. Vitamin D and Colon Cancer. *World J. Gastrointest. Oncol.* **2014**, *6* (11), 430 – 437.

(112) Garland, C. F.; Garland, F. C.; Gorham, E. D.; Lipkin, M.; Newmark, H.; Mohr, S. B.; Holick, M. F. The Role of Vitamin D in Cancer Prevention. *Am. J. Public Health* **2006**, *96* (2), 252 – 261.

(113) Cui, M.; Klopot, A.; Jiang, Y.; Fleet, J. C. The Effect of Differentiation on 1,25 Dihydroxyvitamin D -Mediated Gene Expression in the Enterocyte-Like Cell Line, Caco-2. *J. Cell. Physiol.* **2009**, *218* (1), 113 – 121.

(114) Brozek, W.; Manhardt, T.; Kállay, E.; Peterlik, M.; Cross, H. S. Relative Expression of Vitamin D Hydroxylases, CYP27B1 and CYP24A1, and of Cyclooxygenase-2 and Heterogeneity of Human Colorectal Cancer in Relation to Age, Gender, Tumor Location, and Malignancy: Results from Factor and Cluster Analysis. *Cancers (Basel).* **2012**, *4* (3), 763 – 776.

(115) Lin, J.; Zhang, S. M.; Cook, N. R.; Manson, J. E.; Lee, I.-M.; Buring, J. E. Intakes of Calcium and Vitamin D and Risk of Colorectal Cancer in Women. *Am. J. Epidemiol.* **2005**, *161* (8), 755 – 764.

(116) Holt, P. R.; Kozuch, P.; Mewar, S. Colon Cancer and the Elderly: From Screening to

Treatment in Management of GI Disease in the Elderly. *Best Pract. Res. Clin. Gastroenterol.* **2009**, *23* (6), 889–907.

(117) Ma, Y.; Trump, D. L.; Johnson, C. S. Vitamin D in Combination Cancer Treatment. *J. Cancer* **2010**, *1*, 101–107.

(118) Kumagai, T.; O'Kelly, J.; Said, J. W.; Koeffler, H. P. Vitamin D2 Analog 19-nor-1,25-Dihydroxyvitamin D2: Antitumor Activity Against Leukemia, Myeloma, and Colon Cancer Cells. *J. Natl. Cancer Inst.* **2003**, *95* (12), 896–905.

(119) Medh, R. D. Microarray-Based Expression Profiling of Normal and Malignant Immune Cells. *Endocr. Rev.* **2002**, *23* (3), 393–400.

(120) Bikle, D. D.; Elalieh, H.; Welsh, J.; Oh, D.; Cleaver, J.; Teichert, A. Protective Role of Vitamin D Signaling in Skin Cancer Formation. *J. Steroid Biochem. Mol. Biol.* **2013**, *136*, 271–279.

(121) Ferguson-Yates, B. E.; Li, H.; Dong, T. K.; Hsiao, J. L.; Oh, D. H. Impaired Repair of Cyclobutane Pyrimidine Dimers in Human Keratinocytes Deficient in p53 and p63. *Carcinogenesis* **2008**, *29* (1), 70–75.

(122) Lee, J. H.; Park, S.; Cheon, S.; Lee, J. H.; Kim, S.; Hur, D. Y.; Kim, T. S.; Yoon, S. R.; Yang, Y.; Bang, S. I.; Park, H.; Lee, H. T.; Cho, D. 1,25-Dihydroxyvitamin D3 Enhances NK Susceptibility of Human Melanoma Cells via Hsp60-Mediated FAS Expression. *Eur. J. Immunol.* **2011**, *41* (10), 2937–2946.

(123) Davis-Yadley, A. H.; Malafa, M. P. Vitamins in Pancreatic Cancer: A Review of Underlying Mechanisms and Future Applications. *Adv. Nutr.* **2015**, *6* (6), 774–802.

(124) Moy, F.-M.; Bulgiba, A. High Prevalence of Vitamin D Insufficiency and Its Association with Obesity and Metabolic Syndrome among Malay Adults in Kuala Lumpur, Malaysia. *BMC Public Health* **2011**, *11* (1), 735.

(125) Christakos, S.; Ajibade, D. V; Dhawan, P.; Fechner, A. J.; Mady, L. J. Vitamin D: Metabolism. *Endocrinol. Metab. Clin. North Am.* **2010**, *39* (2), 243–253.

(126) Bikle, D. D. Vitamin D Metabolism, Mechanism of Action, and Clinical Applications. *Chem. Biol.* **2014**, *21* (3), 319–329.

(127) Brożyna, A. A.; Jóźwicki, W.; Janjetovic, Z.; Slominski, A. T. Expression of Vitamin D-Activating Enzyme 1α-Hydroxylase (CYP27B1) Decreases during Melanoma Progression. *Hum. Pathol.* **2013**, *44* (3), 374–387.

(128) Martin, A.; David, V.; Quarles, L. D. Regulation And Function Of The FGF23/Klotho Endocrine Pathways. *Physiol. Rev.* **2012**, *92* (1), 131–155.

(129) Chanakul, A.; Zhang, M. Y. H.; Louw, A.; Armbrecht, H. J.; Miller, W. L.; Portale, A. A.; Perwad, F. FGF-23 Regulates CYP27B1 Transcription in the Kidney and in Extra-Renal Tissues. *PLoS One* **2013**, *8* (9), 1 – 11.

(130) Morris, H. A.; Anderson, P. H. Autocrine and Paracrine Actions of Vitamin D. *Clin. Biochem. Rev.* **2010**, *31* (4), 129 – 138.

(131) St-Arnaud, R.; Messerlian, S.; Moir, J. M.; Omdahl, J. L.; Glorieux, F. H. The 25-Hydroxyvitamin D 1-Alpha-Hydroxylase Gene Maps to the Pseudovitamin D-Deficiency Rickets (PDDR) Disease Locus. *J. Bone Miner. Res.* **1997**, *12* (10), 1552 – 1559.

(132) Haussler, M. R.; Haussler, C. A.; Jurutka, P. W.; Thompson, P. D.; Hsieh, J.-C.; Remus, L. S.; Selznick, S. H.; Whitfield, G. K. The Vitamin D Hormone and Its Nuclear Receptor: Molecular Actions and Disease States. *J. Endocrinol.* **1997**, *154* (3 Suppl), S57 – S73.

(133) Kitanaka, S.; Takeyama, K.; Murayama, A.; Sato, T.; Okumura, K.; Nogami, M.; Hasegawa, Y.; Niimi, H.; Yanagisawa, J.; Tanaka, T.; Kato, S. Inactivating Mutations in the 25-Hydroxyvitamin D3 1 α -Hydroxylase Gene in Patients with Pseudovitamin D-Deficiency Rickets. *N. Engl. J. Med.* **1998**, *338* (10), 653 – 662.

(134) Anderson, P. H.; May, B. K.; Morris, H. A. Vitamin D Metabolism: New Concepts and Clinical Implications. *Clin. Biochem. Rev.* **2003**, *24* (1), 13 – 26.

(135) Tuckey, R. C.; Li, W.; Zjawiony, J. K.; Zmijewski, M. A.; Nguyen, M. N.; Sweatman, T.; Miller, D.; Slominski, A. Pathways and Products for the Metabolism of Vitamin D3 by Cytochrome P450scc. *FEBS J.* **2008**, *275* (10), 2585 – 2596.

(136) Cheng, J. B.; Levine, M. A.; Bell, N. H.; Mangelsdorf, D. J.; Russell, D. W. Genetic Evidence That the Human CYP2R1 Enzyme Is a Key Vitamin D 25-Hydroxylase. *Proc. Natl. Acad. Sci. U. S. A.* **2004**, *101* (20), 7711 – 7715.

(137) Grahn, R. A.; Ellis, M. R.; Grahn, J. C.; Lyons, L. A. A Novel CYP27B1 Mutation Causes a Feline Vitamin D-Dependent Rickets Type IA. *J. Feline Med. Surg.* **2012**, *14* (8), 587 – 590.

(138) Binkley, N.; Gemar, D.; Engelke, J.; Gangnon, R.; Ramamurthy, R.; Krueger, D.; Drezner, M. K. Evaluation of Ergocalciferol or Cholecalciferol Dosing, 1,600 IU Daily or 50,000 IU Monthly in Older Adults. *J. Clin. Endocrinol. Metab.* **2011**, *96* (4), 981 – 988.

(139) Kanis, J. A. Vitamin D Analogs: From Renal Bone Disease to Osteoporosis. *Kidney Int.* **2016**, *56*, S77 – S81.

(140) Barycki, R.; Sicinski, R. R.; Plum, L. A.; Grzywacz, P.; Clagett-Dame, M.; DeLuca, H. F. Removal of the 20-Methyl Group from 2-Methylene-19-nor-(20S)-1 α ,25-

Dihydroxyvitamin D3 (2MD) Selectively Eliminates Bone Calcium Mobilization Activity. *Bioorg. Med. Chem.* **2009**, *17* (22), 7658‑7669.

(141) Masuda, S.; Strugnell, S. A.; Knutson, J. C.; St-Arnaud, R.; Jones, G. Evidence for the Activation of 1α-Hydroxyvitamin D2 by 25-Hydroxyvitamin D-24-Hydroxylase: Delineation of Pathways Involving 1α,24-Dihydroxyvitamin D2 and 1α,25-Dihydroxyvitamin D2. *Biochim. Biophys. Acta - Mol. Cell Biol. Lipids* **2006**, *1761* (2), 221‑234.

(142) Rhieu, S. Y.; Annalora, A. J.; Gathungu, R. M.; Vouros, P.; Uskokovic, M. R.; Schuster, I.; Palmore, G. T. R.; Reddy, G. S. A New Insight into the Role of Rat Cytochrome P450 24A1 in Metabolism of Selective Analogs of 1α,25-Dihydroxyvitamin D3. *Arch. Biochem. Biophys.* **2011**, *509* (1), 33‑43.

(143) Koren, R.; Hadari-Naor, I.; Zuck, E.; Rotem, C.; Liberman, U. A.; Ravid, A. Vitamin D Is a Prooxidant in Breast Cancer Cells. *Cancer Res.* **2001**, *61* (4), 1439‑1444.

(144) Jones, G.; Byford, V.; West, S.; Masuda, S.; Ibrahim, G.; Kaufmann, M.; Knutson, J. C.; Strugnell, S.; Mehta, R. Hepatic Activation and Inactivation of Clinically-Relevant Vitamin D Analogs and Prodrugs. *Anticancer Res.* **2006**, *26* (4 A), 2589‑2595.

(145) http://www.webmd.com/rheumatoid-arthritis/ss/slideshow-ra-overview.

(146) Jones, G.; Prosser, D. E.; Kaufmann, M. Cytochrome P450-Mediated Metabolism of Vitamin D. *J. Lipid Res.* **2014**, *55* (1), 13‑31.

(147) Brown, A. J.; Dusso, A. S.; Slatopolsky, E. Vitamin D Analogues for Secondary Hyperparathyroidism. *Nephrol. Dial. Transplant* **2002**, *17* (10), 10‑19.

(148) Thomas, R.; Kanso, A.; Sedor, J. R. Chronic Kidney Disease and Its Complications. *Prim. Care* **2008**, *35* (2), 329‑344.

(149) Cheng, S.; Coyne, D. Oral Paricalcitol for the Treatment of Secondary Hyperparathyroidism in Chronic Kidney Disease. *Ther. Clin. Risk Manag.* **2006**, *2* (3), 297‑301.

(150) Bolasco, P. Treatment Options of Secondary Hyperparathyroidism (SHPT) in Patients with Chronic Kidney Disease Stages 3 and 4: An Historic Review. *Clin. Cases Miner. Bone Metab.* **2009**, *6* (3), 210‑219.

(151) Pilz, S.; Tomaschitz, A.; Ritz, E.; Pieber, T. R. Vitamin D Status and Arterial Hypertension: A Systematic Review. *Nat Rev Cardiol* **2009**, *6* (10), 621‑630.

(152) Bosworth, C.; de Boer, I. H. Impaired Vitamin D Metabolism in CKD. *Semin. Nephrol.* **2013**, *33* (2), 158‑168.

(153) Meisner, L. F. Topical Composition for the Treatment of Psoriasis and Related Skin

Disorders. US7670620 B2 Patents November 8, 2001.

(154) Masudata, S.; Strugnell, S.; Calverley, M. J.; Makin, H. L. J.; Kremer, R.; Jones, G. In Vitro Metabolism of the Anti-Psoriatic Vitamin D Analog, Calcipotriol, in Two Cultured Human Keratinocyte Models. *J. Biol. Chem.* **1994**, *269* (7), 4794‒4803.

(155) Brown, A. J.; Slatopolsky, E. Vitamin D Analogs: Therapeutic Applications and Mechanisms for Selectivity. *Mol. Aspects Med.* **2008**, *29* (6), 433‒452.

(156) Tominaga, Y. Current Status of Parathyroidectomy for Secondary Hyperparathyroidism in Japan. *NDT Plus* **2008**, *1* (3), iii35-iii38.

(157) Murayama, E.; Miyamoto, K.; Kubodera, N.; Mori, T.; Matsunaga, I. Synthetic Studies of Vitamin D3 Analogues. VIII. : Synthesis of 22-Oxavitamin D3 Analogues. *Chem. Pharm. Bull. (Tokyo)*. **1986**, *34* (10), 4410‒4413.

(158) Akizawa, T.; Akiba, T.; Hirakata, H.; Kinugasa, E.; Tominaga, Y.; Fukagawa, M.; Yokoyama, K.; Zhang, W.; Linde, P. G.; Suzuki, M. Comparison of Paricalcitol With Maxacalcitol Injection in Japanese Hemodialysis Patients With Secondary Hyperparathyroidism. *Ther. Apher. Dial.* **2015**, *19* (3), 225‒234.

(159) Veldurthy, V.; Wei, R.; Oz, L.; Dhawan, P.; Jeon, Y. H.; Christakos, S. Vitamin D, Calcium Homeostasis and Aging. *Bone Res.* **2016**, *4*, 1‒7.

(160) Eelen, G.; Verlinden, L.; Rochel, N.; Claessens, F.; De Clercq, P.; Vandewalle, M.; Tocchini-Valentini, G.; Moras, D.; Bouillon, R.; Verstuyf, A. Superagonistic Action of 14-Epi-Analogs of 1,25-Dihydroxyvitamin D Explained by Vitamin D Receptor-Coactivator Interaction. *Mol. Pharmacol.* **2005**, *67* (5), 1566‒1573.

(161) Werck-Reichhart, D.; Feyereisen, R. Cytochromes P450: A Success Story. *Genome Biol.* **2000**, *1* (6), 1‒9.

(162) Fukushige, H.; Hildebrand, D. F. Watermelon (Citrullus Lanatus) Hydroperoxide Lyase Greatly Increases C6 Aldehyde Formation in Transgenic Leaves. *J. Agric. Food Chem.* **2005**, *53* (6), 2046‒2051.

(163) Hasemann, C. A.; Kurumbail, R. G.; Boddupalli, S. S.; Peterson, J. A.; Deisenhofer, J. Structure and Function of Cytochromes P450:a Comparative Analysis of Three Crystal Structures. *Structure* **2016**, *3* (1), 41‒62.

(164) Nebert, D. W.; Wikvall, K.; Miller, W. L. Human Cytochromes P450 in Health and Disease. *Philos. Trans. R. Soc. B Biol. Sci.* **2013**, *368* (1612), 20120431.

(165) Ozben, T. Mechanisms and Strategies to Overcome Multiple Drug Resistance in Cancer. *FEBS Lett.* **2006**, *580* (12), 2903‒2909.

(166) Li, Q.; Fang, Y.; Li, X.; Zhang, H.; Liu, M.; Yang, H.; Kang, Z.; Li, Y.; Wang, Y. Mechanism of the Plant Cytochrome P450 for Herbicide Resistance: A Modelling Study. *J. Enzyme Inhib. Med. Chem.* **2013**, *28* (6), 1182‒1191.

(167) Ortiz de Montellano, P. R. Hydrocarbon Hydroxylation by Cytochrome P450 Enzymes. *Chem. Rev.* **2010**, *110* (2), 932.

(168) Ortiz de Montellano, P. R. Cytochrome P450-Activated Prodrugs. *Future Med. Chem.* **2013**, *5* (2), 213‒228.

(169) Estabrook, R. W.; Hildebrandt, A. G.; Baron, J.; Netter, K. J.; Leibman, K. A New Spectral Intermediate Associated with Cytochrome P-450 Function in Liver Microsomes. *Biochem. Biophys. Res. Commun.* **1971**, *42* (1), 132‒139.

(170) Sevrioukova, I. F.; Poulos, T. L. Structure and Mechanism of the Complex between Cytochrome P4503A4 and Ritonavir. *Proc. Natl. Acad. Sci. U. S. A.* **2010**, *107* (43), 18422‒18427.

(171) Hamdane, D.; Xia, C.; Im, S.-C.; Zhang, H.; Kim, J.-J. P.; Waskell, L. Structure and Function of an NADPH-Cytochrome P450 Oxidoreductase in an Open Conformation Capable of Reducing Cytochrome P450. *J. Biol. Chem.* **2009**, *284* (17), 11374‒11384.

(172) Hrycay, E. G.; O'Brien, P. J. Cytochrome P-450 as a Microsomal Peroxidase Utilizing a Lipid Peroxide Substrate. *Arch. Biochem. Biophys.* **1971**, *147* (1), 14‒27.

(173) Kumar, S. Engineering Cytochrome P450 Biocatalysts for Biotechnology, Medicine, and Bioremediation. *Expert Opin. Drug Metab. Toxicol.* **2010**, *6* (2), 115‒131.

(174) Wanwimolruk, S.; Prachayasittikul, V. Cytochrome P450 Enzyme Mediated Herbal Drug Interactions (Part 1). *EXCLI J.* **2014**, *13*, 347‒391.

(175) Bachi, A.; Dalle-Donne, I.; Scaloni, A. Redox Proteomics: Chemical Principles, Methodological Approaches and Biological/Biomedical Promises. *Chem. Rev.* **2013**, *113* (1), 596‒698.

(176) Hong, C.-C.; Tang, B.-K.; Hammond, G. L.; Tritchler, D.; Yaffe, M.; Boyd, N. F. Cytochrome P450 1A2 (CYP1A2) Activity and Risk Factors for Breast Cancer: A Cross-Sectional Study. *Breast Cancer Res.* **2004**, *6* (4), R352‒R365.

(177) Narasimhulu, S. New Cytochrome P450 Mechanisms: Implications for Understanding Molecular Basis for Drug Toxicity at the Level of the Cytochrome. *Expert Opin. Drug Metab. Toxicol.* **2010**, *6* (1), 1‒15.

(178) Panigrahy, D.; Kaipainen, A.; Greene, E. R.; Huang, S. Cytochrome P450-Derived Eicosanoids: The Neglected Pathway in Cancer. *Cancer Metastasis Rev.* **2010**, *29* (4), 723‒

735.

(179) Nakagawa, Y.; Ishii, E. Changes in Arachidonic Acid Metabolism and the Aggregation of Polymorphonuclear Leukocytes in Rats with Streptozotocin-Induced Diabetes. *Biochim. Biophys. Acta - Mol. Basis Dis.* **1996**, *1315* (2), 145 – 151.

(180) Spector, A. A. Arachidonic Acid Cytochrome P450 Epoxygenase Pathway. *J. Lipid Res.* **2009**, *50* (Supplement), S52 – S56.

(181) Guengerich, F. P.; Munro, A. W. Unusual Cytochrome P450 Enzymes and Reactions. *J. Biol. Chem.* **2013**, *288* (24), 17065 – 17073.

(182) Nes, W. D. Biosynthesis of Cholesterol and Other Sterols. *Chem. Rev.* **2011**, *111* (10), 6423 – 6451.

(183) Ong, C. E.; Pan, Y.; Mak, J. W. The Roles of Cytochromes P450 in Vascular Biology and Cardiovascular Homeostasis. *Int. J. Clin. Exp. Med.* **2017**, *10* (1), 1624 – 1636.

(184) Tuck, S. F.; Patel, H.; Safi, E.; Robinson, C. H. Lanosterol 14 Alpha-Demethylase (P45014DM): Effects of P45014DM Inhibitors on Sterol Biosynthesis Downstream of Lanosterol. *J. Lipid Res.* **1991**, *32* (6), 893 – 902.

(185) Wang, Z.; Schuetz, E. G.; Xu, Y.; Thummel, K. E. Interplay between Vitamin D and the Drug Metabolizing Enzyme CYP3A4. *J. Steroid Biochem. Mol. Biol.* **2013**, *136*, 54 – 58.

(186) Knutson, J. C.; DeLuca, H. F. 25-Hydroxyvitamin D3-24-Hydroxylase. Subcellular Location and Properties. *Biochemistry* **1974**, *13* (7), 1543 – 1548.

(187) Jones, G.; Strugnell, S. A.; Deluca, H. F. Current Understanding of the Molecular Actions of Vitamin D. *Physiol Rev* **1998**, *78* (4), 1193 – 1231.

(188) Makin, G.; Lohnes, D.; Byford, V.; Ray, R.; Jones, G. Target Cell Metabolism of 1,25-Dihydroxyvitamin D3 to Calcitroic Acid. Evidence for a Pathway in Kidney and Bone Involving 24-Oxidation. *Biochem. J.* **1989**, *262* (1), 173 – 180.

(189) Prosser, D. E.; Kaufmann, M.; O'Leary, B.; Byford, V.; Jones, G. Single A326G Mutation Converts Human CYP24A1 from 25-OH-D3-24-Hydroxylase into -23-Hydroxylase, Generating 1α,25-(OH)2D3-26,23-Lactone. *Proc. Natl. Acad. Sci.* **2007**, *104* (31), 12673 – 12678.

(190) Annalora, A. J.; Goodin, D. B.; Hong, W.-X.; Zhang, Q.; Johnson, E. F.; Stout, C. D. Crystal Structure of CYP24A1, a Mitochondrial Cytochrome P450 Involved in Vitamin D Metabolism. *J. Mol. Biol.* **2010**, *396* (2), 441 – 451.

(191) Ferla, S.; Aboraia, A. S.; Brancale, A.; Pepper, C. J.; Zhu, J.; Ochalek, J. T.; DeLuca, H. F.; Simons, C. Small-Molecule Inhibitors of 25-Hydroxyvitamin D-24-Hydroxylase

(CYP24A1): Synthesis and Biological Evaluation. *J. Med. Chem.* **2014**, *57* (18), 7702 – 7715.

(192) Hewison, M.; Zehnder, D.; Bland, R.; Stewart, P. M. 1alpha-Hydroxylase and the Action of Vitamin D. *J. Mol. Endocrinol.* **2000**, *25* (2), 141 – 148.

(193) Armbrecht, H. J.; Zenser, T. V; Davis, B. B. Conversion of 25-Hydroxyvitamin D3. To 1, 25-Dihydroxyvitamin D3 and 24,25-Dihydroxyvitamin D3 in Renal Slices from the Rat. *Endocrinology* **1981**, *109* (1), 218 – 222.

(194) St-Arnaud, R.; Naja, R. P. Vitamin D Metabolism, Cartilage and Bone Fracture Repair. *Mol. Cell. Endocrinol.* **2011**, *347* (1 – 2), 48 – 54.

(195) Omdahl, J. L.; Morris, H. A.; May, B. K. Hydroxylase Enzymes of the Vitamin D Pathway: Expression, Function, and Regulation. *Annu. Rev. Nutr.* **2002**, *22* (1), 139 – 166.

(196) Kim, S. Y. The Pleiomorphic Actions of Vitamin D and Its Importance for Children. *Ann. Pediatr. Endocrinol. Metab.* **2013**, *18* (2), 45 – 54.

(197) Nykjaer, A.; Fyfe, J. C.; Kozyraki, R.; Leheste, J.-R.; Jacobsen, C.; Nielsen, M. S.; Verroust, P. J.; Aminoff, M.; de la Chapelle, A.; Moestrup, S. K.; Ray, R.; Gliemann, J.; Willnow, T. E.; Christensen, E. I. Cubilin Dysfunction Causes Abnormal Metabolism of the Steroid Hormone 25(OH) Vitamin D3. *Proc. Natl. Acad. Sci. U. S. A.* **2001**, *98* (24), 13895 – 13900.

(198) Olmos-Ortiz, A.; Avila, E.; Durand-Carbajal, M.; Díaz, L. Regulation of Calcitriol Biosynthesis and Activity: Focus on Gestational Vitamin D Deficiency and Adverse Pregnancy Outcomes. *Nutrients* **2015**, *7* (1), 443 – 480.

(199) Pike, J. W.; Meyer, M. B. The Vitamin D Receptor: New Paradigms for the Regulation of Gene Expression by 1,25-Dihydroxyvitamin D3. *Endocrinol. Metab. Clin. North Am.* **2010**, *39* (2), 255 – 269.

(200) Hamamoto, H.; Kusudo, T.; Urushino, N.; Masuno, H.; Yamamoto, K.; Yamada, S.; Kamakura, M.; Ohta, M.; Inouye, K.; Sakaki, T. Structure-Function Analysis of Vitamin D 24-Hydroxylase (CYP24A1) by Site-Directed Mutagenesis: Amino Acid Residues Responsible for Species-Based Difference of CYP24A1 between Humans and Rats. *Mol. Pharmacol.* **2006**, *70* (1), 120 -128.

(201) Chiellini, G.; Rapposelli, S.; Zhu, J.; Massarelli, I.; Saraceno, M.; Bianucci, A. M.; Plum, L. A.; Clagett-Dame, M.; DeLuca, H. F. Synthesis and Biological Activities of Vitamin D-like Inhibitors of CYP24 Hydroxylase. *Steroids* **2012**, *77* (3), 212 – 223.

(202) Posner, G. H.; Helvig, C.; Cuerrier, D.; Collop, D.; Kharebov, A.; Ryder, K.; Epps, T.; Petkovich, M. Vitamin D Analogues Targeting CYP24 in Chronic Kidney Disease. *J.*

Steroid Biochem. Mol. Biol. **2010**, *121* (2), 13 – 19.

(203) Posner, G. H.; Wang, Q.; Han, G.; Lee, J. K.; Crawford, K.; Zand, S.; Brem, H.; Peleg, S.; Dolan, P.; Kensler, T. W. Conceptually New Sulfone Analogues of the Hormone 1 α ,25-Dihydroxyvitamin D₃: Synthesis and Preliminary Biological Evaluation. *J. Med. Chem.* **1999**, *42* (18), 3425 – 3435.

(204) Petkovich, M.; Jones, G. CYP24A1 and Kidney Disease. *Curr. Opin. Nephrol. Hypertens.* **2011**, *20* (4), 337 – 344.

(205) Nagamani, S.; Muthusamy, K.; Marshal, J. J. E-Pharmacophore Filtering and Molecular Dynamics Simulation Studies in the Discovery of Potent Drug-like Molecules for Chronic Kidney Disease. *J. Biomol. Struct. Dyn.* **2016**, *34* (10), 2233 – 2250.

(206) Hanzlik, R. P.; Kishore, V.; Tullman, R. Cyclopropylamines as Suicide Substrates for Cytochromes P-450. *J. Med. Chem.* **1979**, *22* (7), 759 – 761.

(207) Zhang, X.; Li, X.-X.; Liu, Y.; Wang, Y. Suicide Inhibition of Cytochrome P450 Enzymes by Cyclopropylamines via a Ring-Opening Mechanism: Proton-Coupled Electron Transfer Makes a Difference. *Front. Chem.* **2017**, *5* (3), 1 – 10.

(208) Seward, H. E.; Roujeinikova, A.; McLean, K. J.; Munro, A. W.; Leys, D. Crystal Structure of the Mycobacterium Tuberculosis P450 CYP121-Fluconazole Complex Reveals New Azole Drug-P450 Binding Mode. *J. Biol. Chem.* **2006**, *281* (51), 39437 – 39443.

(209) Gomaa, M. S.; Lim, A. S. T.; Wilson Lau, S. C.; Watts, A.-M.; Illingworth, N. A.; Bridgens, C. E.; Veal, G. J.; Redfern, C. P. F.; Brancale, A.; Armstrong, J. L.; Simons, C. Synthesis and CYP26A1 Inhibitory Activity of Novel Methyl 3-[4-(Arylamino)phenyl]-3-(Azole)-2,2-Dimethylpropanoates. *Bioorg. Med. Chem.* **2012**, *20* (20), 6080 – 6088.

(210) Aboraia, A. S.; Yee, S. W.; Gomaa, M. S.; Shah, N.; Robotham, A. C.; Makowski, B.; Prosser, D.; Brancale, A.; Jones, G.; Simons, C. Synthesis and CYP24A1 Inhibitory Activity of *N*-(2-(1*H*-Imidazol-1-yl)-2-Phenylethyl)arylamides. *Bioorg. Med. Chem.* **2010**, *18* (14), 4939 – 4946.

(211) Ferla, S.; Gomaa, M. S.; Brancale, A.; Zhu, J.; Ochalek, J. T.; DeLuca, H. F.; Simons, C. Novel Styryl-Indoles as Small Molecule Inhibitors of 25-Hydroxyvitamin D-24-Hydroxylase (CYP24A1): Synthesis and Biological Evaluation. *Eur. J. Med. Chem.* **2014**, *87*, 39 – 51.

(212) Schuster, I.; Egger, H.; Nussbaumer, P.; Kroemer, R. T. Inhibitors of Vitamin D Hydroxylases: Structure-Activity Relationships. *J. Cell. Biochem.* **2003**, *88* (2), 372 – 380.

(213) Peehl, D. M.; Seto, E.; Hsu, J.-Y.; Feldman, D. Preclinical Activity of Ketoconazole in

Combination With Calcitriol or the Vitamin D Analogue Eb 1089 in Prostate Cancer Cells. *J. Urol.* **2002**, *168* (4), 1583 – 1588.

(214) Ly, L. H.; Zhao, X. Y.; Holloway, L.; Feldman, D. Liarozole Acts Synergistically with 1 α ,25-Dihydroxyvitamin D3 to Inhibit Growth of DU 145 Human Prostate Cancer Cells by Blocking 24-Hydroxylase Activity. *Endocrinology* **1999**, *140* (5), 2071 – 2076.

(215) Schuster, I.; Egger, H.; Herzig, G.; Reddy, G. S.; Schmid, J. a; Schüssler, M.; Vorisek, G. Selective Inhibitors of Vitamin D Metabolism--New Concepts and Perspectives. *Anticancer Res.* **2006**, *26* (4A), 2653 – 2668.

(216) Schuster, I.; Egger, H.; Bikle, D.; Herzig, G.; Reddy, G. S.; Stuetz, A.; Stuetz, P.; Vorisek, G. Selective Inhibition of Vitamin D Hydroxylases in Human keratinocytes1. *Steroids* **2001**, *66* (3 – 5), 409 – 422.

(217) Yee, S. W.; Simons, C. Synthesis and CYP24 Inhibitory Activity of 2-Substituted-3,4-Dihydro-2H-Naphthalen-1-One (Tetralone) Derivatives. *Bioorg. Med. Chem. Lett.* **2004**, *14* (22), 5651 – 5654.

(218) Aboraia, A. S.; Makowski, B.; Bahja, A.; Prosser, D.; Brancale, A.; Jones, G.; Simons, C. Synthesis and CYP24A1 Inhibitory Activity of (E)-2-(2-Substituted Benzylidene)- and 2-(2-Substituted Benzyl)-6-Methoxy-Tetralones. *Eur. J. Med. Chem.* **2010**, *45* (10), 4427 – 4434.

(219) Yee, S. W.; Campbell, M. J.; Simons, C. Inhibition of Vitamin D3 Metabolism Enhances VDR Signalling in Androgen-Independent Prostate Cancer Cells. *J. Steroid Biochem. Mol. Biol.* **2006**, *98* (5), 228 – 235.

(220) Holick, M. F. Sunlight and Vitamin D for Bone Health and Prevention of Autoimmune Diseases, Cancers, and Cardiovascular Disease. *Am J Clin Nutr* **2004**, *80* (6), 1678 – 1688.

(221) ww.specs.net.

(222) Ferla, S. Small Molecule Inhibitors of CYP24A1 for the Treatment of Various Cancers, PhD Thesis. *Cardiff Univ.* **2013**.

(223) Annalora, A. J.; Goodin, D. B.; Hong, W.-X.; Zhang, Q.; Johnson, E. F.; Stout, C. D. Crystal Structure of CYP24A1, a Mitochondrial Cytochrome P450 Involved in Vitamin D Metabolism. *J. Mol. Biol.* **2010**, *396* (2), 441 – 451.

(224) Alonso, H.; Bliznyuk, A. A.; Gready, J. E. Combining Docking and Molecular Dynamic Simulations in Drug Design. *Med. Res. Rev.* **2006**, *26* (5), 531 – 568.

(225) Bawden, D. Computerized Chemical Structure-Handling Techniques in Structure-Activity Studies and Molecular Property Prediction. *J. Chem. Inf. Comput. Sci.* **1983**, *23* (1), 14 –

22.

(226) Rai, D. K.; Rieder, E. Homology Modeling and Analysis of Structure Predictions of the Bovine Rhinitis B Virus RNA Dependent RNA Polymerase (RdRp). *Int. J. Mol. Sci.* **2012**, *13* (7), 8998–9013.

(227) Wieman, H.; Tøndel, K.; Anderssen, E.; Drabløs, F. Homology-Based Modelling of Targets for Rational Drug Design Homology-Based Modelling of Targets for Rational Drug Design. *Mini-Reviews Med. Chem.* **2004**, *4*, 793–804.

(228) Berman, H. M.; Westbrook, J.; Feng, Z.; Gilliland, G.; Bhat, T. N.; Weissig, H.; Shindyalov, I. N.; Bourne, P. E. The Protein Data Bank. *Nucleic Acids Res.* **2000**, *28* (1), 235–242.

(229) Arnold, K.; Bordoli, L.; Kopp, J.; Schwede, T. The SWISS-MODEL Workspace: A Web-Based Environment for Protein Structure Homology Modelling. *Bioinforma.* **2006**, *22* (2), 195–201.

(230) Chothia, C.; Lesk, A. M. The Relation between the Divergence of Sequence and Structure in Proteins. *EMBO J.* **1986**, *5* (4), 823–826.

(231) Thompson, J. D.; Higgins, D. G.; Gibson, T. J. CLUSTAL W: Improving the Sensitivity of Progressive Multiple Sequence Alignment through Sequence Weighting, Position-Specific Gap Penalties and Weight Matrix Choice. *Nucleic Acids Res.* **1994**, *22* (22), 4673–4680.

(232) Siam, A.; Brancale, A.; Simons, C. Comparative Modeling of 25-Hydroxycholesterol-7 α -Hydroxylase (CYP7B1): Ligand Binding and Analysis of Hereditary Spastic Paraplegia Type 5 CYP7B1 Mutations. *J. Mol. Model.* **2012**, *18* (2), 441–453.

(233) Zalewski, A.; Ma, N. S.; Legeza, B.; Renthal, N.; Flück, C. E.; Pandey, A. V. Vitamin D-Dependent Rickets Type 1 Caused by Mutations in CYP27B1 Affecting Protein Interactions With Adrenodoxin. *J. Clin. Endocrinol. Metab.* **2016**, *101* (9), 3409–3418.

(234) Sievers, F.; Wilm, A.; Dineen, D.; Gibson, T. J.; Karplus, K.; Li, W.; Lopez, R.; McWilliam, H.; Remmert, M.; Söding, J.; Thompson, J. D.; Higgins, D. G. Fast, Scalable Generation of High‐quality Protein Multiple Sequence Alignments Using Clustal Omega. *Mol. Syst. Biol.* **2011**, *7* (1), 539.

(235) Lovell, I.W.; Davis, W.B.; Arendall, P.I.W.; Bakker, J.M.; Word, M.G.; Prisant, J. S.; Richardson, D. C. Structure Validation by C α Geometry: Φ / ψ and C β Deviation. Proteins: Structure. *Funct. Genet.* **2003**, *50* (3), 437–450.

(236) Gomaa, M. S.; Simons, C.; Brancale, A. Homology Model of 1 α ,25-Dihydroxyvitamin D3 24-Hydroxylase Cytochrome P450 24A1 (CYP24A1): Active Site Architecture and Ligand Binding. In *Journal of Steroid Biochemistry and Molecular Biology*; 2007; Vol. 104, 53–

60.

(237) http://www.chemcomp.com/MOE-Molecular_Operating_Environment.htm.

(238) Fiser, A. Template-Based Protein Structure Modeling. *Methods Mol. Biol.* **2010**, *673*, 73 – 94.

(239) di Luccio, E.; Koehl, P. A Quality Metric for Homology Modeling: The H-Factor. *BMC Bioinformatics* **2011**, *12* (1), 48 – 66.

(240) http://mordred.bioc.cam.ac.uk/~rapper/rampage.php.

(241) http://services.mbi.ucla.edu/ERRAT/.

(242) http://services.mbi.ucla.edu/Verify_3D/.

(243) Bowie, J. U.; Luthy, R.; Eisenberg, D. A Method to Identify Protein Sequences That Fold into a Known Three-Dimensional Structure. *Science.* **1991**, *253* (5016), 164 – 170.

(244) Luthy, R.; Bowie, J. U.; Eisenberg, D. Assessment of Protein Models with Three-Dimensional Profiles. *Nature* **1992**, *356* (6364), 83 – 85.

(245) Wiederstein, M.; Sippl, M. J. ProSA-Web: Interactive Web Service for the Recognition of Errors in Three-Dimensional Structures of Proteins. *Nucleic Acids Res* **2007**, *35*, W407 – W410.

(246) Wilson, K. A.; Bär, S.; Maerz, A. L.; Alizon, M.; Poumbourios, P. The Conserved Glycine-Rich Segment Linking the N-Terminal Fusion Peptide to the Coiled Coil of Human T-Cell Leukemia Virus Type 1 Transmembrane Glycoprotein gp21 Is a Determinant of Membrane Fusion Function. *J. Virol.* **2005**, *79* (7), 4533 – 4539.

(247) Oezguen, N.; Kumar, S.; Hindupur, A.; Braun, W.; Muralidhara, B. K.; Halpert, J. R. Oezguen, N.; Kumar, S.; Hindupur, A.; Braun, W.; Muralidhara, B. K.; Halpert, J. R. Identification and Analysis of Conserved Sequence Motifs in Cytochrome P450 Family 2: Functional and Structural Role of a MOTIF (187)RFDYKD(192) Iin CYP2B Enzymes. *J. Biol. Chem.* **2008**, *283* (31), 21808 – 21816.

(248) Ost, T. W. B.; Miles, C. S.; Munro, A. W.; Murdoch, J.; Reid, G. A.; Chapman, S. K. Phenylalanine 393 Exerts Thermodynamic Control over the Heme of Flavocytochrome P450 BM3. *Biochemistry* **2001**, *40* (45), 13421 – 13429.

(249) Gotoh, O. Substrate Recognition Sites in Cytochrome P450 Family 2 (CYP2) Proteins Inferred from Comparative Analyses of Amino Acid and Coding Nucleotide Sequences. *J. Biol. Chem.* **1992**, *267* (1), 83 – 90.

(250) Williams, P. A.; Cosme, J.; Sridhar, V.; Johnson, E. F.; McRee, D. E. Mammalian Microsomal Cytochrome P450 Monooxygenase. *Mol. Cell* **2016**, *5* (1), 121 – 131.

(251) Strushkevich, N.; MacKenzie, F.; Cherkesova, T.; Grabovec, I.; Usanov, S.; Park, H.-W. Structural Basis for Pregnenolone Biosynthesis by the Mitochondrial Monooxygenase System. *Proc. Natl. Acad. Sci.* **2011**, *108* (25), 10139–10143.

(252) http://bioinf.cs.ucl.ac.uk/psipred.

(253) Kakarala, K. K.; Jamil, K. Protease Activated Receptor-2 (PAR2): Possible Target of Phytochemicals. *J. Biomol. Struct. Dyn.* **2015**, *33* (9), 2003–2022.

(254) Yamamoto, K.; Masuno, H.; Sawada, N.; Sakaki, T.; Inouye, K.; Ishiguro, M.; Yamada, S. Homology Modeling of Human 25-Hydroxyvitamin D3 1-Hydroxylase (CYP27B1) Based on the Crystal Structure of Rabbit CYP2C5. *J. Steroid Biochem. Mol. Biol.* **2004**, *89*, 167–171.

(255) Yamamoto, K.; Uchida, E.; Urushino, N.; Sakaki, T.; Kagawa, N.; Sawada, N.; Kamakura, M.; Kato, S.; Inouye, K.; Yamada, S. Identification of the Amino Acid Residue of CYP27B1 Responsible for Binding of 25-Hydroxyvitamin D3 Whose Mutation Causes Vitamin D-Dependent Rickets Type 1. *J. Biol. Chem.* **2005**, *280* (34), 30511–30516.

(256) https://www.schrodinger.com/maestro.

(257) Desai, N. C.; Joshi, V. V.; Rajpara, K. M.; Vaghani, H. V.; Satodiya, H. M. Facile Synthesis of Novel Fluorine Containing Pyrazole Based Thiazole Derivatives and Evaluation of Antimicrobial Activity. *J. Fluor. Chem.* **2012**, *142*, 67–78.

(258) Pandey, G.; Bhowmik, S.; Batra, S. Synthesis of 3 H - Pyrazolo [3 , 4 - C] - Isoquinolines and Thieno [3, 2-C]- Isoquinolines via Cascade Imination / Intramolecular Decarboxylative Coupling. *Org. Lett.* **2013**, *15* (19), 5044–5047.

(259) Parmar, K. C.; Vora, J. J.; Vasava, S. B. Synthesis, Spectral and Microbial Studies of Some Novel Schiff Base Derivatives of 4- Methylpyridin-2-Amino Pyridine. *J. Chem. Pharm. Res.* **2009**, *6* (4), 1205–1210.

(260) Yadav, U. N.; Shankarling, G. S. Room Temperature Ionic Liquid Choline Chloride-Oxalic Acid: A Versatile Catalyst for Acid-Catalyzed Transformation in Organic Reactions. *J. Mol. Liq.* **2014**, *191*, 137–141.

(261) Vilsmeier, A.; Haack, A. Über Die Einwirkung von Halogenphosphor Auf Alkyl‑formanilide. Eine Neue Methode Zur Darstellung Sekundärer Und Tertiärer P‑alkylamino‑benzaldehyde. *erichte der Dtsch. Chem. Gesellschaft* **1927**, *60*, 119–122.

(262) Rajput, A. P.; Girase, P. D. Review Article on Vilsmeier-Haack Reaction. *Int. J. Pharm. Chem. Biol. Sci.* **2012**, *3* (1), 25–43.

(263) Yadlapalli, R. K.; Chourasia, O. P.; Vemuri, K.; Sritharan, M.; Perali, R. S. Synthesis and

in Vitro Anticancer and Antitubercular Activity of Diarylpyrazole Ligated Dihydropyrimidines Possessing Lipophilic Carbamoyl Group. *Bioorganic Med. Chem. Lett.* **2012**, *22* (8), 2708–2711.

(264) Abdul, N.; Farooqui, M.; Farooqui, M. Kinetic of Permagnetic Oxidation of Thiophene-2-Aldehyde in Acidic Media. *Int. J. Chem. Stud.* **2013**, *1* (4), 50–54.

(265) Basheer, K. M.; Joseph, J.; Damodaran, T.; Nair, R. Kinetics of the Oxidation of Benzhydrols with Permanganate under Phase Transfer Catalysis in Organic Solvents. *Mod. Res. Catal.* **2013**, *2*, 35–38.

(266) Peter, K.; Vollhardt, C.; Schore, E. N. Organic Chemistry Structure and Function. *W. H. Free. Co.* **2003**, fourth edition.

(267) Woodman, E. K.; Chaffey, J. G. K.; Hopes, P. A.; Hose, D. R. J.; Gilday, J. P. N,N′-Carbonyldiimidazole-Mediated Amide Coupling: Significant Rate Enhancement Achieved by Acid Catalysis with Imidazole・HCl. *Org. Process Res. Dev.* **2009**, *13*, 106–113.

(268) Buchholz, M.; Heiser, U.; Schilling, S.; Niestroj, A. J.; Zunkel, K.; Demuth, H.-U. The First Potent Inhibitors for Human Glutaminyl Cyclase: Synthesis and Structure−Activity Relationship. *J. Med. Chem.* **2006**, *49* (2), 664–677.

(269) Ye, C. M.; Ariffin, A.; Khan, M. N. Solvent Effects on Alkaline Hydrolysis of N-Benzylphthalimide in Mixed Water-Acetonitrile and Mixed. *Indian J. Chem.* **2005**, *44*, 2055–2059.

(270) Hay, M. P.; Wilson, W. R.; Moselen, J. W.; Palmer, B. D.; Denny, W. A. Hypoxia-Selective Antitumor Agents. 8. Bis(nitroimidazoly1)alkanecarboxamides: A New Class of Hypoxia-Selective Cytotoxins and Hypoxic Cell Radioseneitisers. *J. Med. Chem.* **1994**, *37*, 381–391.

(271) Bergstrom, C. P.; Sloan, C. P.; Lau, W.-Y.; Smith, D. W.; Zheng, M.; Hansel, S. B.; Polson, C. T.; Corsa, J. A.; Barten, D. M.; Felsenstein, K. M.; Roberts, S. B. Carbamate-Appended N-Alkylsulfonamides as Inhibitors of Gamma-Secretase. *Bioorg. Med. Chem. Lett.* **2008**, *18* (2), 464–468.

(272) Popkov, S. V.; Skvortsova, M. N. A New Method for the Synthesis of N-(2-Aminoethyl)azoles by Alkylation of Azoles with 2-Alkyl-4,5-Dihydrooxazoles. *Russ. Chem. Bull.* **2006**, *55* (10), 1848–1851.

(273) Gibson, M. S.; Bradshaw, R. W. The Gabriel Synthesis of Primary Amines. *Angew. Chemie Int. Ed. English* **1968**, *7* (12), 919–930.

(274) Khan, M. N. Suggested Improvement in the Ing-Manske Procedure and Gabriel Synthesis

of Primary Amines: Kinetic Study on Alkaline Hydrolysis of N-Phthaloylglycine and Acid Hydrolysis of N-(O-Carboxybenzoyl)glycine in Aqueous Organic Solvents. *J. Org. Chem.* **1996**, *61* (23), 8063‑8068.

(275) Khan, S. B.; Hassan Khan, M. T.; Jang, E. S.; Akhtar, K.; Seo, J.; Han, H. Tyrosinase Inhibitory Effect of Benzoic Acid Derivatives and Their Structure-Activity Relationships. *J. Enzyme Inhib. Med. Chem.* **2010**, *25* (6), 812‑817.

(276) Bratenko, M. K.; Chornous, V. A.; Vovk, M. V. 4-Functionally Substituted 3-Heterylpyrazoles: III. * 3-Aryl (Heteryl) Pyrazole-4-Carboxylic Acids and Their Derivatives. *Russ. J. Org. Chem.* **2001**, *37* (4), 552‑555.

(277) Lin, C. M.; Wong, F. F.; Huang, J. J.; Yeh, M. Y. An Efficient and Convenient Method for Synthesis of 1-Substituted Imidazoles. *Heterocycles* **2006**, *68* (7), 1359‑1370.

(278) http://www.biosolveit.de/.

(279) Zhu, J.; Barycki, R.; Chiellini, G.; DeLuca, H. F. Screening of Selective Inhibitors of 1 α ,25-Dihydroxyvitamin D$_3$ 24-Hydroxylase Using Recombinant Human Enzyme Expressed in Escherichia Coli. *Biochemistry* **2010**, *49* (49), 10403‑10411.

(280) Vinh, T. K.; Ahmadi, M.; Lopez Delgado, P. O.; Fernandez Perez, S.; Walters, H. M.; Smith, H. J.; Nicholls, P. J.; Simons, C. 1-[(Benzofuran-2-yl)phenylmethyl]-Triazoles and -Tetrazoles - Potent Competitive Inhibitors of Aromatase. *Bioorganic Med. Chem. Lett.* **1999**, *9* (14), 2105‑2108.

(281) Saberi, M. R.; Shah, K.; Simons, C. Benzofuran- and Furan-2-yl-(Phenyl)-3-Pyridylmethanols: Synthesis and Inhibition of P450 Aromatase. *J. Enzyme Inhib. Med. Chem.* **2005**, *20* (2), 135‑141.

(282) Taban, I. M.; Zhu, J.; DeLuca, H. F.; Simons, C. Synthesis, Molecular Modelling and CYP24A1 Inhibitory Activity of Novel of (*E*)-N-(2-(1*H*-Imidazol-1-yl)-2-(Phenylethyl)-3/4-Styrylbenzamides. *Bioorg. Med. Chem.* **2017**, *25* (15), 4076‑4087.

(283) Taban, I. M.; Zhu, J.; DeLuca, H. F.; Simons, C. Analysis of the Binding Sites of Vitamin D 1 α -Hydroxylase (CYP27B1) and Vitamin D 24-Hydroxylase (CYP24A1) for the Design of Selective CYP24A1 Inhibitors: Homology Modelling, Molecular Dynamics Simulations and Identification of Key Binding Requirements. *Bioorg. Med. Chem.* **2017**, http://dx.doi.org/10.1016/j.bmc.2017.05.055.

(284) Murugan, R.; Ramamoorthy, K.; Sundarrajan, S.; Ramakrishna, S. Magnesium Oxide Nanotubes: Synthesis, Characterization and Application as Efficient Recyclable Catalyst for Pyrazolyl 1,4-Dihydropyridine Derivatives. *Tetrahedron* **2012**, *68* (35), 7196‑7201.

(285) Kira, M.A. Abdel- Rahman, M.O. and Gadalla, K. Z. The VILSMIEZR-RAACK- III Cyclization of Hydrazons pyrazoleS. *Tetrahedron Lett.* **1969**, *2*, 109 110.

(286) Paul, N.; Muthusubramanian, S. Temperature-Dependent Product Selectivity in the Vilsmeier - Haack Reaction on Bis (Phenylhydrazones) of Bis (Aroylmethyl) Sulfides (1,1 ' -[Thiobis(methylene)]bis[bis[arylmethanone]bis(2-Phenylhydrazones)): Synthesis of 3-Aroylindoles (= Aryl (1 H -Ind. *Helv. Chim. Acta* **2013**, *96*, 452 – 457.

(287) Chornous, V. A.; Mel, N. V; Bratenko, M. K.; Vovk, M. V. 4-Functionally Substituted 3-heterylpyrazoles:VII. 3-Aryl(heteryl)-1-Phenyl-4-Pyrazolecarbonylisothiocyanates. *Russ. J. Org. Chem.* **2002**, *38* (3), 405 – 410.

(288) Ainsworth, C.; Jones, R. G. Isomeric and Nuclear-Substituted β -Aminoethyl-1,2,4-Triazoles. *J. Am. Chem. Soc.* **1955**, *77* (4), 621 – 624.

(289) Sobhani, S ; Honarmand, M. 2-Hydroxyethylammonium Acetate: A Reusable and Cost Task-Specific Ionic Liquid Promoting One-Pot, Three-Component Synthesis of 2-Amino-3,5-Dicarbonitrile-6-Thio-Pyridines. *Comptes Rendus Chim.* **2013**, *16* (3), 279 – 286.

(290) Sobhani, S.; Nasseri, R.; Honarmand, M. 2-Hydroxyethylammonium Acetate as a Reusable and Cost-Effective Ionic Liquid for the Efficient Synthesis of Bis(pyrazolyl)methanes and 2-Pyrazolyl-1-Nitroalkanes. *Can. J. Chem.* **2012**, *90* (10), 798 – 804.

(291) Nnamani, I. N.; Joshi, G. S.; Danso-Danquah, R.; Abdulmatik, O.; Asakuru, T.; Abraham, D. J.; Safo, M. K. Pyridyl Derivatives of Benzaldehyde as Potential Antisickling Agents. *Chem. Biodivers.* **2008**, *5* (9), 1762 – 1769.

(292) Aggarwal, V. K.; de Vicente, J.; Bonnert, R. V. A Novel One-Pot Method for the Preparation of Pyrazoles by 1,3-Dipolar Cycloadditions of Diazo Compounds Generated in Situ. *J. Org. Chem.* **2003**, *68* (13), 5381 – 5383.

(293) Taylor, P.; Zhou, Z.; Zhang, Y. An Efficient and Green One-Pot Three-Component Catalyzed by 2-Hydroxy Ethylammonium Propionate. *Green Chem. Lett. Rev.* **2014**, *7* (1), 18 – 23.

(294) Chattha, F. A.; Munawar, M. A.; Nagra, S. A.; Ashraf, M.; Khan, M. A.; Kosur, S. Synthesis of 3-Aryl-1H-Indazoles and Their Effects on Plant Growth. *J. Plant Growth Regul.* **2013**, *32* (2), 291 – 297.

(295) Hamama, Wafaa S.; Gouda, Moustafa A.; Badr, Marwa H.; Zoorob, H. H. Synthesis of Some New Fused and Binary 1,3,4-Thiadiazoles as Potential Antitumor and Antioxidant Agents. *J. Heterocycl. Chem.* **2013**, *50*, 787 – 794.

(296) Wang, R.; Lu, Y.; Wang, S. Comparative Evaluation of 11 Scoring Functions for Molecular

Docking. *J. Med. Chem.* **2003**, *46* (12), 2287–2303.

(297) Schuster, I.; Egger, H.; Herzig, G.; Reddy, G. S.; Schimid, J. A.; SCHÜSSLER, M.; VORISEK, G. Selective Inhibitors of Vitamin D Metabolism - New Concepts and Perspectives. *Anticancer Res.* **2006**, *26* (4A), 2653–2668.

(298) Gildner, P. G.; Gietter, A. A. S.; Cui, D.; Watson, D. A. Benzylation of Nitroalkanes Using Copper-Catalyzed Thermal Redox Catalysis: Toward the Facile C-Alkylation of Nitroalkanes. *J. Am. Chem. Soc.* **2012**, *134* (24), 9942–9945.

(299) Li, Y.; Deng, P.; Zeng, Y.; Xiong, Y.; Zhou, H. Anti-Selective Asymmetric Henry Reaction Catalyzed by a Heterobimetallic Cu–Sm–Aminophenol Sulfonamide Complex. *Org. Lett.* **2016**, *18* (7), 1578–1581.

(300) Ono, N. The Nitro-Aldol (Henry) Reaction. In *The Nitro Group in Organic Synthesis*; John Wiley & Sons, Inc., 2001; pp 30–69.

(301) Qin, D.-D.; Lai, W.-H.; Hu, D.; Chen, Z.; Wu, A.-A.; Ruan, Y.-P.; Zhou, Z.-H.; Chen, H.-B. Highly Enantioselective Henry Reactions of Aromatic Aldehydes Catalyzed by an Amino Alcohol-copper(II) Complex. *Chemistry* **2012**, *18* (34), 10515–10518.

(302) Brun, E. M.; Gil, S.; Parra, M. Enantioselective α-Alkylation of Unsaturated Carboxylic Acids Using a Chiral Lithium Amide. *Tetrahedron: Asymmetry* **2001**, *12* (6), 915–921.

(303) Kureshy, R. I.; Das, A.; Khan, N. H.; Abdi, S. H. R.; Bajaj, H. C. Cu(II)-Macrocylic [H4]Salen Catalyzed Asymmetric Nitroaldol Reaction and Its Application in the Synthesis of α1-Adrenergic Receptor Agonist (R)-Phenylephrine. *ACS Catal.* **2011**, *1* (11), 1529–1535.

(304) Sasai, H.; Suzuki, T.; Arai, S.; Arai, T.; Shibasaki, M. Basic Character of Rare Earth Metal Alkoxides. Utilization in Catalytic Carbon-Carbon Bond-Forming Reactions and Catalytic Asymmetric Nitroaldol Reactions. *J. Am. Chem. Soc.* **1992**, *114* (11), 4418–4420.

(305) Angelini, T.; Ballerini, E.; Bonollo, S.; Curini, M.; Lanari, D. A New Sustainable Protocol for the Synthesis of Nitroaldol Derivatives via Henry Reaction under Solvent-Free Conditions. *Green Chem. Lett. Rev.* **2014**, *7* (1), 11–17.

(306) Häring, M.; Pettignano, A.; Quignard, F.; Tanchoux, N.; Díaz Díaz, D. Keratin Protein-Catalyzed Nitroaldol (Henry) Reaction and Comparison with Other Biopolymers. *Molecules* **2016**, *21* (9), 1122–1130.

(307) Langer, O.; Dollé, F.; Valette, H.; Halldin, C.; Vaufrey, F.; Fuseau, C.; Coulon, C.; Ottaviani, M.; Någren, K.; Bottlaender, M.; Maziére, B.; Crouzel, C. Synthesis of High-Specific-Radioactivity 4- and 6-[18F]fluorometaraminol- PET Tracers for the Adrenergic

Nervous System of the Heart. *Bioorg. Med. Chem.* **2001**, *9* (3), 677 – 694.

(308) Bhabak, K. P.; Arenz, C. Novel Amide- and Sulfonamide-Based Aromatic Ethanolamines: Effects of Various Substituents on the Inhibition of Acid and Neutral Ceramidases. *Bioorg. Med. Chem.* **2012**, *20* (20), 6162 – 6170.

(309) Youn, S. W.; Kim, Y. H. Facile Synthesis of 2-Nitroalkanols Mediated with LiAlH4 as Catalyst. *Synlett* **2000**, *2000* (6), 880 – 882.

(310) Lodh, R.; Sarma, M. J.; Borah, A. J.; Phukan, P. Selective Synthesis of Nitroalcohols in the Presence of Ambersep 900 OH as Heterogeneous Catalyst. *Monatshefte f{ü}r Chemie - Chem. Mon.* **2015**, *146* (6), 969 – 972.

(311) Lee, D.-M.; Lee, J.-C.; Jeong, N.; Lee, K.-I. Asymmetric Transfer Hydrogenation of 2-Tosyloxy-1-(4-Hydroxyphenyl)ethanone Derivatives: Synthesis of (R)-Tembamide, (R)-Aegeline, (*R*)-Octopamine, and (*R*)-Denopamine. *Tetrahedron: Asymmetry* **2007**, *18* (22), 2662 – 2667.

(312) Gowda, D. C.; Prakasha Gowda, A. S.; Baba, A. R.; Gowda, S. Nickel-Catalyzed Formic Acid Reductions. A Selective Method for the Reduction of Nitro Compounds. *Synth. Commun.* **2000**, *30* (16), 2889 – 2895.

(313) Bosiak, M. J.; Pakulski, M. M. Asymmetric Reduction of ??-Keto Aldoxime O -Ethers. *Synthesis (Stuttg).* **2011**, *0* (2), 316 – 324.

(314) Gupta, P.; Rouf, A.; Shah, B. A.; Mukherjee, D.; Taneja, S. C. Efficient Preparation of Biologically Important 1,2-Amino Alcohols. *Synth. Commun.* **2013**, *43* (4), 505 – 519.

(315) Mizoroki, T.; Mori, K.; Ozaki, A. Arylation of Olefin with Aryl Iodide Catalyzed by Palladium. *Bull. Chem. Soc. Jpn.* **1971**, *44* (2), 581.

(316) Heck, R. F.; Nolley, J. P. Palladium-Catalyzed Vinylic Hydrogen Substitution Reactions with Aryl, Benzyl, and Styryl Halides. *J. Org. Chem.* **1972**, *37* (14), 2320 – 2322.

(317) Brown, J. M.; Cooley, N. A. Carbon-Carbon Bond Formation through Organometallic Elimination Reactions. *Chem. Rev.* **1988**, *88* (7), 1031 – 1046.

(318) Du, Z.; Zhou, W.; Bai, L.; Wang, F.; Wang, J. X. In Situ Generation of Palladium Nanoparticles: Reusable, Ligand-Free Heck Reaction in PEG-400 Assisted by Focused Microwave Irradiation. *Synlett* **2011**, *0* (3), 369 – 372.

(319) Schuster, I.; Egger, H. Acylated Aminoalkanimidazoles and - Triazoles. Patent US5622982. Google Patents April 22, 1997.

(320) Wittig, G.; Schöllkopf, U. Über Triphenyl-Phosphin-Methylene Als Olefinbildende Reagenzien. Mitteil. *Chem. Ber.* **1954**, *87* (9), 1318 – 1330.

(321) Hurd, C. D. Wittig Reaction. *Q. Reports Sulfur Chem.* **1969**, *4*, 159–227.

(322) Zhang, J.; Tang, Y. Iron-Catalyzed Regioselective Oxo- and Hydroxy-Phthalimidation of Styrenes: Access to α-Hydroxyphthalimide Ketones. *Adv. Synth. Catal.* **2016**, *358* (5), 752–764.

(323) Screttas, C. G.; Steele, B. R.; Micha-Screttas, M.; Heropoulos, G. A. Aryllithiums with Increasing Steric Crowding and Lipophilicity Prepared from Chlorides in Diethyl Ether. The First Directly Prepared Room-Temperature-Stable Dilithioarenes. *Org. Lett.* **2012**, *14* (22), 5680–5683.